AD-A122 613 GEOLOGY OF A STABLE INTRAPLATE REGION: THE CAPE VERDE/CANARY BASIN(U) NAVAL OCEAN RESEARCH AND DEVELOPMENT ACTIVITY NSTL STATION MS J A BALLARD

UNCLASSIFIED MAR 82 NORDA-45 F/G 8/10 NL

1/2

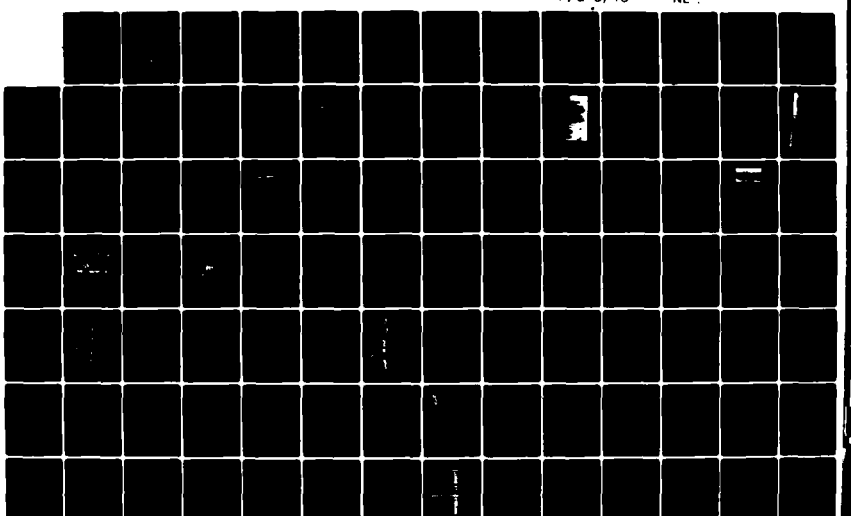

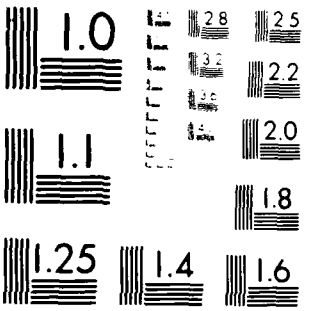

NORDA Report 45

Geology of a Stable Intraplate Region: The Cape Verde/Canary Basin

J. Alan Ballard

Ocean Measurement Program
Ocean Programs Management Office

March 1982

Approved for Public Release
Distribution Unlimited

Naval Ocean Research and Development Activity
NSTL Station, Mississippi 39529

Foreword

This report evaluates a unique bathymetric, magnetic, and seismic data set in terms of the geological history of a major ocean basin. It develops a seismic-stratigraphic classification for deep sea sediments and proposes a tectonic development history within the framework of sea floor spreading theory. The study will be useful to oceanographers, geologists, and geophysicists attempting to synthesize large quantities of data in order to construct a model for regional development.

G.T. Phelps, Captain, USN
Commanding Officer
NORDA

Executive Summary

Bathymetric, structural, and isopach maps have been compiled for an intraplate portion of the African Plate in the east central North Atlantic. These maps, when supplemented with geomagnetic data, provide a means for differentiating the effects of primary and secondary tectonism on present morphology.

Although the Cape Verde/Canary Basin is underlain by Mesozoic age crust and has been a deep ocean area since that time, most of the geologic events controlling present morphology are of Tertiary age. Reflector D1, a seismic event identified from the African continental margin by Seibold and Hinz (1974), can be correlated with an upper Cretaceous black carbonaceous shale throughout the basin. D1 is uplifted across the Cape Verde Rise and depressed by the weight of the Cape Verde Pedestal, suggesting that the Cape Verde Islands were not a significant topographic feature during the Mesozoic. Unconformities and condensed sections in DSDP sites and unconformities on seismic reflection records indicate a possible Eocene age uplifting. Extensive island volcanism and sill and dike emplacement occurred during Miocene. Many abyssal hills and small scale faults are related to this Miocene tectonic phase. Island volcanism has a continuing influence on the sedimentary sections.

The 'J' anomaly is a structural and magnetic manifestation of changes in sea-floor spreading patterns near the end of M-sequence time (120-125 myBP). Increases in spreading rates were accompanied by increases in the volume of the Mid-Atlantic Ridge (Hays and Pitman, 1973), Late Cretaceous rise in sea level, generation of Cretaceous Magnetic 'Quiet Zone' crust, and the initiation of post M-sequence fracture zones.

Seismic-stratigraphic facies analyses show that the Cape Verde/Canary Basin was probably above the carbonate compensation depth during Early Cretaceous and Late Jurassic, was a stagnant basin during Late Cretaceous, and was partially uplifted and eroded during Eocene. Most Tertiary sediments are prograding seaward in a relatively low energy transport mode. The abyssal plain is expanding westward by filling the valleys between abyssal hills and, in some instances, completely covering abyssal hills.

Executive Summary (continued)

Turcotte and Oxburgh (1973) suggested that the membrane stresses caused by northward shifting of the African Plate is capable of generating zones of weaknesses. These weakness zones could be expected to localize island volcanism, create north/south-trending faults, and promote the emplacement of dike swarms and volcanic abyssal hills. The membrane stress model fits Cape Verde/Canary Basin observations better than the 'hot spot' model (Morgan, 1971) or the propagating fracture model (LePichon and Fox, 1971).

Acknowledgements

The successful completion of a project of this magnitude would not be possible without the assistance and cooperation of a great many people. To the officers and crews of the Navy's research fleet and to shipmates too numerous to mention individually, I extend sincere appreciation for never compromising the quality of data collected despite the sometimes trying conditions. Louis G. Hemler and Steve Madosik III contributed many hours of data processing instruction, assistance, and encouragement throughout the life of the project. Carl Mueller assisted with the preparation of illustrations.

Drs. Conrad Neumann, Roy Ingram, John Rogers, and Walter Wheeler, University of North Carolina, Chapel Hill, N.C., contributed valuable advice and suggestions for improving this manuscript. Dr. Joel Watkins, Gulf Oil Co., Houston, Tex., critically reviewed the entire manuscript and suggested several significant changes in focus by providing important preprints and difficultly obtainable references. Many of the ideas presented here are the result of continuing discussions with my colleagues in the Navy's ocean science community. Those reading all or parts of the manuscript and offering suggestions for improvement included Allen Lowrie, David Handschumacher, Peter Fleischer, J. E. Matthews, T. L. Holcombe, Julius Egloff, Anne Einwich, Peter Vogt, and H. C. Eppert. In addition, Allen Lowrie provided indispensable assistance with translations. The work was supported by DCNM (D) funding (DDF Programs).

Contents

Contents (continued)

Contents (continued)

Contents (continued)

Contents (continued)

Illustrations, Tables, and Plates

Illustrations, Tables, and Plates (continued)

Illustrations, Tables, and Plates (continued)

TABLES

PLATES

Geology of a Stable Intraplate Region: The Cape Verde/Canary Basin

I. Introduction

A. Regional Setting

Within the context of plate tectonics, morphology of the original sea floor is the result of faulting and volcanism at the mid-ocean ridge. Fracture zones, the scars left by transform faults, are superimposed on the topographic fabric. Original sea floor cools, becomes draped with sediments, and decreases in elevation as it moves away from the ridge crest. Consequently, crustal ages and sediment thickness increase, and volcanism, earthquakes, and heat flow decrease in intensity and in number away from the spreading center.

Geologic processes associated with plate generation stop at some distance from the ridge crest. The effects of additional subsidence, volcanism, sedimentation, faulting and uplift are intermixed with original volcanism, faulting, and sedimentation. As a result, detailed mapping of surface and subsurface topographies, structures, and sediment distribution is necessary to differentiate the effects of primary and secondary diastrophism and related geologic processes to the present morphology of the plate and determine regional geologic history.

The Cape Verde/Canary Basin, an intraplate area south of the Azores-Gibraltar Ridge and west of the African Continental Margin (Fig. 1), is uniquely suited for the study of the effects of secondary intraplate diastrophism. On the basis of earthquake frequency and magnitude, and heat flow rate (Fig. 2), the basin is tectonically stable. Nevertheless, this area contains the most active volcano in the Atlantic Ocean, south of Iceland (Naval Oceanographic Office, 1965); two non-linear volcanic island groups with the oldest fossils found on any eastern Atlantic island (Colom, 1955); indications of episodic volcanism since Jurassic time (Dillon and Sougy, 1974); evidence of widespread Tertiary epeirogenic uplift (Watkins and Hoppe, 1979); and small scale vertical faulting, volcanism, horsts, and grabens and other suggestions of recent intraplate tectonism (Jones et al., 1966).

Speculative studies based on widely spaced and randomly distributed sampling have illustrated geologic complexities in the Cape Verde/Canary Basin, but have provided few unequivocal solutions to geologic problems. For example, abyssal hills in the basin may have been formed near the ridge crest by volcanism and faulting and undergone only minor later constructional modifications (Rona et al., 1974) or abyssal hills may indicate recent intraplate volcanism and faulting (Jones et al., 1966). Hayes and Rabinowitz (1975) project basin fracture zones across all post-Early Jurassic sea floor in contrast to western Atlantic fracture zones which are mostly confined to Cretaceous and younger sea floor (Vogt and Einwich, 1979). In the eastern Atlantic, the magnetic 'J' anomaly is well developed and correlated with Mesozoic sequence magnetic anomalies M2-M4 (Hayes and Rabinowitz, 1975; Ballard et al., 1976) or anomalies M16-M17 (Barrett and Keen, 1976; Uchupi et al., 1976). Jurassic volcanism has been reported from the Cape Verde Islands (Machado, Ageredo Leme, and Manjardino, 1967, quoted in Dillon and Sougy, 1974), although Hallam (1971) believes the oldest volcanics are Upper Cretaceous lavas and tuffs, and Bebiano (1932) dates the initiation of volcanism as Oligocene. In the Canary Islands, sediments may unconformably overlie plutonic rocks (D. A. Andrews-Jones, 1971, quoted in Dillon and Sougy, 1974) or igneous rocks may be

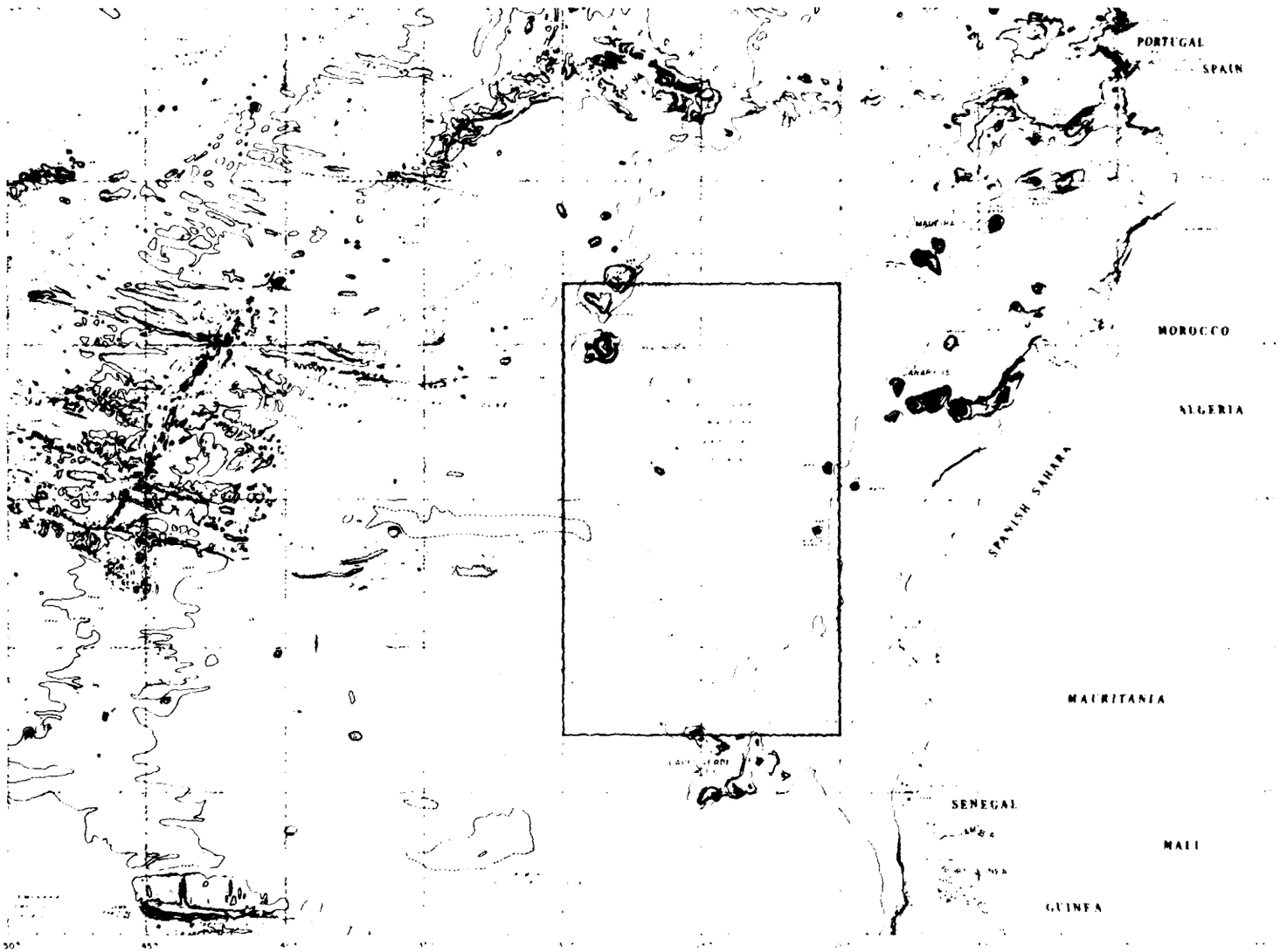

Figure 1. Geography and generalized bathymetry, eastern North Atlantic. Heavy lines enclose area covered in detail in this report. Base map from Uchupi et al. (1976).

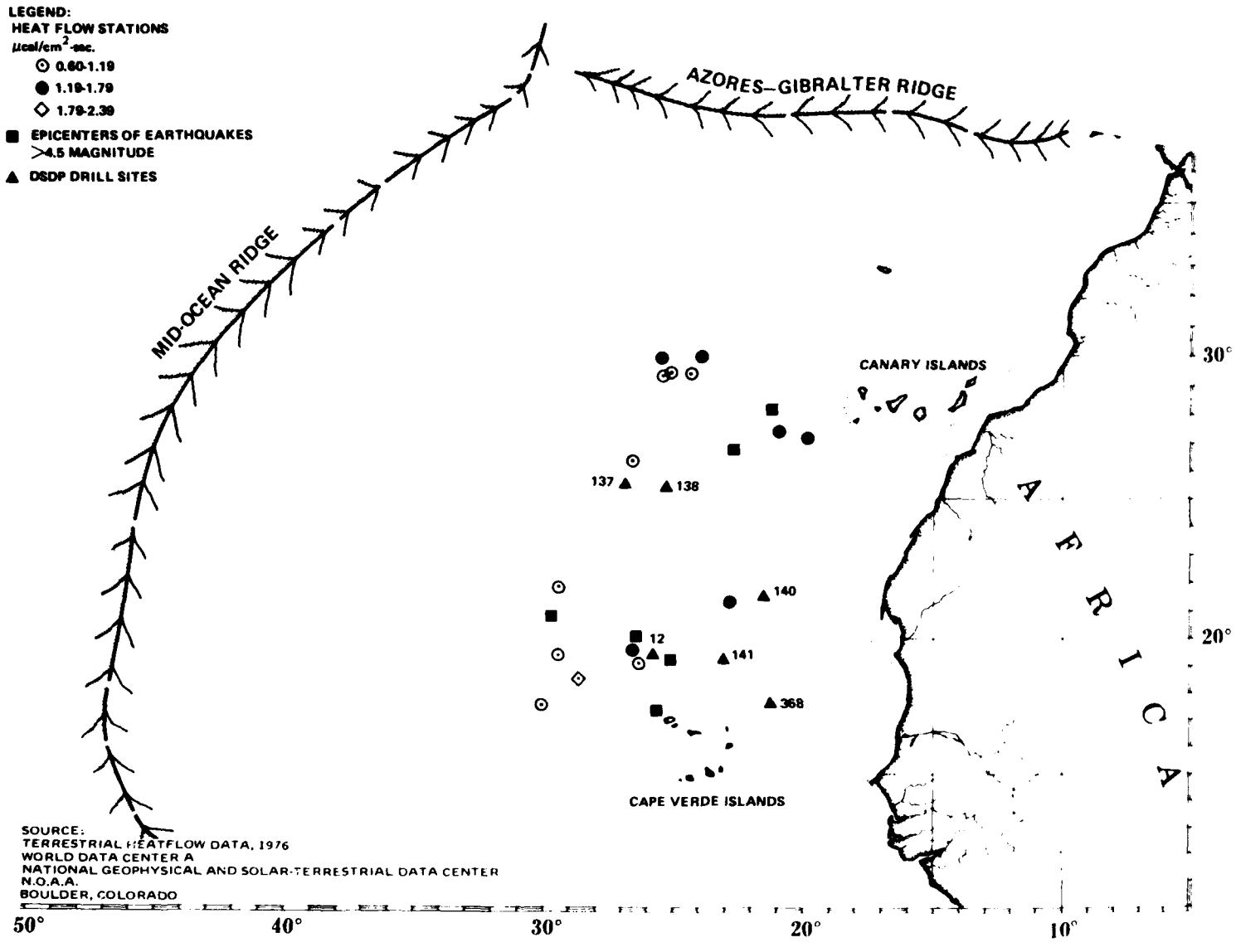

Figure 2. Heat flow measurements and earthquakes recorded from the eastern North Atlantic

intruded into older sedimentary rocks (Rothe and Schminke, 1968). A 'hot spot' trail may be the cause for the location and origin of both the Cape Verde and the Canary Islands (Morgan, 1971; Burke and Wilson, 1972; Wilson, 1973; and Vogt, 1974a, 1974b); but LePichon and Fox (1971) and Anguita and Hernan (1975) believe that a propagating fracture model better accounts for the zones of weakness along which the Canary Islands were formed.

The portion of the Cape Verde/Canary Basin studied for this report (Fig. 1) lies wholly within the bounds of the African Plate (Fig. 3). Availability and adequacy of data controlled the limits of the area. Total area is approximately 1,470,000 km^2.

B. Statement of Problem

To resolve some of the controversies engendered by previous narrowly focused studies, this study will assess the relative importance of primary and secondary volcanism, epeirogenic uplift and subsidence, and determine the sequence of tectonic events that have modified Cape Verde/Canary Basin morphology since its formation and rifting away from the Mid-Atlantic Ridge. The geologic factors that must be considered in the solution to these problems include:

- temporal and spatial distribution of fracture zones, small scale faults, abyssal hills and seamounts;

- locations of depocenters, relationship between depocenters and post-rifting diastrophism, correlation of sediment distribution with island volcanism, seismic stratigraphic evidence for recent unwarping and the timing of such events; and

- the age of the sea floor, and the tectonic significances of tne 'J' anomaly, the M-sequence, and the Cretaceous magnetic 'Quiet Zone.'

Ultimately, the results of these analyses will be viewed in terms of 'hot spot,' propagating fracture, and membrane stress tectonism, all of which have been proposed as mechanics for post-rifting diastrophism and the formation of intraplate structures. These data will be constrained to reject all but the most plausible explanation.

C. Method of Study

The studies previously cited show that questions concerning the origin and development of the Cape Verde/Canary Basin cannot be resolved by considering only a single aspect of the geologic regime. Accordingly, I assembled and processed archived seismic reflection, bathymetric, and magnetic analog profiles in order to prepare bathymetry, structure, isopach, seismic stratigraphy, and magnetic geochronology maps for the study area. Several orders of magnitude more data were used in these compilations than were used in previously published compilations (see Hayes and Rabinowitz, 1975; Rona et al., 1970; Ewing et al., 1972; and Uchupi et al., 1976, for examples). The regional geological framework was established from Deep Sea Drilling Project (DSDP) core logs extracted from DSDP volumes 2, 14, and 41, and from published descriptions of the geology of the Cape Verde and the Canary Islands, and the West African Continental Margin. These data were synthesized and evaluated to seek answers to those questions previously posed.

1. Sources of Data

The data assembled for this study represents the results of more than a quarter-century collection effort by government agencies and academic institutions. Many of these data were collected as by-products of expeditions not intended to provide information on geologic problems, thus track orientation and spacing relative to the features being mapped are not necessarily optimal.

(a) Bathymetry: The Defense Mapping Agency Hydrographic/Topographic Center

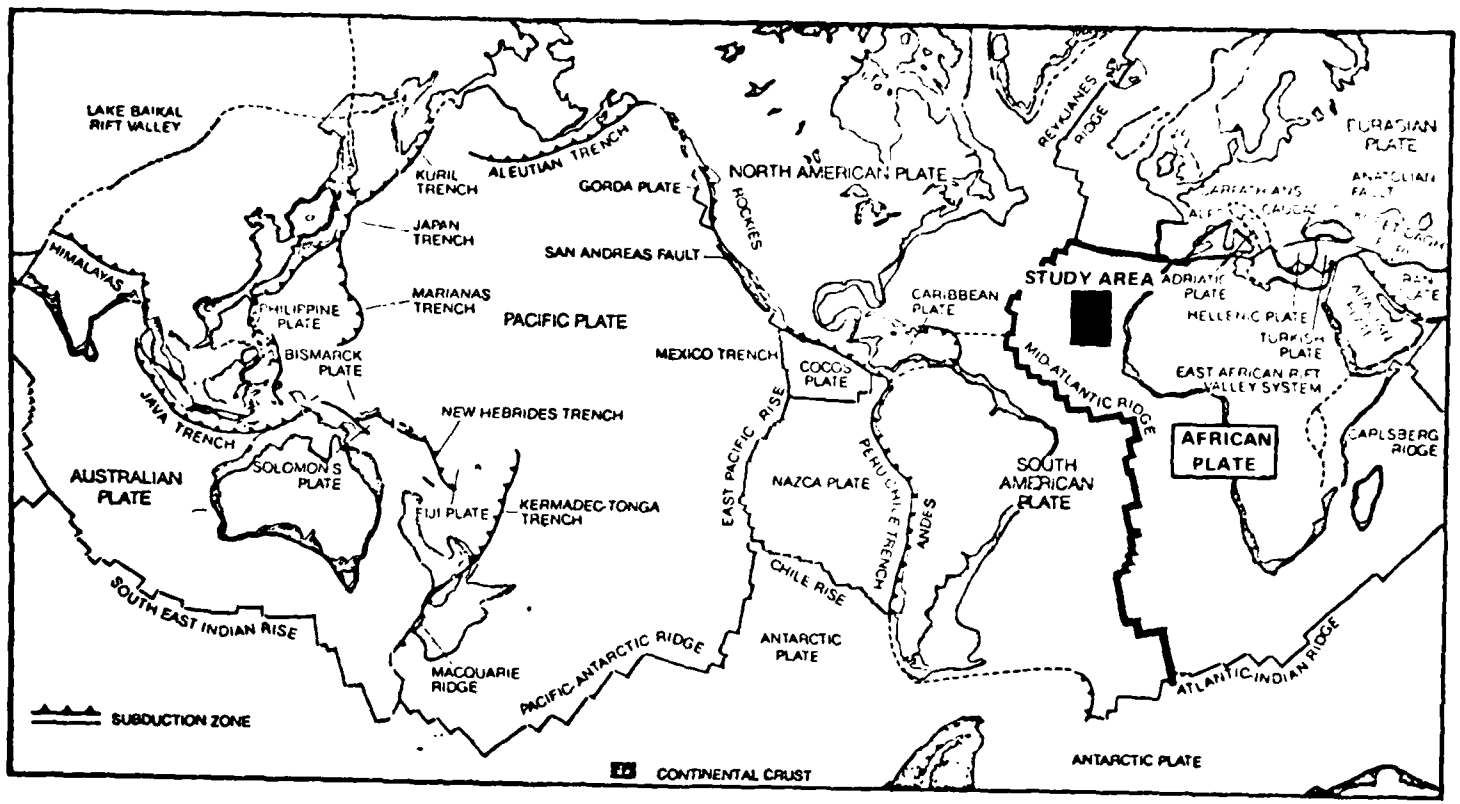

Figure 3. Worldwide distribution of lithospheric plates and other first-order structural and topographic features. African Plate boundaries are emphasized. The study area is indicated by black rectangle. Base map from Dewey (1972).

(DMAHTC) furnished collection sheets of random track lines as the data base for the bathymetry map (Plate I). These data were divided into pre-1965 and post-1965 compilations because the increase in navigation and data recording equipment quality during the mid-1960's provided an additional level of quality control.

(b) Normal Incidence Seismic Reflection Profiles: Between 1967 and 1975, the Naval Oceanographic Office collected most of the single-channel, normal incidence seismic reflection profiles available for this area; I was senior scientist on cruises in 1968, 1973, and 1975 that covered portions of the mapped area. The National Geophysical and Solar-Terrestrial Data Center (NGSDC) provided other random track data, including several cruises made by Lamont-Doherty Geological Observatory, Woods Hole Oceanographic Institution, and other domestic and foreign sources routinely supplying data to NGSDC. Approximately 125,000 km of track lines were processed to produce the structure and the isopach maps.

(c) Geomagnetic Data: Magnetic profiles were selected from geomagnetic data available through the National Geomagnetic Data Bank maintained by the Naval Oceanographic Office, NSTL Station, Mississippi. Because numerous geomagnetic data compilations and interpretations of sea floor spreading anomaly patterns have been published for the North Atlantic, I selected only those magnetic profiles that would add new coverage and for which seismic reflection profiles were available.

2. Data Processing and Analysis

Data assembled from various data banks and supplemented by several cruises in which I participated were redacted to Plates I-III.

(a) Bathymetry: DMAHTC routinely corrects random track bathymetric data for transducer depth and in accordance with Matthews' Tables, for variations of the speed of sound in water. On the assumption of inferior navigation and depth recorder accuracy, pre-1965 data were position-adjusted relative to post-1965 line crossings. I discarded as unreliable pre-1965 lines requiring position shifts of more than a few coordinate minutes. Verified collection sheets were contoured at 100 m intervals on a PS-4 (1° longitude = 4 inches) Mercator projection base chart. Contoured maps were photographically reduced to PS-2 (1° longitude = 2 inches) scale for presentation. In contouring submarine topography, shapes and distribution of features are rigidly controlled by track spacing. North of 26°N and in other limited areas, sounding tracks are sufficiently dense to permit correlative contouring. In areas of lesser track density, contouring is biased by the assumption of prevalent topographic trends.

(b) Seismic Reflection Profiles: Most published reports using normal incidence seismic reflection profiles as data sources are primarily reconnaissance studies using widely spaced reflection profiles as one would use geologic cross sections to interpret structural relations. Constraints on these earlier studies include the availability of a reliable velocity/depth function, poor quality of navigational and recording equipment that limited data quality, and interpretational problems such as side echoes, slope corrections, and multiple reflections. Techniques for collection, reduction, and interpretation of these data are treated in detail in the Appendix (Chapter 7).

NGSDC furnished microfilm copies or photographs of original records. Photographic enlargement to an 18-inch width permitted tracing of reflectors onto an overlay, and digitization with an X-Y coordinate table digitizer (Appendix). I corrected digital data for water velocity variations in accordance with Matthews. Tables and for velocity increase with depth in the sediment section by using an average velocity gradient of 1.799 sec-1 (Appendix).

Corrected depths to basement and corrected sediment thickness were plotted on PS-4 scale base charts at 3-minute increments and contoured in 200 m intervals. Final plots were photographically reduced to PS-2 scale.

Seismic profiler data and bathymetric data collected simultaneously will not necessarily produce compatible depths. Bathymetric data are corrected for transducer depth prior to correction for water velocity variations. Seismic source and receiver tow depths were not used in qualitative reconnaissance studies and, until recently, not recorded.

(c) Geomagnetic Data: Magnetic profiles were digitized with a table digitizer prior to removal of regional magnetic fields and diurnal effects to obtain anomaly amplitudes relative to the 1965 International Geomagnetic Reference Field. Published magnetic profiles were photographically enlarged to PS-2 horizontal scale to match the horizontal scale of original data; vertical scales of published magnetic profiles were not corrected. Comparisons of anomaly wavelengths and amplitudes with published magnetic profiles and models permitted correlation with Mesozoic anomalies.

II. Regional Geology

A. Introduction

Geologic history of the Cape Verde/ Canary Basin (Fig. 1) is derived from studies of the African Continent and Continental Margin, inferences based on analyses of geomagnetic lineations, information on petrology and tectonics provided by nearby islands, and sedimentary sections from six DSDP drill sites. African continental geology establishes a structural framework for the area prior to the creation of the modern Atlantic Ocean basin, geomagnetic analyses suggest a chronology for ocean basin information, and stratigraphic sections constructed from outcrops of island rocks and DSDP drill logs provide evidence for geologic evolution of the region.

B. Historical Background

Pliny the Elder introduced the term Canary Island into Western European literature in his description of Juba II's expedition to these islands in 40 B.C. Juba II, King of Mauritan a, was impressed by the multitudes of arge dogs (Canes, hence the name Canary) sharing these islands with the Gauches, a Berber people originally from North Africa (Encyclopedia Britannica, 1975, p. 502).

Between the 15th Century and the coming of oil-powered shipping, the larger of the Canary Islands served as replenishing stations for ships bound south and west from European ports. Seamen aboard these vessels provided the first cursory descriptions of the area. These early explorers noted that the Canary Islands are emergent portions of a pedestal centered near 28°N, 16°W (Fig. 1). The seven major islands comprise a land area of approximately 7270 km^2 and include the highest mountain in the Atlantic Ocean - Pico de Teide in Tenerife. This peak, active as recently as 1949 (Naval Oceanographic Office, 1965) and emitting steam as recently as 1968, rises 3720 m above sea level. The average heights of all the western islands exceed 1200 m.

In 1936, Wust suggested that the term Canary Basin replace Murray's more general descriptive term Monaco Deep (Fairbridge et al., 1966, p. 580). Wust described the Canary Basin as a group of east/southeast-trending seamounts rising above the Canary Abyssal Plain (Heezen et al., 1959) and the Madeira Abyssal Plain (Heezen and Laughton, 1963). The northwest African continental rise and the Canary and Madeira volcanic plateaus are included in the Canary Basin.

Southward, the Canary Basin evolves indistinctly into the Cape Verde Basin. Wust, also in 1936, used the term Cape Verde Basin as a replacement for Murray's ill-defined Chun and Mosely Deeps (Fairbridge et al., 1966, p. 580. The Cape Verde Islands are the central topographic and structrual feature of the Cape Verde Basin (Fig. 1).

The Cape Verde Archipelago consists of ten inhabited islands, nine smaller islets, and at least one large submerged seamount. The land areas cover 4035 km^2. These islands are centered near 16°N, 24°W, approximately 460 km west of Dakar, Senegal, and 2400 km east of the Mid-Atlantic Ridge. The Cape Verde Islands, uninhabited when discovered, were settled by the Portuguese between 1457 and 1462.

The name, Cape Verde, obtains from the fact that the rainfall in the upper elevations supports lush vegetation clearly visible from the sea. The lower slopes are hotter, drier, and more barren than the Canary Islands (Ballard and Michael-Thome, in press). Into the first half of the 20th Century, the Cape Verdes, like the Canaries, served as replenishing stations for ships bound for the Cape of Good Hope.

The Cape Verde Islands are divisible into two groups, according to their geographic positions. Six of the islands comprise the northern or windward group, while the remaining four comprise the southern, or leeward group. Erosion has reduced most elevations in the easternmost islands (Sal, Boa Vista, and Maio) to little more than 100 m. Topography on all other islands except Sao Vicente, is rugged with plateau levels at several hundred meters. The island of Fogo consists of a single, active, conical volcano, Pico, which rises 2829 m above sea level, making it the second highest peak in the Atlantic Ocean. Pico's eruption of June-August, 1951, was the latest of 26 eruptions recorded since 1500, thus making it the most active volcano in the Atlantic, south of Iceland. Ash from the 1951 outburst, which locally accumulated to 20 cm thicknesses, was rapidly worked into the soil and is not readily obvious a decade and a half after the eruption (Van Padang et al., 1967).

From the times of Columbus onward, thousands of ships crossed the Cape Verde/Canary Basin with scant concern for its shape and dimension. Nearly four centuries after their discovery, Charles Darwin collected igneous rock from Sao Tiago (Part, 1950). In the fall of 1838, the U.S. Exploring Expedition, enroute from Madeira to Rio de Janeiro, made enough soundings to define the shapes of the Canary and Cape Verde pedestals (Wilkes, 1845). Fifteen years later USS DOLPHIN, equipped with a sounding machine, completed the first detailed transoceanic bathymetric profile during its passage from Yucatan to Senegal (Fig. 4). Subsequent explorations by CHALLENGER (1873-76), GAUSS (1901-1903), QUEST (1922-1923), METEOR (1925-1927) and many others added to the bathymetric data base and established the approximate form and dimension of the area. By 1958, sufficient data had accumulated to permit Bruce Heezen, Marie Tharp and their co-workers to classify sea floor physiography and establish submarine geomorphology as a viable branch of marine science (Heezen et al., 1959). The establishment of the bathymetric framework of the sea floor was a vital precursor to the development of the theory of sea floor spreading.

C. West African Geologic Background

At approximately 30.5°N, the South Atlas lineament crosses the coastline (Watkins and Hoppe, 1979) separating alpine orogenic belts to the north from the West African craton to the south. The craton consists of a series of basins and rises, some of which preceded Atlantic Ocean rifting and some of which were formed by post-rift subsidence (Dillon and Sougy, 1974; Watkins and Hoppe, 1979). On the West African craton, exposed rocks consist of folded Precambrian and Paleozoic sediments immediately south of the South Atlas lineament, Precambrian granitized basement extending to about the latitude of Cap Blanc, and folded and metamorphosed Paleozoic sediments reaching to about 20°N. These rocks are onlapped by a Mesozoic-Cenozoic coastal plain sedimentary sequence reaching from the latitude of the Canary Islands to the latitude of the Cape Verde Islands (Dillon and Sougy, 1974).

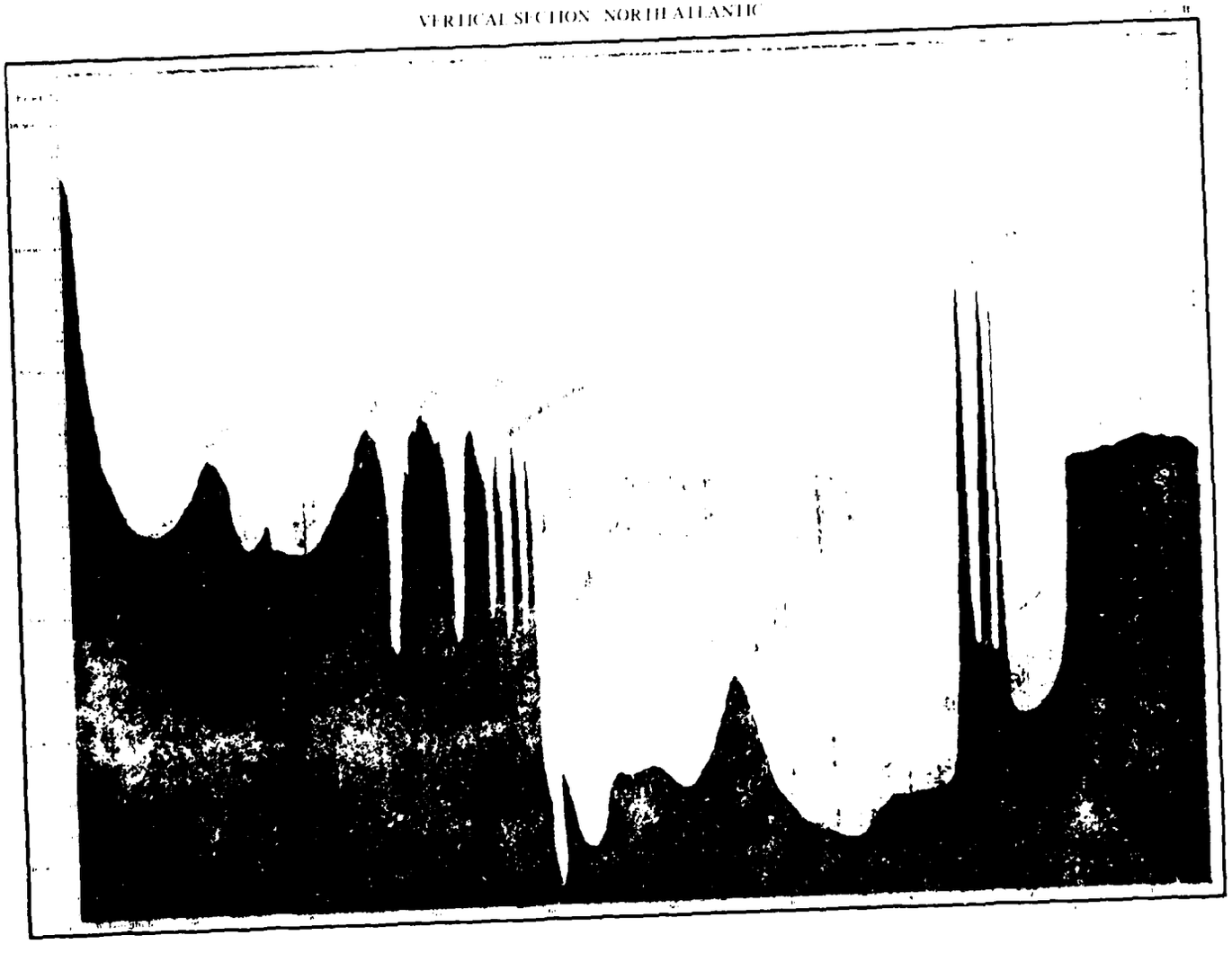

Figure 4. Cross-section of the Atlantic Ocean drawn from bathymetric data collected by sounding machine aboard USS DOLPHIN. From Maury, M.F. (1855). Physical Geology of the Sea. Harpers, New York, 389 p.

The Cenozoic sedimentary veneer is identified as deep-sea sediments by Watkins and Hoppe (1979).

The West African craton was subjected to glaciation in the late Precambrian and subsequent transgressions from which a shallow marine sequence of limestones and shales were deposited. In the Paleozoic, periods of deposition in shallow intracratonic basins alternated with periods of erosion (Dillon and Sougy, 1974). Marine sediments appear lower in the stratigraphic section in the northern portions of West Africa than in southern portions. This observation is consistent with the suggestion of a north to south opening of the Atlantic (Dillon and Sougy, 1974).

West Africa has probably acted as a stable block since Precambrian times. Along the continental margin, basins have been formed by downwarping and faulting of the basement. Sills and dike swarms occurred during Permian time, probably in response to basement unwarping. Early Triassic faulting created graben basins similar to those in North America, probably leading to the formation of a modern Atlantic Ocean. Oceanic crust began forming during late Jurassic. By the end of Mesozoic time a thick wedge of sediments had formed a fan structure which is largely responsible for the present-day continental slope and rise (Dillon and Sougy, 1974).

D. Opening of the North Atlantic Ocean

The Triassic tectonic activity that created fault basins in both eastern North America and northwest Africa was very likely the precursor to the plate breakup that eventually created the modern Atlantic Ocean (Heirtzler, 1974). The North Atlantic Ocean began to form about 200 myBP along a WNW-ESE directional split between North America and Northwest Africa (Hallam, 1971). Evidence of Triassic period rifting includes the extrapolation of magnetically dated portions of the sea floor to the continental margins assuming constant spreading rates on the basis of identifiable and dated magnetic anomalies; the calibration of oceanic basement by DSDP holes 105 (162 myBP) and 100 (155 myBP), both of which recovered Jurassic marine fauna; and the occurrence of Triassic basins and dikes in both North America and West Africa (Heirtzler, 1974).

The distribution of sediments in western Africa indicates that North America and Africa split apart in a north to south direction (Dillon and Sougy, 1974). By approximately 140 myBP, the South Atlantic Ocean had begun opening (Hallam, 1971). If the continents broke apart along the Jurassic magnetic 'Quiet Zone' as C.L. Drake, J.I. Ewing and H. Stockard (quoted by Hallam, 1971) believe, then portions of the Canary Islands are situated in continental crust, but all of the Cape Verde Islands are on oceanic crust.

E. Geology of the Canary Islands

The Canary Islands, one of the major sources of volcanic debris in the eastern North Atlantic Ocean south of Gibraltar, are centered near 16°W and 28°N (Fig. 1). Dillon and Sougy (1974), Grunau et al. (1975), and Watkins and Hoppe (1979) have summarized most of the available information concerning the geology of the Canary Islands, but left unresolved conflicts relating to their origins.

The Canary Islands are subaerial exposures of a submarine ridge located about 3000 km to the east of the Mid-Atlantic Ridge and about 300 km west of the African continent. In plane view, the Canary Island pedestal is "L" shaped, with one limb trending approximately east-west parallel to projected African Plate fracture zone trends and the other limb trending north-northeast, subparallel to extrapolated Mid-Ocean Ridge and Atlas trends. The base of the ridge is about 2000 m below sea level.

Rocks of the Canary Island are mainly igneous, as are rocks of the Cape Verde Islands 1500 km to the southwest. Exposed rocks consist of a basement group separated from an overlying basalt group by an intervening unconformity. The basement group is a complex suite of plutonic mafic and ultramafic rocks, pillow lavas and associated submarine volcanic rocks, and intercalcated sedimentary rocks (Dillon and Sougy, 1974).

The plutonic rocks are a complex mixture of peridotites, pyroxenites, and gabbro dikes forming 80% of the exposed section and trending north-northwest parallel to faults and the horizontal limb of the 'L' shaped ridge (Dillon and Sougy, 1974). Gastesi (1973) believes that the plutonic mafic and ultramafic rocks exposed on the island of Fuerteventura may represent a fragment of ocean floor, while Hallam (1971) suggests that these rocks are continental fragments.

Sedimentary rocks, interlayered with the basement group, consist of marine limestones, shales, cherts, marls, siltstones, and sandstones. Late Cretaceous foraminifera occur in limestones, and lower-middle Miocene reef fossils occur in other zones (Uchupi et al., 1976).

Intense deformation complicates stratigraphic relationships. Some investigators (D.A. Andrews-Jones, 1971, quoted in Dillon and Sougy, 1974) believe that the sediments unconformably overlie the plutonic rocks, and are thus younger than the igneous rocks. Rothe and Schmincke (1968) maintain that the igneous rocks were intruded into the older sedimentary sequences.

Further complicating age relationships is the placement of most of the Canary Island Archipelago east of the magnetic quiet zone boundary (Plate IV) and thus onto seafloor reasonably presumed to be older than 150 myBP. On the other hand, radiometric (K-Ar) age determinations from the plutonic rocks exposed on Fuerteventura obtained a maximum age of 38.6 myBP (Oliogocene) for these strata (Uchupi et al., 1976).

The basalt group overlies the plutonic and related rock sequences. The 1000 m thick sections of tabular, subaerial flow basalt suggests that the islands formed as large composite shield cone volcanoes (Dillon and Sougy, 1974). After building above sea level, the volcanoes collapsed and undoubtedly contributed large quantities of pyroclastic debris to the surrounding sea floor (Schmincke, 1967). These volcanoes apparently began forming during early to middle Miocene and continued into the Pliocene before diminishing. A second period of volcanism began during the Pleistocene and has continued, at least, to the middle of the 20th Century (Naval Oceanographic Office, 1965).

Several authors have attributed the formation of the Canary Islands to a mantle plume or 'hot spot.' Burke and Wilson (1972) believed that the Canaries were formed over a 'hot spot' that became active during the Miocene. Wilson (1973) thought that the Canary Islands marked the site of a young 'hot spot.' Vogt (1974a and 1974b) suggested that the spacing of Canary Island volcanoes indicates that a 'hot spot' is responsible for their formation if it is assumed that crustal blocks break into horizontal and vertical equidimensional pieces, thus making volcano spacing indicative of depth to source.

On the other hand, Anguita and Hernan (1975) argue that inter-island age distance relationships are inconsistent with reasonable seafloor spreading velocities. These authors found that each island has undergone two periods of of vulcanism of 4.5 to 6.0 my each. A quiescent period of 3-8 my separated the two periods of active vulcanism. To form these islands a 'hot spot' diameter must exceed 400 km or intermittently start and stop. They suggest that linearity of alignment of island vulcanism and times of starting and ending of each cycle of vulcanism imply the existence of a westward-propagating fracture being fed from a mantle or lower crustal magma source.

F. Geology of the Cape Verde Islands

The Cape Verde Archipelago consists of 10 islands and several small islets on top of two extensive submarine pedestals centered near 16°N, 24°W (Fig. 1). These pedestals are arranged in the shape of the letter 'T', with the cross-bar trending NE-SW and the vertical bar NE-SE. The pedestal beneath Sal, Boa Vista, Maio, Sao Tiago, Fogo and Brava is more than 400 km long, but less than 40 km across at the widest point. The pedestal is flat-topped with submarine slopes averaging 3° to 4°. Steeper slopes are common toward the southeast end. Sao Nicolau, Santa Luzia, Sao Vicente, Santa Antao and a large submarine volcano rising to within 50 m of sea level lie on the NW/SE-trending pedestal. This pedestal, about 220 km long by 70 km wide, is bound by slopes whose gradients average 4°. Bases of both pedestals are at about 3300 m below sea level.

The area between the pedestals is a gentle southwestward-sloping valley with a concave profile and at least two deep water channels near the center (Fig. 5). These channels may be the conduits through which slope sediments are moved out to area base-level. The passage between Sao Nicolau and Boa Vista reaches depths of 3150 m, only slightly higher than areas surrounding the pedestals. The lack of a topographic connection between the pedestals also implies the absence of structural connections. This conclusion is supported by seismic profiles.

Because the Cape Verde Islands lie athwart major shipping lanes and have long served as supply stations, the Cape Verde Islands were often visited, although seldom studied. The BEAGLE (1832-1836), VINCENNES (1838-1842), EREBUS (1839-1843), CHALLENGER (1872-1876), GAUSS (1901-1903), QUEST (1922-1923), and METEOR (1925-1927) expeditions all collected samples from the islands. Although Darwin called at Sao Tiago and compiled the first geologic information about the islands, it was not until the present century that the first geologic mapping was sponsored by the Portuguese Government (Bebiano, 1932). Sousa Torres and Pires Soares (1946) and Part (1950) studied sedimentary rocks and fossils.

Prior to Bebiano's work, geologists commonly accepted a suggestion that Cape Verde igneous rocks included a Precambrian continental basement complex. In fact, the Cape Verde Islands are mainly volcanic in nature, with basic extrusives the dominant rock (Table I). Bebiano (1932) reported that 83% of basic extrusives were basalt lavas and pyroclastics with minor amounts of acidic and intermediate types. Part (1950) grouped volcanic rocks into (a) olivine basalts, the most common rock type; (b) nepheline basalts, typical of recent lavas; (c) phonolites, extrusive equivalents of nepheline synenites; (d) trachytes, with high silica contents relative to phonolites; and (e) melilites-basalts-tuffs, low silica feldspathoids indicating recent basic volcanism.

Volcanism has been the continuing factor in the formation of the Cape Verde Archipelago. Cape Verde volcanism began in early Tertiary, possibly Eocene, when lower Cretaceous limestones and grits (angular, fragmental sandstones) were folded, covered by flood basalts and intruded by lamprophyre dikes (Bebiano, 1932). Igneous rocks make up 95% of the exposed rocks, and nepheline basalts, tephrites, and phonolites are still being formed by Pico.

Sedimentary rocks provide more information about the evolution of the Cape Verde Islands than similar rocks provide for other Atlantic islands. Sediments in Maio reach elevations of 265 m, thickness of 433 m, and have dips up to 90°. Elsewhere in the islands, sediments seldom exceed 25 m in thickness and dips are less than 50°. Limestones comprise some 90% of the sedimentary rocks. The remainder consists of conglomerates, tuffaceous sandstones, calcarenites, and minor argillaceous sediments (Sousa

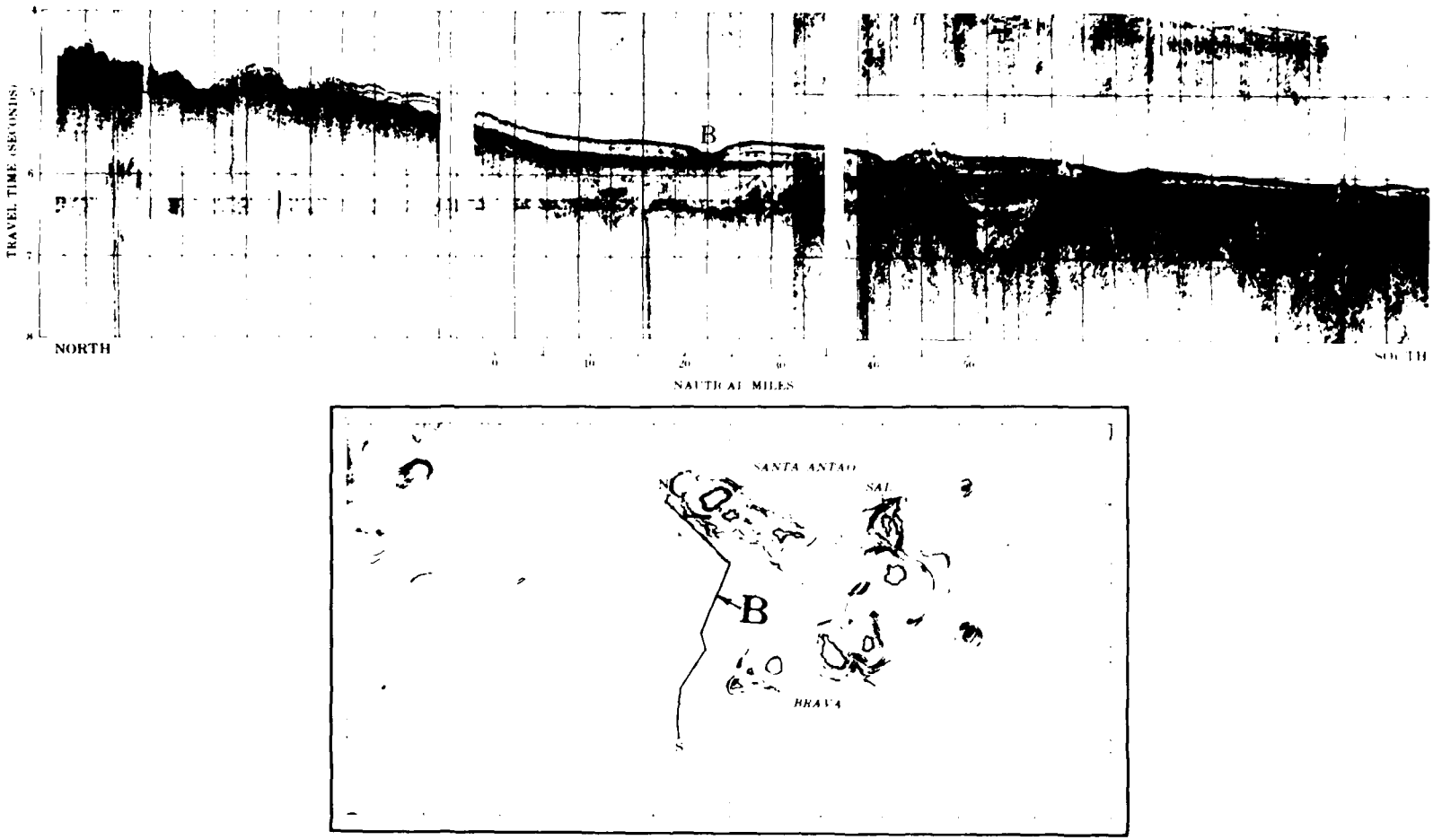

after Ballard and Hemler (1969)

Figure 5. Submarine channels on Cape Verde Rise. These distributary channels are 3-5 km wide and about 150 m deep on this crossing. They bifurcate and become wider and more shallow downslope.

Table 1. Generalized Stratigraphic Table for the Cape Verde Islands (Modified from Bebiano, 1932)

Quaternary	Calcareous Beach and Dune Sands; Basalts and Ash	Stage IV
TERTIARY:		
Late Tertiary	Basalt, alkali-basalt, and ash; phonolite, intrusions of nepheline-syenite, nepheline monozonite, and essexite	Stage III
Miocene	Conglomerates, clays, and limestones	
Oligocene	Basalt and ash (main basalt series)	Stage II
Eocene	Earliest sills of Maio	Stage I
CRETACEOUS:		
Post-Aptian	Maio, Sao Tiago	
Aptian	Limestones of Maio	
Barremian[1]	Basic lavas and tuffs of Maio	
Neocomian	Limestones and grits of Maio	
JURASSIC:		
Portlandian	Deep-water limestones with "Aptychi" on Maio and Boa Vista	
U. Jurassic[2]	Intrusion of nepheline synenites and emplacement of carbonatite of Brava	
(M. Jurassic-doubtful)		

[1]Hallam (1971).

[2]Machado, Azeredo, Leme, and Monjardino (1967), quoted in Dillon and Sougy (1974).

Torres and Pires Soares, 1946; Part, 1950). Active sand dunes cover large areas on Boa Vista and Sal.

Geomorphic and faunal evidence suggest that the easternmost group of islands (Sal, Boa Vista, Maio) are the oldest members of the Archipelago. Sousa Torres and Pires Soares (1946) and Colom (1955) report the presence of Upper Jurassic (Portlandian) limestones from Maio and possibly from Boa Vista. Fossiliferous pelagic sediments of both Early Cretaceous (Valanginian-Albian) and Middle Cretaceous (Cenomanian) ages have been found on Maio, and similar deposits seem to be present on Sal and Boa Vista (Sousa Torres and Pires Soares, 1946). Apparently the Cape Verde Rise was the site of deep water sedimentation as long ago as 150 myBP and a source capable of providing angular fragments for sandstones existed 120 myBP.

The oldest rocks recorded from the Windward Group (Sao Nicolau to Santo Antao) are late Cretaceous fossiliferous marly limestones from Sao Nicolau, the easternmost island. Other members of the Archipelago and the probable order of age are: Sao Tiago, probably Late Cretaceous; Sao Vicente, Eocene; Santa Antao, Miocene; Brava, probably Pliocene; and Fogo, Pleistocene (Sousa Torres and Pires Soares, 1946).

The Cape Verde Islands may have begun to form by submarine volcanic processes between Late Jurassic (Dillon and Sougy, 1974) and Middle Cretaceous (Barremain) (Hallam, 1971). The breakthrough of the Atlantic Ocean into the southern basin was followed by marked Middle Cretaceous (Albian-Cenomanian) sea level transgressions which reached a maximum in Late Cretaceous (Campanian) (Hallam, 1971). Subsequently, sea level regressed, and by late Maestrictian, emergence took place and consequent denudation removed much of the Mesozoic sedimentary covering of the islands (Hallam, 1971). Erosion, subsidence and the formation of littoral and dune deposits composed of marine and volcanic debris characterized intervolcanic times. In Maio, Lower Cretaceous, and possible Upper Jurassic, sediments are of neritic type deposited in marginal seas (Sousa Torres and Pires Soares, 1946). In the Miocene, sedimentation occurred on Sao Nicolau and Sao Tiago, and Middle Miocene (Vindobonian) age strata are found on all the islands except Brava and Fogo (Part, 1950). Sea level transgressions were probably renewed in the Pliocene, but during the Pleistocene, there were sea level regressions with renewed volcanism continuing till the present (Sousa Torres and Pires Soares, 1946). Local variations in the generalized sections exist because of the general westward decrease in age of the various islands.

The decrease in age in a westerly direction may imply 'hot spot' generation (Wilson, 1973; Vogt, 1974a and 1974b). However, the periodicity of the long continued history of tectonic activity for these islands, the incomplete knowledge of stratigraphy and structure for these islands, and the lack of precise knowledge of the mechanics of 'hot spot' tectonics would seem to make such an explanation an oversimplification.

G. Geology at DSDP Sites

1. Cape Verde Rise

The Cape Verde Rise spans more than 5° of latitude west of the African Continental Rise, and sedimentological effects of the Cape Verde Rise can be seen as far west as the foothills of the mid-ocean ridge. Four of the six holes drilled by DSDP in the area covered by this report were located on the Cape Verde Rise. These drill holes provide determination of subbottom sediment types and ages, depositional environment, and the nature of the volcanic basement. The following core descriptions and paleontological age determinations were extracted from DSDP volumes 2, 14 and 41.

(a) Site 12: DSDP Site 12 was located on the northern slope of the Cape Verde Rise about 300 km northwest of the Cape

Verde Archipelago (Plate I). The total drilled depth of 218 m was only a small portion of the estimated one kilometer thick sediment section (Plate III). Between the water-sediment interface and the paleontologically defined Eocene horizon at 161 m, sediments consist of 4 m of foram-nannofossil chalk oozes and altered volcanic ash clays interspersed with unaltered volcanic ash layers between 42 m and 115 m. From 115 m to 161 m, the only sample recovered was a siliceous clay with abundant devitrified shards. Between a depth of 161 m and the total hole depth of 218 m, recovered sediments were volcanic ash layers, clays with devitrified shards, and abundant chert fragments. Pyritized radiolaria contained in clay layers, possibly composed of altered volcanic debris, indicated an Eocene age for the oldest recovered fossilized sediment (Peterson et al., 1970). Average sedimentation rates ranged between 3 m/my and 4 m/my.

Volcanic debris increases with depth, suggesting that Cape Verde volcanism was a more significant sediment source during mid-Tertiary than during late Tertiary and Pleistocene. In addition, the relative absence of foraminifera in recovered sediments indicates that, during mid-Tertiary, Site 12 lay below the carbonate compensation depth (Peterson et al., 1970).

(b) Site 141: DSDP Site 141 was located north of the Cape Verde Archipelago about the same distance from the Islands as Site 12 (Plate I). The 294 m drill hole penetrated three sedimentary units and a highly altered basalt. The upper 84 m consisted of a foram-nannofossil chalk ooze ranging in age from Pleistocene to Early Pliocene, and Early Pliocene to possibly Middle Miocene chalk to marl ooze. Clay content increased and fossil content decreased downward. Unit 2 is approximately 200 m of zeolitic clay whose color varies with depth, but whose composition does not. The lower part of Unit 2 is a deep-sea type brown clay continuing an altered volcanic ash layer. The third sedimentary layer is a subarkosic sand of possible granitic origin presumed to represent the lowest 8 m of the sedimentary section.

Site 141 was selected in order to permit drill sampling of diapiric structures (Fig. 6) initially reported from the Cape Verde Rise by Ballard and Hemler (1969). These structures have been attributed to dikes and plugs formed by secondary tectonic activity (Ballard and Hemler, 1969), differential compaction around pre-existing irregularities in the volcanic basement-layer 2 (Collette and Rutten, 1970), sedimentary diapirism caused by weight of overlying material (Lancelot and Embley, 1978) and a deep-ocean salt layer formed during a time of restricted oceanic circulation (Schneider and Johnson, 1970; Rona, 1969; Pautot et al., 1970). Recovered core samples indicate that these diapiric structures are composed of fractured, altered serpentinized basalt. Hayes, Pimm et al. (1972) conclude that these diapirs are basalt plugs that have altered hydrothermally under a sediment cap.

Middle Miocene age sediments occur at a depth of only 2.5-3.0 m subsurface depth at a piston coring site located near 22°30°N, 25°30°W (Embley and Jacobi, 1977). An intrusive basalt plug may have forced Miocene sediments to the surface at this location.

The carbonate-noncarbonate sediment transition occurs at 4232 m below sea level, which is about 400 m shallower than similar transitions at nearby drill sites. This suggests about 400 m uplift since Pliocene. Uplift must be localized because DSDP Site 12, 150 km to the east, shows no evidence of uplift (Hayes, Pimm et al., 1972).

(c) Site 140: Site 140 was drilled into a thick sequence of lower Continental Rise sediments overlying Late Jurassic age sea floor (Plate IV). The subbottom profiler record across the Lower Continental Rise (Fig. 7) shows a uniform section of apparently alternating layers of undeformed, thinly bedded turbidites

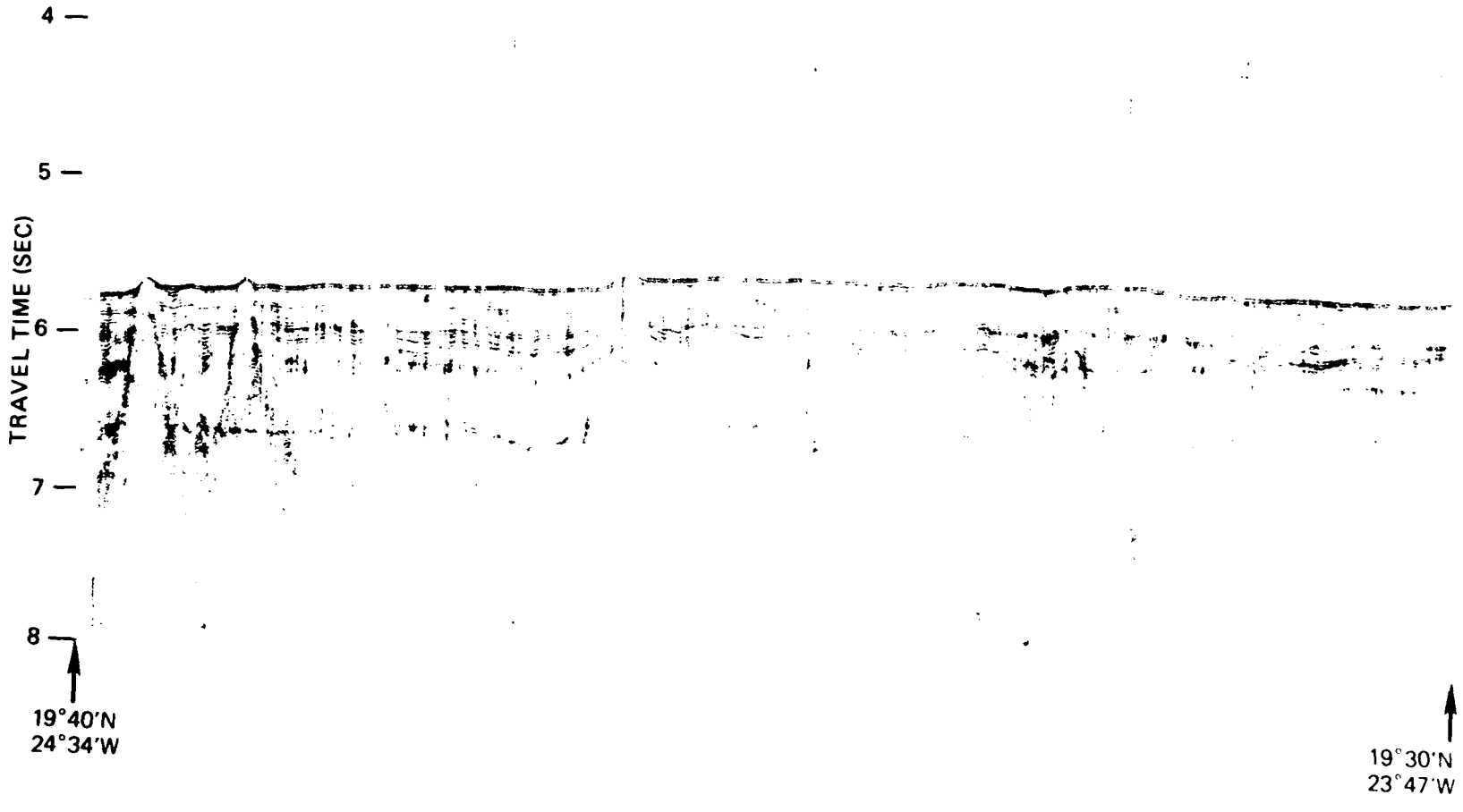

Figure 6. Diapirs on the Cape Verde Rise. Surface relief is about 30-40 m. Depth difference on upslope-downslope sides of diapir near center of illustration is about 35 m. The high amplitude reflector at about 6.5 seconds is correlated with Reflector D1.

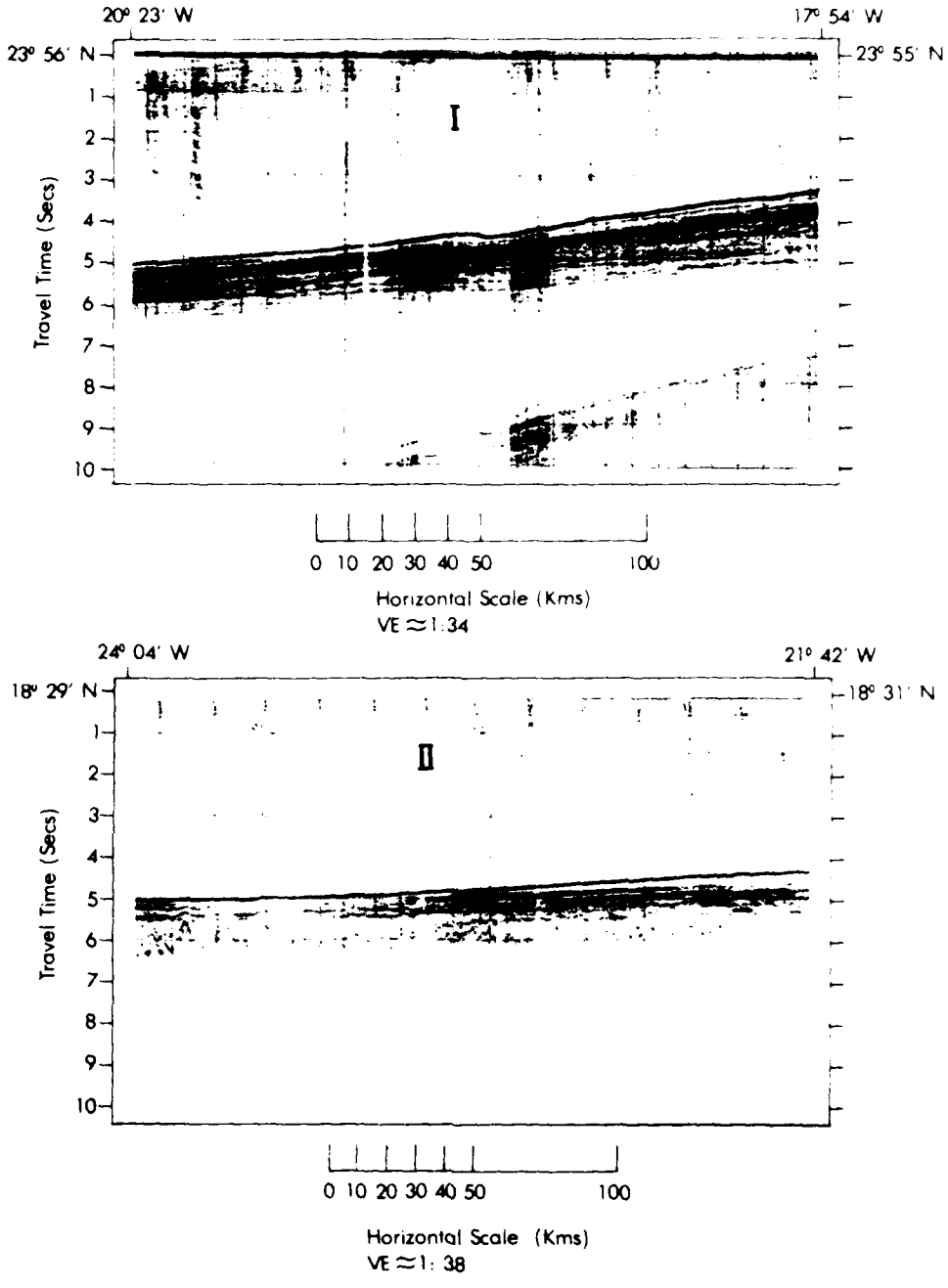

Figure 7. Seismic reflection profiles across the African Continental Rise. Profile I: Example of oblique progradational seismic stratigraphic facies; probable slump scar near center of section. Profile II: Example of sigmoid progradational seismic stratigraphic facies.

and pelagic sediments prograding seaward. The upper surface of layer 2, acoustic basement, is not visible on seismic profiles. Hayes, Pimm et al. (1972) report that a nearby seismic refraction station indicated a total sediment thickness of 1.5 - 2.0 km.

The total drilled depth at Site 140 was 651 m. The upper 150 m of sediment was a chalk ooze. The age assigned to this sediment ranges from Recent to possibly Late Pliocene and the sedimentation rate was estimated to be 20 m/my. The underlying layer was 75 m of deep-sea clays with interspersed sandy silt lenses, containing Middle Early Miocene foraminifera, diatoms, and radiolaria. A calculated sedimentation rate of less than 1 m/my suggests that the uncored interval between 210 and 235 m depth represents an Early to Middle Miocene hiatus. It is not possible to determine if the "pre-Middle Miocene" nonfossiliferous clays present at Site 141 are indicative of a similar hiatus. The third differentiable unit was a 384 m section of silty clays with a few thin sand beds which become lithified to siliceous mudstones and cherts with increasing depths. The time of deposition for this unit is believed to span the entire Lower Tertiary.

The deepest six meters of Site 140 was a silty clay with thin, interspered sandy silts and silty sands containing poorly preserved marine fossils of Upper Cretaceous (Maestrichtian) age. In addition, thin beds of fine to medium grained arkosic sands are scattered throughout the lowermost section. The high content of orthoclase feldspars, angular to subrounded quartz grains, the heavy mineral suite, and the sharp upper and lower contacts indicate that these layers represent turbidite flows derived from a granitic source area (Hayes, Pimm et al., 1972). The African continent was the likely provenance for these turbidites because Part (1950) reported the complete absence of alkaline rhyolites from the Cape Verde Islands.

At Site 140, weathered volcanic debris was a less significant component of the sedimentary section than at other Cape Verde Rise drilling sites. Overall, sediments from Site 140 seem to have more of a deep-water, open-ocean aspect than those from other sites. Scarce and poorly preserved pre-Middle Miocene calcareous fossils suggest that the carbonate compensation depth was greater than 4800 m below sea level, at that time.

(d) Site 368: DSDP Drill Site 368 was located about 200 km NE of the archipelago in a sediment section thicker than the resolving power of single-channel seismic equipment. Three lithostratigraphic units were identified from the 984.5 m of drilled section.

The upper 265 m of cored sediment consisted of interbedded marls and oozes with abundant nannofossils. Silt-size quartz, feldspars, and heavy minerals are present near the top of the section, but are nearly absent from a depth of a few meters to a depth of 185 m, then abruptly increase below 185 m, perhaps reflecting changes in regional volcanism. Detrital clay and calcium carbonate content fluctuate inversely throughout this 265 m section. Fossil nannoplankton and radiolaria are Early Miocene and younger.

The middle sedimentary section consists of 675 m of silty clays and claystone that become indurated to shales about 700 m below the sea floor. The lower one-third of this section contains shales, claystones, and layers and nodules of porcellanite, an induration product of clays and marls; scattered, thin beds and laminae of graded sands and silts indicative of turbidity current activity; and flecks, streaks, laminae, and halos of black stains that may indicate manganese. The section between 750 m and 950 m depth is similar to the upper part except for increases in detrital material such as heavy minerals, plant debris, pyrite, dolomite crystals, and fish debris. Paleontological age dating of this section was not

possible, but estimated sedimentation rates suggested an Early Miocene to Late Cretaceous age.

The lowermost unit penetrated was 35 m of dark shales containing abundant organic debris interbedded with diabase sills. Foraminifera, nannoplankton, and radiolarians are concentrated in thin silt layers within the shale zones. The several thin and one thick (12.5 m) section of igneous rocks were interpreted as sills because of the sharpness of contacts and evidence of contact metamorphism (Lancelot, Seibold et al., 1978). The shales in this shale-sill series are assigned an Upper Cretaceous age; the sills are radiometrically age-dated as Miocene.

2. Cape Verde/Canary Basin

(a) Site 138: DSDP Site 138 was located on the Cape Verde/Canary Abyssal Plain about 130 kms east of Site 137. An 1800 m relief seamount lies between the sites. At Site 138, silty clay interbedded with quartz sand layers comprises the upper 150 m. Radiolaria and diatom fossils indicated that Early Miocene age sediments occurs at 52 m, Early Oligocene at 110 m, and Early Eocene at about 150 m depths. A 90 m thick layer of unfossiliferous, indurated, brown clay underlies the upper zone. The third layer at Site 138 was 150 m of indurated mudstone with brown clays and scattered 5-10 cm thick chert layers. Fossil radiolaria indicate that this section was deposited during Early Paleocene-Late Cretaceous (Danian-Campanian) time. The lowermost rocks recovered from Site 138 were about 35 m of cyclic alternations of dolomitic clays and carbonaceous silty muds. Within this section, a 150 cm thick basalt flow and two ash layers show that Late Cretaceous (Cenomanian) volcanoes were active. Site 138 terminated in a coarse-grained basalt at a cored depth of 437 m. This basalt was interpreted as a sill because sediments immediately above the basalt are younger than those found above basalt at Site 137 (Hayes, Pimm et al., 1972). The upper 400 m of sediments accumulated at average rates of 3-10 m/my.

(b) Site 137: Site 137 was located in the abyssal hills province. At this site, 397 m of sediment overlies brecciated, serpentinized basalt that was probably formed at the surface (Hayes, Pimm et al., 1972). The upper 245 m of sediment was unfossiliferous deep-sea brown clay. Between 0 and 58 m depth, the silt fraction consists primarily of terrigenous minerals, while in the 58-245 m zone, zeolites are very common silt component. Thirty-two meters of Late Cretaceous (Cenomanian to Turonian) carbonaceous clays and cherts underlie the brown clay. The lowermost sediment fron Site 137 was 120 m of semi-consolidated marl and chalk ooze with foraminifera concentrated in thin layers, suggesting redeposition from the distal portions of a turbidite flow. Layer 2 basalt was recovered from the bottom of Site 137. Its age was estimated as 101 my. Sedimentation rates were calculated to be less than 3 m/my for deep-sea brown clays. Site 137 was above the carbonate compensation depth before Middle Late Cretaceous (Turonian), but has been below the carbonate compensation depth since then (Hayes, Pimm et al., 1972).

H. Summary

West Africa has been supplying sediments to the Atlantic Ocean since oceanic crust began forming during the Jurassic. The Jurassic-Cretaceous limestone, clay, carbonaceous shale sequence indicates a deepening and stagnating condition in the depositional area. Devitrified shards, altered volcanic ashes, zeolitic clay and silts, and intrusive sills and dikes are among the evidence that volcanism became an important sediment source during the Cretaceous.

Sediments recovered by DSDP drilling in the Cape Verde/Canary Basin and the Cape Verde Rise show affinities with the stratigraphic sections from the Canary and Cape Verde Islands. Wide-spread distributory channels engraved in the surface of the Cape Verde Rise (Fig. 5) show that these islands are still an important source of detritus.

Sedimentation rates, as determined by drilling, vary with physiographic location. Continental rise and abyssal plain drill sites accumulated sediments at rates that ranged from 50 m/my down to 3 m/my. Sediments accumulated in the abyssal hills province at less than 3 m/my.

The presence of barren, brown, deep-sea clays and the relative abundance of silica-rich sediments suggests that much of the sea floor in the area sank below the carbonate compensation as it spread away from the Mid-Atlantic Ridge, and then built above the carbonate compensation depth in the area of rapid sediment accumulation. Early and Middle Tertiary unwarping also raised localized portions of the sea floor above the carbonate compensation depth.

III. Submarine Geomorphology

A. Introduction

A bathymetry chart (Plate I) and a structure-contour map (Plate II) were prepared for the Cape Verde/Canary Basin. The bathymetry map will aid in the description and classification of present sea floor surfaces such as the continental rise, abyssal plain, abyssal hills and seamounts. Plate II, a structure map contoured on acoustic basement, will aid in the identification and localization of fracture zones, faults and structural controls on sedimentation. The purpose of this section is the description of geomorphic processes producing present surface configurations, the determination of structural influences on present geomorphic processes, and the definition of a regional stage of development. Heezen et al. (1959) divided the Cape Verde/Canary Basin into continental rise, abyssal hills, Cape Verde Abyssal Plain, and Cape Verde Plateau physiographic provinces. Since 1959, most bathymetric studies have added soundings and refined physiographic classifications and boundaries, but have made few significant revisions to Heezen's original work. Figure 8 is a physiographic chart based on bathymetric data assembled for this study.

B. Bathymetry

1. Continental Rise

Heezen et al. (1959) define a continental rise as a smooth, seaward sloping, pelagic apron lying at the base of the continental slope and bridging the gap between the continent and the floor of the abyss. Commonly, continental rises are divided into upper and lower segments on the basis of decreasing seaward gradients which range from less than 1/100 at the slope margin to greater than 1/700 at the abyssal plain boundary. Local relief on the continental rise seldom exceeds 20 m, except where submarine canyons or seamounts breach the sediment cover.

In Figure 8, the continental rise is divided into upper and lower segments based on a decrease in slope. The upper part of the rise is best developed seaward of the eastern boundary seamounts and the Canary Island rise. In this area, surface slopes decrease from about 1/60, near the seamounts, to about 1/200 near the the Upper/Lower Continental Rise transition. Shallow slides and continental rise swells typical of steep depositional environments characterize the area mapped as Upper Continental Rise (Fig. 9). Irregularities in the contours north of the Cape Verde Rise suggest similar features.

The lower continental rise widens and steepens toward the south as the topography comes increasingly under the influence of the Cape Verde sediment provenance. On the E-W profile (Fig. 10) along 28°N, the surface gradient is about 1/680 and the lower edge of the continental rise, as indicated by a slope break, is located at about 24°45'W. A second E-W profile (Fig. 10) about 250 km farther south shows that the gradient has steepened to slightly less than 1/500 and that the rise has been extended westward by about a half degree. On a third topographic profile

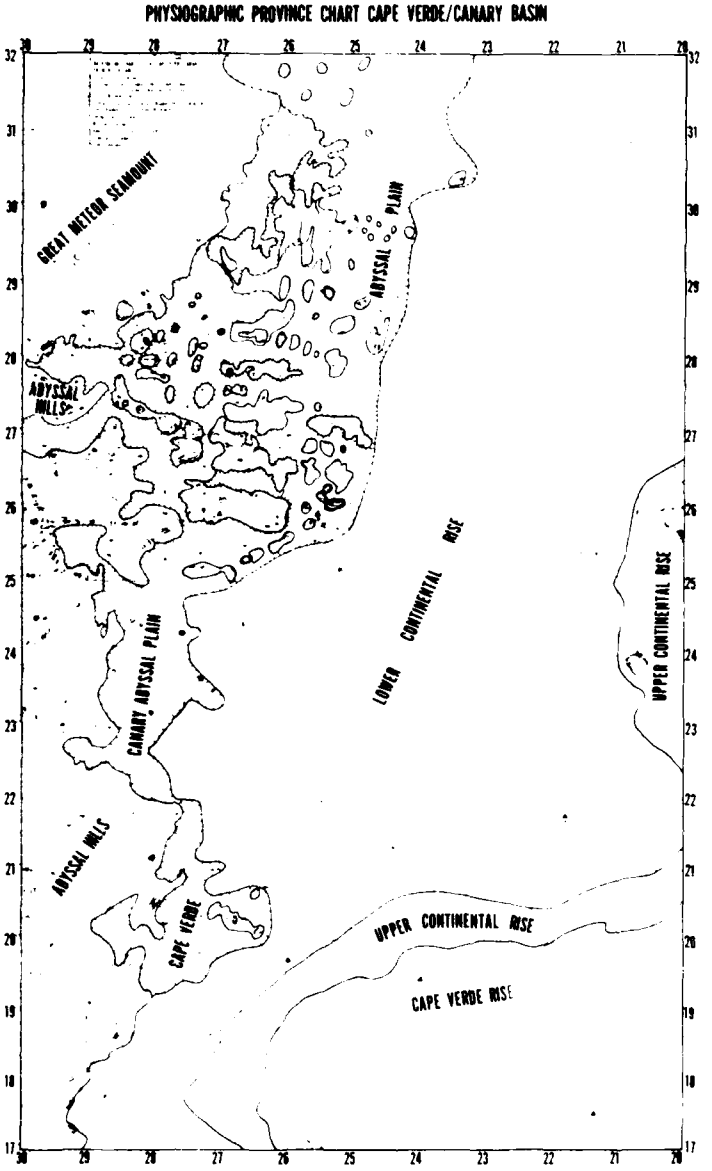

Figure 8. Cape Verde/Canary Basin Physiographic Provinces. Plate I, with 1000 m contours enhanced, is the base map. Nomenclature after Heezen et al., 1959. Closed contours on Cape Verde/Canary Abyssal Plain indicate locations of abyssal hill groups.

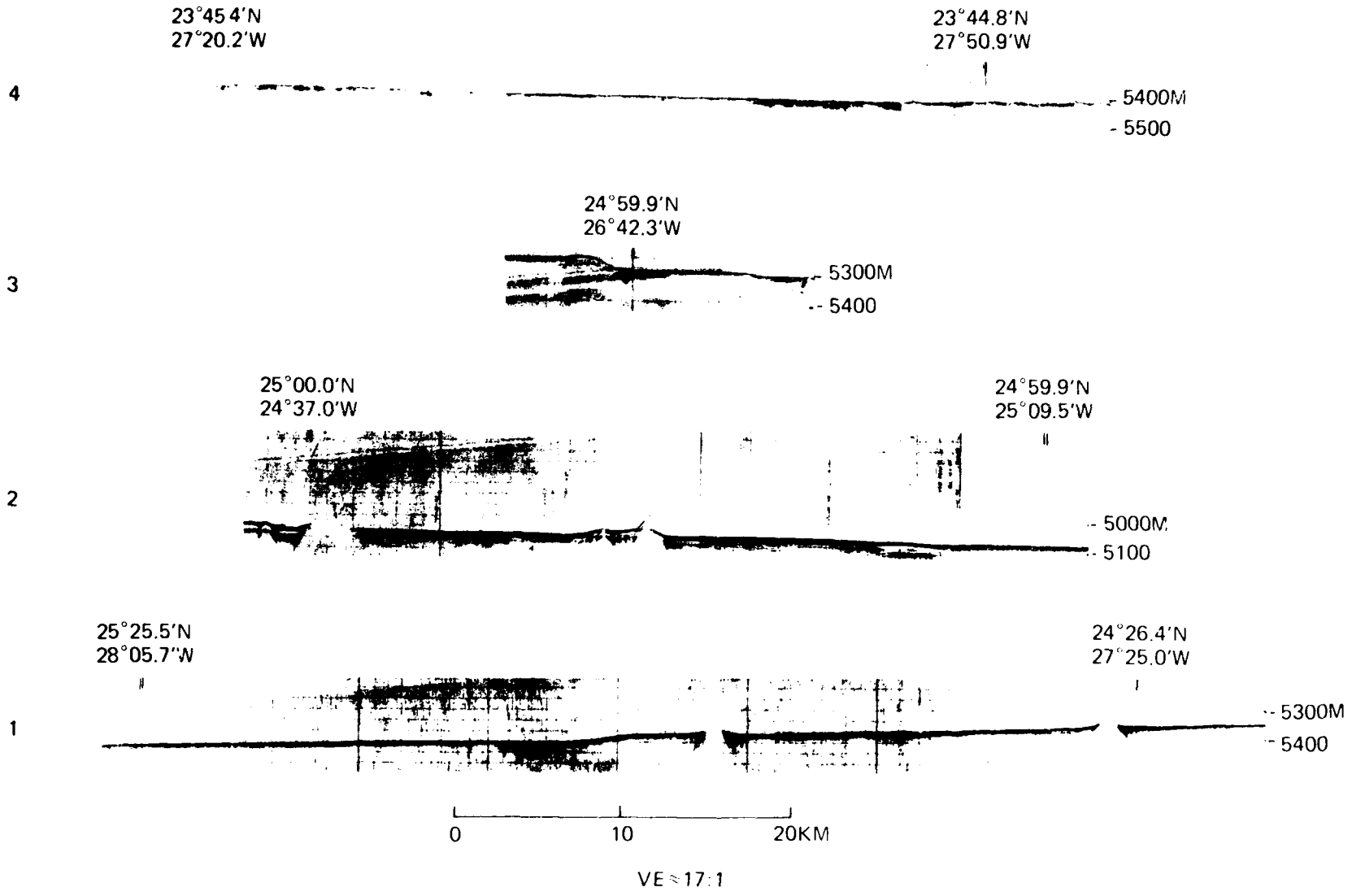

Figure 9. 3.5 kHz bathymetric profiles on the lower continental rise and abyssal plain. Profiles 1 and 2 show gradational contacts between continental rise and abyssal plain. Profile 3 shows sediment dammed behind a small hill forming the continental rise/abyssal plain contact. Surface crenulations on profile 4 may indicate the toe of a slump. Small hills on profiles 1 and 2 illustrate the relief of small hills less than the contour resolution. Vertical exaggeration approximately 1:17.

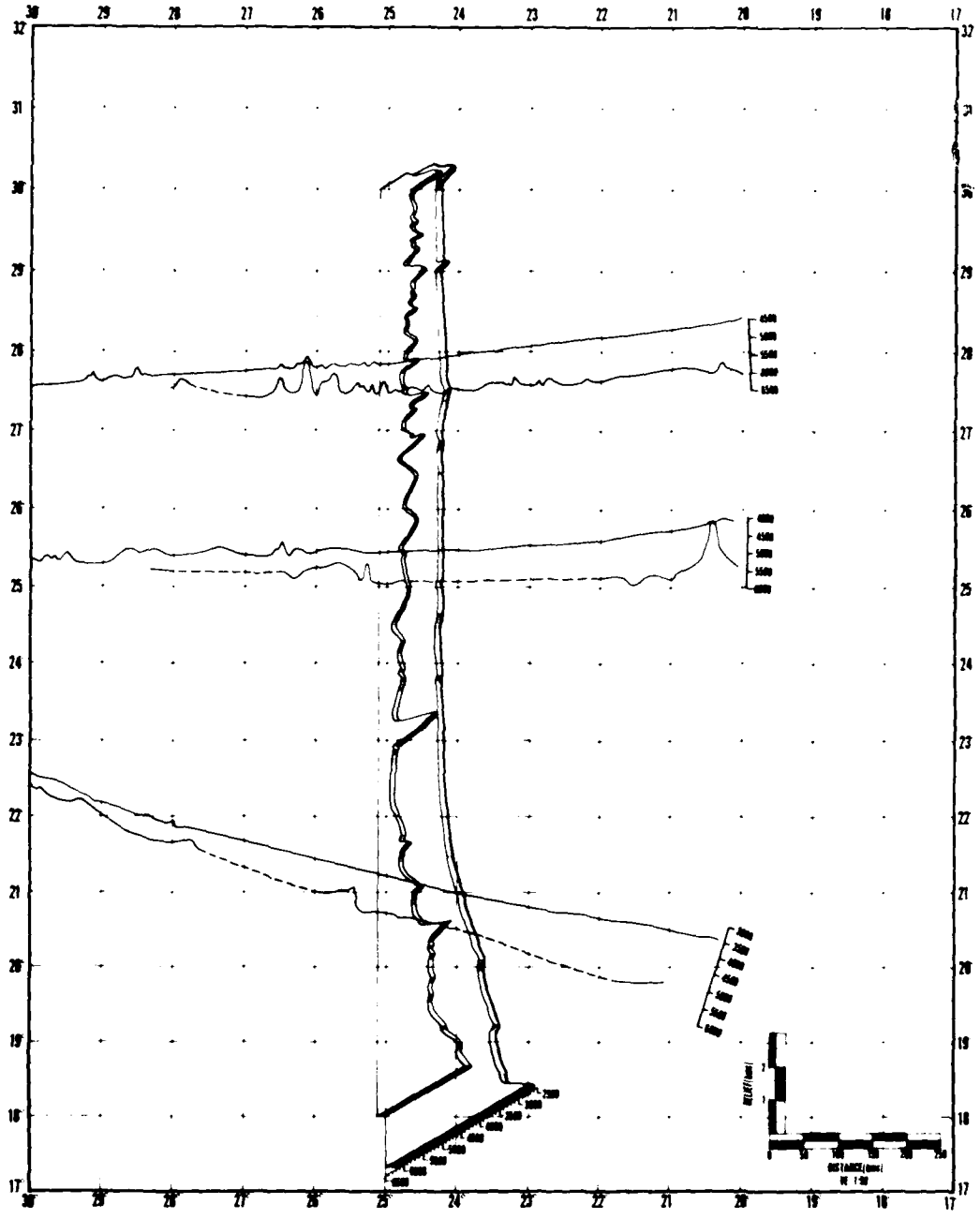

Figure 10. Topographic and structural profiles accross Cape Verde/Canary Basin reconstructed from PLATES I and II. Note abrupt steps in Cape Verde Rise basement south of about 22°N.

(Fig. 10), an additional 450 km farther south, the upper part of the rise has seaward gradients of about 1/340 while downslope gradients decrease to about 1/600 at the terminus. The westernmost extension of the lower continental rise reaches 28°W between 22° and 25°N.

Figure 9, lines 1-4, illustrates local relief of less than 100 m on the continental rise. The 100 m contour interval of the bathymetry chart (Plate I) is incapable of resolving these features.

The convexity and smoothness of the rise surface implies seaward progradation. The apparent low angle outcrops at the slope break (Fig. 9, line 1) could be due to progradation, aggradation or slumping. Low angle dip reversals near the center of the depression (Fig. 9, line 1) suggest slumping as a probable cause.

Embley et al. (1978) attribute hyperbolic echoes on bathymetric records on the continental rise at about 24-26°N to erosion or selective deposition by northward-flowing, contour-following currents. The bathymetric and the seismic profiles used in this study suggest that creep and slumping are major modes of sediment transport (Fig. 9, lines 2 and 4), but contour current erosion is not apparent.

Figure 9 (lines 1 and 3) shows the sharp change that marks the seaward termination of the lower continental rise. Line 3 shows that sediment ponding behind a basement high might be responsible for the boundary, while line 1 suggests that a local base level has been reached.

2. Cape Verde/Canary Abyssal Plain

The abyssal plain in the mapped portion of the eastern North Atlantic is different from abyssal plains of the western North Atlantic. Both have surface slopes of less than 1/1000 (Heezen et al., 1959), but sediment on the Cape Verde/Canary Abyssal Plain is much thinner, causing basement highs to breach the sediment cover. Consequently, abyssal plains appear as small sediment ponds separated by abyssal hills. The north-south topographic profile (Fig. 10), and Figure 11, A and B, are examples of localized abyssal plains typical of the Cape Verde/Canary Basin.

Depths of the various abyssal plains appear to be tectonically influenced with the shallower abyssal plains located in the northern portions of the basin. Abyssal plain depths average about 5200 m near 28°N 28°W, 5300 m at 25°N 28°W, and 5400 m at 22°N 28°W. A portion of this difference may be due to sediment contributed by the Azores Plateau and Iberian Peninsula, but the high incidence of faulting and volcanism seaward of the lower continental rise implies tectonism as a major factor. Figure 11, A and B, shows two segments of the abyssal plain at different levels. Segment B is graben faulting on the abyssal hill that forms the western boundary of the abyssal plain segment and is a barrier to eastward movement of sediment.

3. Abyssal Hills

Abyssal hills, small hills usually less than 20 km wide and rising less than 1000 m above the ocean basin floor, are the earth's most widely distributed physiographic feature (Heezen et al., 1959; Shipley, 1978). Abyssal hill provinces form seaward boundaries of abyssal plain provinces except in the Cape Verde/Canary Basin were abyssal plain sediments onlap the flanks of abyssal hills. West of 29°W, abyssal hills predominate relative to abyssal plain. Figure 11 shows examples of abyssal hills with relief less than 100 m, indicating that the bathymetry chart (Plate I) shows fewer abyssal hills than are actually present.

Plate I and Figure 11 show two types of abyssal hills. One type is a single sharp peak without apparent sediment cover, slopes with gradients of more

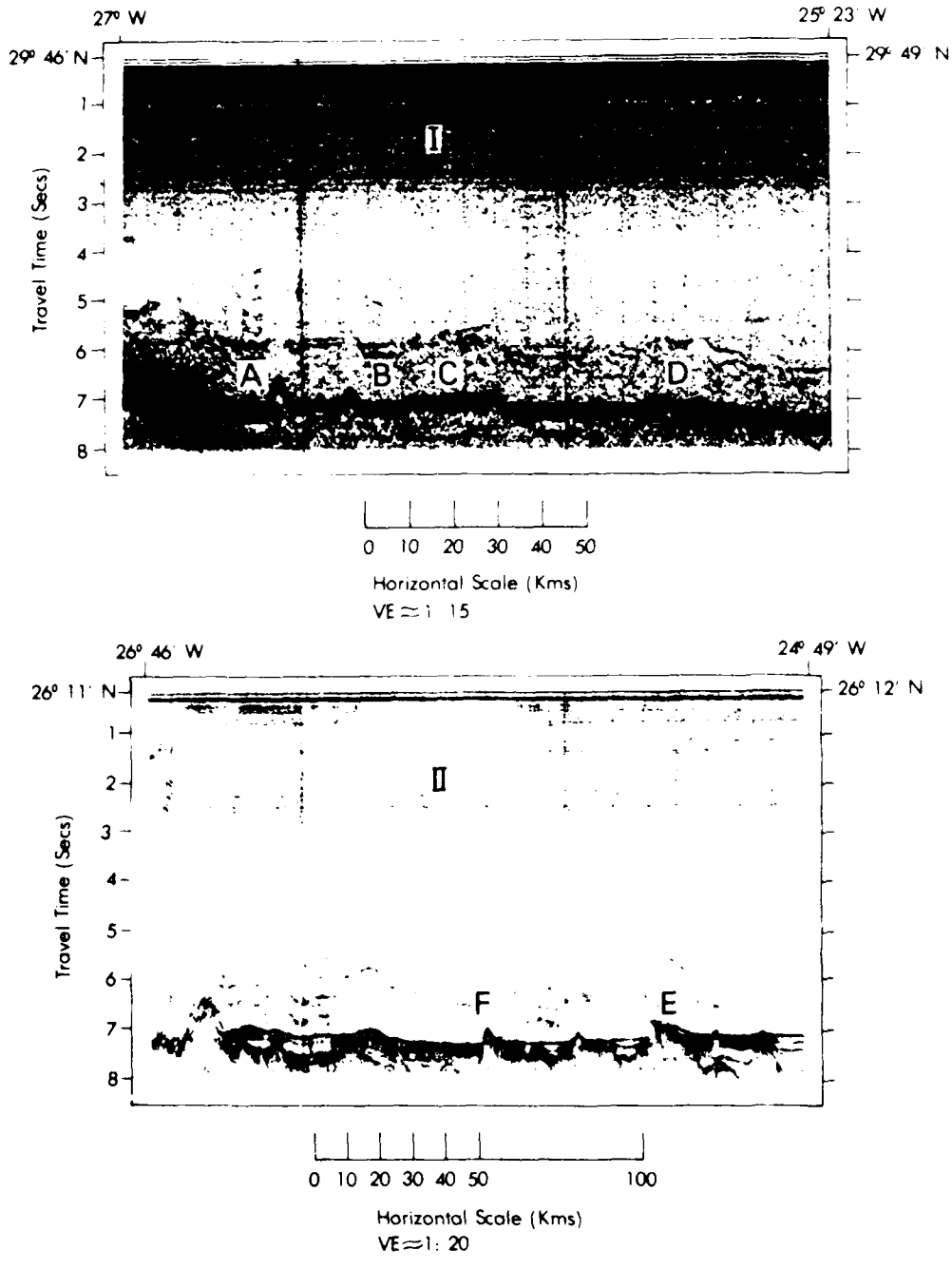

Figure 11. Structures observed on typical seismic reflection profiles: I: A and B: apparent grabens showing sediment ponding. C and D: apparent horsts. II: E and F: vertical faulting. Only relative motion can be determined from seismic profiles. The relatively lower surface level of the graben implies that B is an example of recent faulting or that the ridge to west of B is elongate thus forming a barrier to eastward moving sediments. C, D, E, and F are examples of abyssal hills.

than 1/10 and profile widths of less than 5-10 km. The other type is a broader feature relative to its height, has slopes with gradients of less than 1/20, and profile widths of 15 km or more. Frequently, measurable thickness of sediment will be draped over broad abyssal hills and multiple peaks will rise above the average crest of these features. Broad abyssal hills have mappable areas of 200-400 km^2.

Jones et al. (1966) describe an abyssal hill near 29°20'N, 25°20'W that they consider typical of the larger abyssal hills. This hill rises about 600 m above the sea floor and is believed to be a volcano because of its topographic form and the 40 km^2 caldera-like summit depression. Luyendyk (1970) studied elongate abyssal hills in the Northeast Pacific which averaged about 400 km^2 in area and about 300 m relief. He concluded that some were shield volcanoes and others were horst structures. Both types are present in the Cape Verde/Canary Basin but volcanoes appear to predominate. The multiple peaks commonly seen on abyssal hills (Plate I) are possibly related to shifts of eruptive centers during volcanic activity (Jones et al., 1966). Jones et al. (1966) report no prominent directional trend in the elongation of the hills in their small study area, although Rona et al. (1974) found a northeast trend to abyssal hills in the east central North Atlantic. Plate I does not show a directional trend for the Cape Verde/Canary Basin.

4. Cape Verde Rise

The Cape Verde Rise is a prominent sedimentary apron surrounding the base of the Cape Verde Pedestal. The Rise is separated from the African Continental Rise by a broad sill reaching 22°W and lying less than 3100 m deep (Plate I). North and northwest of the Cape Verde Islands, the boundary between the Cape Verde Rise and the Upper continental Rise is arbitrarily placed where surface slopes decrease to less than 1/100. Surface gradients become progressively steeper upslope, resulting in a concave profile and implying a relatively high energy depositional environment.

Overall, the surface of the rise is quite smooth except for an occasional basement peak penetrating the sediment cover and a widespread network of small erosional channels trending toward the northwest. A typical erosional channel (Fig. 12) is less than 10 km wide, 40-80 m deep, slopes northwestward with gradients of 1/100 - 1/200, and has a small levee on one side. Steepened channel gradients relative to Cape Verde Rise gradients show active erosion and suggest that these channels serve as conduits for moving sediments from the Cape Verde Islands to the abyssal floor.

5. Seamounts

Seamounts are topographic features with a circular or elliptical base, at least 1000 m relief, and comparatively steep slopes (Heezen et al., 1959). In the Cape Verde/Canary Basin, seamount groups are located along the western edge of the area north of 29°N and south of 21°N, and along the upper continental rise at the eastern boundary (Plate I). An isolated seamount is located between DSDP Sites 137 and 138 (Fig. 13).

Great Meteor Seamount, discovered and named in the 1937 cruise of German Research Ship METEOR, is the southernmost of a chain of large seamounts extending northward to the Azores Plateau (Pratt, 1963). The base of the seamount is elliptical and has an area of more than 10,000 km^2. The seamount, to a depth of about 2000 m, has an average gradient of about 1/4. Below 2000 m, gradients decrease to 1/12 or less. The seamount is level and less than 300 m deep; minimum depths recorded by USNS LYNCH (Cruise LY-33, November-December 1973) were 214 m and 266 m on different parts of the summit. Great Meteor Seamount has the general aspect of a guyot, possibly because of wave planation and relative sea level fluctuation during the Miocene, or post-Miocene sea level fluctuations and isostatic sinking (Pratt, 1963).

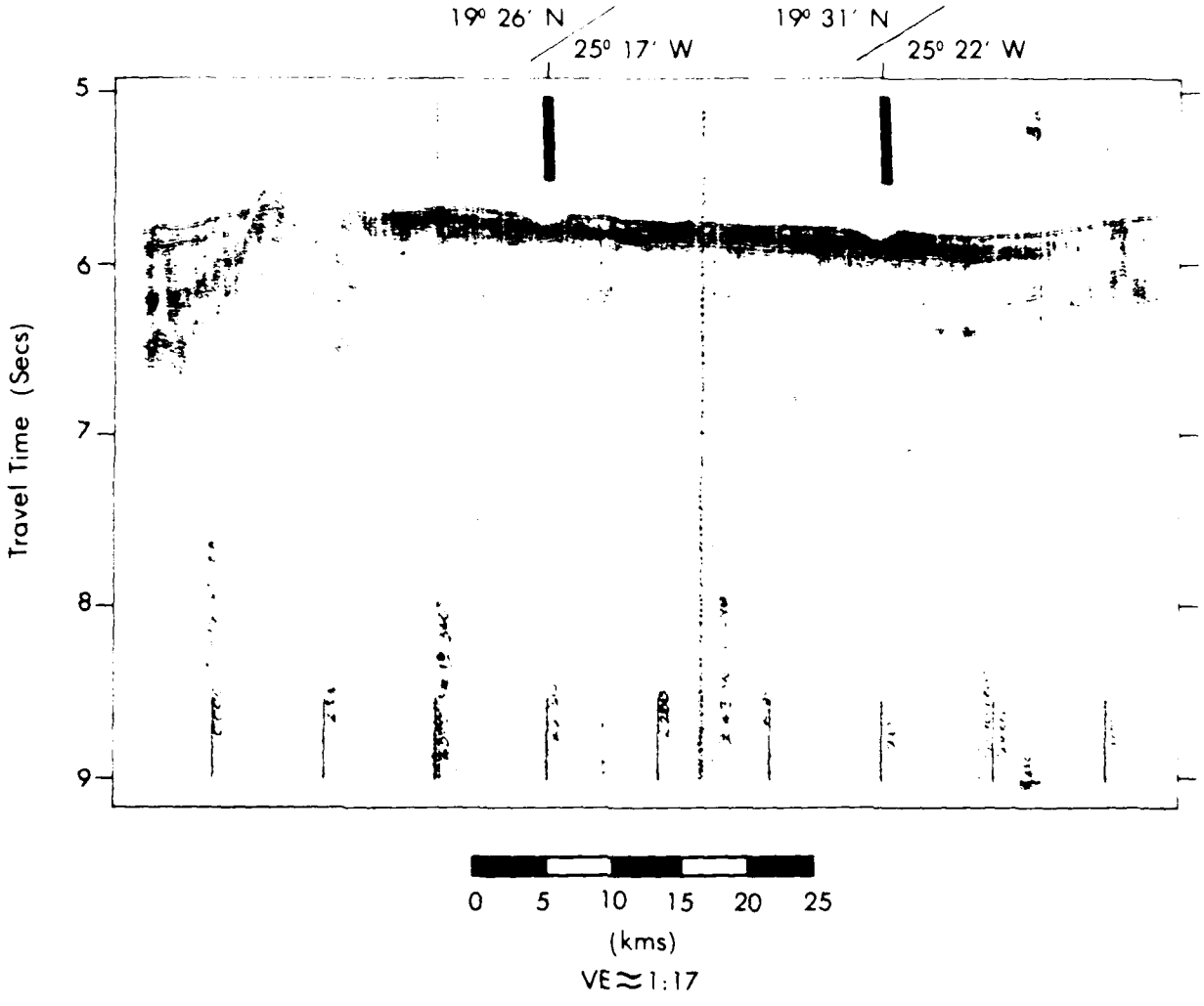

Figure 12. Two crossings, about 12 km apart, of an erosional channel on the Cape Verde Rise. At these locations, the channel is about 4 km wide and about 80 m deep. The axis of the channel slopes northwestward at about 1.160. The levee is most pronounced on the northeast side of the channel.

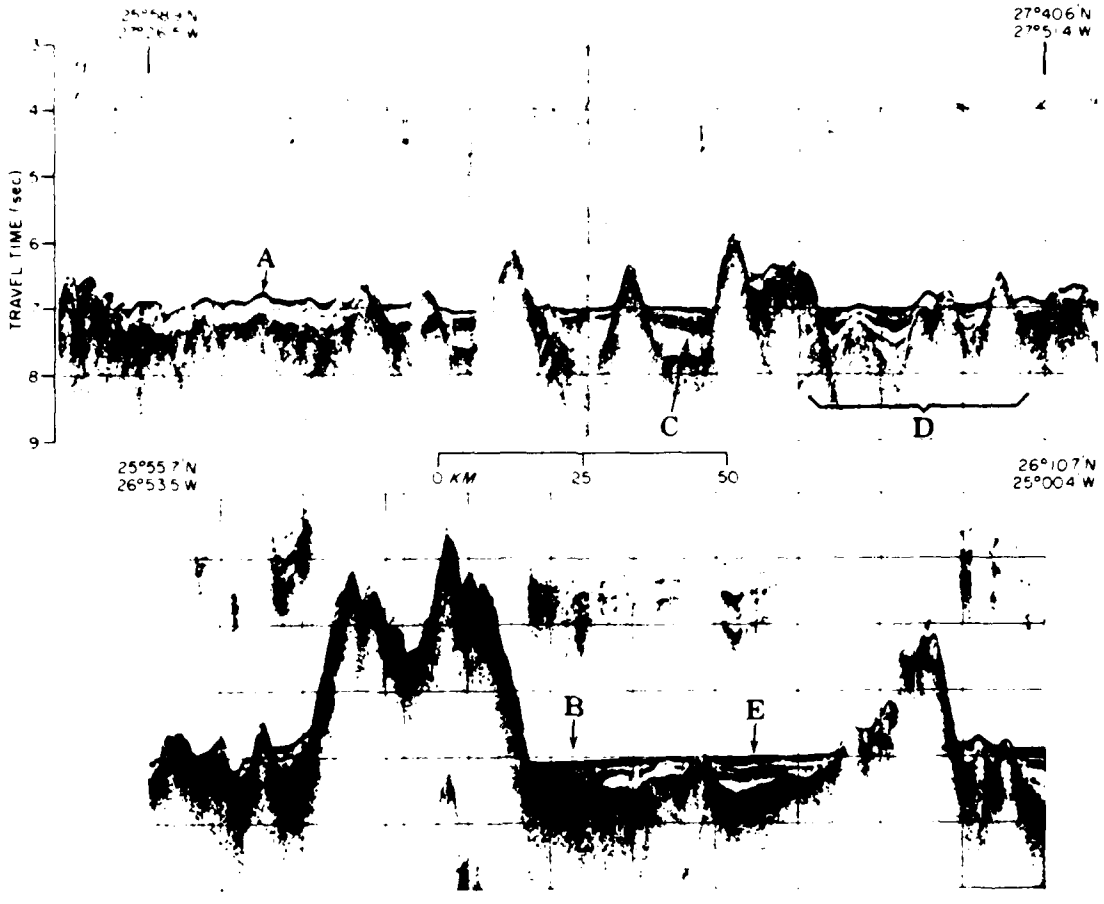

Figure 13. Typical seismic reflection patterns in the Cape Verde/Canary Basin. A. Draped acoustically transparent facies. B. Simple parallel reflectors typical of turbidity or strong bottom current deposition. C. Lower acoustically transparent zone. D. Irregular acoustically opaque reflections typically identified as an acoustic basement. E. Smooth, acoustic basement probably caused by sills or later extrusives. Also location of DSDP Drill Site 138.

The seamounts south of 21°N are small compared to Great Meteor. Summits are seldom shallower than 2200 m, areas of deepest closed contours seldom exceed 1500 km^2 and slope gradients vary between 1/3 and 1/15 (Plate I). Steeper slopes face eastward. Sediment moats around one of the seamounts were interpreted as selective deposition from a northeastward-flowing bottom current (Lowrie et al., 1977) rather than the result of isostatic adjustment due to crustal loading.

The eastern boundary seamounts are aligned along a northeast trend connecting the Cape Verde and Canary Islands (Plate I). These seamounts are intermediate in size relative to other seamounts in the area. Echo Bank (Fig. 14) rises to about 300 m subsurface, but all other seamounts in the group have summit depths of about 1000 m. The average area of the base of these seamounts is about 1200 km^2.

C. Basement Structure

1. Fracture Zones

Fracture zones are defined as long, narrow bands of grossly irregular topography characterized by volcanoes, linear ridges, and scarps typically separating distinctive topographic provinces with different regional depths. Because most fracture zones lie within crustal plates and are produced by transform faults at the spreading axis, many fracture zones can occur within a single rigid plate moving on a sphere (Menard and Chase, 1970).

Cape Verde/Canary Basin fracture zones are typically described from topographic, seismic, or magnetic profiles as graben-like structures with about 40 km width and 100-200 m relief (Rona and Fleming, 1973). On the African Plate, fracture zones are spaced about 100 km apart and trend about N80°W (Uchupi et al., 1976). Plate IV shows the fracture zones mapped in the Cape Verde/Canary Basin from the data compiled for this report.

The fracture zone that approximately parallels 27°N is probably typical of Cape Verde/Canary Basin features (Plate IV). This structure has an average width of 25 to 30 km and a maximum depth greater than 6 km. Topography of the flanking ridge is characterized by its variability in which minimum relief is 200-400 m and maximum relief is about 1000 m. Flanking ridges trend subparallel to the 27°N fracture zone. Sediments in the 27°N fracture, usually greater than 600 m, are thick enough to mute the underlying topography.

Fracture zones (Plate IV) were initially mapped on the basis of structure, topography, and sediment thickness, and confirmed by magnetic profiles. Magnetic signatures of fracture zones characteristically have long wavelengths parallel to fracture trends and short wavelengths perpendicular to fracture trends (Handschumacher and Andrews, 1975). Depth to basement is a useful criterion for recognizing fracture zones because depths greater than 6000 m constitute only about 2% of the surface of earth. Width is a less reliable criterion because boundary topography is characteristically variable. Sediments in fracture zones east of 29°W appear to be turbidites in 400-800 m thick ponds interrupted by irregularities in the basement floor.

Topographic and structure profiles lack the resolution to define relative motion along a fracture zone. In fact, it is impossible to determine the amount of offset without the aid of geomagnetic profiles. Conversely, structure can cause offsets in magnetic anomalies. Thus, a grid survey with closely spaced tracks (cf 10-20 km) is required to correlate magnetic, topographic, and structural lineations and locate fracture zones. Previous interpretations of fracture zone dimensions, regional distributions, and offsets and relative motion patterns based on data from widely spaced track lines (Rona et al., 1970; Harbison et al., 1973; and Rona and Fleming, 1973) are not valid as indicated by the distribution of these features on Plates I-IV.

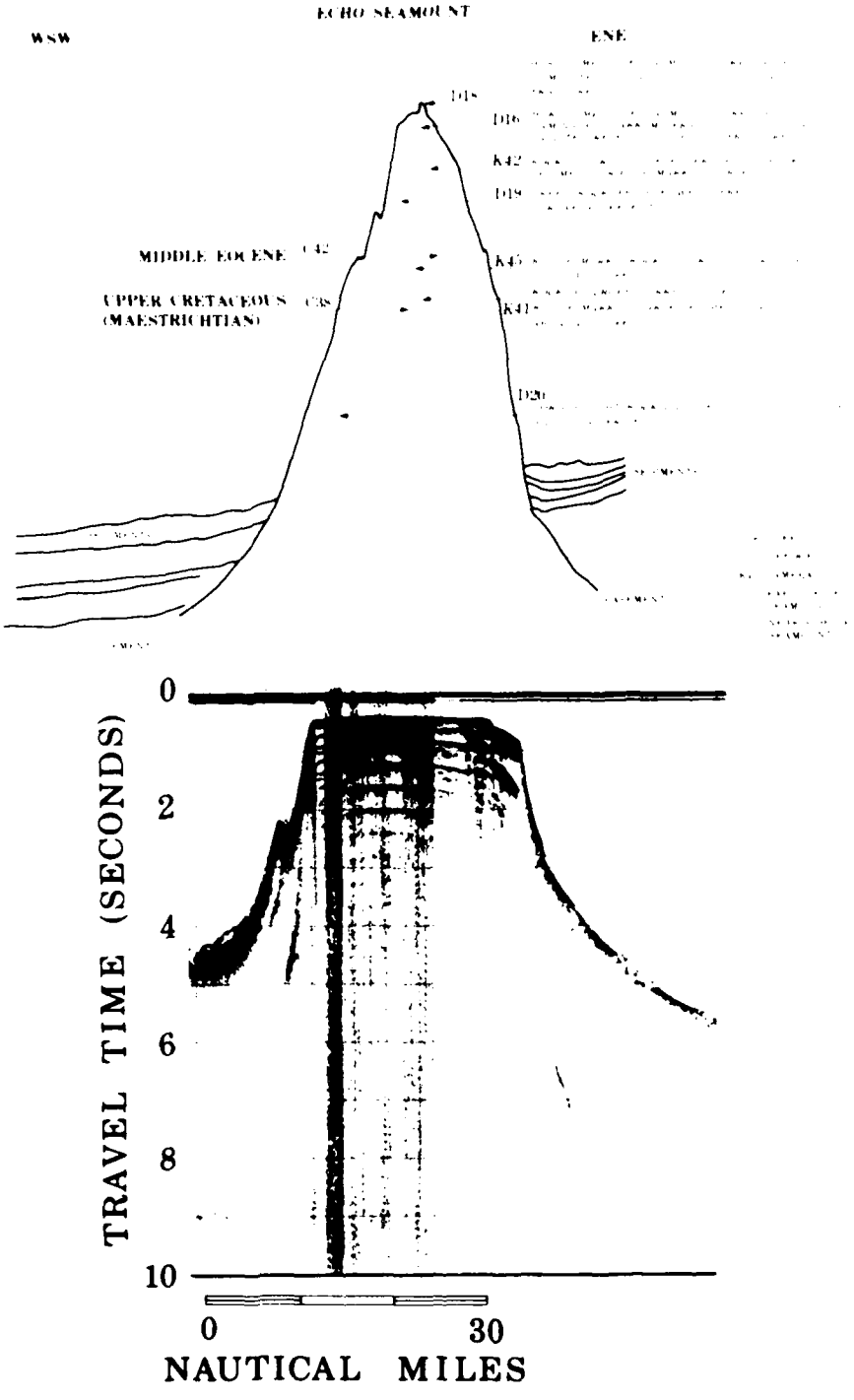

Figure 14. Paleontologic, stratigraphic analysis of Echo Bank, Cape Verde/Canary Basin by Martin Weiss, Naval Oceanographic Office (Unpublished File Illustration). All samples recovered were indurated, marine sedimentary rocks. Lower portion is original bathymetric profile with different horizontal scale than upper portion.

2. High Angle Faulting

The structure-contour map (Plate II) shows that acoustic basement north of 26°N and west of the Canary Islands is broadly warped. Seismic profiles from this area show numerous high angle faults (Fig. 11-C). These faults typically have throws of 200-400 m, and displace acoustic basement and all overlying sediments. In some instances, faulting appears to be very recent, with the apparent downthrown block showing little change in sediment thickness relative to the apparent upthrown side. In other cases (Fig. 11-B), the apparent downthrown side shows evidence of rapid deposition. Determination of absolute fault motion is not always possible with single channel seismic reflection records.

Another area of faulting is located west of the Cape Verde Islands in an area of apparent broad unwarping (Plate IV). Displacements on these faults are comparable to those north of 26°N. Differences of numbers of faults in the two areas probably reflect differences in density of seismic profiles.

The relationship between faulting and other structural elements in the area is not clear. Some abyssal hills appear to be bound by normal faults, thus forming horsts. However, most abyssal hills do not have associated faults. In several instances faults appear to cross fracture zones. In another case, faults form boundaries of a fracture zone indicating post-rifting tectonism along the fracture zone or sedimentation that has not been influenced by topography.

3. Structure of Cape Verde Rise

The Cape Verde Rise, beneath its sediment cover, extends north to about 21°N and west to about 28°W (Plate II). The southern boundary is outside the charted area, and the eastern boundary is obscured beneath sediments thicker than the resolving power of single channel seismic equipment. Lancelot, Seibold et al. (1977) note that the broad rise shown by the bathymetry map (Plate I) is the surface expression of a smooth, northwest/southeast-trending rise with an average depth of 7 seconds (cf 5300-5500 m) below sea level. This rise appears to connect the Cape Verde Pedestal with Cape Verde in Senegal (Lancelot, Seibold et al., 1977).

Weigal and Wissman (1977), reporting results of refraction seismic surveys on the eastern Cape Verde Rise, note that acoustic basement is correlative with a 5.2 km/sec layer. They identify the 5.2 km/sec layer as layer 2. Layer 2 can be traced on seismic profiles throughout the Cape Verde/Canary Basin except where obscured by sills and/or excessive sediment thickness.

North of the pedestal, acoustic basement reaches regional depths across two northward-facing, terrace-like escarpments, each with about 600 m relief (Fig. 10). These terraces can be traced westward on seismic profiles around the base of the Cape Verde Pedestal. Basement roughness increases from east to west, particularly west of the Cape Verde Islands, where a group of seamounts causes basement level to be about 1000 m higher than average basement level in the Basin. A zone of diapiric structures (Fig. 6) roughly coincides with the zone of basement relief shown trending northwest from about 19°N, 24°W (Plate IV).

D. Crustal Depth/Age Relationship

Sea floor subsides as it moves laterally from a spreading center. Subsidence is thought to be caused by complex interaction between mantle degassing, mineralogic phase changes, mantle counterflow, cooling and contraction of layers 2 and 3, and erosion and sedimentation, but is independent of sea floor spreading rates. Age of the sea floor can be estimated when regional basement depth and sediment thickness are known and mantle cooling, contraction, degassing and counterflow are assumed constants (Menard, 1969; Sclater et al., 1971; Sclater and Detrick, 1973).

In practice the age-depth relationship is determined by defining average regional basement depths and estimating sediment thickness from seismic reflection profiles, correcting for isostatic loading effects, and then comparing results with sea floor ages interpolated from magnetic anomaly correlations and DSDP age data. With this procedure, Menard (1969) empirically determined average subsidence rates of 90 m/my for the 0-10 myBP time period, 33 m/my for 10-40 myBP time period and 20 m/my for the 40-70 myBP time period. In addition, Menard (1969) estimated an average subsidence rate of 20 m/my for the time period between 70-140 myBP.

Total subsidence near the center of Cape Verde/Canary Basin (24°N, 26°W) is approximately 3500 m at Menard's (1969) rates if a crustal age of 120 myBP is assumed (Plate IV). Total depth to basement is 6200 m if the mean depth of the ridge crest is assumed to be 2700 m (Tucholke, Vogt et al., 1979). Average measured depth to basement at 24°N, 26°W is 6200 m (Plate II).

Tucholke, Vogt et al. (1979) established an empirical age depth curve for North Atlantic Ocean crust. To derive this curve these authors used sediment thickness (S) corrected for isostatic loading effects to determine sediment-free basement depth (Z). Topographic corrections are applied to sediment-free basement depths to determine average corrected basement depth. The isostatic loading correction factor of 0.66 is determined from $(\rho_m-\rho_s)/(\rho_m-\rho_w)$, where ρ_m is the density of the mantle (3.3 g/cm^3 assumed), ρ_s is the sediment density (1.8 gm/cm assumed), and ρ_w is 1.03 g/cm^3, the average density of water. These parameters are combined in the equation $Z = D + 0.66S$.

DSDP Site 137 illustrates the application of this procedure. At this location, sea floor depth is 5361 m and measured sediment thickness is 397 m, but is isostatically corrected to 262 m (0.66 x 397). Sediment-free basement depth is 5623 m (5361 + 262). A crustal depth estimate of 5830 m is derived from Menard's (1969) subsidence rates and the assumption of 102 myBP crustal age for Site 137. These estimated depths are within a contour interval of Site 137 basement depth shown on Plate II.

In order to estimate a subsidence anomaly for the Cape Verde Rise, I assumed that the 122 myBP isochron passes near 19°N, 26°W (Plate IV). Average regional crustal depth for 122 myBP North Atlantic sea floor is about 5600 m (Tucholke, Vogt et al., 1979). Sea floor depth at 19°N, 26°W is 4200 m (Plate I), and sediments are approximately 800 m thick. Sediment-free basement depth is calculated as 4728 m (4200 + (0.66) 800).

A topographic correction must be applied to sediment-free basement depth to determine basement depth because of uplifting of the Cape Verde Pedestal. The topographic correction is determined by correcting regional crustal depth for sediment overburden and subtracting the sediment-free basement depth (Tucholke, Vogt et al., 1979). The topographic correction at 19°N, 26°W is 344 m (5600 - 528 - 4728 = 344).

Basement depth adjusted for Cape Verde Pedestal uplift is 5072 m and the measured depth to acoustic basement is 5000 m (Plate II). These data suggest that the Cape Verde Rise has been uplifted 344 $\pm$ one contour interval. The results obtained agree with Hayes, Pimm et al. (1972) estimate of 400 m uplift between DSDP Sites 12 and 141, but are well below the 1000 m uplift for the Cape Verde Rise estimated by Lancelot, Seibold et al. (1977). Accuracy of the results is dependent on the reliable detection and identification of layer 2 as an acoustic basement and the determination of a velocity function to correct the thickness of overlying sediments.

IV. Age of the Sea Floor in the Cape Verde/Canary Basin

A. Introduction

Knowledge of the age of the sea floor is necessary to establish a time frame for the gelogic evolution of the Cape Verde/ Canary Basin. In this section, radiometric and Paleontologic age data from DSDP and other literature are used to update the geochronologic framework within which magnetic reversal sequences are fitted. Magnetic reversal sequences are used to revise previously published isochron charts for M-sequence anomalies, extend the J-anomaly across the Cape Verde Rise and delineate areas of Cretaceous 'Quiet Zone' crust with greater precision than possible from previous studies.

B. Sea Floor Age Data

Age calibrations in the Cape Verde/ Canary Basin include radiometric and micropaleontologic age dates for DSDP Sites 137 and 138 (Pimm, Hayes et al., 1972); Jurassic age fossils from Maio in the Cape Verde Islands (Colom, 1955); and late Cretaceous foraminiferal limestones unconformably overlying lithologically correlative Jurassic-Cretaceous siliceous deposits on Fuerteventura, Gomera, and La Palma in the Canary islands (Gastesi, 1970).

The age of the basement at DSDP Site 137 is assumed to be 103-106 myBP (van Hinte, 1967a). This age is defined by a nannoplankton flora 3 m above the basalt-sediment interface (Hayes, Pimm et al., 1972) and extrapolation of the average rate of sediment accumulation (2 m/my). The geomagnetic age of the basement is approximately 97 myBP according to Larson and Pitman's (1972) correlations, and approximately 111 myBP by Pitman and Talwani's (1972) calender. Hayes, Pimm et al. (1972) belive that highly altered basalt sampled at DSDP Site 137 is the upper surface of the crust.

The deepest sampled igneous rocks at DSDP Site 138 are altered basalts. Hayes, Pimm et al. (1972) believe the basalt layer to be approximately 95 myBP on the basis of fossils recovered from the sediments immediately overlying the basalt. Geomagnetic extrapolations by Pitman and Talwani (1972) show that oceanic crust at this location is about 103 myBP. Vogt and Einwich (1979) use Van Hinte's (1976a) Cretaceous time scale to assign an age of 110-115 myBP to the crust at Site 138.

In order to reconcile these age discrepancies, Hayes, Pimm et al. (1972) note that the age of the oldest sediment at DSDP sites may not be the same as that of the underlying basement because of unrecognized sedimentary hiatuses, the erroneous identification of sills as true basement, and the relatively low interval velocities in the overlying sediments. These authors anticipate that 50 to 100 m of sediment lie between the presumed sill and true basement although seismic profiles (Fig. 13-B) do not give any indication of deeper reflectors. If these additional sediments exist, and if sediments have accumulated at an average rate of 10 m/my, then basement would be 10 my older than the sill sampled. This extrapolation produces estimated basement ages of 105-110 myBP and is compatible with geomagnetic deductions.

Fossiliferous limestones and cherts of Maio provide age information about the Cape Verde Islands. Ammonites recovered from these rocks were dated as Late Jurassic and thought to have been deposited on the sea floor before the Cape Verde Islands were uplifted (Colom, 1955). Radiometric ages from Maio (Grunau et al., 1975) are Miocene and do not provide any information about the age of the crust in this area.

C. Magnetic Geochronology

Sea floor spreading creates new lithosphere at a mid-ocean ridges by the interjection of molten magma into existing host rock until the host rock

and the magma assume similar petrologic characteristics. As the temperature of these new pieces of sea floor decrease to less than the Curie Point, their rock masses become magnetized in the direction of the earth's prevailing magnetic field. Because the earth's magnetic field periodically reverses its polarity, an alternating series of positively and negatively magnetically polarized rock masses are generated. In recent years, profiles of alternations of magnetic polarities have been interpreted to establish a geomagnetic time scale in terms of conventional geochronology.

Widely spaced, usually randomly oriented magnetic profiles helped establish the age and the tectonic history of the sea floor in the eastern North Atlantic (Pitman and Talwani, 1972; Rona and Fleming, 1973: Hayes and Rabinowitz, 1975; Ballard et al., 1976; Uchupi et al., 1976). Such studies identified the Jurassic Magnetic 'Quiet Zone', the M-sequence and J-anomaly, the Cretaceous magnetic 'Quiet Zone' and the Cenozoic anomaly sequence as significant magnetic elements between the African Continental Margin and the Mid-Atlantic Ridge. These analyses conclude that the initial North American-African continental breakup began about 180 myBP, and the sea floor spreading has continued since that time at an average half-rate of about 1.5 cm/yr (Heirtzler, 1974).

To isolate major structural elements and establish a magnetic chronology, published magnetic profiles were combined with a selection of magnetic records collected concurrently with seismic profiles. For clarity, these data are presented as E/W profiles (Fig. 15), N/S profiles (Fig. 16), a tectonic summary chart showing anomaly correlations, assigned ages, and other structural elements (Plate IV), and isochron chart (Fig. 17) assigning geologic ages to the oceanic crust in the study area.

1. Jurassic Magnetic 'Quiet Zone'

The eastern boundary of the charted area (PLATE IV) is the Jurassic Magnetic 'Quiet Zone' previously delineated in both the eastern and the western North Atlantic basins (Pitman and Talwani, 1972). The Jurassic 'Quiet Zone' is positioned on the basis of decreased anomaly amplitudes, but definite correlations are hampered by the presence of seamounts along the lower continental rise that may be related to the 'Quiet Zone'/M-sequence boundary. In the 'Quiet Zone,' familiar sea floor spreading characteristics of anomaly linearity, continuity, and correlation are difficult to establish with routinely collected and processed data because of the very low anomaly amplitudes. However, profiles collected with near-bottom magnetometers in magnetic 'Quiet Zones' in other parts of the world shows numerous low-amplitude, but correlative, events (Handschumacher, Pers. Comm., 1979).

The origin of the Jurassic 'Quiet Zone' is unresolved. Among the proposals offered for 'Quiet Zone' origin are:

(a) Thickness of the sediment cover over the lower continental rise attenuates magnetic anomalies;
(b) Magnetic intensity decreases with increasing geologic age;
(c) A series of horizontal lava flows of differing polarities in which destructive interference of individual magnetic anomalies diminishes the summed amplitudes;
(d) Secondary tectonism destroys residual magnetism;
(e) Origin of magnetic 'Quiet Zone' sea floor near the magnetic equator and the subsequent shift of the magnetic equator of the northward drift of spreading sea floor;
(f) Very long periods of geologic time without polarity reversals; or
(g) Very rapid polarity reversals generating short wavelength, low amplitude, magnetic anomalies.

Handschumacher and Kroenke (1978) demonstrated that a rapid reversal sequence occurring during a period of uniform sea floor spreading would create short wavelength, low amplitude anomalies, and

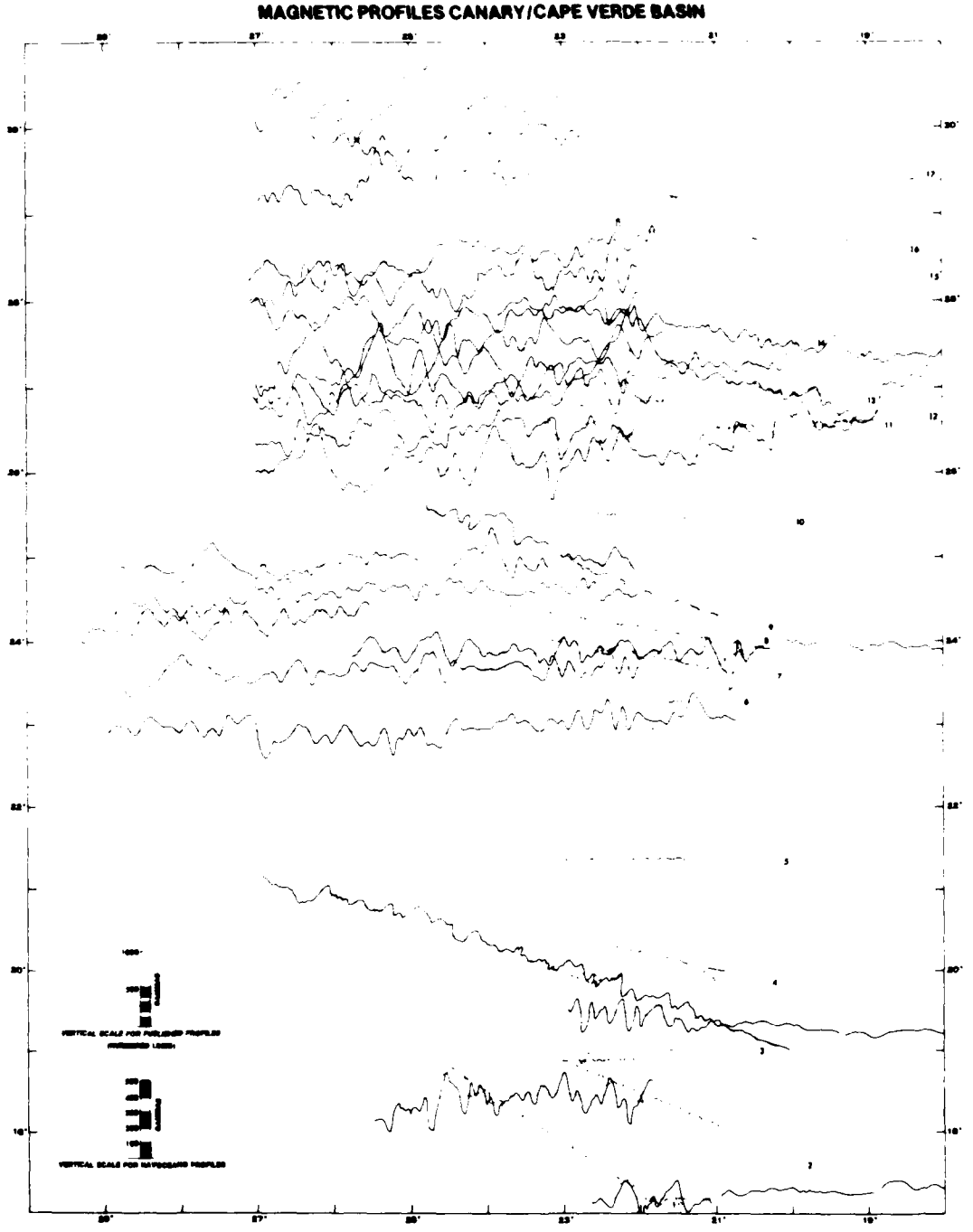

Figure 15. E-W magnetic profiles from the Cape Verde/Canary Basin. Numbered profiles are from Hayes and Rabinowitz (1975). Other profiles are from the magnetic data bank maintained by the U.S. Naval Oceanographic Office at NSTL Station, Mississippi.

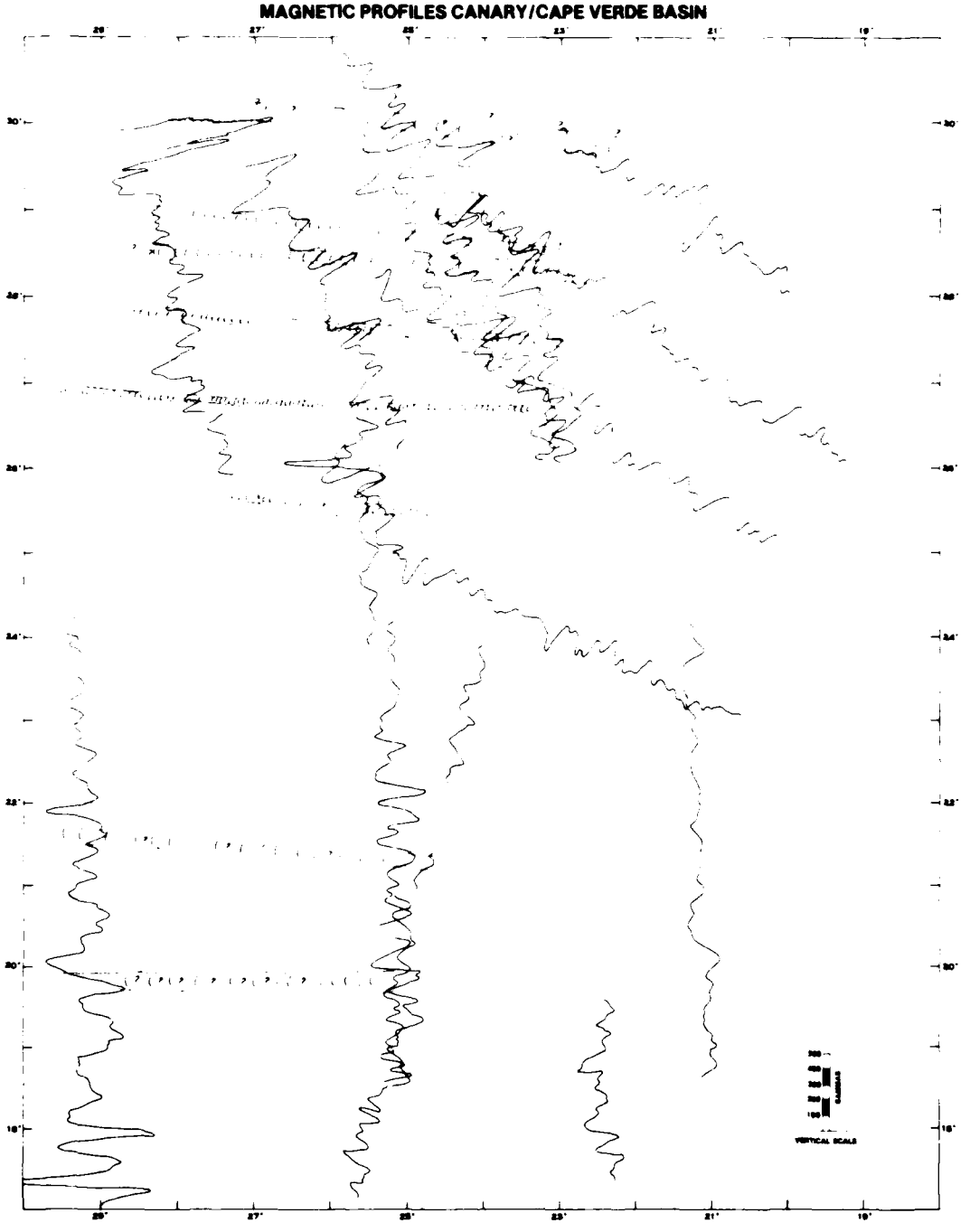

Figure 16. N-S magnetic profiles from the Cape Verde/Canary Basin. Probable fracture zones indicated. Profiles previously unpublished.

that these anomalies can be correlated in the Pacific. If this origin obtains for the Atlantic Jurassic 'Quiet Zone,' then this boundary is very likely to be an isochron and not time transgressive as Hayes and Rabinowitz (1975) believe. The most reasonable age estimate for this isochron is 146 myBP (Oxfordian) (Van Hinte, 1976a).

2. M-Sequence

The broad band of Mesozoic anomalies (M-sequence) that parallel the African Continental Margin (Plate IV) is one of the most striking magnetic features in the eastern North Atlantic. Vogt et al. (1971) originally described and named this sequence of sea floor spreading anomalies and their corresponding isochrons from data collected by USNS KEATHLEY in the southwest North Atlantic. Subsequently, Pitman and Talwani (1972) identified similar features in the eastern North Atlantic and established isochrons correlative with the KEATHLEY lineations and other Mesozoic anomalies on a world-wide scale. They numbered these lineations M-1 through M-25 (M-Mesozoic) and revised the time scale to conform to their spreading model. Larson and Hilde (1975) recognized an M-0 event and extended the time scale to range between M-0 at 108 myBP and M-25 at 153 myBP. Vogt and Einwich (1979) revised the calibration for the Mesozoic sequence in the western Atlantic and adapted the M-sequence lineations to the geologic time scale proposed by Van Hinte (1976a, b), thus changing the time span to 111 myBP-149 myBP.

Anomaly resolution typical of Pacific magnetic data is not attainable in the Atlantic because of greater geologic complexity and slower spreading rates. Anomalies on adjacent profiles could not always be correlated with complete certainty, but sequential patterns considered in the context of the entire data set allowed the identification of some anomalies on every profile. Along-strike amplitude variations, particularly prevalent between about M-14 and M-4 times, secondary vulcanism that distorts sea floor spreading anomaly patterns and minor navigational discrepancies all contribute to the difficulty of comprehensive correlations over appreciable distances. On Plate IV, anomaly correlations are shown where they can be identified with reasonable confidence. The anomaly labeling pattern is adapted from the Pacific M-sequence studies of Larson and Hilde (1975). M-2, the youngest of the M-sequence anomalies that can be correlated throughout the surveyed area, is dated as Early Cretaceous (Neocomian) by Van Hinte (1976a). M-17 (Fig. 15) is a distinctive and easily correlated anomaly as is M-18 which Van Hinte (1976a,b) locates at the Cretaceous/Jurassic boundary. M-22, a pronounced low located west of the Continental Rise Seamounts, is useful as an index for aligning profiles. Between M-22 and the Jurassic 'Quiet Zone,' anomaly amplitudes decrease with increasing ages. As a result, recognition and correlation of M-23 and older anomaly sequences are difficult (Fig. 15; Plate IV).

Within the correlated M-sequence anomalies an average half spreading rate of about 1.5 cm/yr obtains (Plate IV). No significant differences in spreading rates are apparent during either the Late Jurassic or the Early Cretaceous. Spreading rates during the time of formation of Cretaceous 'Quiet Zone' sea floor may have been slightly faster (cf 2 cm/yr), but lack of magnetic definition does not permit precise determination.

The correlation sequence shown in Plate IV does not require the numerous fracture zones shown by previously published correlations. The change in trend of the M-sequence from 0° azimuth south of about 23° to an azimuth of about 030° north of about 24° might relate to major fracturing as shown by Hayes and Rabinowitz (1975). However, changing trends also correlate with changes in Mid-Ocean Ridge and continental trends. Trend changes are not related to major fracturing because spreading rates on

either side of the trend change are similar, positions of correlated anomalies are within the limits of navigational inaccuracies and are frequently distorted by the location of basement relief, and trend changes are compatible with similar non-fracture zone related trend changes in the Western Atlantic (Vogt and Einwich, 1979).

3. The 'J' Anomaly

The 'J' Anomaly, first described by Heezen et al. (1959), is a high amplitude, double-peaked magnetic feature recognizable in eastern and western North Atlantic basins. This sequence of two to four polarity events is best developed in the eastern North Atlantic north of the new England Seamount-Canary Islands lineation where it is associated with a pronounced structural and topographic feature (Hayes and Rabinowitz, 1975; Ballard et al., 1976). A similar double-peaked magnetic feature can be traced from the latitude of the Canary Islands to the Cape Verde Islands (Plate IV). In this part of the Cape Verde/ Canary Basin, the 'J' Anomaly does not seem to be related to structural relief.

Hayes and Rabinowitz (1975) and Ballard et al. (1976) are among those who identify the M2-M4 sequence as the 'J' Anomaly of Pitman and Talwani (1972). Conversely, Uchupi et al. (1976) correlate the 'J' Anomaly with the positive polarity event M-15 in the eastern Atlantic, while Hayes and Rabinowitz (1975) do not consistently recognize an M-15 event. Barret and Keen (1976) believe that anomalies M-16 - M-17 represent the negative trough of the 'J' Anomaly in the western Atlantic. The correlations in Plate IV show M-2 - M-4 as the 'J' Anomaly and date its time of occurrence as Early Cretaceous (Neocomanian) or 121-123 myBP by Van Hinte's (1976a) calendar.

Amplitudes and wavelengths associated with the 'J' Anomaly are not characteristic of normal, sea floor spreading, magnetic features. The breakup in M-sequence linearity and uniformity began during the 'J' Anomaly time. The causes of the transition from M-sequence to Cretaceous 'Quiet Zone' are not known, but Pitman and Talwani (1972) conclude that the Mid-Ocean Ridge axis shifted westward north of the Canary Island lineation, after the formation of the 'J' Anomaly. I believe this ridge axis shift was one manifestation of a changing tectonic regime, possibly the expansion of the Mid-Atlantic Ridge, that created fracture zones, led to the initiation of volcanism, and the subsequent beginning of uplift in the Cape Verde/Canary Basin.

4. Cretaceous Quiet Zone

West of M-2 - M-4, magnetic profiles show high amplitude anomalies, frequently with long periods on east-west profiles (Fig. 15) and short periods on north-south profiles, (Fig. 16), with few recognizable sea floor spreading patterns and no correlatable sequences. This portion of eastern Atlantic sea floor is called the Cretaceous 'Quiet Zone' and is believed to indicate crust formed during a period of few magnetic reversals (Larson and Hilde, 1975). Although Pacific magnetic anomalies conform to 'Quiet Zone' description (Handschumacher, 1979, pers. comm.), the North Atlantic north of 17° shows a noisy magnetic signature over crust of approximately 80 to 110 myBP, and cannot be accurately described as 'Quiet Zone.'

Vogt and Einwich (1979) consider possible causes of the Cretaceous 'Quiet Zone' such as basement topography, intrabasement magnetization contrasts, and long-term geomagnetic fluctuations and conclude that none of these explanations are satisfactory. These authors believe that changes in magnetic patterns beginning near the end of the M-sequence indicate a change in geologic processes at the Mid-Atlantic Ridge at the time this portion of crust was being formed. The increasing irregularities in the younger Mesozoic reversal sequence (M-1 - M-5) relative to regular anomalies of the M-16 - M-22 portion support Vogt and Einwich's (1979) conclusion

that changes began before the end of the M-sequence. Evidence presented in this study indicating that smaller scale faulting is largely confined to the area defined as Cretaceous 'Quiet Zone,' also suggests changes in the geologic processes occurring during the development of this portion of sea floor.

The absence of sea floor spreading anomalies prevents magnetically dating Cretaceous 'Quiet Zone' sea floor. However, the present consensus age for anomaly M-4 is 123 myBP and for anomaly number 34, the oldest of the Tertiary sequence of sea floor spreading anomalies, is 81 myBP. Thus, the changes in geologic processes that produced the Cretaceous 'Quiet Zone' are confined to Middle Cretaceous time (Fig. 17).

5. Cenozoic Anomaly Sequence

The extreme northwest corner of the study area is crossed by anomalies 34, 32, and 25 (Pitman and Talwani, 1972). Van Hinte (1976a) assigns ages of 81 myBP to anomaly 34 and 70 myBP to anomaly 32. Pitman and Talwani (1972) date anomaly 25 as 61 myBP. Anomalies 34, 32 and 25, in concert with other Cenozoic magnetic lineations, trend about 030° north of 24°N, but almost due north, south of about 23°N. This trend seems to indicate preservation of spreading patterns established at the time of initial North American/African rifting or relatively recent reorientation of the African Plate north of 24°N.

D. Summary

Figure 17 illustrates the age of the sea floor in the Cape Verde/Canary Basin. The Cretaceous-Jurassic boundary is positioned on the basis of the correlation of anomaly M-18 and is dated at 135 myBP (Van Hinte, 1976a). Positions of Late Jurassic stage isochrons are interpolated from M-sequence age dates proposed by Van Hinte (1976b). The Tertiary-Cretaceous boundary and the Upper (Senonian) Cretaceous-Middle Cretaceous boundary are interpolated from correlations published by Pitman and Talwani (1972). Independent data to assess their reliability are not available.

Between Late Jurassic (Oxfordian) and Early Cretaceous (Aptian) times, sea floor formed at a relatively constant half rate of about 1.5 cm/yr. As shown in Plates I and II, Early to Middle Oxfordian sea floor is marked by a concentration of seamounts. The significance of these seamounts, which are approximately coincident with the Jurassic 'Quiet Zone'/M-sequence boundary, is not known, but their positions suggest a basic change in spreading rates, plate orientation, or the locations of zones of crustal weaknesses due to vertical tectonism.

Most crust in the Cape Verde/Canary Basin is of Early to Middle Cretaceous age (Fig. 17). Early Cretaceous (Neocomian) age crust underlies most of the Cape Verde Islands. Extrapolation of Portlandian age crust would include the island of Maio from which Jurassic fossils have been reported. The age of the crust may be greater than the ages of the Cape Verde and Canary Islands.

The breakup of sea floor spreading uniformity began during the late part of Early Cretaceous (Aptian) as indicated by the deterioration in the quality and confidence in M-5 to M-1 correlations. The eastern Atlantic 'J' Anomaly (M-2 - M-4) and its mirror image in the western Atlantic imply that the anomaly and its associated structural relationship must have been generated at, or very near, the axis of the Mid-Atlantic Ridge.

The Cretaceous 'Quiet Zone' was formed on crust of Middle Cretaceous age. There is no evidence to indicate changes in spreading rates because the data are not capable of being resolved with sufficient precision to measure spreading rates accurately.

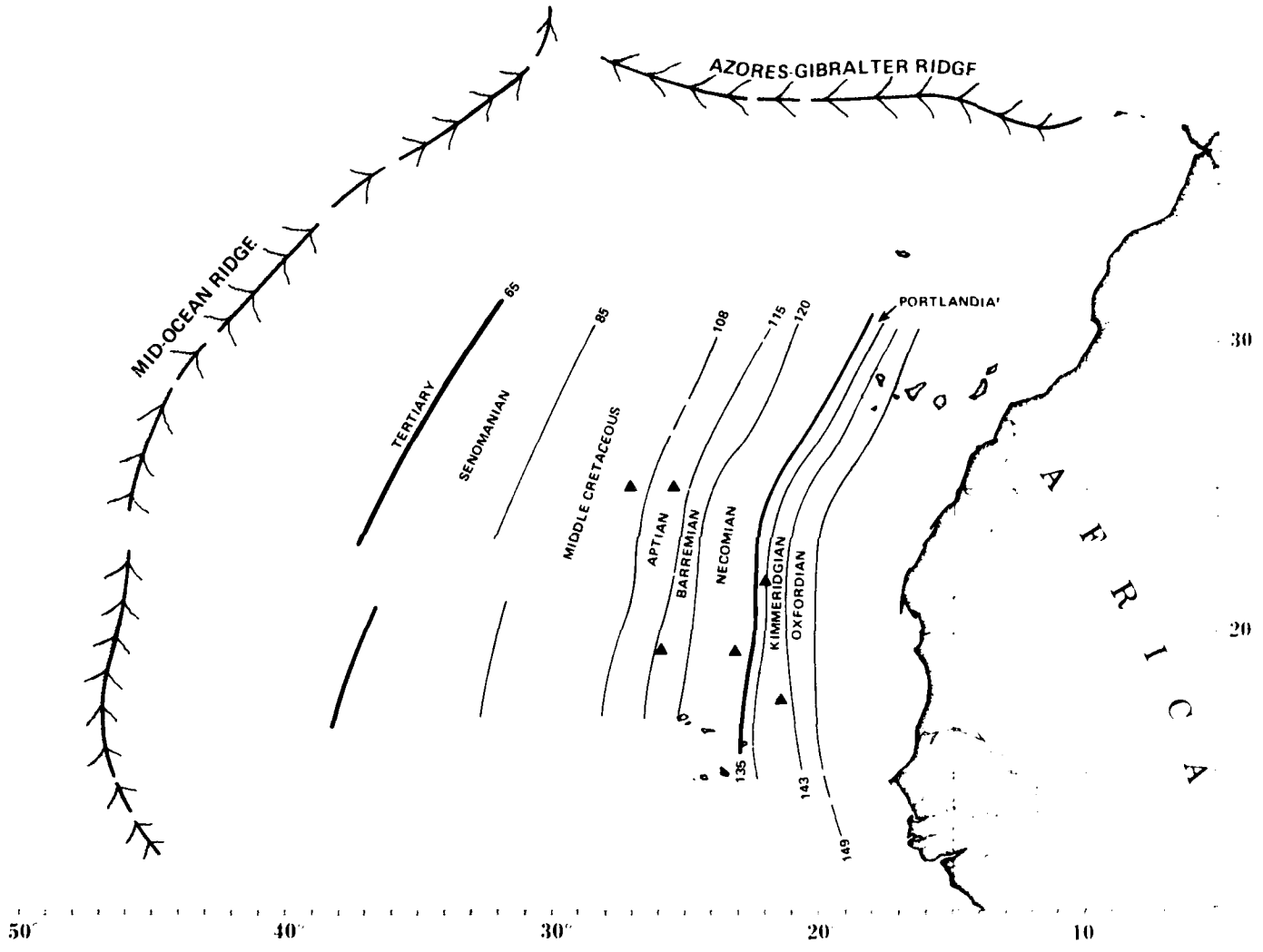

Figure 17. Age of the sea floor in the Cape Verde/Canary Basin based on magnetic anomaly correlations. Triangles indicate locations of DSDP drill holes. Heavy lines at 65 myBP and 135 myBP indicate the Tertiary/Cretaceous and Cretaceous/Jurassic time boundaries, respectively. Neocomian includes Berriasian, Valanginian, and Hauterivian stages, and Senomanian includes Coniacian, Santonian, Campanian, and Maestrichtian stages. The data prohibit more precise dating.

V. Sediment Distribution Patterns in the Cape Verde/Canary Basin

A. Introduction

Previous studies of the distribution of sediments in the eastern Atlantic Ocean (Collette et al., 1969; Ewing et al., 1972; Uchupi et al., 1976; Embley et al., 1978) have been based on widely spaced sub-bottom profiles. As a result, published sediment isopach charts are produced as uncorrected time sections, usually contoured in fractions of seconds, rather than as thickness sections contoured in corrected meters. Interpretations of these charts are limited to such generalities as delineating areas of thick and thin sediment accumulations.

Seismic reflection profiles contain stratigraphic information in addition to providing sediment thickness and basement topographic configurations. This information may be recovered by qualitative analyses of variations in reflection amplitude and continuity, and relationships between reflectors. The process of interpreting high density, normal incidence, seismic reflection records in geologic terms is defined as seismic stratigraphy.

Instrumental and environmental limitations must be recognized and removed from the data prior to interpretation. This step is necessary because seismic stratigraphy is a limited art in which imagination and pattern recognition are confined by fundamental considerations. Thus, successful stratigraphic interpretation of seismic data is a combination of principles, experience and imagination (Sheriff, 1977).

This section will present a sediment isopach map, classify ocean basin sediments according to seismic reflection patterns, and map the distribution of seismic reflection facies and discuss their geologic significance.

B. Sediment Thickness

Plate III is an isopach map of lithologic material overlying acoustic basement and represents, for the most part, unconsolidated sediments interspersed with volcanic flows and sills. The isopach map was prepared by scaling reflection times from about 125,000 track-km of single channel seismic reflection records at three-minute intervals, converting these data points to sediment thickness by applying an average velocity correction factor (Appendix) and plotting in proper geographic position on PS-4 base charts. Due to the use of an average velocity gradient, total sediment thickness values contain an error that increases with increasing thickness.

Topography, sediment supply, and tectonic history control sediment distribution in the Cape Verde/Canary Basin. Sediments are more than a kilometer thick along the continental rise except where larger seamounts penetrate the sediment cover (Plate III). North of about 21°N, isopach contours develop an approximate N 30° E trend roughly paralleling the African Continent and suggesting that the majority of sediments are derived from that source. South of 21°N and west of about 25°W, isopach contours tend to parallel the Cape Verde Pedestal and indicate that the islands are an increasingly important source.

Between about 23°N and 25°N, 1000 m sediment thickness extends at least 150 km farther west than in other parts of the basin. This depocenter may be the result of regional downwarp relative to the Cape Verde Rise uplift (Lancelot, Seibold et al., 1977) and the broad upwarp west of the Canary Islands (Uchupi et al., 1976).

West of about 23°W and north of about 26°N, topography dominates sediment distribution. Sediment ponding is widespread with adjacent sediment ponds at different topographic levels (Fig. 18, A, B, C), but much of the sediment distribution appears to be due to

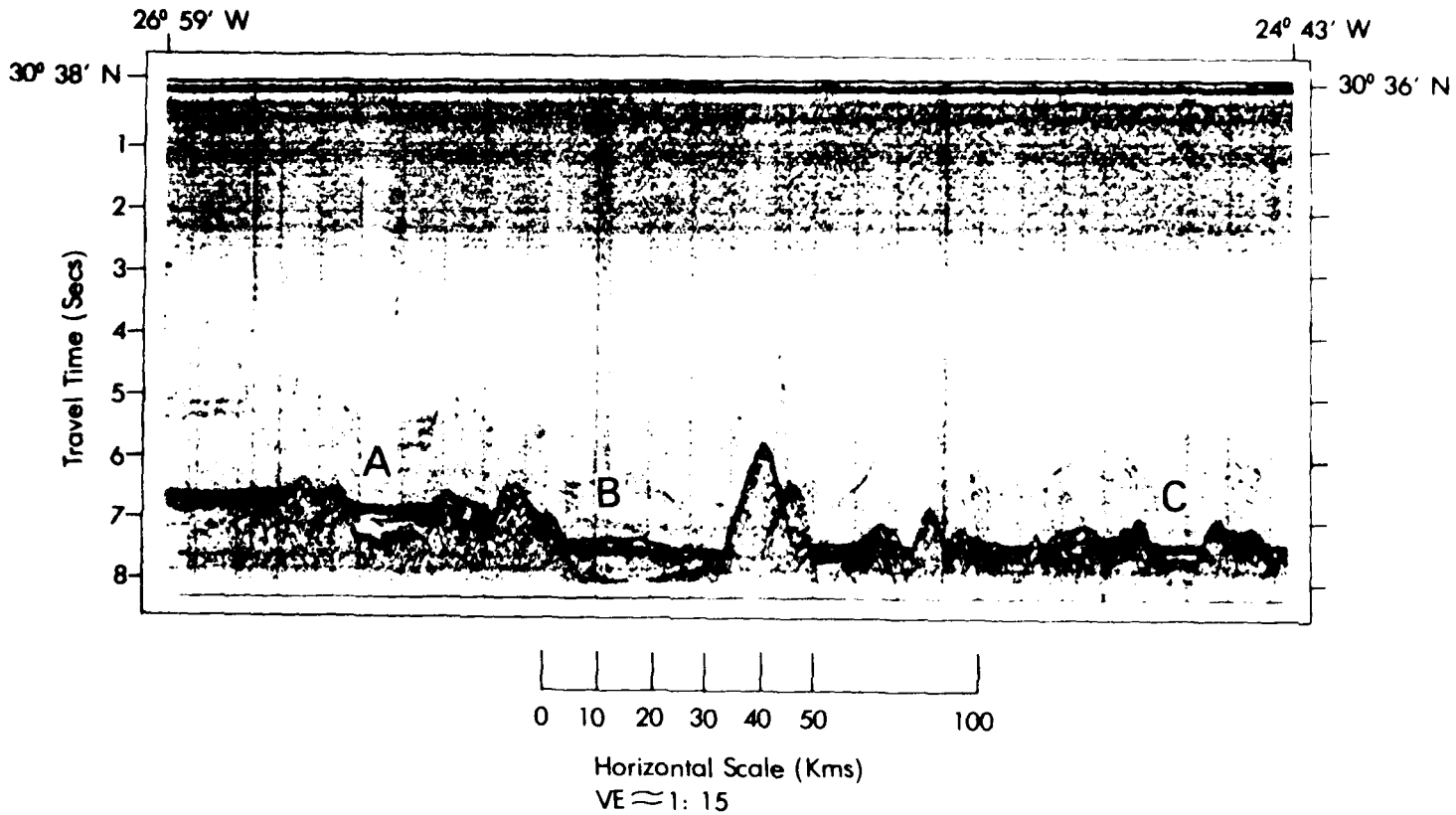

Figure 18. Examples of sediment ponding in the Cape Verde/Canary Basin. The different levels of ponds A and B suggest that B is a recent graben or the abyss. hill between A and B and the abyssal hills east of B are linear ridges capable of blocking sed' 'ent movement.

filling between basement highs and subsequent faulting that produced the present ponded appearance. Sediments in the ponds are about 200-400 m thicker than those in the intervening areas (Plate III). North of 26°N, several sediment ponds have linear, nearly E-W trends. These depocenters appear to coincide with fracture zones. Sediment thickness in these fracture zones average 200-400 m greater than thickness in non-fractured areas (Plate III).

Ewing et al. (1972) and Lowrie et al. (1978) attribute some lineation patterns to redistribution of sediments by northward-flowing contour currents and deposition from suspended nepheloid layers. Although these factors lead to some variations in sediment thickness, an analysis of depositional facies as determined from seismic profiles suggests that these processes, particularly contour current deposition, are too limited in area to be a significant contributor to present depositional patterns. Examination of published bottom photographs (Lowrie and Escowitz, 1969) shows a tranquil bottom environment with no apparent current effects visible except around the flanks of seamounts.

Ewing et al. (1972) suggest that aeolian transport of terrigenous material derived from the North African deserts and increased biologic productivity associated with coastal upwelling are significant contributors to the total sediment column. The major sources of sediments presently being deposited in the lee of the Cape Verde Pedestal are erosion of volcanic rocks of the islands, transportation and redeposition of shelf sediments, open ocean planktonic sedimentation, and windblown volcanic ash and dust (Rothe, 1973). Seibold and Hinz (1974) report that up to three-fourths of Quarternary sediment layers on the shelf and slope east of the Canary Islands consist of plankton, but that the shelf and slope east of the Cape Verde Islands are being built with only 10-20% carbonate content.

C. Seismic Stratigraphy

1. Instrumentation Background

Normal incidence marine seismic reflection records are three-dimensional (apparent position, reflection time, and relative amplitude) presentations of two-dimensional (thickness or time and continuity or space) information bearing some similarity to geologic cross-sections. Record abscissas show time measured in minutes and hours. Time can be converted to geographic position when combined with navigation records. The ordinate is time measured in seconds, which can be used to represent vertical distance below sea level when corrected for velocity variations and gradients in the sediments and the overlying water column, and when reflections from dipping interfaces are corrected for horizontal offsets of the reflection point (Appendix).

The gray tones of variable density seismic reflection records are qualitative measures of the intensities of the reflected signals and noises and represent the Z-axis in a three-dimensional presentation. According to manufacturers, the white to black spectrum of variable density recording paper is equivalent to 23 db dynamic range. Tone patterns that reflected signals of varying intensities create can be related to the underlying geologic regime.

As discussed in the Appendix, the geologic data presented on seismic records are interspersed with noises that are complex functions of the instruments used, environmental noises at the time data were collected, and peculiarities in the reflectivity of the geologic section being traversed. Bubble pulse generated noise obscures subtle details of the geology and is the most severe instrumental limitation to the interpretation of analog-processed, single-channel data. Bubble pulses on filmed record copies can be identified from source and receiver geometry, but can only be removed by deconvolution of magnetic tape recorded digital data.

2. Relationship Between Geology and Reflection Patterns

Intensity of the reflected wave or signal amplitude is the measured quantity that is presented as the Z-axis of marine normal incidence seismic reflection records. Amplitude of the reflected signals is directly related to acoustic impedance, which is the product of the density-velocity relationship and a continous function of the geologic column (Appendix).

Density and velocity in unconsolidated marine sediments are controlled by complex variations in porosity, grain size, composition, shape and sorting, packing, degree of induration, and fluid saturation. These sediment properties vary in both horizontal and vertical directions. The distribution of these properties establishes a relationship between acoustic stratification and geology of the traversed area.

Relative signal reflection amplitude, reflection continuity and abundance, and reflection configuration can be readily determined from seismic reflection records. These records can be qualitatively related to such lithologic factors as lateral variation in gross lithology, velocity-density contrast, and fluid content. Stratigraphic factors that can be inferred from reflection records are bed thickness and spacing, bedding continuity, depositional process, sediment source direction, and subsidence, uplift, and erosion in the depositional environment. Because the influence of each of these properties cannot be independently evaluated, seismic reflections cannot always be related to rock interfaces or to abrupt changes in lithology. Seismic profiles must be correlated with coring data to quantify geologic relationships.

Particular patterns of reflected energy can be related to particular seismic stratigraphic facies. A seismic-stratigraphic facies is a three-dimensional, areally definable unit with a unique and identifiable reflection pattern, amplitude, continuity, frequency, and interval velocity (Sangree and Widmier, 1977). Seismic-stratigraphic facies are mappable information.

3. Reflection Patterns in Deep Ocean Environments

Figures 19 and 20 illustrate classifications of reflection patterns and seismic-stratigraphic facies for deep water clastic sediments. These classifications, modified from Sangree and Widmier (1977), are limited to those reflection configurations likely to be observed on single-channel seismic records from ocean basins and adjacent continental margins.

(a) Non-Stratified Reflection Patterns: Figure 20 defines three classes of non-stratified reflectors. Acoustically transparent reflector patterns (Fig. 13-A) do not reflect significant amounts of the particular wavelength seismic energy transiting the section, while acoustically opaque reflection patterns (Fig. 13-D) indicate that most of the incident seismic energy has been reflected or scattered. The terms 'acoustically transparent' and 'opaque' used in describing seismic reflectors are qualitative adaptions from optics and have no precise geologic meaning. Also, the earth acts as a low-pass filter and selectively reflects higher seismic frequencies with increasing depth in the sedimentary section; thus a buried transparent reflection configuration may be both geologically and geophysically different from a surface acoustically transparent zone.

A variation of an acoustically transparent pattern is a zone without coherent internal reflectors, but with energy returns well above the background noise level (Fig. 21-2). Sangree and Widmier (1977) label such sequences as 'chaotic' reflection patterns and attribute them to post-depositional disturbances, such as bioturbation, slumping, and current erosional/depositional scars, that produce diffractions, discontinous layering, and internal contortions. Chaotic

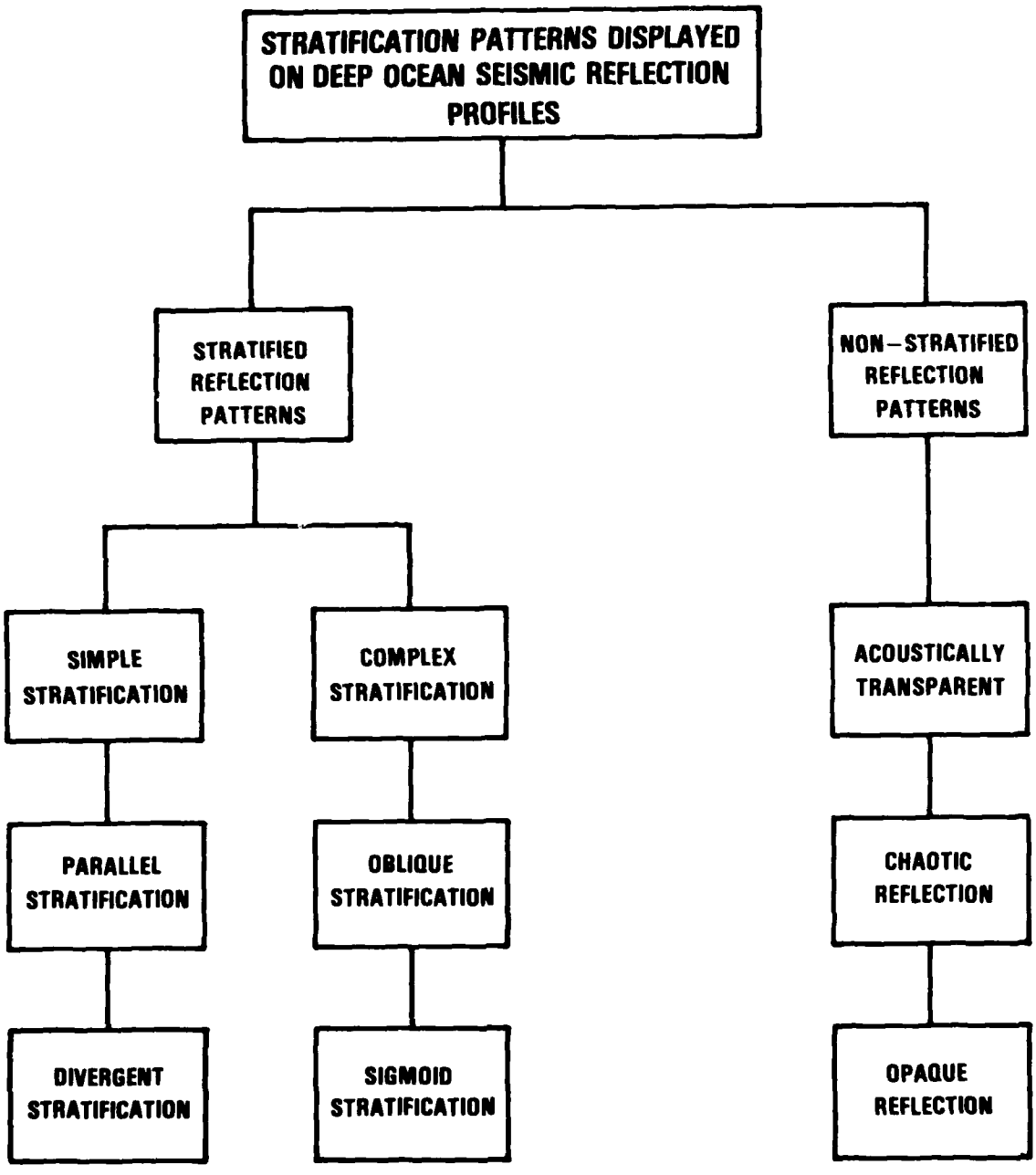

Figure 19. Classification of reflection patterns from deep ocean seismic reflection profiles. See text for definitions and Figures 13, 21, 22, and 25 for examples. (Adapted from shallow water seismic reflection patterns defined by Sangree and Widmier (1977).)

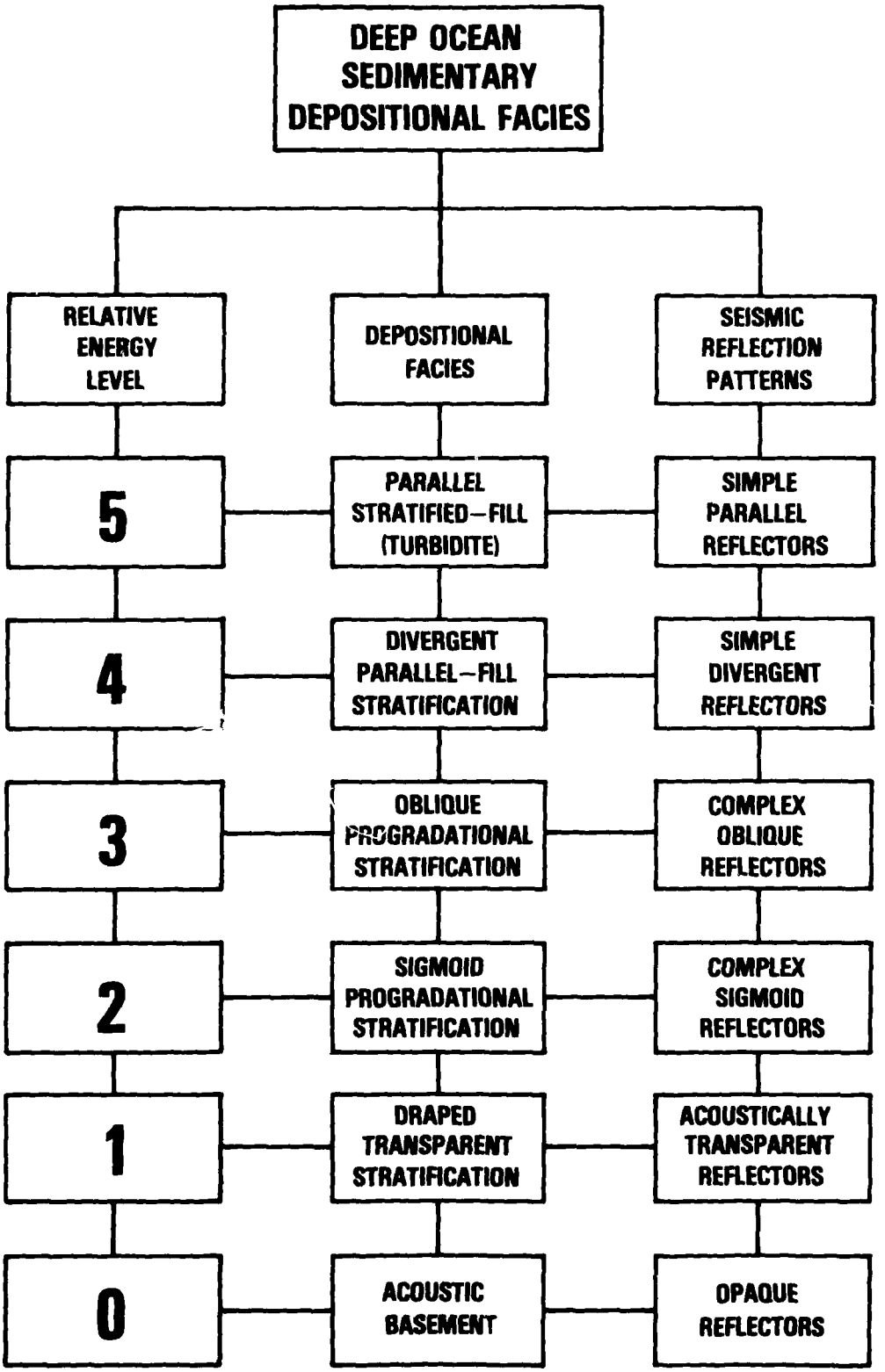

Figure 20. Classification of deep ocean seismic-stratigraphic facies.

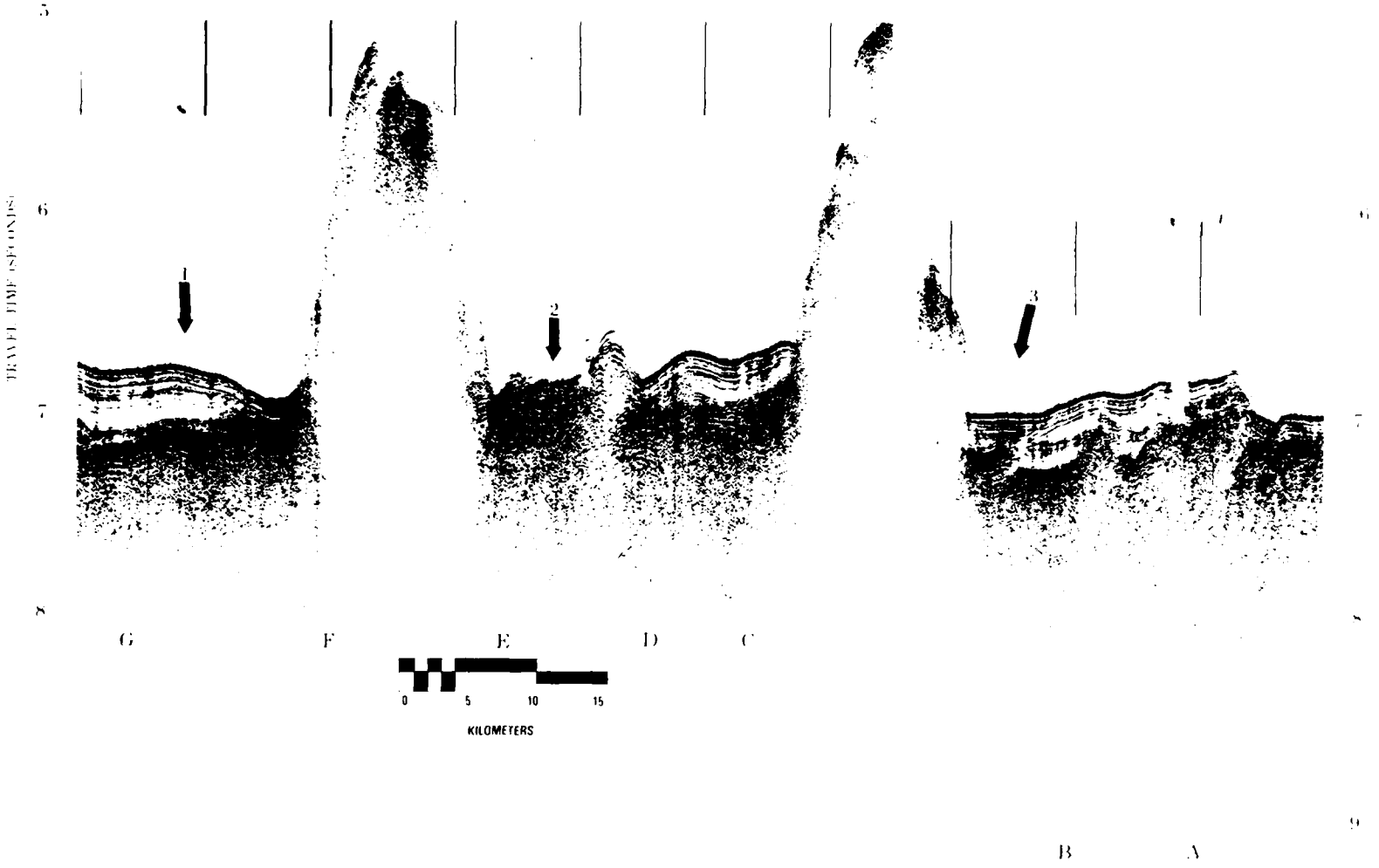

Figure 21. Examples of Stratification Patterns. 1) Sigmoid Stratification Pattern. This sequence grades into other types of stratified reflection patterns. 2) Chaotic Reflection Pattern. 3) Parallel Stratification. Figure illustrates two crossings of KANE seamount.

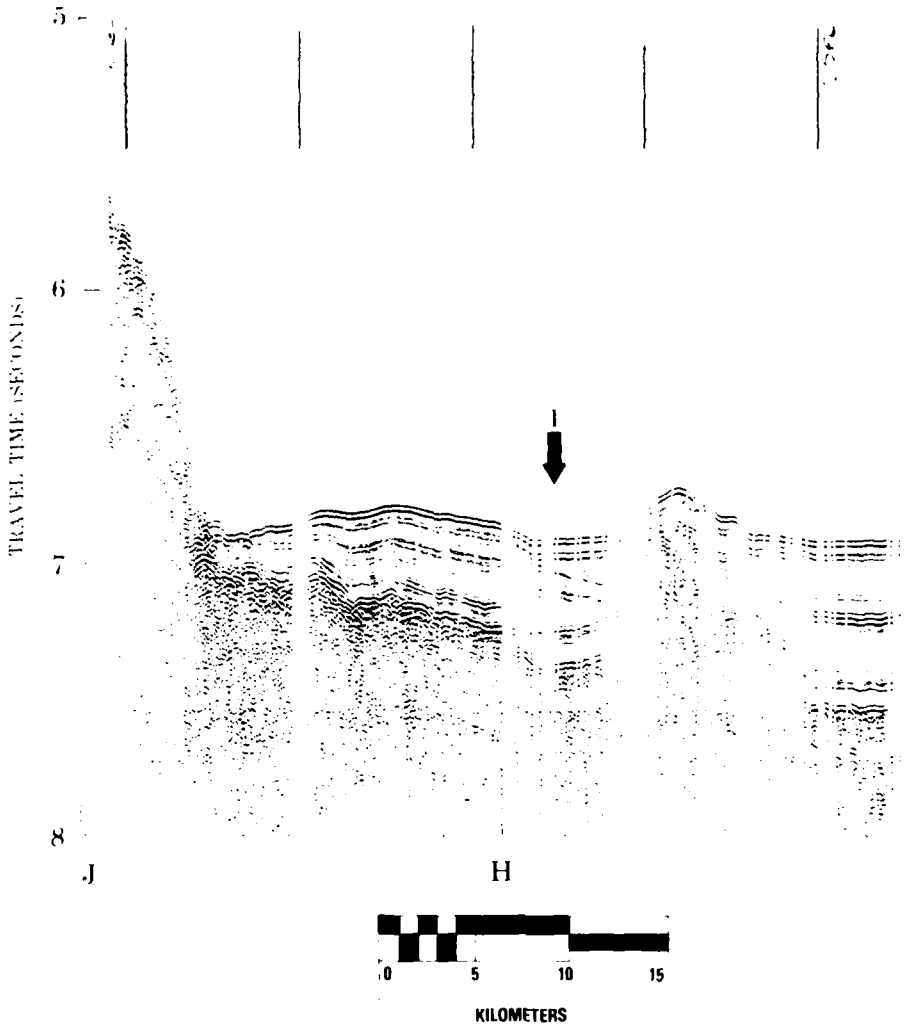

Figure 22. Divergent Reflection Stratification Pattern.

reflection patterns are usually associated with more energy intensive depositional processes or with some post-depositional tectonic activity that has altered original layering.

Acoustically transparent reflection patterns in the deep ocean tend to represent pelagic, fine-grained lithologically homogenous, low energy deposits. These reflectors commonly drape over existing basement topography like a sheet and frequently show a surface that is simply smoothed basement relief. Continuity and amplitude of surface reflections are high, but scattered internal reflectors are weak and discontinuous, suggesting dewatering of sediments, restrictive distribution by bottom currents, or local slumping. A secondary cause of acoustic transparency, particularly near the bottom of a thick section, may be attenuation of the higher frequencies resulting in long wavelength, low frequency energy incapable of resolving thin layering (Appendix).

Opaque reflecting zones are high amplitude, unstratified reflectors generally called 'acoustic basement' that are assumed to represent the surface on which the sedimentary section is deposited. High amplitudes and reverberation levels screen deeper reflectors. However, recent multichannel seismic profiles have resolved gross layering in 'acoustic basement' (Watkins, Pers. Comm., 1979). Opaque reflection patterns can be subdivided into those reflectors with a relatively smooth upper surface, typical of sills and laccoliths (Fig. 13-E) and reflectors with a rugged upper surface suggesting extrusive volcanism (Fig. 13-D).

(b) Stratified Reflection Patterns: Stratified reflection patterns are generated by alternating successions of high and low reflection amplitude sediments deposited on parallel or subparallel interfaces. The nomenclature of Sangree and Widmier (1977) permits stratified patterns to be subdivided into simple and complex types. This distinction is based on the reflective surfaces's relationship to underlying layers, and the energy of deposition.

Simple parallel and simple divergent stratification patterns are characterized by uniform reflection amplitudes probably related to repetitive depositional energy levels. Simple reflection patterns (Fig. 21-3) indicate uniform rates of sediment accumulation, and cyclic repetition of sediment inputs on a stable or uniformly subsiding surface. On the other hand, divergent stratification patterns (Fig. 22) imply variations in the rate of deposition, progressive tilting of the depositional surface, variations in the inputs of detrital and pelagic sediments or a combination of all these factors (Sangree and Widmier, 1977).

As reflection amplitudes decrease both the proportion of coarse detritus and the energy of deposition decrease. Intermediate amplitude parallel to gently divergent stratification configurations on the lower continental rise are correlated with deep marine hemipelagic clays and oozes commonly interbedded with coarse silts deposited from the distal portions of low velocity turbidity currents or deep water, bottom contour following currents (Sangree and Widmier, 1977). Simple parallel stratification patterns, commonly associated with abyssal plains, are alterations of turbidite sequences and pelagic clays. Deposits of these types suggest periods of high energy sedimentation interspersed with periods of low energy sedimentation. The numerous shallow channels incised into the lower continental rise are probably scars left by turbidity current erosion as well as channels for guiding turbidity currents to the abyssal plain floor.

Complex stratification patterns are indicative of the relationship between sedimentation rates, subsidence rates, and system energy levels. Oblique reflections (Fig. 7-I) suggest the outbuilding from a common upper depositional surface such as might occur during the formation of a delta or deposition

and outbuilding along an insular or continental shelf. On the other hand, the sigmoid reflection pattern, which forms a gentle S-shaped pattern from shallow to deep water shows progradation from a major sediment source. The gentle dips of sigmoid reflection patterns imply that progradation exceeds subsidence (Fig. 7-II). Both sigmoid and oblique reflection patterns, when found in an ocean basin, are typically composed of fine-grained pelagic sediments interspersed with fine-grained, suspensed load, detrital sediments.

(c) Boundary Reflection Patterns: The upper and lower boundaries of seismic reflection sequences frequently make a unique statement about the depositional history of that sequence. Sangree and Widmier (1977) recognize three upper boundary configurations and three lower boundary configurations (Fig. 23).

Upper and lower concordant boundaries are most frequently associated with simple parallel and divergent reflection patterns. Seismic reflections of these types typically represent marine clays and oozes deposited by low-energy currents, although high speed intermittent currents may deposit sediments with concordant boundaries. Onlap and downlap boundary types are also associated with low energy deep ocean deposits such as oozes, marls, clays, and low velocity turbidity current deposits.

Seismic stratigraphic facies with a toplap upper boundary is frequently found in association with deltaic deposits or deep ocean deposits associated with strong currents. Erosional truncation boundaries in deep ocean sedimentary sequences are found in the vicinity of seamounts, where distributary channels cross the continental slope and rise, and where deep ocean currents impinge on the sea floor (Sangree and Widmier, 1977).

D. Seismic Stratigraphic Facies Distribution

Relative system energy levels suggest five marine stratigraphic facies in the Cape Verde/Canary Basin. Four facies can be mapped (Fig. 24).

Oblique progradational facies is best developed along the upper continental and insular rises and around seamounts. The slightly concave upper surface of the sequence indicates sufficient system energy for some portion of the sediment load to bypass the nearest available depositional site. Oblique progradational facies may also be found around basin floor seamounts where deposits are formed by the deceleration of bottom currents downstream from an obstruction (Lowrie et al., 1978).

Sigmoid progradational facies occurs during a stable lower continental rise gradually encrouching upon an abyssal floor. Sigmoid progradational facies covers the majority of the mapped area (Fig. 24). This distribution implies that the Cape Verde/Canary Basin is tectonically stable and/or that the supply of sediment exceeds the rate of downwarping. The gentle S-shaped surface of the sigmoid progradational facies suggests that the system energy is insufficient to transport the majority of the sediments beyond the closest depositional site.

The divergent parallel-fill stratification facies (Fig. 20) is the result of sediment being rapidly dumped into a basement or topographic depression. In the Cape Verde/Canary Basin, this facies is not mapped because it usually occurs beneath the parallel stratified-fill turbidite facies mapped as the abyssal floor facies in Figure 24. Both facies suggest episodic influxes of sediments under the influence of excess motive force.

The draped acoustically transparent facies (Fig. 13-A) indicates a low energy environment with a much higher proportion of pelagic sediments than

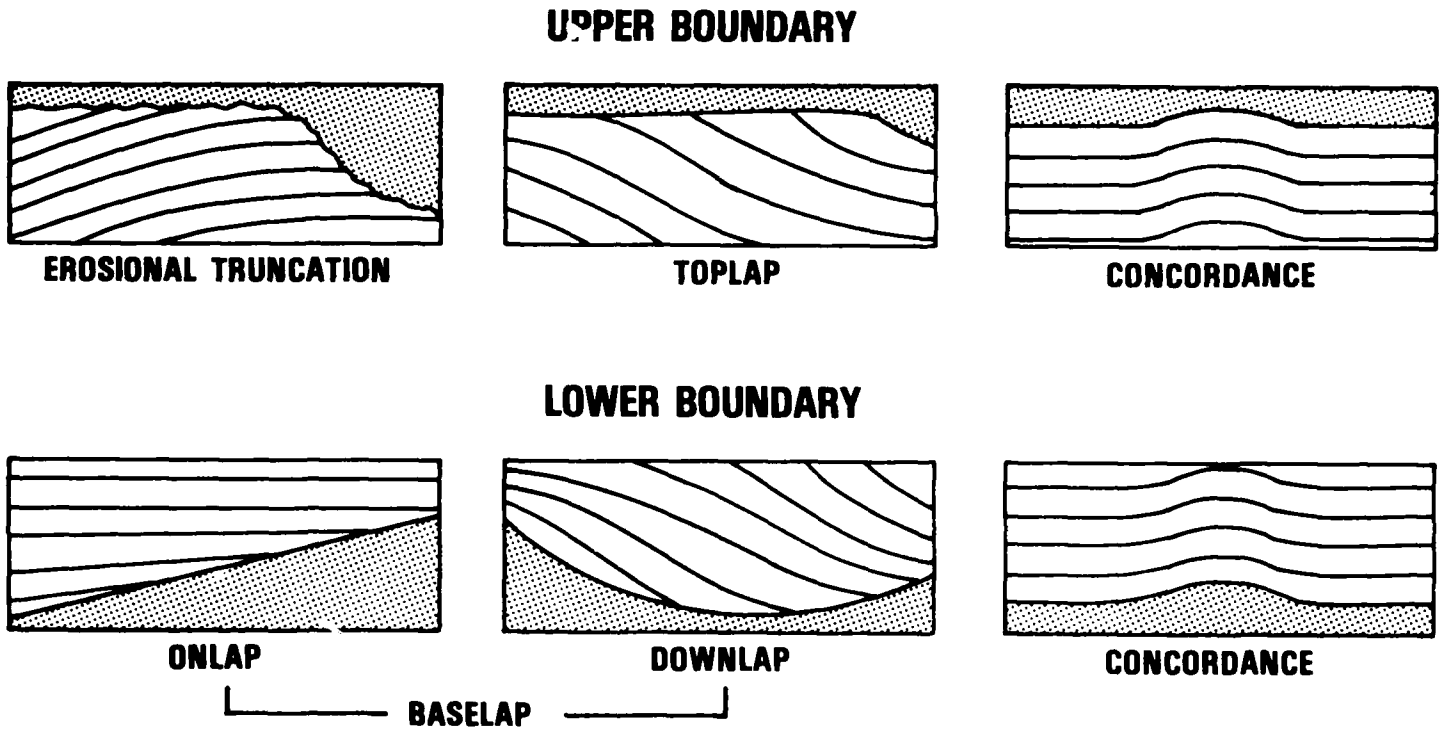

Figure 23. Upper and Lower Seismic Reflection Boundaries. (From Sangree and Widmier, 1977). Examples of downlap (Fig. 22), onlap (Fig. 25), erosional truncation (Figs. 21 and 13), and concordance (Fig. 7), boundaries are illustrated.

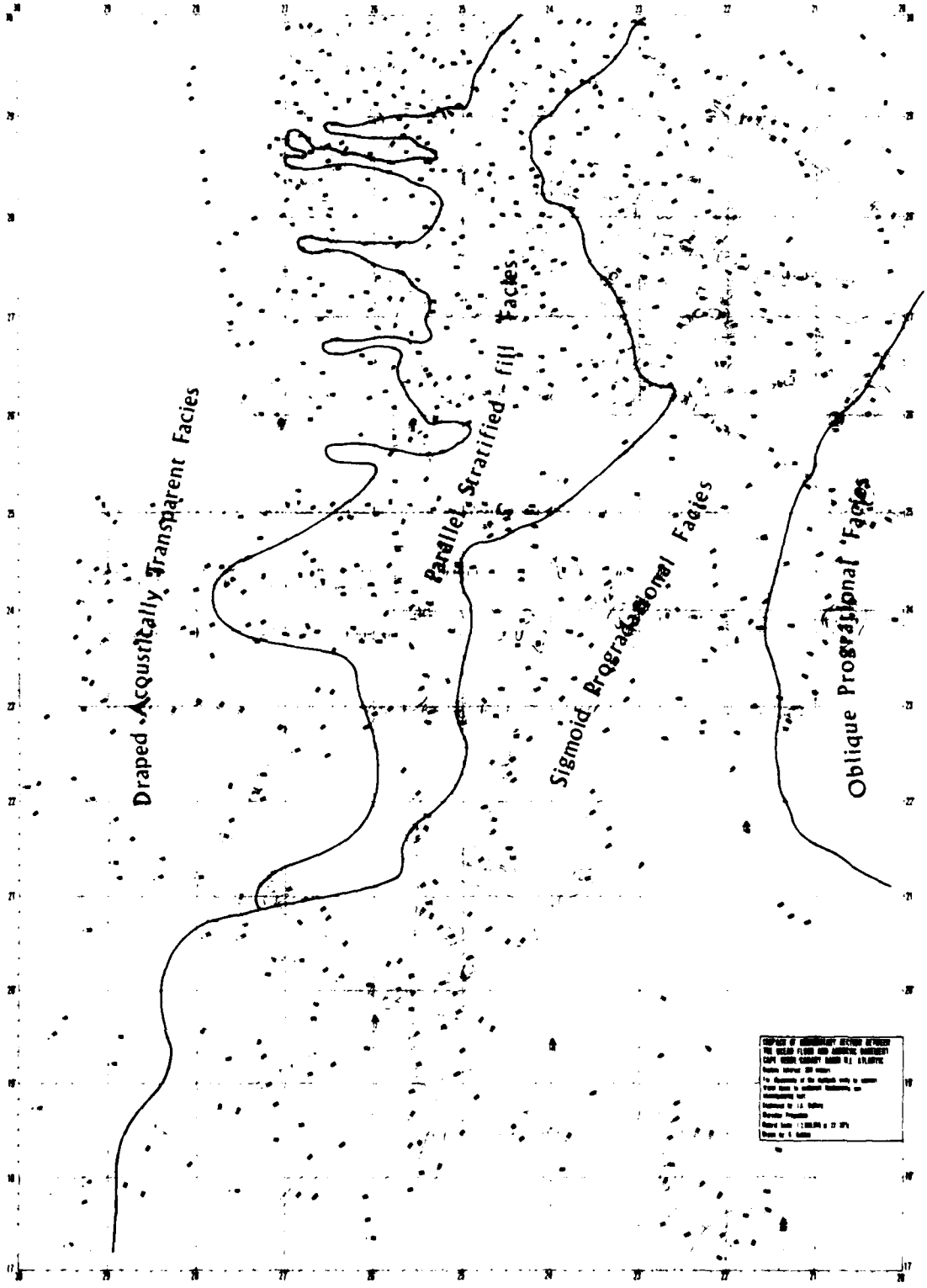

Figure 24. Seismic-stratigraphic Facies Map Cape Verde/Canary Basin. The boundaries between facies are transitional. See Figures 13, 21, and 22 for examples of facies types.

other seismic-stratigraphic facies. The uniform blanketing of basement topography defines relative regional stability, and a uniform rate of sediment supply without bottom currents capable of influencing sediment deposition. The paucity of internal reflectors implies that the sediment transportation system has insufficient energy to bring coarser grained material into the depositional area, that porosity is uniformly high, and that sediment dewatering has not produced areas of increased lithfication and greater density.

E. Regional Reflection Correlations

Lithologies and an unconformity from DSDP sites correlated with four seismic reflection events in the Cape Verde/ Canary Basin and Rise, and adjacent continental rise (Fig. 25). Seibold and Hinz (1974) labelled the lowermost reflector D1, the intermediate reflector A, and the uppermost reflector D2. An unconformity formed on Upper Eocene sediments is identified at DSDP Sites 12 and 140 on the Cape Verde Rise, and 368 and 369 along the Continental Rise (Uchupi et al., 1976). These reflectors can be traced over large parts of the Cape Verde/Canary Basin.

Reflector D1 (Seibold and Hinz, 1974) correlates with black carbonaceous shales 945 m deep in DSDP hole 368. These Upper Cretaceous (Albian (?) -- Turonian) shales are interbedded with Miocene age diabase sills (Lancelot, Seibold et al., 1977).

The characteristic acoustic signature of D1 is identifiable beneath about one kilometer of sediment along the Lower Continental Rise west of Senegal. D1 is unwarped about 500-600 m, in concordance with the entire sedimentary section, across the northern Cape Verde Rise. This change in elevation is probably due to Middle Tertiary uplifting of the Cape Verde Rise.

D1 becomes indistinguishable among the high amplitude reflectors on the crest of the Cape Verde Rise; but a similar reflector in a similar stratigraphic position can be identified beneath the more transparent sediments on the western slope of the rise. West of the Rise, the D1-type reflector can be correlated from profile to profile as far west as about 28°W and as far north as about 25°30°N. About 25 km south of DSDP Site 138, the D1-type reflector pinches out against a small basement rise.

At Site 138, cherty, pyritiferous, carbonaceous black mud occurs between depths of 400-435 m. This lithologic unit is dated as Late Early (Cenomanian) Cretaceous (Hayes, Pimm et al., 1972). At Site 137, about 130 km west of Site 138, nannomarl and chalk oozes containing pyrite and chert occur between 257-275 m depths. This unit is also dated as Cenomanian by Hayes, Pimm et al. (1972). Lithologic and seismic similarities, and stratigraphic position are evidence of correlativity between D1 and the similar reflector seen on the seismic profiles (Fig. 25).

On another seismic section between Dakar and the Cape Verde Pedestal, D1 occurs as a horizontal reflector at a depth of 5.6 sec below sea level. About 100 km east of the islands, D1 abruptly slopes westward beneath the Pedestal, at a gradient of about 1/100, to a depth of 6.6 sec. The abrupt downwarping of D1 is likely caused by isostatic loading imposed on the crust by the Cape Verde Islands and provides an upper limit for the age of the Cape Verde Islands.

Lancelot, Seibold et al. (1977) believe that the carbonaceous shales of reflector D1 are indicative of Middle to Late Cretaceous anoxic environments in deep parts of the North American Basin. If anoxic conditions existed at that time, the entire east central North Atlantic Basin would have been affected.

Horizon A is a Middle to Upper Eocene chert sequence usually interspersed with zeolitic clays and altered volcanic debris (Uchupi et al., 1976). In the Cape Verde/Canary Basin, Horizon A lies 0.4 to 0.6 sec above reflector D1 (Lancelot, Seobold et al., 1972, and Fig. 25).

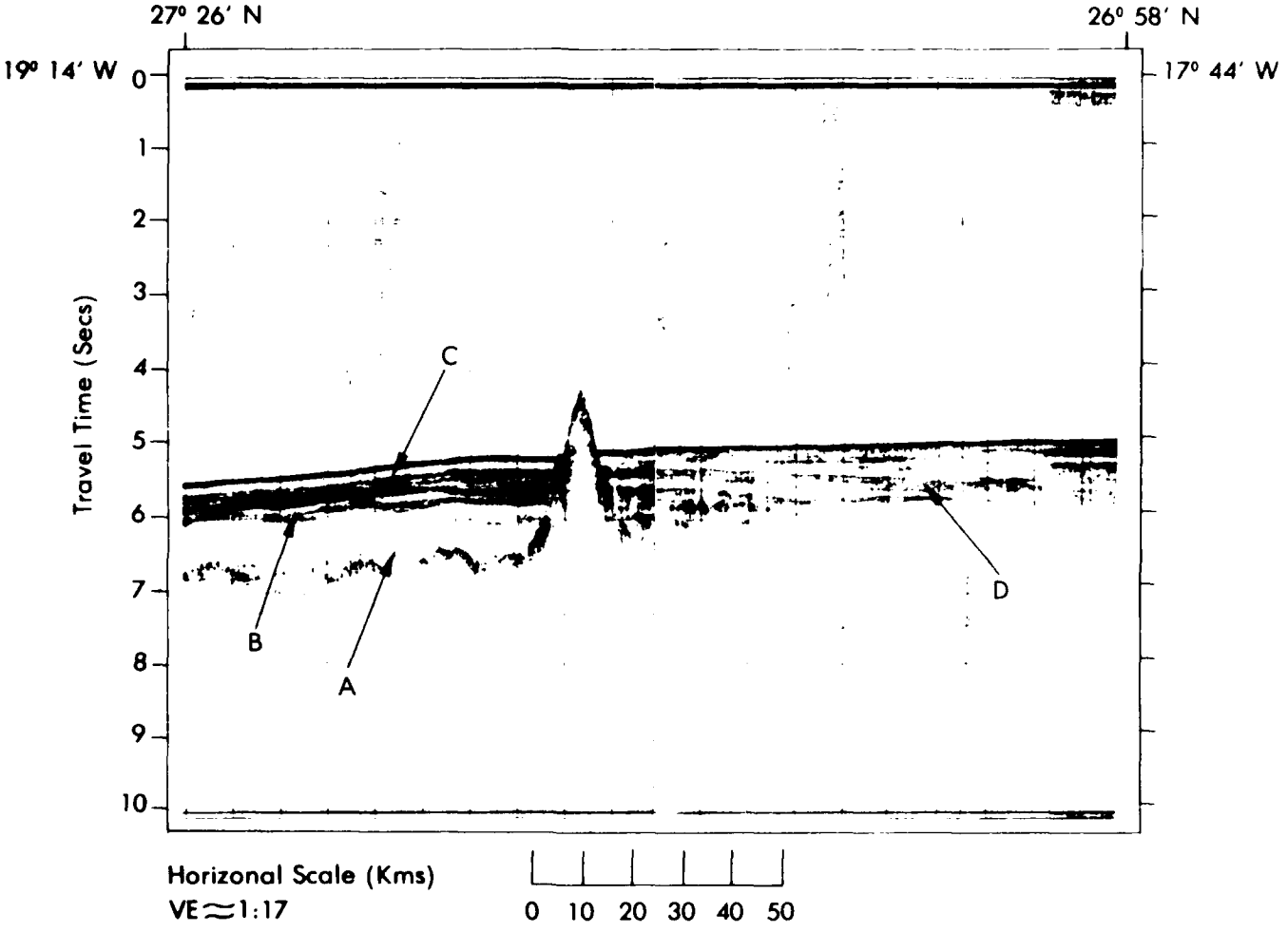

Figure 25. Correlatable Reflection Events in the Cape Verde/Canary Basin. Points A and C indicate reflectors D1 and D2 of Seibold and Hinz (1974) traced from type sections on the continental slope west of Senegal. Point B is Horizon A, and Point D is a Pre-Miocene unconformity that probably correlates with Upper Eocene unconformities detected at several DSDP drill sites.

On the Cape Verde Rise, a multi-layered, variable amplitude reflector 0.6 sec above and conformable with D1 can be traced on various profiles to a Middle Eocene clay in DSDP Hole 140. Similar reflectors can be located at appropriate depths in numerous seismic sections (Fig. 25) and possibly correlated with sediments identified as Horizon A in DSDP Holes 137, 138, 141 (Hayes, Pimm et al., 1972) and 12 (Peterson et al., 1970). In my opinion, Horizon A is not acoustically defined with sufficient clarity to be correlated with the confidence shown by Uchupi et al. (1976).

D2 is the uppermost reflector defined by Seibold and Hinz (1974). D2 correlates with the Middle Miocene transition from carbonate-poor sediments to nannofossil marls and oozes identified in DSDP Holes 140, 141, and 368 (Uchupi et al., 1976). D2 is difficult to correlate from one seismic section to another because of interference from numerous high amplitude reflectors in the upper 200 m of the section.

An angular unconformity, stratigraphically similar to the unconformity detected at several DSDP sites, can be identified on reflection profiles crossing seamounts located at about 17°N, 22°W; 25°50'N, 19°30'W; and 27°N, 17°30'W. These seamounts are flanked by thick sedimentary sections of simple parallel to slightly divergent reflectors with concordant boundaries. The seamount at 27°N, 17°30'W is the example illustrated in Figure 25.

Figure 25 shows an angular unconformity sloping toward the Continental Rise with a gradient of about 1/230. Overlying parallel reflectors onlap the unconformity that lies between the surface and a nearly horizontal reflector that may be equivalent to Horizon A. Sediments overlying the unconformity are between 300 and 450 m thick. At sedimentation rates of 27 m/my for the most recent 2 myBP and about 10 m/my for the remainder of Neogene time (Lancelot, Seibold et al., 1977), 300 m of sediments would be deposited in about 27 my or since Late Oligocene. The Pre-Miocene age for this unconformity is compatible with age estimates for the unconformity detected at DSDP sites on the Cape Verde and Continental Rises, and for an unconformity east of the Canary Islands mapped by Watkins and Hoppe (1979).

VI. Discussion and Conclusions

During the past two decades, history and development of passive Atlantic continental margins have become thoroughly documented. However, studies of tectonic features in the deep ocean basins seaward of passive margins, particularly the central Northeast Atlantic, have lagged. The prevalence of low energy sedimentation regimes and the historical paucity of earthquakes illustrate the present state of crustal stability. Nevertheless, long continued volcanism, widespread unconformities, complex relationships between fracture zones and vertical faults, and the variability of magnetic anomaly patterns testify to a rich and varied tectonic history. Thus, the purpose of this section is to fit observational data into a tectonic framework and gain some insight into the geologic development of the Cape Verde/ Canary Basin.

Seismic-stratigraphic facies distribution indicates that the Cape Verde/ Canary Basin has been a relatively stable deep water area in recent times. The widespread distribution of low energy progradational facies (Fig. 25) suggests that progradation is a major growth form for the insular and continental rises. The distribution of draped, acoustically transparent facies shows that large areas are beyond the reach of turbidity current or sheet flow sedimentation. Turbidite deposition is expanding abyssal plains by encroaching on abyssal hills (Fig. 24). Localization of chaotic reflection patterns (Fig. 21) implies that current controlled sedimentation is areally inconsequential at present. Slumps, creep and other forms of mass wasting are significant depositional processes (Egloff, 1973; Embley et al., 1978). Watkins and Hoppe (1979)

confirm that gravity sliding and debris and turbidite flows are common off the Atlantic margin of northwest Africa and suggest that similar mechanisms may account for widespread Oligocene and Miocene unconformities.

Before the present sedimentation regime obtained, two phases of tectonism controlled the distribution of sediments in the Cape Verde/Canary Basin. The first phase began concurrently with the formation of sea floor at the Mid-Atlantic Ridge and reflects sea floor subsidence to regional base levels. The second tectonic phase involved epeirogenic uplift of the Cape Verde and Canary Rises, the initiation of volcanism that led to formation of the Islands, faulting and diapirism. Each phase produced a distinct impact on sedimentation and seismic reflection character.

Basin DSDP Sites 137 and 138, and others nearby, penetrated Lower and Middle Cretaceous carbonate sediments formed when sea floor was above the carbonate compensation depth. Subsequent subsidence below the carbonate compensation depth caused deep sea clays with siliceous fossils to replace carbonates as the dominant sediment. This sedimentation pattern accounts for the acoustic transparent zone overlying acoustic basement (Fig. 13-C).

Carbonaceous black shales, described from DSDP Site 368, indicates stable, stagnant conditions during Aptian-Turonian time (Lancelot, Seibold et al., 1977). Cenomanian age reflector D1 has been traced from the shelf of the edge of the Cape Verde Rise (Seibold and Hinz, 1974), although Wissman (1979) doubts that shelf and slope reflectors can be continued to the Continental Rise. A reflector occupying a similar stratigraphic position to D1 (Fig. 25) can be traced from the lower Rise near DSDP Site 368, possibly as far west as 27°W. The distribution of D1 indicates anoxic conditions and basin wide stability during part of Late Cretaceous.

Changes in sea floor spreading rates may have caused oceanic stagnation. P. R. Vogt (Pers. Comm., 1979) believes that spatial constraints require a significant increase in sea floor spreading rates beginning near the end of M-sequence time, although on topographic evidence (Plate II) a spreading rate increase does not appear justified. Hays and Pitman (1973) show that increasing spreading rates are accompanied by increasing cross-sectional areas of mid-ocean ridges and increasing ridge volume could cause sea level transgressions, as occurred around the North Atlantic in Late Cretaceous. Because ridge expansion would change circulation patterns, there may have been a short but important interval of stagnation as one regime of deep circulation was replaced by another (Hays and Pitman, 1973).

The epeirogenic uplifting phase of tectonic development was superimposed on the sea floor subsidence phase during Early Tertiary. Regional unwarp of the Cape Verde Rise lifted the area south of about 21°N and increased the deposition of clastics relative to other sediments, as shown by core logs from DSDP Sites 12, 140, and 368.

Seismic profiles and logs from DSDP Sites 12 and 368 indicate that Eocene sediments thin across the Cape Verde Rise, although the record is incomplete because an Eocene unconformity marks the top of the section. A similar situation obtains from the Canary Rise where Watkins and Hoppe (1979) show that Eocene age sediments thin over the crest of the arch because uplift began prior to deposition. These results are compatible with radiometric ages obtained by Grunau et al. (1975) from the Canary and Cape Verde Islands and geologic mapping by Bebiano (1932) who dated the earliest sills on Maio as Eocene. Other evidence for dating the beginning of regional tectonism as Eocene include unconformities around seamounts (Fig. 25) and volcanism as indicated by zeolites in core samples.

Bond (1977) analyzed African marine transgressions relative to North and South American and European sea level stands. He concluded that Africa was epeirogenically uplifted, rather than the older continents subsiding, after Micoene, and, possibly, before Miocene. These events were concurrent with Cape Verde and Canary Rise uplifting and generated relative, and probably absolute, downwarping along the continental margin and in the basin between the rises.

Sarnthein (1977) examined sand fractions from central Northeastern Atlantic DSDP cores in terms of provenance and depositional environments. In order for the observational data to fit the geologic model, he concluded that the area between 14°N and 20°N was shifted northward by 6 to 7 degrees of latitude between Early Miocene and Pleistocene. This conclusion is compatible with the LePichon et al. (1973) view that all plates have moved toward the North Pole since the Cretaceous.

Jurassic volcanism has been reported (Machado, Azeredo Leme, and Manjardino, 1967, quoted in Dillon and Sougy, 1974) from the Cape Verde Islands. Seismic profiles show Cenomanian age reflector D1 downwarped by the weight of the Cape Verde Pedestal east of the islands and uplifted across the northern part of the Rise. The oldest unconformity detectable on seismic profiles is Eocene, implying that the Pre-Cretaceous uplift and volcanism was not a significant factor in the development of the islands.

Volcanism began in the Cape Verde Islands during Oligocene (Bebiano, 1932). Absent or condensed Oligocene sections in Cape Verde Rise DSDP drill holes support the evidence that regional upwarping preceded volcanism. The major phase of volcanism began during Miocene (Dillon and Sougy, 1974). Radiometric dating indicates that sills and dikes were emplaced on the islands and in the basins at this time (Grunau et al., 1975; Lancelot, Seibold et al., 1977). Diapirs may have been related to this phase of volcanism.

Although the Cape Verde/Canary Basin is located on Cretaceous and Late Jurassic crust (Fig. 17), analyses of magnetic anomaly patterns produce ambiguities in understanding tectonic development. The Jurassic 'Quiet Zone'/M-Sequence boundary is an expression of a major tectonic event. The Jurassic sea level transgression, which reached a maximum during Oxfordian time, could relate to this boundary (Hallam, 1971), but the data lack the resolution to support or refute this hypothesis.

M-sequence anomalies parallel the African Continental Rise. Magnetic profiles shown in Figures 15 and 16 suggest that fracture zones did not appear in the central Northeastern Atlantic until near the end of M-sequence time and that they are confined to late Early Cretaceous and younger sea floor. There is no evidence for the numerous fracture zones offsetting the M-sequence as shown by several authors (Rona and Fleming, 1973; Hayes and Rabinowitz, 1975; Uchupi et al., 1976). Vogt and Einwich (1979) and Vogt (Pers. Comm., 1979) note that few M-sequence fracture zones are found in the Western North Atlantic and that major fracturing did not begin in the Western Atlantic until very late in M-sequence time.

Eastern North Atlantic magnetic anomalies formed during early Late Cretaceous and afterward have unusually large and irregular amplitudes and wavelengths (Fig. 15). These anomalies cannot be correlated and, therefore, provide only negative evidence of the tectonic history.

Events that created the present form of the Cape Verde/Canary Basin began in the upper part of the Early Cretaceous (Aptian). The high amplitude 'J' Anomaly indicates changes in the form in which ocean crust was being generated. This change probably was a response to sea floor spreading rate increases and the beginning of volume changes in the Mid-Atlantic Ridge. Ridge expansion and contraction is likely responsible for Late Cretaceous sea level transgression and Early Tertiary regression.

Late Cretaceous uplift of the Cape Verde and Canary Rises has been suggested, but evidence for uplift is ambiguous. Seismic profiles do not show obvious thinning above reflector Dl although reflector Dl is uplifted over the northern part of the Cape Verde Rise. Evidence for widespread Eocene uplift is unequivocal. Volcanism began during Oligocene, expanded during Miocene, and continues to the present. Pre-Tertiary volcanism, although possible, did not make an impact on sedimentation as demonstrated by DSDP cores. Miocene epeirogenic uplifting in West Africa accompanied volcanism and uplift on the Cape Verde and Canary Islands and Rises. These vertical movements may have been concurrent with a postulated, 600 km or more, northward lateral movement of the entire African Plate. Table II is a summary of the geologic events that shaped the present form of the Cape Verde/Canary Basin.

The chronology of tectonism is preserved in the geologic record, but evidence for the mechanism producing tectonism of this magnitude is much more subtle and subject to speculation. The island archipelagoes, the boundary seamounts, and the abyssal hills that Jones et al. (1966) believe are volcanoes may be remnants of a 'hot spot' trail (Morgan, 1971; Burke and Wilson, 1972; Wilson, 1973; Vogt, 1974 a,b). For a 'hot spot' to form these features in the order in which they were formed, the 'hot spot' would have to be decoupled from the lithosphere and have moved independently of the lithosphere (Anguita and Hernan, 1975). LePichon and Fox (1971) and Anguita and Hernan (1975) suggest a propagating fracture as the mechanism for the formation of the Canary Islands, but efforts to correlate island volcanism with east-west fracture zones have been unsuccessful.

Turcotte and Oxburgh (1973) offer two alternate explanations to the 'hot spot' and propagating fracture mechanisms for the formation of intraplate structures. In the first case, they note that thermal stresses produced by the cooling of oceanic lithosphere produces tension parallel to the spreading center where the plate was formed. As a result, the stress field will be aligned parallel to magnetic anomalies and perpendicular to fracture zones (Turcotte and Oxburgh, 1973). Based on the trends of the fracture zones between 26°N and 30°N and mapped magnetic anomalies (Plate IV), the direction of thermally generated stresses should be NNE with tensional fracturing oriented NNW, i.e., in the direction of maximum shear or about 45° to magnetic anomaly trends. Small scale faulting (Plate IV) in abyssal hill areas is oriented very nearly parallel to anomaly trends rather than at an acute angle as is expected. In addition, thermal stresses would be maximized shortly after the crustal layer was formed, resulting in fracture zones extending across the M-sequence and grabens in M-sequence crust. The small scale faults are relatively recent events as shown by offsets in both basement and overlying sediments (Fig. 11).

As an alternate mechanism for the development of intraplate structure, Turcotte and Oxburgh (1973) note that stress patterns may be developed in lithosphere by membrane stresses related to sea floor spreading on a non-spherical earth. When a portion of lithosphere that has been created near the equator is shifted poleward, that portion of lithosphere is forced to lengthen its radius of curvature, thus creating tensional stresses along the margins. Membrane stresses are the result of stretching the plate to different radii of curvature. When the thickness of lithosphere is small compared to its area, bending stresses developed by plate movement to a different latitude will be small when compared with membrane stresses. Magnitude of the stresses will be greatest at 45° latitude because the change in the radii of curvature of the earth is a maximum at 45° latitude. Turcotte and Oxburgh (1973) conclude that if the radius of

Table II. Geologic Summary of the Cape Verde/Canary Basin

PLEISTOCENE	Localized uplifts diminishing, progradational growth of continental and insular rises, continuing volcanism.
PLIOCENE	Area above CCD, extensive volcanism in both island groups and possibly in abyssal hill areas.
MIOCENE	Uplifting of northwest Africa and Canary pedestal produces wide-spread unconformities, plate motion develops northward component, wide-spread faulting and emplacement of diapirs and abyssal hills, volcanism continues.
OLIGOCENE	Area largely below CCD, beginning of volcanism and uplifting in the Canary Islands, extensive volcanism in Cape Verde Islands.
EOCENE	Area below CCD, widespread erosional unconformity, regional upwarping of the Cape Verde Rise begins.
PALEOCENE	Stable, deep water basin, continental and pelagic sediments deposited on Cretaceous—Jurassic crust, unimpeded circulation.
L. CRETACEOUS	Basin-wide deposition of black carbonaceous shales (reflector D1), restricted circulation, area below CCD, regional volcanism connected with seamounts and west Africa rather than islands, foram limestones in Fuerteventura and La Palma.
E. CRETACEOUS	Mid ocean ridge volume changes, end of 'M-Sequence' of sea floor spreading anomalies and initiation of Cretaceous 'Quiet Zone' anomalies, area above CCD.
L. JURASSIC	Deep-water sediments containing 'Aptychi' being deposited in area of present Cape Verde Islands, area above CCD, 'M-Sequence' of sea floor spreading anomalies being formed.
E. JURASSIC	End of Jurassic 'Quiet Zone' sequence of geomagnetic anomalies, initial opening of North Atlantic Ocean after period of Late Triassic graben faulting in northeast North America and northwest Africa.

curvature of a circular segment of a spherical shell (large area relative to thickness) is increased, the edge of the shell will undergo tangential stresses, but the center of the shell will be in compression. They also estimate that the magnitude of stresses required to stretch a segment of shell from one radius of curvature to a slightly different radius of curvature is about 5.7×10^9 dynes/cm^2 which is considered adequate to fracture the lithosphere. Magma from the asthenosphere would then rise along cracks through the lithosphere.

Plate motions on a non-spherical earth require finite extensions to relieve membrane stresses, such as the estimated 4.8 km extension of the 36 km wide Rhine graben (Turcotte and Oxburgh, 1973). Grabens, fracture zones, and crustal fracturing leading to broad areas of magmatic extrusions, as well as local volcanism, and highly variable heat flow could be expected as a result of tensional stresses. Compressional stresses cause reverse and thrust faulting and diapirism leading to uplift, subsidence, and local volcanism.

Sykes and Sbar (1974), in their study of intraplate stress distribution, show an earthquake with tensional focal mechanism along the Mid-Atlantic Ridge, west of the study area. These authors also show a thrust fault with compressive focal mechanism on the African Plate south of the Cape Verde Islands. These two examples of intraplate stress distribution fit the membrane stress model postulated by Turcotte and Oxburgh (1973).

Other examples of observational data that fit the membrane stress model include the faults shown in Plate IV which trend north-south, are of relatively recent origin, and appear to cut across fracture zones. In the Northern Hemisphere, a northward plate shift would, according to Turcotte and Oxburgh (1973, create compressional cracks propagating southward. In addition, crustal compression would likely generate stress relief features such as diapirs, abyssal hills, and submarine volcanoes. These factors are characteristic of the Cape Verde/Canary Basin.

Membrane stresses could be generated in response to a northward component of sea floor motion by the African Plate. Observed structures are compatible with compressive membrane stresses. To demonstrate the validity of the membrane stress model or any other proposed model requires the compilation and synthesis of an enormous quantity of data concentrated in a very small area. This step is necessary because many of the previous conclusions about the nature and developmental history of the ocean basins have resulted from probability analyses of widely scattered survey data. Statistical approaches to the determination of local and regional geologic history is of questionable validity because of growing evidence for significant geologic heterogeneity and because of the realization that for each hypothesis proposed, there are observational examples and counter examples.

VII. Appendix. Instrumental and Environmental Limitations to the Interpretation of Single-Channel Seismic Reflection Records

A. Introduction

Normal incidence seismic reflection records are simply graphic displays of the total travel time of sound waves between a sound source, an impedance mismatch within the stratigraphic column, and a receiver. Before these records can be meaningfully related to variations in geological interfaces which they approximate, one must understand the behavior of acoustic energy, the equipment with which it is generated and received, and the environmental effects on the paths that it follows. Therefore, the purpose of this appendix is to describe how the collection of single-channel seismic data may be fitted to a specific objective, and to define limits of accuracy and consistency of essentially qualitative data that are to be used quantitatively. Accordingly, both the basic principles involved, and the operational techniques employed for the two types of sound sources commonly used by oceanographic institutions to collect single-channel seismic data, are outlined.

In order to collect data more applicable to the solution of problems, it is important that equipment and technique be configured for the specific objective. For example, if the operational area consists of a thick section of uniform sediments, and the objective is to delineate the distribution of probable upper Tertiary reflectors, the equipment and technique used would be quite different from those with the goal of mapping "acoustic basement" topography beneath a variable thickness sediment cover. Other factors that should be evaluated before data collection begins are the amount of noise generated by the survey vessel, the towing operation, and the environment.

Once the data are collected, it is necessary to consider the distortions, to both the transmitted and received signals, introduced by instrumentation before desired signals and other periodic events on the seismic record can be separated and the relationship between recorded signals and noises established. Also, compressional wave velocity variations, ray path and reflecting point variations, and amplitude variations contribute to the recording of data that are not true depictions of unique geologic events.

Once a reflected event representative of a geological variation is identified, the event must be positioned with respect to the geometries of the reflecting surfaces and the recording equipment. The magnitude of errors inherent in conversion of analog data to a digital format with an x-y coordinate digitizer must be evaluated with respect to the scale of the original recordings or the enlargement of the archived data films. Figure 26 is a sketch of a typical single-channel seismic operation at sea and a block diagram of equipment commonly used.

B. Sound Energy Sources

For more than half a century, geophysicists have worked to obtain continuous seismic representation of subsurface geology. Research to achieve this goal led to the development of nondestructive, rapidly repeatable acoustic sources for the seismic reflection profiling technique which has found great applicability in the deep ocean basins.

One of the first reported uses of nondestructive or nonexplosive sources to measure sediment thickness in water-covered areas was Smith's (1958b) attempt to use a 12 kHz transducer to determine thickness and accumulation rates of recent sediments in Lake Mead. To improve instrumentation, MacClure et al. (1958) experimented with lower frequency transducers and developed the "Sonoprobe," which operated at 3.8 and 6.([illegible] lower frequencies and

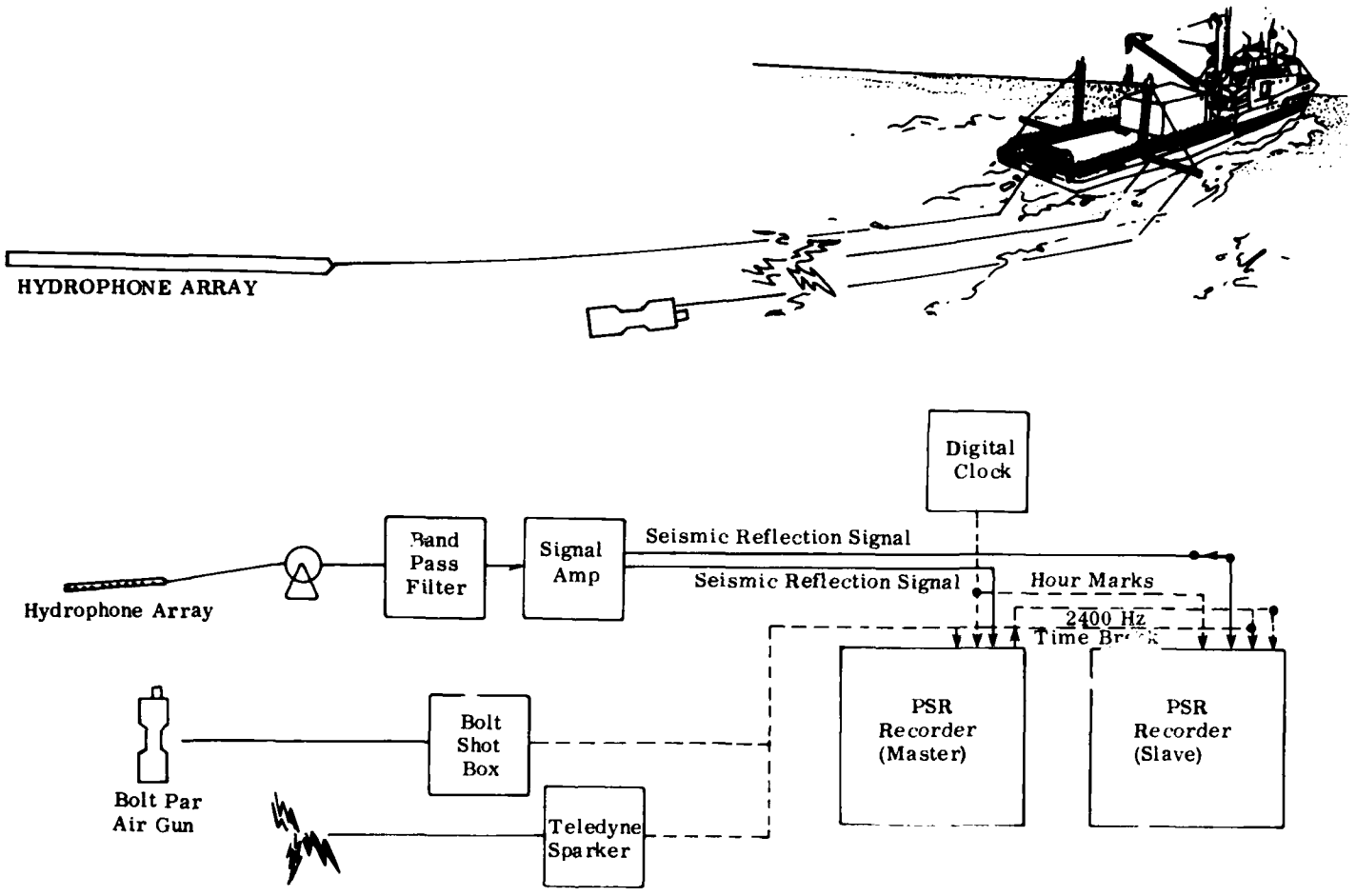

Figure 26. Sketch of a standard towing arrangement and block diagram of a typical single-channel shipboard seismic reflection configuration. In routine operations, a single source is used. The filter and amplifier are usually packaged in a single unit.

higher power thus obtained fostered several orders of magnitude improvement over previous efforts. Other nonexplosive source experiments were reported by Anderson (1953), who described the acoustic behavior of an electrical spark in seawater, and Padberg (1958), who pointed out the advantages of high pressure air discharges as a seismic source. Other acoustic devices designed to operate in water-covered areas included propane/oxygen exploders, eddy-current transducers, displacement transducers, electrolysis generators, vacuum imploders, and explosively released steam. Despite these advances, the first successful marine reflection profiler used small blocks of fuse-detonated TNT fired at two- or three-minute intervals as an energy source (Ewing and Tirey, 1961).

1. Characteristics of a Nondestructive Source

Sound sources must have certain common characteristics in order to qualify as a nondestructive, continually operating, marine seismic energy source. A source should have a broad frequency range in order to provide high frequencies for improved resolution and low frequencies for maximum penetration. Other characteristics include (1) very short time period between initiation of the source discharge and maximum power output of the initial pulse in order to obtain maximum power transfer to the water column, and the higher frequencies and improved resolution; and (2) no bubble pulse associated with initial discharge in order to give a single output and an unequivocal reflected signal.

To make shipboard operations feasible, a source must be sturdy enough to be towed at 18.5 km (10 knots) or more; flexible enough to be discharged as slow as once per minute, or as fast as once per second; and mechanically and electrically simple enough to achieve low initial cost, operational reliability, and ease of maintenance by relatively inexperienced people. In addition, shipboard feasibility is enhanced if the source does not require extensive pre-installation modifications to the ship and is sufficiently lightweight so that it may be launched or recovered under rigorous sea conditions without danger to the few people usually available for handling assistance. Finally, a source is not acceptable if it is destructive to marine life or if it produces offensive by-products.

Obviously, no particular sound source is uniquely suited for all applications. Therefore, the assembler of a seismic profiling system must make value judgments based on his particular application and his evaluation of the limiting characteristics of an acoustic source.

Because the sparker source is relatively inexpensive to buy and install, easily towed and handled at sea, reliable and easily maintained by frequently inexperienced technicians, and nondestructive to marine life, the Naval Oceanographic Office, as well as many other institutions and agencies with marine geophysics programs, initially chose the sparker as their basic sound energy source. In reaching this decision, the sparker's bubble pulse was perceived as unavoidable, if not helpful; and the sparker's deficiency in the low-frequency portion of the spectrum was considered inconsequential because signal attenuation through the water column is not a serious problem, and ocean-bottom sedimentary layers are frequently thin and respond well to higher frequency sound waves. Later improvements in air gun technology led many oceanographic institutions to adopt air gun energy sources because of their higher power and lower frequency output. Because most of the archived, single-channel seismic data were collected with either sparker or air gun energy sources, only the operation of these sources will be considered in detail.

2. Sparker Seismic Energy Source

Sparkers work because electrical energy storage devices will almost instantaneously (on the order of microseconds)

release most of their energy, which requires several seconds to develop. When the electrodes, between which the energy flows, are immersed in a conducting fluid such as salt water, the energy may be of sufficient intensity to vaporize the fluid between the electrodes, thereby creating a high-intensity, short duration, shock wave.

According to Kramer et al. (1969), the arcing of current from one electrode to another creates a hot and incandescent plasma of steam, ionized copper "gas," and free electrons. Expansion of this "steam" vapor produces the initial shock wave at seismic frequencies. The energy output of the initial pulse is primarily a function of capacitor bank storage voltage because stored energy varies as the square of the voltage, but only as the first power of the capacitance (Knott, 1970). As a result, Knott believes that it is important to operate the sparker at highest possible voltage levels in order to obtain both a high-peak pressure pulse and a long-period bubble pulse, because the length of the bubble-pulse period is indicative of energy output. If a high frequency is required to improve resolution, it may be obtained by reducing capacitance (Knott, 1970).

The size and shape of the initial discharge pulse is related to the number, size, and spacing of electrodes, and to some other rather ill-defined parameters such as water temperature and salinity, and electrode tow depth. These factors are, of course, in addition to the electrical characteristics of the storage units.

In the sparker arrangement used on Naval Oceanographic Office ships, the 30 kJ capacitor banks are charged at 14,500V and then discharged between two 60 mm (1/4 in) copper wires encased, except for tips, in nylon insulation and rigidly separated by a 0.5 m spacer. Because only the tips of the electrodes are exposed to salt water, a point-source is effectively produced.

Figure 27 illustrates the signal waveform typical of this installation.

The "steam" bubble produced by the initial discharge expands to its maximum volume within a few milliseconds and then rapidly collapses. The collapse of the bubble and the rush of water into the created cavity generate a second wave or "bubble" pulse which contains an appreciable portion of the total power available from the sparker. The bubble created by the sparker is unique in that it is created primarily by steam; when the steam condenses on the first oscillation, further oscillations of the bubble pulse are prevented (Fig. 27). According to Kramer et al. (1969), 25 msec is an average bubble pulse period for a 30 kJ sparker, but other records show bubble pulses with periods of about 13 msec (Fig. 27). The approximate peak frequency spectrum of the bubble pulse is the reciprocal of the period and will vary between 30 and 80 Hz for most of the systems commonly used. The oscillation of the bubble pulse can be used to increase the energy radiated at lower frequencies and thus enhance penetration (Kramer et al., 1968).

3. Pneumatic Seismic Energy Source

Despite increases in power output achieved by the use of larger, more powerful capacitors, the sparker remains a very inefficient method for generating seismic energy. To increase the total power output and increase penetration by lowering the frequency spectrum, most oceanographic institutions have added air guns to their inventory of seismic energy sources. Although the costs, operational simplicity, and reliability of air guns and sparkers are comparable, the increase in power and decrease in frequency are paid for by a decrease in resolution caused by the paucity of higher frequencies and the multiplicity of oscillations of the bubble pulse. This latter factor is readily evident in Figure 28, which shows the waveform of a 225 in^3 air gun (Mero and Freitag, 1975).

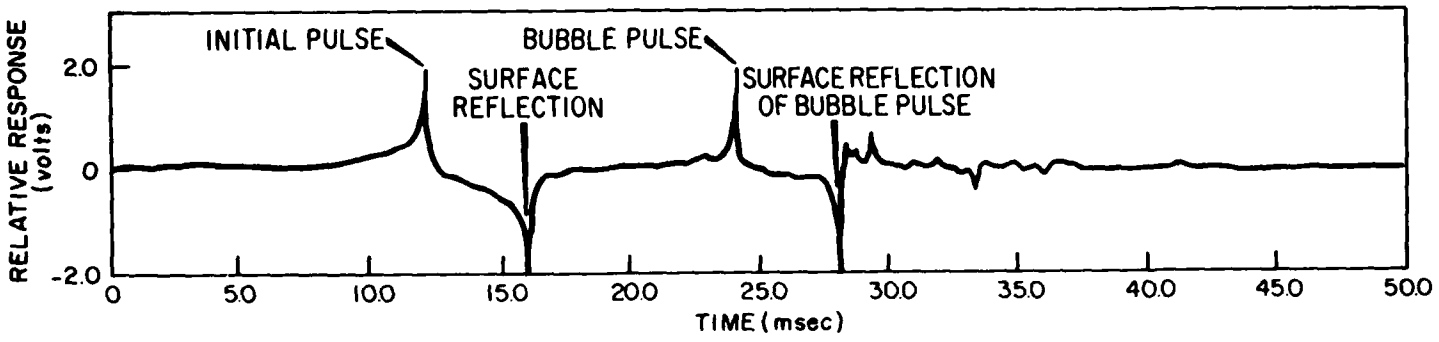

Figure 27. Broadband source signature of a 30-Kj 15-kV single electrode sparker towed at 3.0 m beneath the surface (after Mero and Freitag, 1974).

Air guns produce shock waves because high-pressure air, commonly 2,000 psi, can be explosively released from its storage chamber. This suddenly released air creates a spherical bubble whose pressure is greatly in excess of ambient hydrostatic pressure and generates acoustic energy by displacing a quantity of water. The air bubble oscillates several times (Fig. 28) while rising through the water column and eventually vents to the surface.

Air gun frequency output is a function of air pressure, chamber size, and gun depth (Giles, 1968). Increasing the size of the air chamber has the same effect as increasing the pressure; i.e., it increases the size of the bubble and decreases the frequency. Conversely, an increase in tow depth increases the hydrostatic pressure on the air bubble and results in an increase in frequency.

Greatly increased power outputs may be routinely obtained from air guns relative to sparkers. Calculations show that a 300 in^3 air gun (probably the most common size) is approximately equivalent to a 450,000 J sparker, about three times the size of the largest system presently operating.

Air guns can be grouped in an array of various chamber sizes to greatly enhance the output signal and diminish bubble pulses. Use of multiple air gun arrays requires that several compressors be installed aboard ship. The resulting expense and amount of ship space required for several air compressors make this means of improving the output signal somewhat less than cost effective for institutions conducting multifaceted oceanographic operations. Other available air gun bubble suppression devices include a wave shaper, which is an air chamber insert with a hole cut in the top so that part of the high-pressure air is released explosively, and part is released more slowly in order to counteract bubble pulse development. The device is effective, but requires about twice the air capacity for a given chamber size.

Because of high power and low-frequency spectrum, air guns are used almost exclusively for wide-angle reflection and refraction surveys in the deep ocean. Data collected by these techniques are used to calculate interval velocities and velocity gradients within the sediment column in order that travel times to reflecting horizons can be converted to true depths.

In addition, the signal shape generated by an air gun is extremely repetitive relative to the signal shape generated by a sparker discharge. As a result, the air gun output signal is more amenable to digital signal processing techniques than is a sparker's output signal.

Because of the relatively long time interval between the direct pulse and the oscillations of the bubble pulse -- usually more than 100 msec -- it is possible to resolve reflectors between these two events, assuming that the bubble pulse is identified. If the data are digitally processed, the bubble pulse may be removed by deconvolution techniques.

C. Signal Processing

There may be a millionfold variation in seismic energies from the initial source output to the weakest returning reflection. As a result, some form of online signal processing is required before a seismic cross section can be printed and evaluated. In addition to removing many spurious signals and thus simplifying interpretations, the signal processing equipment also introduces signal distortions that may complicate interpretations for the unwary.

The basic data collection and processing elements for routine, online operations most commonly include hydrophones connected as arrays to receive echoes, preamplifiers to boost signals from the towed hydrophone array, filters to emphasize signals in those frequency ranges containing the most pertinent

information, amplifiers to boost filtered signals to printing levels, and facsimile or line scan recorders to display the data.

In recent years, many technological advances have substituted digital computers for those analog approaches to signal processing. However, for routine reconnaissance operations at sea, and as real-time monitor for digital or multichannel records, data are normally recorded in analog format. If an area is selected for a detailed investigation, then seismic data may be recorded on magnetic tape and subjected to the appropriate digital processing techniques.

1. Signal Detection

A hydrophone is a geophone suitable for use at sea. Geophones operate on either electrodynamic, variable reluctance, or piezoelectric principles. Because electrodynamic-type geophones attempt to measure the displacement of the earth generated by seismic waves, and thus require a simulated separation from the earth, they are not suitable for use at sea. On the other hand, variable reluctance and piezoelectric-type geophones are planted within the medium and are capable of sensing pressure variations. Because pressure is equal to (mass times acceleration)/area, and both mass and area are fixed, measured pressure variations are proportional to acceleration, which is the second-time derivative of displacement.

Variable reluctance geophones generate electrical signals when pressure changes on soft iron diaphragms on opposite sides of the geophone causes the diaphragms to move and thus vary the magnetic reluctance. Reluctance is the magnetic analog of resistance in electrical circuits. Variable reluctance hydrophones are capable of measuring pressure variations, but for a given hydrostatic pressure, the power output increases with increasing frequency (Evenden and Stone, 1971).

Piezoelectricity is a property of certain crystals that causes them to develop an electrical potential when they are deformed. Because certain manufactured materials, notably barium titanite, possess this property and may be cast in any desirable shape or size, they are used almost exclusively in marine hydrophones. Piezoelectric hydrophones produce a voltage output which is proportional to instantaneous water pressure and uniform for a broad range of frequencies. The major disadvantage in piezoelectric hydrophones is that their output impedance is very high so that a transformer is required to match impedances between the hydrophone and the preamplifier (Evenden and Stone, 1971).

The big problem with both variable reluctance and piezoelectric hydrophones is that they are unable to discriminate against pressure variation from any source or direction. To reduce this problem, hydrophones are connected in parallel and/or series-wired linear arrays, and encased in plastic tubing filled with castor oil, kerosene, or similar buoyant dieletric. The dielectric increases hydrophone coupling and decreases salt-water corrosion; buoyance makes depth control possible by selective weighting. The value of hydrophone arrays are discussed in a following section.

2. Preamplification

Preamplifiers are required to supply the additional power that weak signals need to overcome cable losses, to match impedances between the hydrophone array and the cable, and to help suppress the very strong signals radiating directly from the source. These seemingly contradictory requirements are met because seismic preamplifiers require a very high input impedance to match the high impedance of low-frequency hydrophones. For example, the Teledyne Exploration Company's Model 24257 hydrophone array preamplifier has a 510 kΩ input impedance. In addition, preamplifiers are usually relatively low-gain (20 dB)

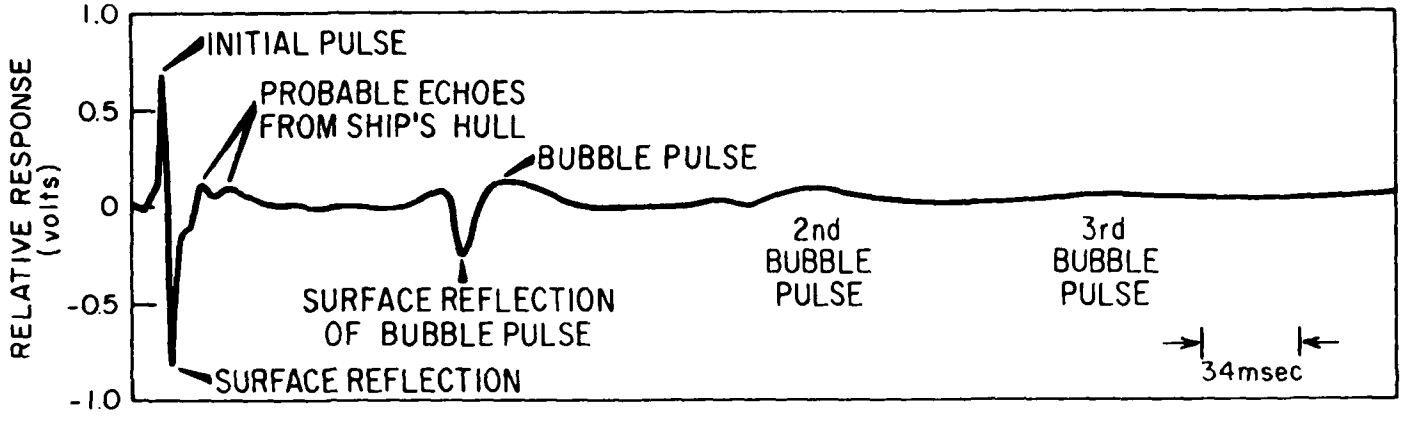

Figure 28. Broadband source signature of 225-in^3 air gun charged to 2000 psi and suspended 4.6 m below the surface. Note complication added by onset of surface reflection of bubble pulse before expansion of air bubble is completed (after Mero and Freitag, 1974).

devices. This combination permits preamplifiers to maximize the weakest signals, which are often those with the lowest frequency, and to minimize the strongest signals if they contain appreciably higher frequency components, because the high input impedance increases the hydrophone array's signal damping capability.

3. Filtering

An electrical filter, as the name implies, is an electronic device which attenuates those signals with frequencies higher or lower than a selected value, and limits recorded data to those ranges that emphasize a particular feature. In this manner, the filter may aid resolution by enhancing higher frequencies, increase penetration by reducing higher frequencies and allowing more gain to be added to the lower frequencies, or by discriminating against cable or array vibrations. Filters are categorized in a variety of fashions depending on whether or not power is required for operation (active or passive), or on which side of their cut-off frequency the passband lies (high-pass or low-pass); or if high-pass, whether or not the inductor has a capacitor in series (with series capacitor, m-derived or without-constant K); or if low-pass, whether or not the inductor has a capacitor in parallel (with capacitor in parallel, m-derived or without, constant K) (Evenden and Stone, 1971). Seismic systems usually have a filter inserted between the preamplifier and the primary amplifier (Fig. 26) or are built as an integral part of the primary amplifier.

(a) Passive Filters

Passive filters require no power for their operation, but suffer from relatively high insertion losses - differences between input and output levels. For this reason, and because of the size and expense of laminated iron core indicators, passive filters are not widely used in marine seismic equipment.

In practical applications, the m-derived passive filter has a very steep slope (greater than 20 dB/octave), but poor impulse response; while the constant-K passive filter has a more gentle slope (greater than 12 dB/octave), but a much better impulse response. As a result, the m-derived filter is more frequently used with amplifiers connected to digital recorders because impulse response is not as important in digital processing as in analog processing (Evenden and Stone, 1971). The constant-K filter seems more suited for amplifiers driving analog recorders.

(b) Active Filters

When a passive filter is energized with a single impulse, which is always made up of equal amounts of all frequencies, the filter responds by attenuating some frequencies and shifting the phases of others (Smith, 1958a). As a result, a single-impulse input emerges from the filters as two or more cycle wave trains. This phenomenon leads to the concept of differentiating and integrating circuits which make active filtering possible.

If the series resistor and capacitor in an RC filter are small enough to make $\omega RC \approx 0$ over a specified frequency range, then the output voltage from the circuit is the "equivalent of passing it through a system whose amplitude-frequency response is directly proportional to frequency, and whose phase-frequency response is a constant 90° lead" (Evenden and Stone, 1971, p. 35). This output response, when measured across the resistor, is commonly referred to as differentiation.

Conversely, if the resistance and capacitance in the RC filter are made very large such that $\omega RC \to \infty$, then the voltage across the capacitor "has an amplitude-frequency response which is a constant 90° lag" (Evenden and Stone, 1971, p. 36). This type circuit response, when measured across the capacitor, is commonly called integration.

A waveform passed through a differentiating circuit emerges as a series of spikes, while the same waveform passed through an integrating circuit emerges as a broad curve. When a differentiator and an integrator operate on the wave form sequentially, a frequency band is defined. Better frequency discrimination and less distortion are achieved by feeding as much as possible of the filtered signal back through an amplifier capable of responding to frequencies all the way down to dc. This feedback process defines as active filter.

Active filters with steep slopes and sharp frequency cutoffs may be obtained by operating several such combinations in tandem. For example, Teledyne Exploration Model 25950 seismic amplifier uses three cascaded stages of active filtering between the preamplifier and the primary amplifier in order to obtain maximum filter slopes of 36 dB/octave. The availability, compactness, and low cost of reliable transistors, resistors, and capacitors combined with easily achievable amplifier stability make active filtering one of the most widely used analog signal processing techniques.

(c) Filter Selection

The tradeoff in filter bandwidth selection is between resolution and noise interference. If the bandwidth is set too wide, the multiplicity of wavelengths of returning signals will constructively and destructively interfere, thus creating signals of different wavelengths and amplitudes that produce a spurious clutter on the record. On the other hand, if the bandwidth is set too narrow, then certain combinations of reflector spacing may well eliminate significant returns and create false 'transparent' zones. The center frequency of a particular bandpass is the square root of the product of the end points. For example, a 20 to 125 Hz bandpass has a center frequency of 50 Hz, i.e., $((20)(125))^{1/2}$. The filtered range should be at least an octave wide -- the higher cutoff frequency twice that of the lower cutoff frequency. Selection of a filter with a very steep low-frequency cutoff slope (24 to 36 dB/octave) helps to remove lower frequency tow noises. The upper frequency cutoff seems to be less critical. If 60 Hz pickup from the ship's electrical system proves troublesome, a notch filter, which severely attenuates signal over a very narrow frequency range, may be used without disturbing the other frequency components. Filters always attenuate some of the signal levels within the bandpass. The insertion loss is frequency-related such that changes in the filter bandpass will necessitate changes in amplification in linear amplifiers.

4. Amplification

The amplitude of the filtered signal is frequently below the threshold printing level of the facsimile or tape recorder being used. To multiply signal voltages to acceptable levels, a high-gain, low-noise amplifier is inserted into the seismic system between the filters and the recorders (Fig. 26).

There are a multitude of seismic amplifier designs, but all have several common characteristics. For example, input impedance is always much lower (10^{-3}) than is true for preamplifiers, and output impedance is even lower (10^{-5}) than the input impedance. Low impedances retard transient 60 Hz electrical pickup.

Many seismic amplifiers can accept signals ranging from 0.3V to 10^{-7}V, and deliver an 0.6V signal after several stages of amplification. Stable low frequency amplification is considered more difficult to obtain than high frequency amplification because capacitive reactance, the capacitor's resistance analog, increases with decreasing frequency. When it is necessary to cascade several transistorized amplifiers to achieve adequate signal gain, the gain in the low-frequency portion of the spectrum is controlled primarily by the reactance of the interstage coupling capacitors (Brophy, 1966).

Among the several schemes for seismic signal amplification, the differential input amplifier is widely used because its amplification factor can be easily controlled by varying the resistance ratio between the two input terminals. The voltage difference between the two input terminals is the signal that is amplified. Other amplifiers are designed to increase the amplifier gain as the signal level decreases. If the gain of each amplifier is automatically adjusted as the signal level varies, then the amplifier is designated automatic gain controlled (AGC). On the other hand, if the amplifier gain is buffered in predetermined steps to a predetermined level, then the amplifier is designated programmed gain controlled (PGC). Both AGC and PGC are commonly supplied options on seismic amplifiers; however, if true amplitude information is required from the data, then PGC recording is necessary.

5. Recording

With the exception of limited areas surveyed with closely spaced grids, structures in the ocean are so poorly known that most seismic lines are essentially reconnaissance lines. When sufficient data have been accumulated to permit the geophysicist to precisely define his requirements, then it may be practical to record data in the more easily processed digital format. However, given the current constraints under which most oceanographic vessels operate, the graphic record made on board ship is most likely to remain the primary seismic data presentation format.

Facsimile or line scan recorders work because the recording paper conducts electricity. When electrical current is applied to the styli carrier bar, the stylus burns the paper wherever the stylus is in contact with the paper at the instant of energizing. Recorders are constructed so that only one stylus touches the paper at any one time. Electronic circuitry necessary to discharge the sound source is usually energized by initial contact between the stylus and the paper, thus, the recorder provides the timing control for the seismic system.

The number of lines per inch of recording controls the ease and reliability of visual correlation. Naval Oceanographic Office uses 150 lines per inch for its master record because the slight offlap of individual line scans produces greater data density and enhances the correlation of subtle effects. The slave recorder is frequently adjusted to 50, 75, or 100 lines per inch, depending on model of recorder and geologic feature being studied. Experience has shown that a slight gray background highlights weaker reflections without detracting from stronger events.

Both wet and dry types of recording papers are widely used. Wet paper probably has a somewhat wide dynamic range, but tends to wrinkle and distort with changes in humidity. Dry paper is immune to humidity changes, but smudges badly and has a print odor that may be offensive in confined quarters aboard ships. Up to 23 dB dynamic range is possible with most of the recording papers now in use (Knott, 1970).

If any secondary data processing is likely to be required, seismic data should be recorded on magnetic tape. Analog recorders have dynamic ranges more than twice the dynamic range of the best variable density recorder. One of the chief advantages of magnetically recorded data is that selected areas can be reprocessed and presented at a horizontal to vertical scale ratio of 1:1. Such a presentation adds an extra dimension to interpretations.

D. Signals, Noises, and Hydrophone Arrays

When a sound wave travels through the ocean, the water is alternately squeezed together (compressed) and stretched apart (rarefied). Because of this phenomenon, devices (hydrophones) capable

of converting mechanical energy (pressure) to electrical signals are used to detect both the intensity and frequency of the passing wave. A hydrophone, however, has two shortcomings. Because it is a pressure-sensitive device, it will respond to any change in pressure, regardless of origin; and because the wavelength of energy at seismic frequencies is very long compared to a practical size for hydrophones (30 m versus 0.03 m), the hydrophone is inherently unable to discriminate against pressure differentials from any direction (Albers, 1965). To reduce the impact of these problems, hydrophones are connected in various configurations called arrays or streamers.

1. Noise Sources and Control

As a sound wave travels outward from its source, its intensity is diminished by spreading of the wave front and absorption by the medium through which it is traveling. Eventually, signal levels decay to an intensity that is less than, or equal to, the environmental noise in which the system is operating, and desirable signals (reflections from subsurface acoustic horizons) are obscured by noise.

Noise, commonly defined as unwanted signal, is actually made up of random and coherent components. Random noise is locally generated, statistically uncorrelated energy, while coherent noise is statistically correlated and behaves in much the same fashion as desirable signal energy. For maximum inhibitory effectiveness, the two must be differentiated and treated in different fashions.

The sum of reverberation and field noises which cannot be rejected establishes the minimum signal level which can be recorded, thus, the incoming signal must exceed these noise levels. The greater the difference between these two values, the greater the clarity of the recording.

Significant noise generators capable of obscuring incoming signals include (1) propeller cavitation, shipboard machinery noises, and ship vibrations; (2) turbulence created by an object being towed through the water; (3) ambient noise created by the prevailing sea state and local faunal sounds; (4) cable strumming and hydrophone acceleration caused by the stress of towing and wave motion; (5) electrical noise caused by the ship's 60 Hz operating power and crosstalk between various electrical conductors; and (6) reverberations. Other undesirable effects such as multiples, diffractions, and bubble pulses are often recorded, but these are functions of the source or the geological environment and will be discussed along with structural interpretations.

2. Cavitation and Other Ship Noise

Local hydrostatic pressures may be reduced to less than the ambient vapor pressure of water by extreme agitation, such as that due to propeller blades driving into the water. When this situation obtains, bubbles are formed. When these bubbles move into areas of higher pressure and oscillate, noise is emitted just as in bubble pulse oscillations associated with seismic sources. This noise is called cavitation, and serves not only as a source of undesirable signal, but also as a baffle capable of screening seismic returns.

Mechanical vibrations produced by operating machinery directly coupled to the ship's hull are capable of producing noise at seismic frequencies. The relative intensities of mechanically coupled and cavitation noises are functions of ship's speed and displacement. At slow speeds (15 km/h), the mechanical noises predominate, while at higher speeds (greater than 22 km/h), cavitation becomes most important (National Defense Research Comm., 1946). Low-frequency (30-40 Hz) rhythmic noise frequently seen on seismic records, particularly in shallow water, is very likely due to mechanically coupled engine vibrations rather than to propeller noise as suggested by Bedenbender et al. (1970).

The sound field radiated by the ship and its equipment is omnidirectional. As a result, the deleterious effects of this noise source may be reduced by increasing the tow distance, by virtue of the receiving directionality of the hydrophone array, and by raising the low-frequency filter cutoff. As in the case of ambient noise, ship's noise is inversely proportional to frequency at the rate of about 7 dB per octave (National Defense Research Comm., 1946).

3. Turbulent Noise

Turbulent noise, also called flow noise, is created by movement of an object through the water. Pressure distribution around a moving object is usually high at the leading edge, very low along the top, sides, and bottom surfaces, and high at the trailing edge. If the object is blunt, then the distance between the high-pressure zones and low-pressure zones becomes very short, the pressure rises rapidly, the boundary layer becomes separated from the object, and the pressure zones coalesce to form a broad, eddying wake downstream of the object. The effect of turbulent noise can be quite substantial; Bedenbender et al. (1970) report sound pressure spectrum levels in excess of 10 dB re 1 mbar for frequencies less than 80 Hz when the array's tow speed is 18.5 km/h.

The turbulent effect is magnified if the surface of the towed object is rough and the speed is relatively high. For example, Bedenbender et al. (1970) have heuristically determined that surface roughness becomes significant in producing noise when the height of the surface irregularity exceeds 0.06 inch (0.15 cm) divided by the ship's speed in knots. Thus, at 18.5 km/h (10 kn), an irregularity greater than 0.0152 cm (0.006 inch) will cause some turbulence. In practical terms, this means that the hydrophone array should be kept clear of the wake of the ship, sound source, or even the towed magnetometer. In addition, extraneous chafing gear, tape, hose clamps, ballast weights, etc., should be removed or streamlined. Also, it may be necessary to add fairing to the streamer cable to reduce formation of turbulent eddies.

4. Ambient Noise

Sea surface noise generated by wind stress is the dominant source of ambient noise in the open ocean. Figure 29 shows the relationship between wave height, frequency, and sound pressure spectrum level (Urick, 1967): Mean pressure calculations, based on Figure 29, show that ambient wave noise decreases by an order of magnitude for 1, 5, and 8 foot wave heights, when the frequency is raised from 10 Hz to 50 Hz. The frequency-noise levels for 1 to 8 foot wave heights decrease by a factor of about 3 when the frequency is raised from 50 Hz to 100 Hz. Thus, close attention to low-pass filtering and sea state can drastically reduce noise and increase signal resolution.

Raindrops, marine life, and passing ship traffic all contribute to the level of ambient noise at seismic frequencies in the ocean. All these effects are transitory and can seldom be predicted or avoided.

5. Vibration and Acceleration

One need only stand on the afterdeck and watch the motions of a hydrophone array to appreciate the fact that considerable noise is generated by constantly varying tow tension. The pitch, roll, and yaw of the ship all produce static and dynamic pressure variations as well as accelerations in the towed array. At seismic frequencies, noises created by accelerations are an order of magnitude more significant than noises created by other motions and may reach maximum amplitudes of as much as 24 dB (Bedenbender et al., 1970).

On the other hand, Schoenberger and Mifsud (1974) have shown that in relatively calm seas and at towing speeds above 10 km/h that cable noise far outstrips electrical and ambient noises as the major source of undesirable

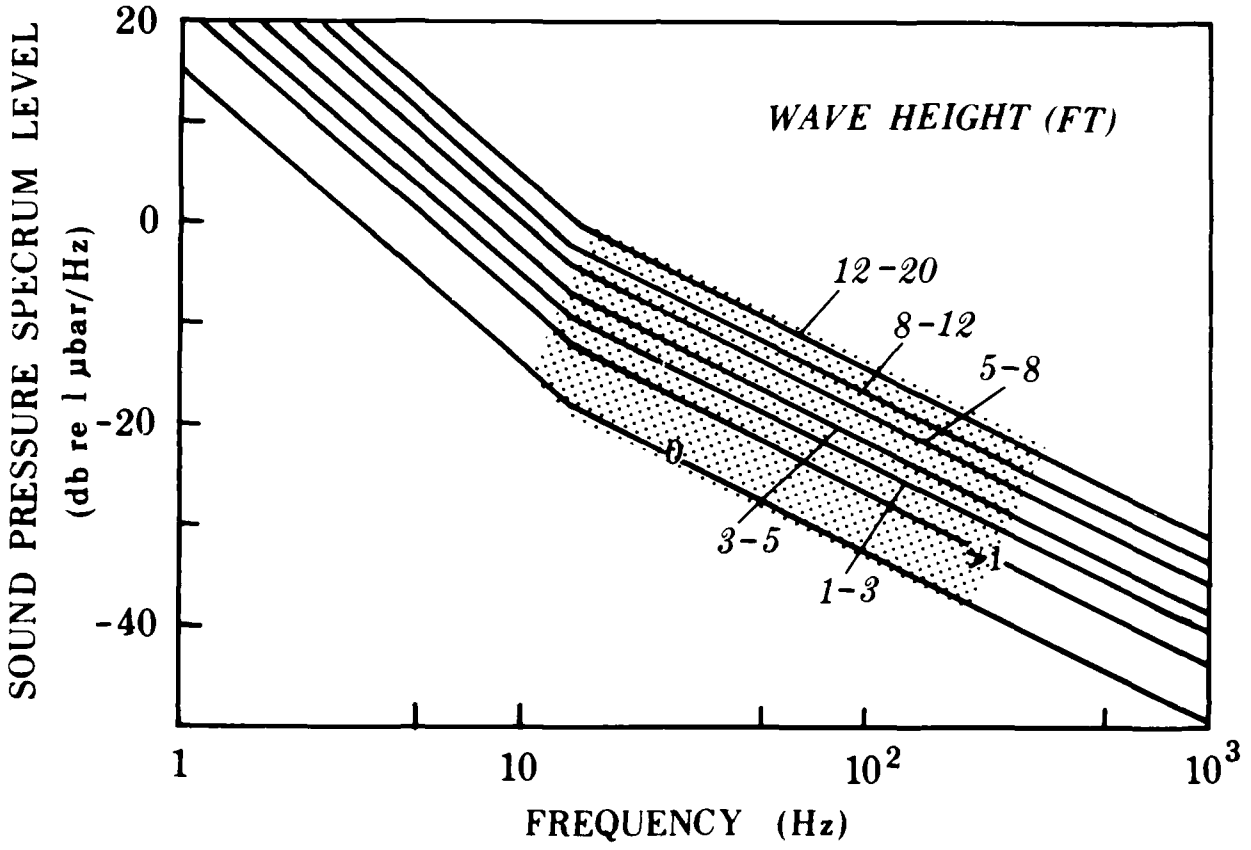

Figure 29. The frequency and intensity of noises generated by waves up to 20 feet high. At seismic frequencies, indicated by stippled zone, wave noises produced by a moderate sea may easily exceed signal levels. After Urick (1976).

signal. Rather than cable strumming, however, these authors believe that pressure fluctuations due to water flow (turbulence) cause much of this noise. Further, these noises occur between 10 and 25 Hz and are difficult to remove by low-frequency filtering.

Most hydrophone arrays include a stretch of compliant section to reduce the effects of cable strumming and vibration. If this proves to be inadequate in a particular installation, some gain may be realized by towing the array with elastic or nylon line, which will serve to further insulate the array from erratic ship motions that induce strumming and accelerations. In addition, the cable fairing recommended to reduce turbulent noise should help reduce strumming.

In addition to producing ambient noise, wave motion (sea state) produces accelerations which can be quite large. Acceleration noises are controlled by mounting crystal hydrophone elements symmetrically about their sensitive axes, thus, a position change is recorded as both positive and negative pressures of equal amplitudes. The sum of these pressures is zero. Acceleration cancellation techniques can provide up to 12 dB improvement in the signal/noise ratio (Luehrmann et al., 1970).

6. Electrical Noise

In permanent ship installations, electrical noises are usually not a significant problem. However, on ships-of-opportunity, transient 60 Hz noise from the ship's operating equipment may intrude into the seismic passband. Thus, it is imperative that all of the seismic equipment be carefully and thoroughly grounded. Even this precaution might not prevent noise override from high-powered transmitters such as the ship's radio. Such noise can be disastrous to the seismic record (Fig. 30). Low ($\approx 10\Omega$) output impedance of the seismic amplifiers will help minimize 60 Hz electrical noise. High-voltage seismic sources, such as a sparker, frequently produce transient spikes on simultaneously recorded data. Physical separation of the sensors and cables or addition of blanking circuits may help alleviate this problem.

7. Reverberation

Reverberation is energy scattered back toward the source by irregularities in the medium and, as such, represents an entirely different class of noise. Reverberation has a practically unpredictable amplitude because the location and the magnitude of the irregularities are continually changing. Volume reverberation is reverberation from the water column caused by air bubbles, suspended solids, marine life, and local fluctuations of sound velocity resulting from random temperature and density variations. Bottom reverberation is a function of bottom sediment size and type, bottom slope or irregularity, area of insonification, frequency, and pulse length.

8. Signal Enhancement and Hydrophone Arrays

The goal of maximizing the signal/noise ratio has been attacked by using multiple groupings of hydrophones in series and/or parallel connection. Linear arrays of hydrophones may achieve directionality because arrays behave as an extended receiver or antenna. In this case, the array is much more sensitive in the plane perpendicular to its linear dimension.

Linear array design is based on the following assumptions: the desired signal originates from a distance sufficiently great so that the signal arrives at the hydrophone array as a plane wave, the incoming signal is in the plane of maximum array sensitivity, and the noise is predominantly local. Within these constraints, the hydrophones are then spaced far enough apart so that the locally generated noises arrive at each hydrophone at a different time and are statistically uncorrelated, while distant signals arrive simultaneously and are summed by the array.

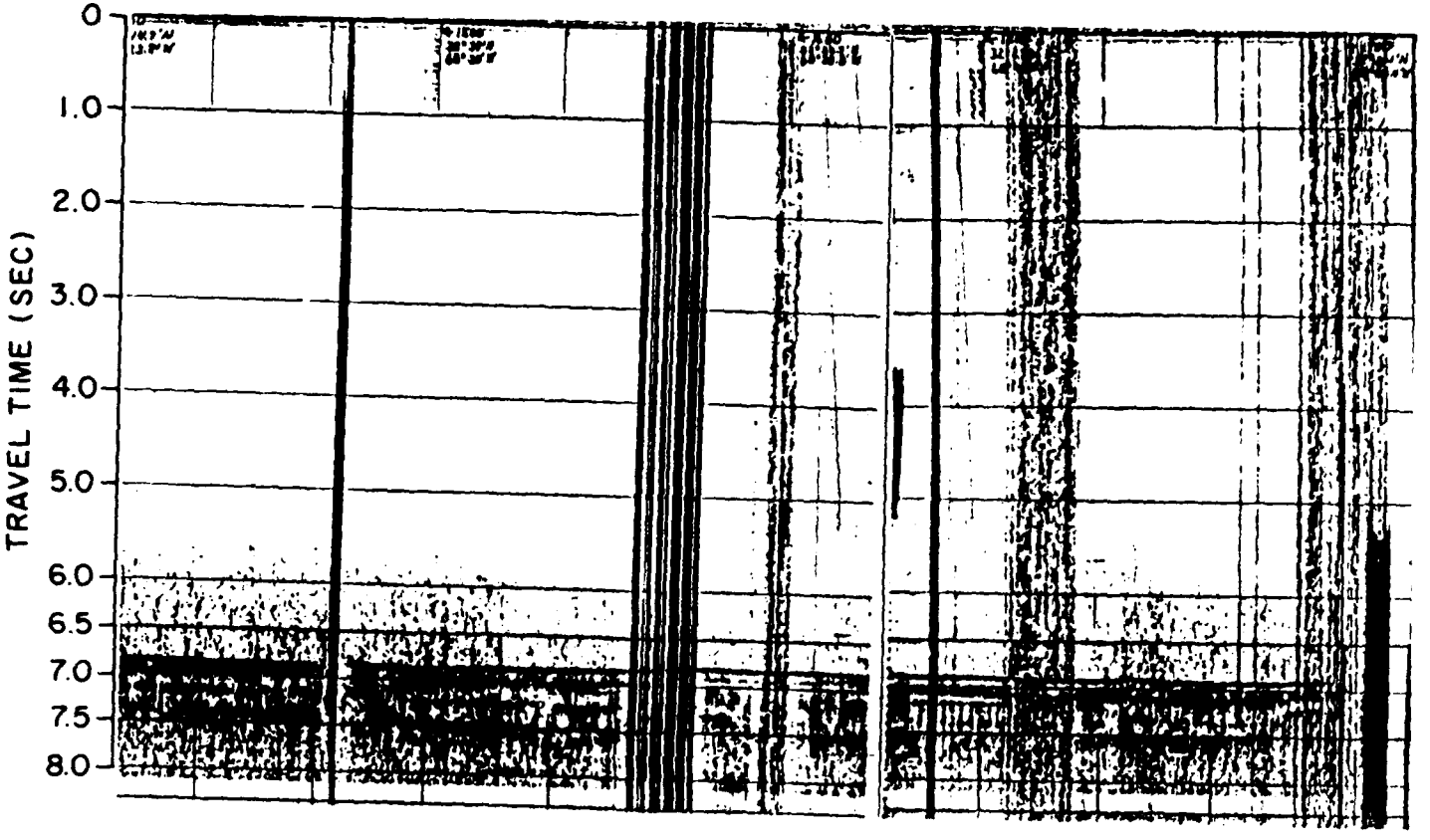

Figure 30. Noise interference on a seismic record. The heavy dark bands near the center of the illustration are radio transmissions picked up by the hydrophone array lead-in cable and the gray areas on the right are passing ship traffic.

Improvement in the signal/noise ratio can be approximated from the number of hydrophones in the array if the noise sources are all random. This improvement occurs because the random noise energy received by each hydrophone is distributed in a normal curve with a standard deviation related to the square root of the number of samples of noise energy. As a result, the total noise energy output of the hydrophone array is the product of the number of hydrophones (n) and the square root of the random noise output of each hydrophone in the array ($n^{1/2}$) (Schoenberger and Mifsud, 1974). Because the signals are identical and in phase, the signal energy output by each hydrophone in the array is not random. Thus, the total signal energy output of the hydrophone array is the product of (n) identical signals from (n) hydrophones. Therefore, the near field, random, signal/noise improvement is approximately equal to ($n^{1/2}$), where (n) is the number of hydrophones in the array.

If the noise is coherent, individual hydrophone elements in the array cannot distinguish noises from signals. Nevertheless, the hydrophones coupled as an array can provide some signal/noise improvement because the array acts as an extended receiver having zones of greater and lesser sensitivities.

The zone of maximum sensitivity (main lobe) is perpendicular to the long axis of the array such that any coherent noise originating outside the main lobe is received with reduced amplitude. The width of the main lobe (directionality of the array) decreases with increasing length of the array and increasing frequency of the received signal (Luehrmann et al., 1970). Simply adding hydrophones to increase the length of the array and increasing the frequency will not solve all the noise problems. In the first case, the array cannot resolve features smaller in lateral extent than the length of the array; and, in the second case, increasing the frequency increases both bottom reverberations and attenuation losses in the bottom (Luehrmann et al., 1970).

The magnitude of the signal/noise increase due to directionality of the array can be estimated, because the main receiving lobe is perpendicular to the long axis of the array and passes through the midpoint of the array. Therefore, the array's total signal power gain ($G^2\theta$) can be taken to have the value (n^2) everywhere inside the beamwidth (λ/D) and zero outside the beamwidth. The array's total noise power gain is ($\lambda/2D$ [n^2]), because of the lack of correlation between the distant noise sources (bottom reverberation, side echoes, etc.) (Horton, 1969). Therefore, the signal/noise improvement factor is ($2D/\lambda$) for the distant noise background when (D) is the length of a hydrophone array made up of (n) equally spaced hydrophones and (λ) is the wavelength of sound (Horton, 1969).

In the case of the Teledyne Exploration model 24257 hydrophone array, widely used for single-channel marine seismic work, 25 groups of two hydrophones each are spaced about 46 cm (18 in) apart to form an 11 m array. A second identical array is attached to form a total of 22 m of active section. The output signal from each hydrophone pair is alternatively fed into two amplifiers. This electronic interlacing minimizes random noise by a factor of 10 or ($100^{1/2}$). The coherent noise reduction factor ($2D/\lambda$) is approximately 1.5, (2[22m]/[30 m]), assuming a center frequency of 50 Hz.

Directional arrays, frequency windows, and bias level controls allow recorder gains to be adjusted in such a fashion that the printed record is most pleasing to the eye, and, perhaps, a bit easier to interpret. But in actual practice, the lineup of events and reflector quality, those factors which enhance visual correlation, are the only signal/noise improvement factors that are really significant. If the noise contaminant comes from directly beneath the hydrophone array (multiples, diffractions, etc.), then the experience and intuition of the analyst becomes the final available filter.

E. Geometrical and Environmental Influences on Record Interpretation

The continuous seismic reflection profiler is a powerful tool for unraveling details of geologic structures and the distribution of probable rock types beneath the ocean floor. However, the system does not provide unique solutions to these complex interrelationships because the nature of the equipment and the complexity of sound waves transmitted over long distance through a varying medium do not allow simplifying assumptions. Therefore, the intent of this section is to point out some of the spurious events that appear on the record, interspersed with true reflections, and which must be accounted for before the full usefulness of this instrument can be realized. For a fully unique solution to geologic complexities, other types of data, such as drillhole samples and magnetic and gravimetric field intensities, must be considered.

1. Ray Paths

Energy can follow at least six different ray paths between the source and receiver (Fig. 31). All of these paths carry information that contributes to the interpretation of seismic profiles. The direct ray's slant range can be determined if the depths of, and horizontal distance between, the source and receiver are known. By the geometric relationship [source depth - receiver depth)^2 + (distance^2]$^{1/2}$, the slant range can be calculated. This value, when divided by an average surface water velocity, should be very close to the measured travel time, verify the source and receiver geometry, and identify a first event on the record. The path length of the surface-reflected ray may also be calculated; however, in deep water and with the relatively slow recording speeds used in single-channel recordings, this step is seldom necessary or easily accomplished.

Expected arrival times of the four bottom-reflected rays can be calculated from source and receiver depths, the water depth, and the assumption of near-normal incidence for the reflected rays. The first arrival should occur at a time determined by ([Z-S) + (Z-R)]C), where (S) and (R) are source and receiver depths, respectively; (Z) is the water depth, and (C) is the average sound velocity in water. The second and third arrivals will occur at [(2Z + S-R) X (C)], respectively. These last two reflections will return simultaneously if the source and the receiver are at the same depth (Fig. 31). If these depths are adjusted to about one-fourth wavelengths of the center frequency, destructive interference would greatly diminish the intensity of the recorded signal, thus making the record easier to interpret. The fourth arrival occurs at ([(Z+S) + (Z+R)] X [C]). This return forms the end of a particular reflection sequence, which, dependent on the geometry, consists of three to four echo sequences.

In addition to the four bottom-reflected ray paths, most marine seismic sources generate one or more bubble pulses of varying intensity that contribute another group of ray paths similar to those shown in Figure 31. Filtering, which helps to isolate frequencies of maximum value, adds several harmonic oscillations to the wave train. Finally, the source energy is usually of such intensity that two or more source-bottom-surface round trips are possible. Thus, the problem of analyzing sub-bottom profiler records is essentially that of identifying the first of these many reflected arrivals from each sub-bottom reflecting horizons, and discarding the remainder.

2. Identification of Reflected Signals

As the source (air gun or sparker) discharges, an initial shock wave is generated. This shock wave, or pulse, has a rise time of only a few microseconds. Since it represents zero time for all practical purposes, this is the pulse whose progress is monitored to determine structure beneath the ocean

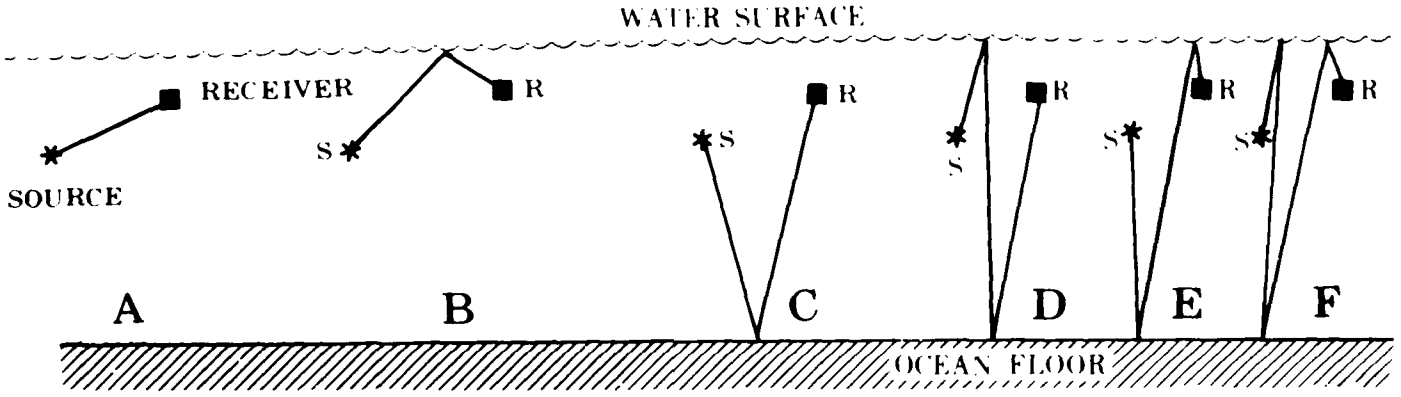

Figure 31. Paths followed by the primary sound ray between source and receiver. A and B are the first dark lines at the top of the record; C through F are rays forming the echo sequence from a single interface. The bubble pulse and other secondary sources generate similar sequences of signals which are recorded along with these echoes.

floor. The various acoustic events following the initial pulse are identified in Figure 31.

Figure 32 is an example of a one-second sweep rate air gun record in which the arrival times of the various signals are noted. The 57 msec time delay represents the time between initiation of the sweep and arrival of the signal at the hydrophone if the time interval between the beginning of the sweep and the discharge of the gun is neglected. Using a surface water velocity of 1.48 km/sec (estimated from Naval Oceanographic Office, SP-68, 1966), the distance from source to receiver is 82 m. This value is reasonable because full deployment of the hydrophone array was not practical in this particular installation.

The surface-reflected pulse (Fig. 31B) normally follows the initial pulse with a time delay indicative of the total depth of the source and the receiver. In Figure 32, the 65 msec event suggests a receiver depth of about 9 m and a source depth of about 1.5 m, both of which are reasonable values for this installation. However, the fact that the 65 msec pulse and its bottom reflection both follow the initial pulse and its bottom reflection with no change in time delay, implies a greater degree of regularity than is likely for towed source and receiver. The increases in amplitude of the bottom-reflected counterparts of the 57 and 65 msec events indicate that the initial events were not in the plane of maximum sensitivity of the hydrophone array, while both reflected events were more nearly so. Most likely, the 65 msec event is an artifact of the outgoing pulse, and the slight variations in amplitude along the horizontal axis are due to the addition of a surface-reflected component.

Again, in Figure 32, the 77 msec event followed 12 msec later by another signal could possibly be caused by the initial pulse bouncing off the ship's hull and then off the water surface. This would mean that the gun was towed about 15 m astern, and the total hydrophone distance was 99 m. These are considered reasonable values for the particular installation used for this record.

The next three events (105, 139, and 167 msec, Fig. 32) could be any number of things, such as surface duct multiples, reverberation from sound hitting the ship's hull, filter ringing, or bubble pulses. Reflections from the ship's hull appear on the record as low energy waves ahead of the bubble pulse, and frequently have a resonant character because the hull tends to reverberate. In addition, other repetitive noises aboard ship, such as paint chipping, heavy machinery, or radio transmission (Fig. 30), can be received and recorded as interference, particularly if shipboard wiring is poorly grounded.

3. Bubble Pulses

Hydraulic afterflow, the temporary storage of kinetic energy not immediately radiated, is inherent in underwater explosions (Kramer et al., 1968). This afterflow is manifest as a series of oscillating bubbles. The size, the period of oscillation, and the identity and control of such bubbles are significant in the interpretation of marine seismic records. In general terms, the air from an air gun or the vapor generated by a sparker expand much more rapidly than they rise through the water column. This factor, coupled with the momentum imparted by the explosion, causes the pressure within the expanding gas bubble to become less than ambient pressure, much in the fashion of a ball containing three orthogonal springs which, from the compressed positions, are stretched past their equilibrium positions. At some diminished pressure, the process reverses and the bubble begins to collapse under the influence of the excess ambient pressure, and the reverse momentum generated by the implosion of the bubble analogous to the contraction of the orthogonal springs. The inward rush of water and the concurrent decrease in bubble size continues until the pressure inside the now-compacted air bubble is greater than

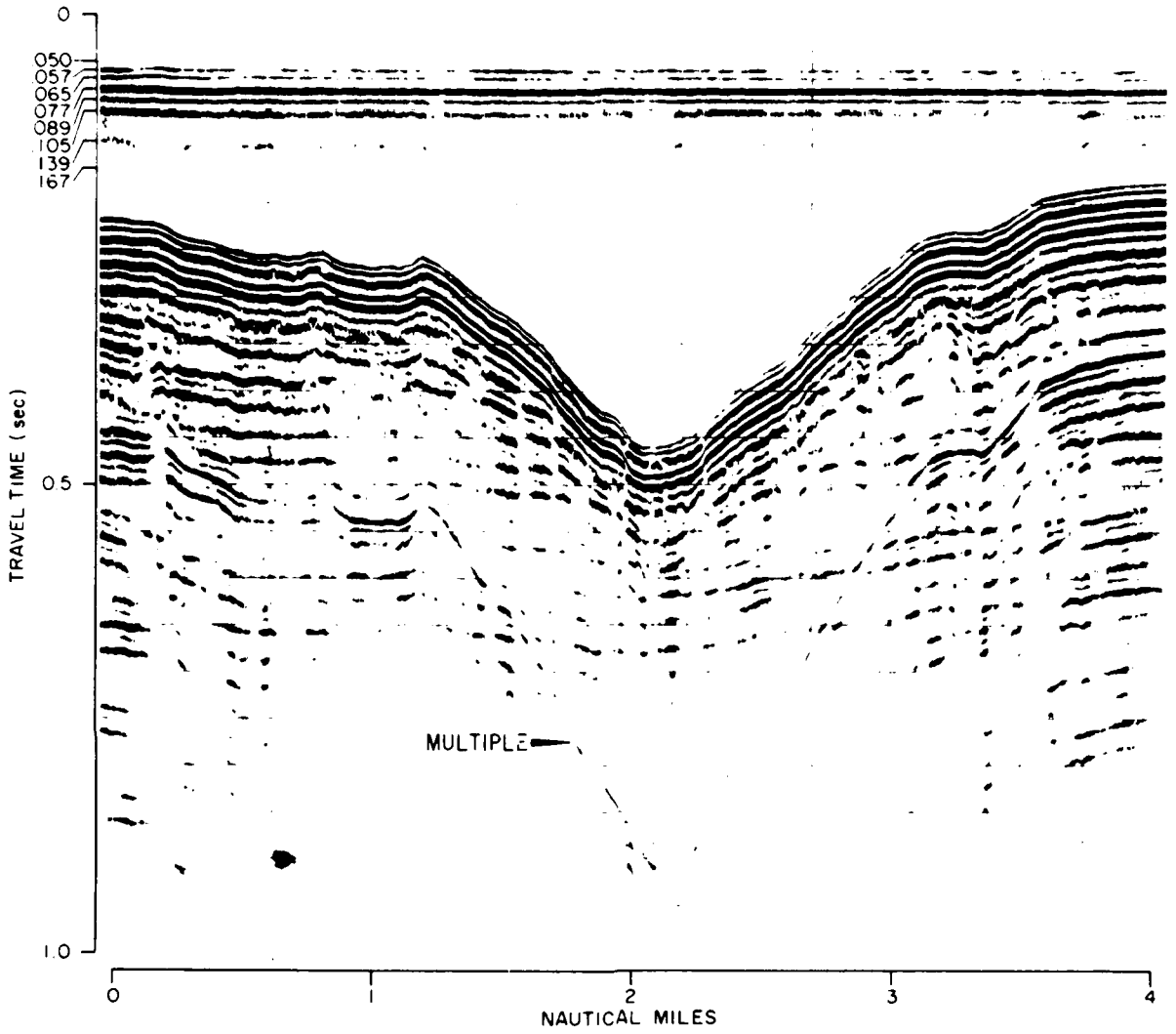

Figure 32. One-second firing rate, one-second sweep rate air gun record across Oceanographer Canyon. The 10 in^{-3} air gun was pressurized to 800 psi and towed about 1.5 m below the surface. The recorded events between 0.057 second and 0.167 second are identified in the text.

the ambient pressure. Also the ambient pressure is decreasing continually because the bubble is steadily rising through the water column. At this point, because of the elasticity of the compressed air within the bubble, the process reverses and a second expansion begins. These alternating expansions and contractions are called bubble pulse oscillations.

Bubble pulses generate compressional waves within seismic frequencies, and continue to do so until the energy is diminished below the threshold of the receiving equipment or the bubble reaches the surface. In the case of a sparker source, only one bubble oscillation is recorded because steam is formed by the discharge and degenerates to water on the compression cycle (Fig. 27).

The air gun wave train in Figure 28 shows three bubble oscillations from a depth of 4.6 m. Not only does the energy diminish rapidly with each bubble oscillation, but the period becomes smaller. Energy is lost by turbulent water flow and other related effects which tend to decrease bubble size. In addition, smaller bubbles rise faster becaus they must move less water, and thus oscillate fewer times (Kramer et al., 1969).

Factors involved in determining bubble pulse periods are charge size and depth of explosion. These parameters are related by the empirical formula $T = [0.000209(KQ)^{1/3}][(d + 33)^{-5/6}]$, where (T) is bubble pulse period in seconds, and (d + 33) is a depth factor in which (d) is the source depth in feet and (33) is the atmospheric pressure correction factor. (K) is a constant equal to 1×10^{10} and 1.36×10^{7}, when (Q), the potential energy of the gas bubble at maximum radius, is expressed in kilojoules (sparker), and foot-pounds (air gun), respectively (Kramer et al., 1969). Based on data given by Kramer et al., 1969, a (Q) value of 40×10^{3} foot-pounds was approximated for the 10 in^3 air gun used for the record in Figure 1. A decrease in air gun operating pressure decreases the bubble pulse period.

The 139 msec event in Figure 32 is undoubtedly the bubble pulse. If the source is a 10 in^3 air gun pressurized to approximately 800 psi and towed at 1.5 m depth, then the bubble pulse period would be about 82 msec, and its arrival time at the hydrophone array would be 57 msec + 82 msec = 139 msec. The width of the return at 139 msec would probably obscure the surface reflection of the bubble pulse even if the bubble did not vent to the surface on the first oscillation as is probable with only a 1.5 m source depth. A high-speed recording oscillograph is usually required to resolve the surface reflection of a bubble pulse (Figs. 27 and 28).

4. Multiples

One of the consistently difficult problems in interpretation of single-channel seismic profiles is the identification and elimination of multiple path arrivals. The bottom-surface-bottom multiple is usually relatively simple to identify. For example, the bottom return (area on left side of Fig. 32) arrives at 266 msec, and the first bottom multiple is very likely the strong echo at 514 msec. The 18 msec difference between the times required for two surface-to-bottom round trips is undoubtedly due to shortening of the multiple's vertical path length relative to the primary's vertical path length, because of the more nearly vertical angle of incidence of the multiple reflected signal. Other factors that con firm the 514 msec event as the true bottom-reflected multiple are the characteristic repetition of shapes and the doubling of apparent dips (Fig. 32).

Intrabed, or 'peg-leg,' multiples are more difficult to identify than bottom-surface-bottom multiples. A simple rule of thumb in visual identification of an internal multiple is to look for changes in position of a reflector with respect

AD-A122 613 GEOLOGY OF A STABLE INTRAPLATE REGION: THE CAPE VERDE/CANARY BASIN(U) NAVAL OCEAN RESEARCH AND DEVELOPMENT ACTIVITY NSTL STATION MS J A BALLARD

2/2

UNCLASSIFIED MAR 82 NORDA-45 F/G 8/10 NL

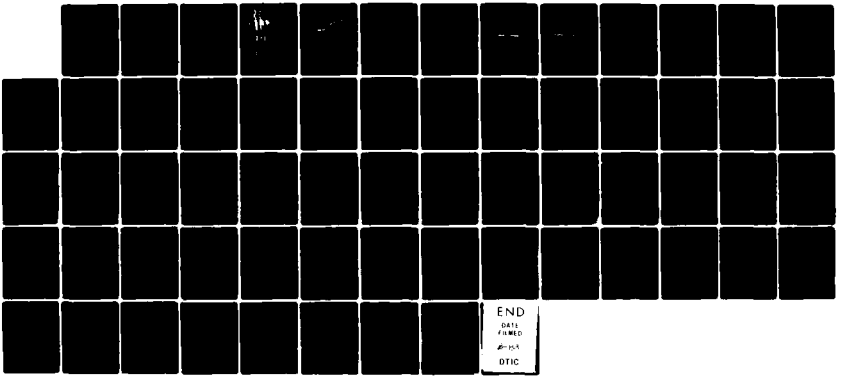

END

DATE FILMED

DTIC

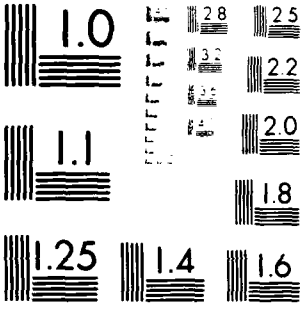

to the position of its suspected multiple. The suspected multiple should be parallel to the primary reflector, but displaced in time. This rule of thumb should be used judiciously because velocity variations between layers can cause apparent displacements (Fig. 33).

Although deep scattering layers and water inhomogeneities may produce multiples at frequencies commonly used for depth soundings, the interference of these factors is unusual at seismic frequencies. Nevertheless, strange events may be recorded for which no source is readily apparent (Fig. 34). The multiple event in Figure 34 is possibly some malfunction of the equipment, some unrecorded peculiarity in the geometry of the installation, or even a flaw on the recording paper. Its effect on the record is obvious.

Qualitative visual analysis is usually limited to the interval between the first bottom echo and the first bottom multiple. Digital data processing techniques are required for complete multiple suppression.

5. Velocity Effects

Compressional wave velocities in oceanic sedimentary and volcanic rocks vary both in horizontal and vertical directions. These velocity variations may cause some inconsistencies in record interpretation unless an allowance is made for their effects.

Low velocity layers within the stratigraphic column have long plagued terrestrial seismologists (Thompson, 1963). Figure 33 shows schematically the effect of thickening and thinning of low-velocity layers on the reflected record section. This figure illustrates that apparent thinning can be produced by increasing either thickness or velocity above a given horizon. For example, the apparent dip of reflectors underlying the head of Oceanographer Canyon (Fig. 32) is undoubtedly exaggerated by the increasing depth of water -- a thickening low-velocity layer in this case -- over the canyon axis.

Similarly, reflectors along the edge of a declivity, such as a canyon wall or slope break, will apear to downbend prior to outcropping when, in reality, these reflectors may outcrop horizontally. The reason is the same; that is, as the bottom slopes downward, the thickness of the slower water path increases while the faster sediment path remains the same. The result will be longer arrival times and an apparent downbending of the reflectors. To determine if velocity variations might be real cause for these effects, the reflections must be corrected for interval velocities and replotted to true scale (i.e., without vertical exaggeration.)

Vertical velocity variations have a profound effect on the apparent shapes of erosional channels and true synclines when these features are displayed on a seismic time section. For example, the apparent syncline at Point A in Figure 35 is very likely to be a true structural feature. Close examination of the reflectors beneath arrow (A) shows that dips become steeper with increasing depth, undoubtedly because the velocity increases with increasing depth, thus displacing successively deeper reflectors progressively upward on a time section. On the other hand, at Point B in Figure 35, an apparent syncline lies directly beneath an erosional channel. Accepting the validity of the coincidence of a syncline beneath an erosional channel does not explain the broadening of the feature with depth. The broadening of the apparent syncline with depth is due to the downward displacement in time of reflectors in response to the increased thickness of the low velocity water layer in the channel, thus resulting in a structure which is the artifact of a velocity anomaly (Tucker and Yorston, 1973).

Velocity variations may cause apparent thinning or apparent dip between reflecting horizons, faults that appear as folds, or horizontal reflectors that appear as gravity slides on the recorded

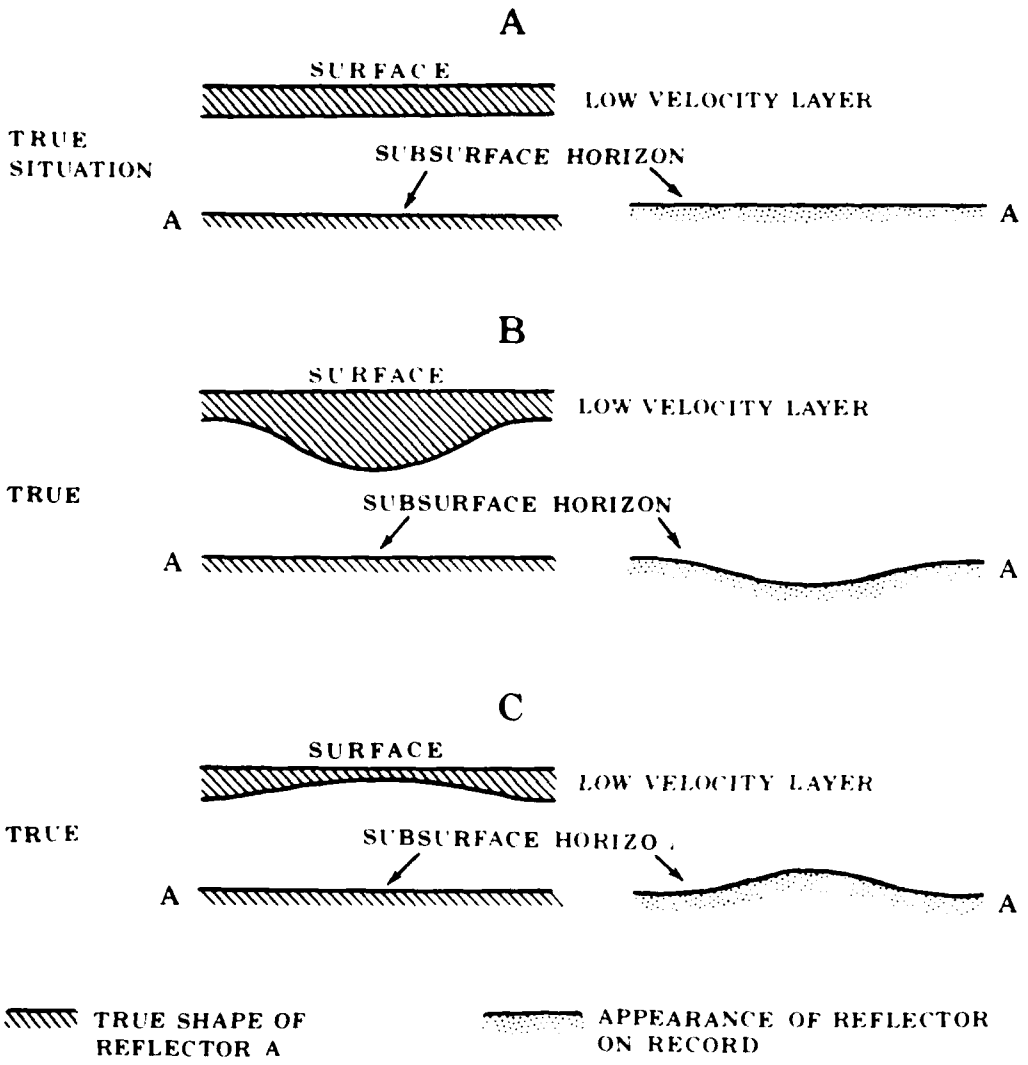

Figure 33. Effect of a low velocity layer on the recorded appearance of a horizontal reflector (after Thompson, 1963).

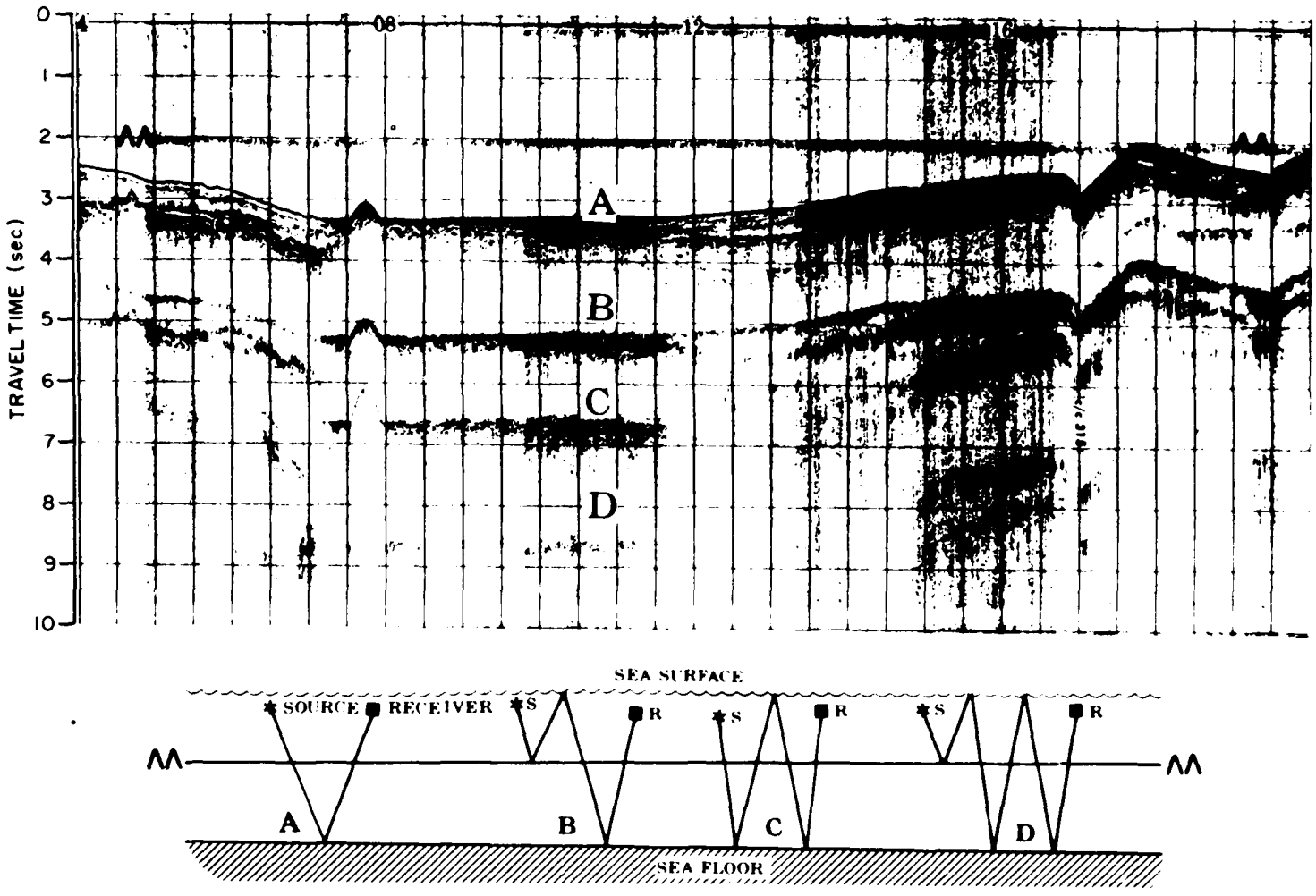

Figure 34. A multiple reflected event of unknown origin. Diagrams B and D are possible ray paths for signals reflecting from the inhomogeneity at 2 seconds, while A and C are the bottom echo and its multiple.

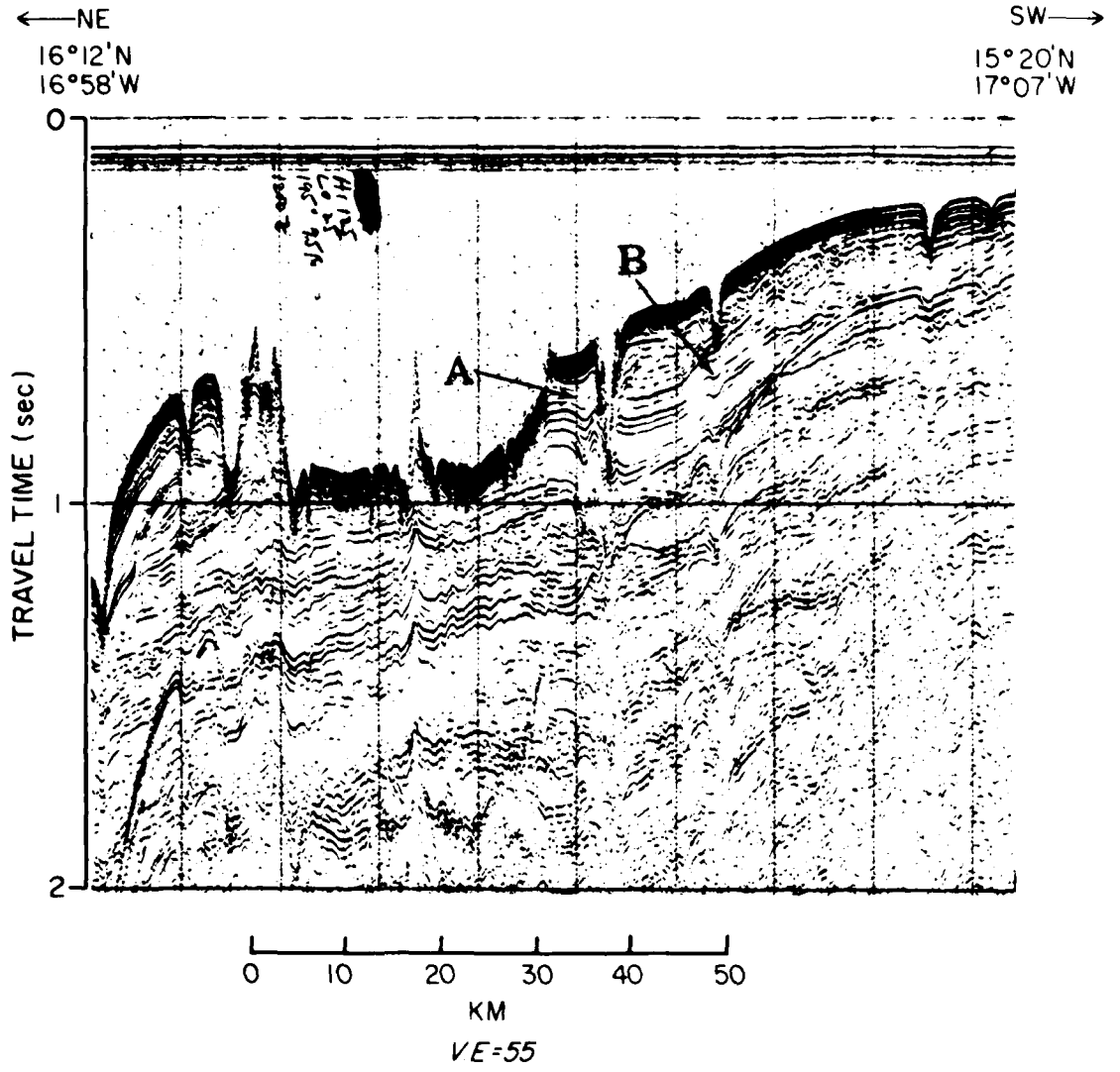

Figure 35. Synclines and erosional valleys along the Senegalese Continental Margin. Point A is an apparent syncline in which the dips of successively deeper reflections increase with depth, possibly because of velocity increases with depth. Point B is an apparent syncline in which dips of successively deeper reflections decrease and the entire structure widens with increasing depth. Point A is interpreted as a true syncline and Point B as an artifact of the increased thickness of an overlying low velocity layer (water, in this instance).

time sections. Tucker and Yorston (1973) maintain that the vagaries of geology are such that any coincidence of surface, near-surface, and subsurface reflectors is sufficient to suspect velocity inconsistencies.

6. Diffraction Effects

A diffraction is the echo pattern produced by energy scattered from a sharp peak, edge, or similar irregularity. Diffractions (side echoes) can cause small, sharp erosional valleys and synclines to appear to be underlain by anticlines (Fig. 36). A diffraction and an anticline can be distinguished because a diffraction is hyperbolic in that its maximum curvature is at the highest point and flattens out uniformly with depth. This situation exists because the point of origin of the diffraction does not move as the observation point is moved along the surface, whereas the apparent reflecting point moves in response to changes in receiver position. The limbs of a true anticline will appear to become less steep with depth because of the normal increase in velocity with depth (Tucker and Yorston, 1973). To detect these differences, the depth section should be replotted without vertical exaggeration because vertical velocity increases cause apparent decreases in vertical exaggeration.

Diffracted water wave arrivals may cause structures that appear as diapirs on the record (Ball, 1969). Diffracted water wave signals are common and may be of sufficient amplitude to obscure the configuration of reflectors beneath the apparent diapir if the reflector is restricted in the area. To determine if a diapir is real, or is a restricted area reflector, square the shallowest water depth over the crest of the suspected diapir, and add this quantity to the square of the horizontal distance from the crest of the ship's position. If this sum approximately equals the square of the water depth directly beneath the ship at the horizontal distance used, then the feature is likely an artifact of diffracted water wave arrivals (Ball, 1969) (Fig. 37).

In the case of a true intrusive or diapir, the actual width of the structure will be obscured by diffractions and weak reflections that occur within the length of the hydrophone array. Normally, lack of alignment of reflectors appearing within the length of the hydrophone array should present no problem except in very shallow water. For example, in 1 km water depth, the difference in arrival times between a sound wave at the first hydrophone in a 22 m long hydrophone array towed 183 m behind the ship, and the last hydrophone in that array, is 0.7 msec (assuming straight line propagation and 1.5 km/sec velocity). On a record in which one second of the vertical scale equals 119 m, this time difference equates to 0.08 mm of record length. In deeper water, the time differences would be less.

The edge of the intrusive is always somewhere inside the apparent limits of the structure. This situation is particularly obvious in cases where basement relief apparently preceded the sediment cover. Then the horizontally layered sediments will appear to have penetrated the sides of the basement high, when in reality, side echoes from the basement high are simply arriving ahead of the true sea floor reflections (Fig. 38). Krause (1962) developed equations for determining horizontal displacement of a diffracted arrival if the apparent slope of the feature producing the diffractions and the depth of the flat sea floor are known. Near Point A in Figure 38, the highest part of the flat sea floor is approximately 4,780 m below sea level, and the apparent slope of the lower part of the intrusive is 15.5°. Using these parameters in the equation $\overline{IJ} = Z_3 \times \tan \phi$, for dips of less than 30°, the horizontal displacement of the side of the intrusive is approximately 660 m (4780 X tan 15.5/2), when $\overline{IJ}$ is horizontal displacement, Z_3 is the depth of deeper flat bottom, and tan ϕ is the apparent dip (Krause, 1962, Eq. 37A). With a ship's speed of

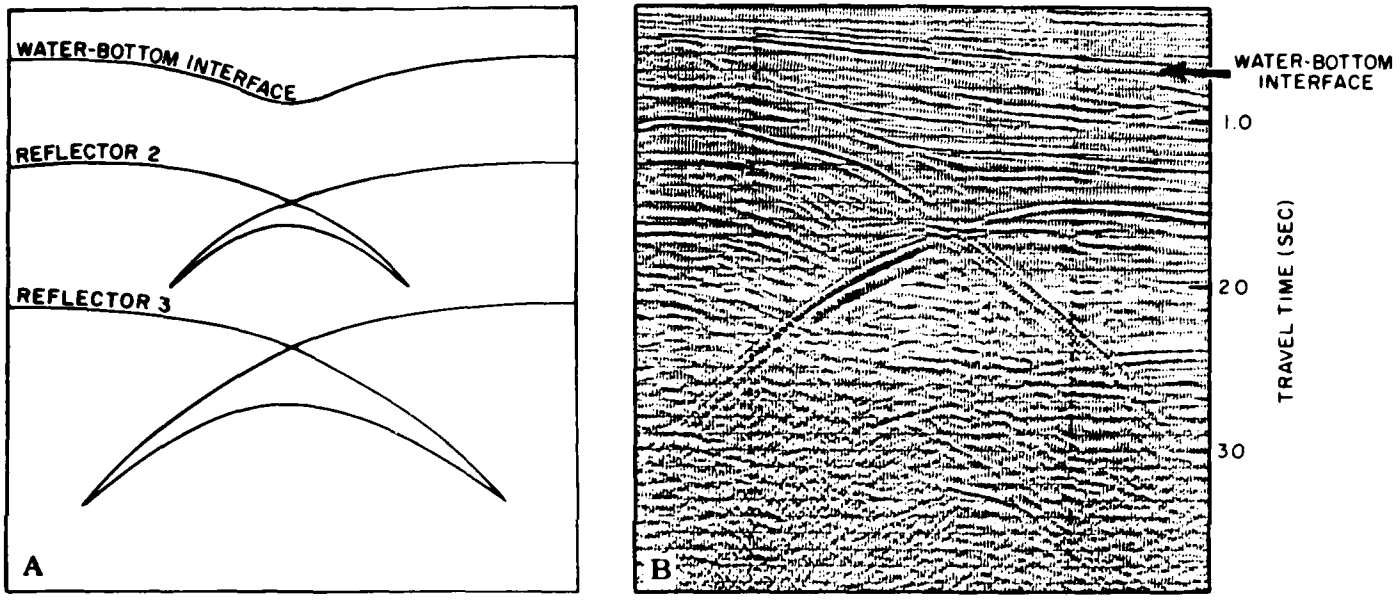

Figure 36. Sketch of an apparent anticline beneath a syncline. This pattern is caused by echoes from the sides of the syncline arriving after the true reflection. The increase in width of the apparent anticline and the decrease in dip of the limbs with the depth are clues to its true source (after Tucker and Yorston, 1973).

SCHEMATIC REPRESENTATION OF A POINT REFLECTOR AND
ACTUAL RECORDING OF A DIAPIR (NEAR POINT REFLECTOR)

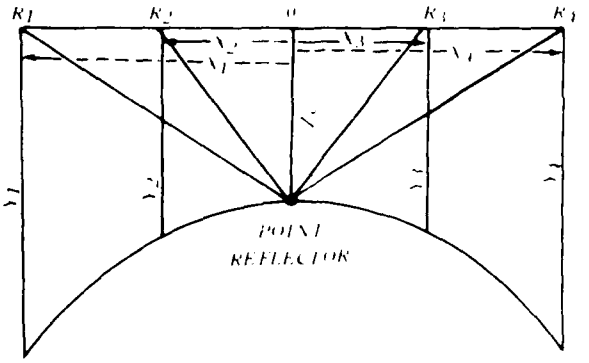

based on data from Ball (1969)

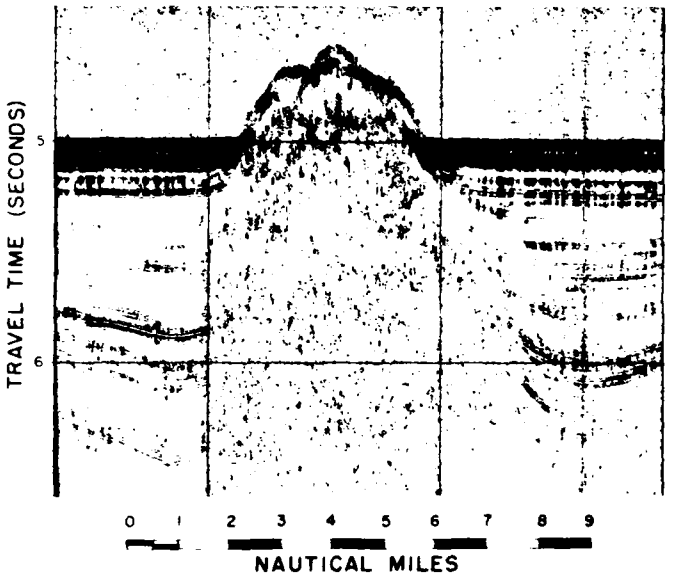

Figure 37. A sketch of Ball's (1969) technique for distinguishing diapirs from restricted area reflectors which generate apparent diapirs. R_1 through R_4 are receiver (ship) position; Z_c is water depth at the center of the structure; X_1 through X_4 are horizontal distances from the center of the structure; and Y_1 through Y_4 are water depths at receiver positions, as read from the record. If $(Z_c)^2 + (X_n)^2 = (Y_n)^2$, then the feature is very likely generated by a diffracted arrival.

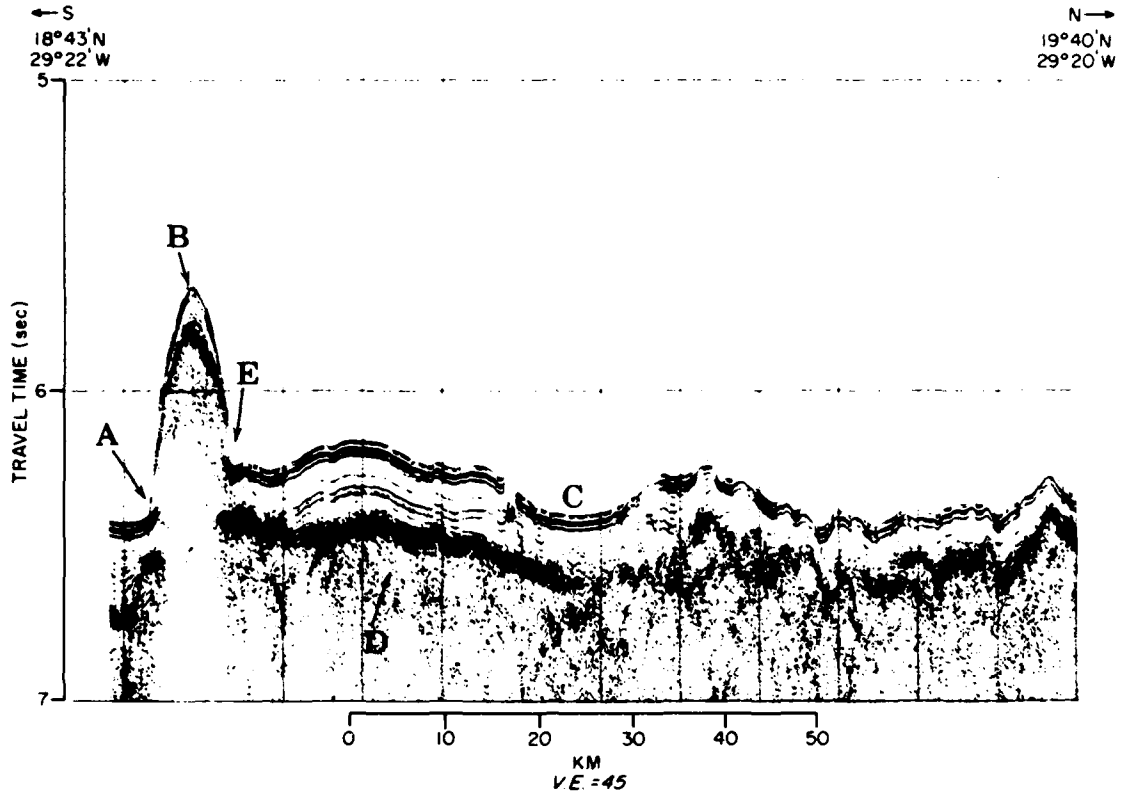

Figure 38. Record illustrating several reflection phenomena: (A) Diffraction arriving ahead of true sea floor reflection; (B) Amplitude decrease due to scattering (divergence) from a convex surface; (C) Amplitude increase due to convergence on concave surface; (D) Smooth basement with suggestion of layering. Reflection of this type may be produced by intrusions such as sills, lithified sediments overlying true volcanic basement, or volcanic debris reworked by currents; (E) Offset sea floor caused by sediment ponding behind peak (B), or by faulting. Sediments are approximately the same thickness on opposite sides of the peak; therefore, faulting appears the more probable.

18 km/h, diffractions from the intrusive begin arriving ahead of the true sea floor reflection about 2 minutes before the actual contact between the sea floor and the intrusive is reached. For slopes greater than 30°, it is necessary to convert apparent slopes to true slopes as illustrated in the section on dip calculations.

Because the insonified area of the bottom and sub-bottom is rather large, signals reflected from surfaces outside the plane of the profile will appear on the profile at apparent depths much greater than their true depths. In addition, reflections from dipping beds are shown as if their arrival paths are vertical rather than perpendicular to the reflector. The result is that the actual locations of dipping reflectors are updip, and shallower than they appear to be from the seismic profile (Ball, 1969). The best way to evaluate these phenomena is to run closely spaced lines with frequent cross checks.

7. Amplitude Effects

The 23 dB dynamic range claimed for the recording papers used with facsimile recorders effectively adds a z-component to standard x/y coordinate recorders. The intensity of the z-component is a qualitative measure of the amplitude of signals arriving at the hydrophone array. The displayed amplitudes represent reflecting horizons which, in turn, may approximately equal lithologic interfaces, and therefore are subject to lateral variations in both form and composition. Thus, even relative amplitude variations are capable of revealing a great deal of additional geological information if amplitude anomalies due to the instruments used and those due to operational geometry can be separated from the total returning energy.

Relative amplitudes may vary in response to source strength and directivity or to receiver coupling and directivity. The signal emitted by the source is capable of shot-to-shot variation. In the case of a sparker, bits of electrodes are spalled with each shot; electrode deterioration can become noticeable after an extended period of operation. The result is a gradual decrease in output energy which appears on the recorder as a gradually decreasing signal. To ameliorate electrode deterioration, the polarity of the electrodes must be changed. Before further evaluation of a relative amplitude change on a sparker record, the operational log should be examined to determine elapsed time since the most recent polarity check.

Similarly, source and receiver depth changes may reinforce or diminish reflected energy by increasing the bubble pulse period and constructively or destructively reinforcing reflected signals.

According to Schoenberger and Levin (1974), when a seismic wave passes through a cyclic section of sediments, the initial pulse is broadened by the generation of a set of intrabed multiples. The lower order multiples have the same phase as the initial pulse and tend to add energies at the lower frequencies. In addition, as the beds become thinner, the amplitude of the reflection will decrease because amplitude is proportional to thickness, but inversely proportional to wavelength (Widness, 1973). Owing to the vertical geometry of the reflectors, some echo sequences may appear on the record with amplitudes that are not related to the physical properties of the sediments in the section.

In addition to frictional absorption, interfering multiples, and other physical peculiarities, the inherent low passband nature of the earth leads to diminution of reflected energy. The proportion of low-frequency energy in the reflected passband increases as reflector depth increases, because the earth selectively attenuates the higher frequencies, thus reducing the overall signal level. After all identifiable sources of amplitude variations related to operational procedures and signal peculiarities have been resolved, those

anomalies remaining are likely to have some measure of geologic significance.

Acoustic energy may converge when reflected from a concave surface or diverge when reflected from a convex surface, thus producing high- and low-amplitude reflection sequences, respectively (Fig. 38). Convergence and divergence are qualitative measures of sub-bottom roughness because signal scattering occurs when sharp local relief (roughness) is greater than the wavelength of the signal divided by eight times the cosine of the angle of incidence (Leong et al., 1971). Although all surfaces are acoustically smooth at normal incidence (cosine of the angle of incidence becomes 0), all seismic energy may not reach the reflecting surfaces at normal incidence, resulting in variable intensity echos because of variations in scattering (Fig. 38).

Scattering, lateral variations in reflector lithology, cementations, and diffracted water wave arrivals from faults and point reflectors may appear on records as variations in relative amplitude with a variety of geometric shapes. For example, pagoda structures noted in the eastern Atlantic (Emery, 1973) and in other areas, may be due to these factors because 3.5 kHz sound waves may be scattered or coalesced by roughness features of less than 2 m relief (Leong et al., 1971).

Structural or facies relationships may be better understood by consideration of qualitative amplitude data (Larner et al., 1973). For example, strong reflections from the evaporitic sequence overlying a salt dome may help distinguish it from a shale dome or a depositional anticline. Marker horizons may be traced and correlated over widely separated areas on the basis of a characteristic reflected signal, one component of which is relative amplitude. Horizon A, a widespread sequence of closely spaced chert beds in the North Atlantic, is a well-known example of this phenomenon.

At a reflecting boundary, the Rayleigh reflection coefficient, a quantitative measure of amplitudes, is the ratio of the acoustic pressures of the incident and reflected waves. At normal incidence, the reflection coefficient (R) is determined from the expression

$$\frac{\rho_2 V_2 - \rho_1 V_1}{\rho_2 V_2 + \rho_1 V_1}$$

in which ρ_1, ρ_2 and V_1, V_2 are the densities and velocities in the upper and lower layers, respectively.

Hamilton (1970) calculated reflection coefficients for a variety of bottom sediment types in three geological environments and derived values between 0.4098 for a coarse-grained continental shelf sand and 0.0941 for an abyssal plain clay. Reflection coefficients are linearly related to porosity by the equation $R = 0.6468 - 0.6456\ (n)$, in which (R) is the reflection coefficient and (n) is porosity (Fass, 1969). Extremely high reflection coefficients for unconsolidated sands have been related to occurrences of natural gas; the reflection coefficient is a measure of fluid saturation because porosity and saturation are inversely proportional to velocity, but directly proportional to density. The sea floor is normally a good reflector because the large increase in densities more than offsets the small velocity variations across the water/sediment interface. Reflection coefficients decrease with depth because the magnitudes of layer-to-layer density/velocity variations decrease with increasing depth. Reflection coefficients can be estimated qualitatively from normal incidence seismic records when the first layer ($\rho_1 V_1$) is of low velocity and low attenuation because the reflection coefficient is frequency independent and is determined by the ratio between direct and reflected peak amplitudes (Hastrup, 1970).

8. Dip Calculations

In areas of constant slope, the recorded dip of bottom and sub-bottom reflectors

is less than the true dip of these reflectors (Krause, 1962). However, the tangent of apparent dip is approximately equal to the sine of true dip up to about 15° when the ship's track is parallel to the direction of true dip. Most oceanic structures have dips less than 15°.

When the relationship between ship's track and true dip is unknown and the apparent dip is greater than 15°, then it is necessary to correct for both ship's heading and apparent dips. The best approach for determining these factors is to calculate apparent dips and track heading at points where record sections intersect, and from these data, calculate true dip in the manner described by Brooks (1970).

Data available at the point of intersection of two tracks are apparent dip and ship's heading for each record. From the geometric relationship, the tangent of the apparent dip is equal to the tangent of the true dip times the cosine of the difference between ship's heading and true dip direction (tan ξ' = tan ξ cosβ' in Brooks' terminology). Of these parameters, only the tangents of apparent dip can be determined from the record, so it is necessary to define two other parameters.

One of these (δ), is the ratio of the tangents of the apparent dip angles from each profile (δ = tan ξ'/tan ξ''); and the other (η), is the cosine of the angle separating the two headings or (η = cos (β' + β'')) (Brooks, 1970). With these values, it is possible to calculate cos β' and cos β'', which are the variations of each track from true dip direction, and then substitute these values into the true/apparent dip relationship. These values are calculated from

$$\text{Cos } \beta' = S[(1-\eta)/(1-2\eta\delta + \delta^2)]^{1/2}$$

$$\text{Cos } \beta'' = [1-\eta^2/(1-2\eta\delta + \delta^2)]^{1/2}$$

which are Brooks' equations 7 and 8, respectively.

For a numerical example, assume that the apparent dip measured on a track bearing 345°T is 24° at the point of intersection, with a track bearing 015°T, and having an apparent dip of 18°. The first step is to calculate δ from tan ξ'/tan ξ''(.4452/.3249 = 1.3703), and then (η), which is cos((360-345) + (15-0)) = cos 30°. Using these values to find cos β' (Brooks' Eq. 7) and cos β'' (Brooks' Eq. 8) yields 0.70631 and 0.49564, respectively. Finally, substituting in tan ξ = tan ξ'/cos β' (0.4452/0.70631 = 0.63032) gives the angle of true dip as 32.22°, and tan ξ = tan ξ''/cos β'' (0.32492/0.49564 = 0.65555) gives the angle of true dip as 33.25°.

9. Vertical Exaggeration

Because the ordinate of the seismic chart recorder represents depth through the water column is seconds, and the abscissa represents distance over the ground in hours, some scale adjustment must be made. Vertical exaggeration, the ratio of horizontal scale to vertical scale, is one measure of this scale disparity.

Vertical exaggeration is calculated by referencing vertical and horizontal scales to unity. For example, in Figure 38, 1 hour of ship's travel time (horizontal scale) is equal to 3 cm of record length, or 16,470 m ground distance. On the vertical scale, 0.5-second travel time is also equal to 3 cm record length, or 366 m uncorrected depth. HS/VS is approximately equal to 45:1, which means that the vertical scale is expanded 45 times relative to the horizontal scale.

The effect of vertical exaggeration is to foreshorten distances and distort the width of features relative to their height, thus making gentle rises apear as precipitous slopes. Conversely, some degree of vertical exaggeration is necessary in order to recognize features that would likely be missed without some added emphasis. If true dips and surface gradients are to be determined,

the effects of vertical exaggeration must be removed either by replotting the record at 1:1 scale, or by dividing the tangent of the apparent slope by the vertical exaggeration to obtain the true tangent of the slope.

When correlating from one record to a record made on a different cruise, one must be aware of the effects of scale differences. This is primarily the reason for operating one recorder at a fixed sweep rate.

10. Resolution

Resolution is the minimum time between reflectors that can be reliably measured from the record. Ultimately, a complex interrelationship between reflector spacing, filter bandwidth, signal/noise (S/N) ratio, velocity/depth profile, source characteristics, and recording speed determines the minimum reflector thickness that can be resolved. Some of these factors can be quantitatively evaluated. Others, such as the S/N ratio, are qualitative and must depend on the experience and intuition of the analyst for meaningful evaluation.

According to Ricker (1953), the individual wave components of a seismic wave train are resolvable only when similar phases are separated in time by an amount greater than 0.428 of the time period of the wave. Based on this observation, the minimum resolvable reflector thickness is: $h = (0.428V/2f)$, where (V) is sound velocity in the sediments and (f) is the dominant frequency. For the case in which the sound speed is 1.5 km/sec and the center frequency is 50 Hz, the minimum resolvable layer thickness would be 6.42 m.

However, on a 4 sec sweep speed seismic record, one second of one-way travel time is represented by 119.06 mm of record width. At that scale, 6.42 m is represented by approximately 1.01 mm. Under the most favorable S/N conditions, approximately 7 m would be the minimum resolution if the outgoing signal were a single pulse.

The reflection group indicative of a single interface is made up of at least four separate events exclusive of the bubble pulse and its associated reflections (Fig. 32). If an average sparker bubble pulse time period of 0.025 sec is assumed, then the onset of the bubble pulse event will occur at 2.98 mm (0.025 sec X 119.05), after the beginning of the initial pulse. In addition, if the bubble pulse has all the ray paths shown in Figure 32, then an additional 0.008 sec (Fig. 27) will elapse before the beginning of the last part of the signal. This time delay is equivalent to a record length of about 1 mm. Thus, the total distance across the record corresponding to the initial wave train is approximately 4 mm, which equates to about 0.017 sec one-way travel time (4/119.06/2), or approximately 25 m at an assumed sound speed of 1.5 km/sec.

Frequently, the bottom return will be considerably wider than 4 mm without being degraded by adverse S/N ratio. In this case, it is safe to assume that layering exists in the upper 25 m, but it is often not possible to determine how many layers are present or how much they are separated.

The velocity/depth relationship is capable of affecting both the amplitude of the recorded signal and the reflector separation that can be resolved. For example, under the influence of a positive density/velocity product (ρc) gradient, reflectors separated about 1/4 wavelength (about 7.5 m for 50 Hz at 1.5 km/sec) will add constructively to produce a return of higher amplitude than either of the component echoes. However, for a negative ρc product gradient (Fig. 39), reflectors separated about $1/4\lambda$ will add destructively, and the total amplitude will be reduced.

These amplitude variations occur because a reflection that returns from a boundary characterized by an increase in ρc product will have the same phase as the initial signal striking the boundary. Conversely, when the structure of the ρc product is such that the overlying layer

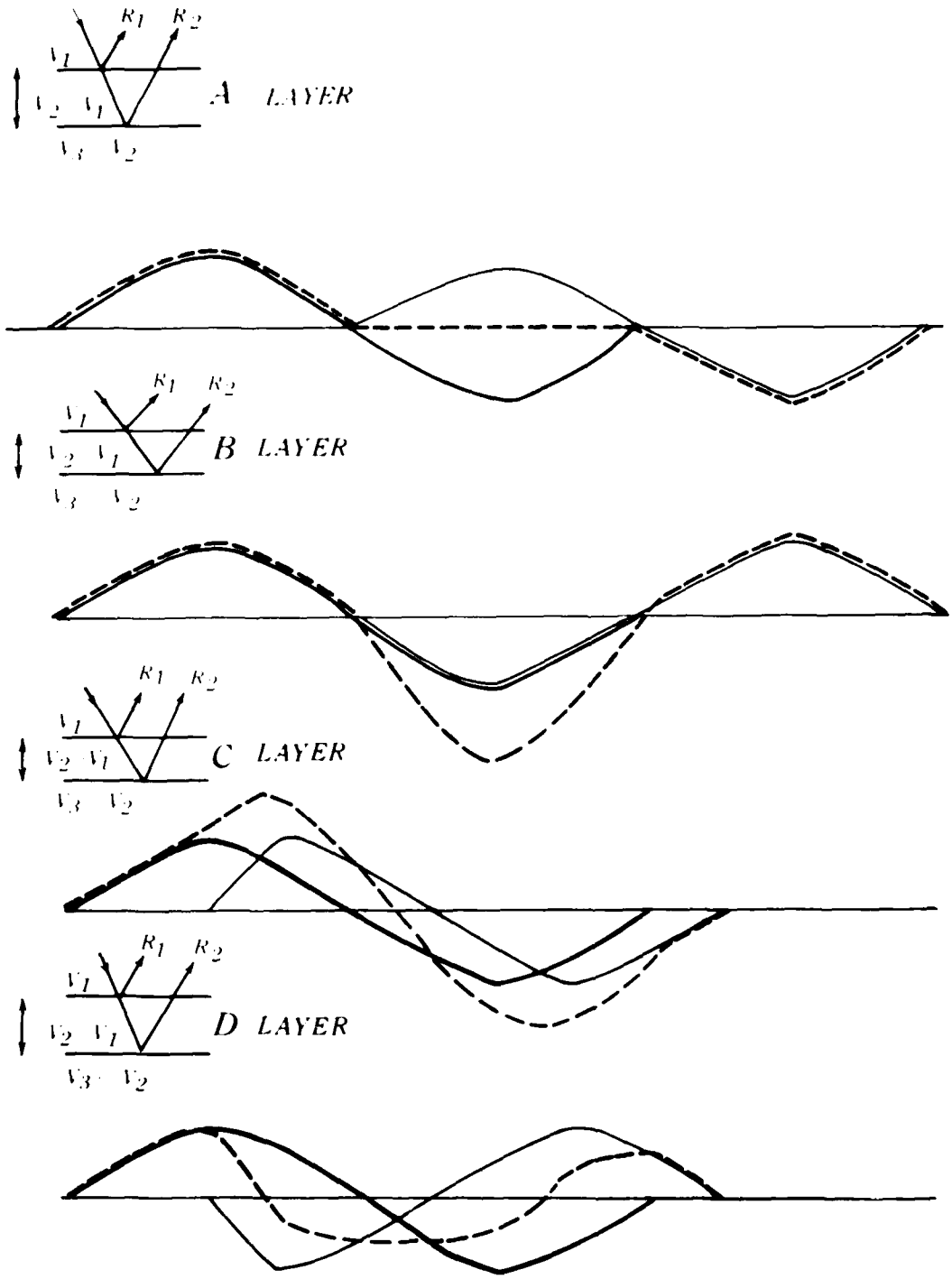

Figure 39. Schematic presentation of the recorded appearance of reflectors from layers with 1/2 wavelength separation (A and B), in which velocity increases with depth (A) and decreases with depth (D). The dashed line represents the combined recorded intensity of the two individual signals (light and heavy lines).

has a higher ρc product than the underlying (Fig. 39), then the seismic waves reflected from either surface of the layer will have different phases. These reflections sum differently from reflections with similar phases. For normal incidence waves, the phase shift will be 180° when the transmitting medium is high density/high velocity (water), and the medium across the reflecting interface is low density/low velocity (air).

Widness (1973) has noted that a reflector 1/8 wavelength thick is capable of returning constructively interfering echoes from both its top and bottom surfaces if the velocity gradient is negative (Fig. 39). The 1/8 λ is defined as the minimum thickness capable of supporting signal coherence at seismic frequencies. However, for 50 Hz reflections, 1/8 λ is about 3.25 m, and the time difference between top and bottom reflections would be 0.0004 sec [(2) X (3.25 m/1.5 km/sec)]. This time difference equates to 0.05 mm, and is not reliably resolvable from the record. As noted previously, about 25 m of subbottom reflection time (4 mm on the record) is required to encompass an entire wave train. If a single cycle of the predominant frequency (50 Hz) is 30 m long, it is unlikely that a portion of a single cycle will ever be recorded, or that constructive or destructive wave interference will be a recording problem.

F. Velocity Gradients and Depth Corrections

If a geological model of the ocean floor is based solely on normal incidence seismic reflection records, it must be considered qualitative, and thus speculative, because of the lack of velocity, density, or other mass physical property data for the sediments. To convert raw reflection data (time sections) to geophysical cross-sections representative of true depths to reflecting horizons, corrections must be made for the variations of velocity with increasing time within the sedimentaton section. Once the velocity model is established, additional meaningful inferences about the physical properties of the sediments may be made.

Velocity gradients are the rates of change of compressional wave velocities with increasing depths. Gradients are usually expressed as an increase in velocity per linear increase in depth or sec^{-1}. In the upper levels of deep ocean marine sediments, these gradients are positive and usually lie between 0.5 and 2.0 sec^{-1} (Houtz et al., 1968).

The purpose of this section is to show how data from other sources may be adapted for determining velocity structure. DSDP Site 138, located at 25°55.37'N, 25°33.79'W, will serve as an example for compilation of a bottom velocity model, because it contains all the necessary parameters to establish a velocity model and some independent measurements against which the model could be verified. USNS LYNCH cruise LY-33A made two crossings of this drill site and detected four persistent reflectors at 0.070, 0.180, 0.250, and 0.460 seconds 2-way travel time (Fig. 39). If the seismic reflection record is interpreted with an assumed sound speed of 1462.8 m/sec (nominally 1/800 sec/fm assumed by most recorders beneath the ocean floor will be 1462.8X (travel time/2), which equals 51, 132, 183, and 336 m, respectively. A check of the coring log for this site (Hayes, Pimm et al., 1972) revealed that a zone of silty clay and sand, identified as early Miocene, extended from 52 to 61 m, that no stratigraphic horizons could be identified near 132 m, that between 175 and 183 m depth the rate of drilling decreased dramatically indicating a harder layer of clay, that an indurated mudstone with chert layers was encountered near 240 m, and that basalt began at 435 m below the water/sediment interface (Fig. 40). Since the correspondence between apparent reflector depths and drilled depths is poor below 51 m, the conclusion is that vertical velocity changes occur with increasing depth within the sediment column.

Figure 40. Comparison of seismic reflection record across DSDP Site 138 and data derived from drilling records. Measured velocities from Hayes, Pimm et al. (1972), instantaneous velocities are calculated using average interval velocity and an approximated initial velocity. Note poor correlation between reflectors and stratigraphy and difference between apparent or uncor rected depths and depths corrected for interval velocity.

To establish sediment velocities that will permit apparent depths shown on the reflection record to be compared with drilled depths, interval velocities must be calculated by dividing drilled depth by the one-way travel time of the appropriate reflection. After calculating interval velocities along the drill hole, the following assumptions are made:

- The 0.070 sec reflector corresponds to the lithologic unit encountered at 52 m; therefore, an interval velocity of 1.486 km/sec is appropriate (Fig. 40).

- The reflector at an apparent depth of 132 m below the ocean floor is an artifact of a gradual change in sediment physical properties or of inexact interval velocity; however, if the abrupt change in drilling rates at 156 m represents an impedance mismatch of sufficient magnitude to produce a reflection, the calculation of an interval velocity between 52 and 156 m of 1.891 km/sec is permitted.

- The indurated clay zone beginning at 175 m may be related to the 0.180 sec reflector, although no reasonable interval velocity will account for the time differences between the 0.07, 0.180, and 0.250 reflections. A sonic velocity measurement for the interval between 183 and 190 m made on board GLOMAR CHALLENGER reports a velocity of 1.823 km/sec (Hayes, Pimm et al., 1972; Table 4, p. 141). An instantaneous velocity calculated for this depth is 1.836 km/sec; the difference between these two values is less than 1%.

- The reflection arriving at 0.250 sec may be due to the same lithology that produces the drilling rate changes near 250 m or the top of the indurated mudstone with chert layers found at a drilled depth of 255 m. The interval velocity within this zone is 2.657 km/sec, which may be excessive.

- The basement reflection arrives at 0.460 km/sec and is representative of the basalt encountered at 437 m below the water/sediment interface. The interval velocity in the zone between the 0.180 and the 0.460 reflectors is 2.007 km/sec.

Given interval velocities and reflection times, the only other parameter required for completing the bottom velocity model is the initial velocity or velocity at the water/sediment interface. Although no velocity measurements were made by GLOMAR CHALLENGER at the water/sediment interfaces, Hamilton (1970) details a technique of very accurately relating initial sediment velocity (V_0) to the velocity of the bottom water if the sediment type can be inferred. According to Hamilton, the ratio of sound velocity in seawater to sound velocity in sediment can be considered a constant for a particular bottom sediment type, because the only changes in sound velocity in the bottom water and sediment pore water are due to temperature and pressure changes. Temperature and pressure effects on the mineral grains are inconsequential, thus, both water and sediment velocities can be corrected to in situ conditions and the ratio between these velocities will be constant. For example, a pelagic silty clay from an abyssal hill area has a water/sediment interface velocity ratio of 0.985, a clayey silt from an abyssal plain has a velocity of 1.003, and a silty clay from a slope environment has a velocity ratio of 0.994 (Hamilton, 1970).

DSDP Site 138 is located near the foot of the African Continental Rise in an area where surficial sediments are described as green, silty clay with sand layers (Hayes, Pimm et al., 1972). The reflection profile across this site (Fig. 13) shows a series of closely spaced reflectors which very likely approximates silty clay continental slope environment. With this assumption and a bottom water velocity of 1515.8 msec at a depth of 5,288 m (Naval Oceanographic Office, SP-68, 1966), the initial bottom velocity (V_0) at the water/sediment interface is 1.507 km/sec (1515.8 X 0.994).

To determine the velocity gradient (a) in the sedimentary section, the gradient equation developed by Houtz and Ewing

(1963) is used. In this equation, $a = (V-V_0)/1/2h$, the layer thickness (h) is divided in half because the instantaneous velocity (V) is an average that is assumed to be representative of the midpoint of the layer.

Average gradient is the most practical parameter for correcting apparent depths to very nearly true depths. Thus, the average velocity for the entire section is 1.90 km/sec (437 m(1/2(0.46 sec))), and the average gradient is 1.799 sec^{-1} when V_0 is 1.507 km/sec.

To determine instantaneous velocity at any depth in the presence of a linear gradient, multiply gradient by depth and add to the intital velocity. For example, at a depth of 428 m in DSDP Site 138, the calculated instantaneous velocity is 2.277 km/sec (V_0 = 1.507, h = 428 m, a = 1.799 sec-1). Between 425 m and 431 m in drill hole 138, three sonic velocity measurements in dolomite silts and carbonaceous muds averaged 2.369 km/sec (Hayes, Pimm et al., 1972; Table 4, p. 141) or less than a 4% difference when compared with a value obtained by an average gradient method.

For correcting apparent reflector depths to more realistic depths, the linear gradient equation can be rewritten in the Houtz and Ewing (1963) format, as $h = V_0(e^{at}-1)/a$. With this equation, the depths to reflecting horizons at drill Site 138 are 54, 147, 211, and 429 m, respectively. Intervals at 147 and 211 m were not cored, and the only indication of lithologic changes are slight changes in the drilling rate (Fig. 40).

The calculated reflection depths permit two conclusions:

- Seismic reflections cannot always be correlated with lithologic horizons.

- When an average linear gradient value is used to calculate depths, variations between true and calculated reflector depths will exist, especially as the sedimentary section becomes thicker. This latter situation occurs because gradients decrease with increasing depth in the sedimentary column. A more realistic travel time vs. velocity curve would show interval velocity decreasing downward as shown by Houtz et al. (1968).

As a rule-of-thumb, a linear gradient should be reasonably satisfactory to a one-way travel time depth of about 0.5 sec. Below that depth, a nonlinear gradient curve should be used if the considerable quantity of refraction data required for its construction are available; otherwise, the limitations of the results should be recognized.

G. Data Conversion

Seismic reflection records, on which isopach and structural contour charts are based, are normally assembled from all available sources. As a result, these data are recorded at a variety of shot repetition rates, recorder speeds, ship speeds, vertical exaggerations, and navigational accuracies. Prior to compilation, the analog records must be put into a digital format. One method of achieving this conversion is with an electro-mechanical digitizer, such as the Edwin Industries 4-place X/Y digitizing table. However, this process introduces errors, the magnitude of which must be considered.

On the 10-second vertical scale record, the worst-case -- 10 seconds of 2-way travel time -- is represented by 3,818 digitizing table units along the record ordinate. This equates to approximately 0.955 table units per 1/4000 sec travel time, or one nominal fathom, the usual recorder scale. Consequently, one digitizing table ordinate unit is approximately 1.94 m (1.047 fm). The record ordinates are always oriented to within $\pm$2.5 table units. This means that elevation differences of 9.7 m are distributed over the digitized width of the record, or that any single digitized value may have $\pm$1 m error because of record misalignment on the digitizing table. If the record length is 12 hours, thus representing 185 to 220 km, then the error introduced by acceptable

alignment of the paper reduces to about 0.092 m/km of track.

Along the abscissa, one hour of ship's travel time (150 lines per inch horizontal scale of the recorder) is equivalent to 483 digitizing table units. If a ship's speed of 16.7 km/h is assumed, then 30 table units represents 1 km. Abscissa orientation variances of $\pm 2\frac{1}{2}$ digitizing table units means that approximately 0.18 km will be distributed over the horizontal scale of the record section being digitized.

The other major source of digitizing error is identification of the onset of the reflection event. For the ocean floor event, several operator checks have shown a reading repeatability of ± 3 table units (5.82 m). The onset of basement and intermediate reflections are much more difficult to determine than the onset of the bottom event. As a result, the absolute depth to basement is estimated to contain as many as five digitizing table ordinate units of error. On a 10 sec vertical scale, 150 lines per inch of horizontal scale record (the maximum case), this equates to approximately 10 m of vertical variation. Ultimately, it is the signal/noise quality of the record that controls the relative accuracy of the determination of reflection time; i.e., good records are easy to pick, poor records are difficult to pick.

After data points are scaled at unfixed, frequent intervals from the original record, they are averaged and compared at 3 min intervals. This means that data points are spaced at even time increments, but at variable distance increments. This procedure is unlikely to produce serious errors in the data because the difference between a maximum ship's speed of 18.50 km/hr and a minimum ship's speed of 12.95 km/hr is only 0.28 km for 3 minutes of steaming time. In fact, the averaging routine serves to smooth some of the vertical fluctuations or jitter introduced in the original data by operator's placement of the cursor or the inconsistency of selecting the onset of deep reflections.

H. Summary

The question that remains after all the environmental, instrumental, and interpretational constraints have been considered is: Do the data present a unique and viable solution to a geologic problem? Although this question can never be precisely answered, the converse -- What would be the effect of not considering these constraints? -- can be approximated. For example, Figure 40 shows that a reflector could be mislocated by about 100 m in 0.5 sec 2-way travel time, unless velocity data are used to correct to more appropriate depths. The effect of incorrect depths on sedimentation rate calculations or structural contours would be considerable. Similarly, failure to consider vertical velocity changes may also lead to interpretation of erosional features as synclines (Fig. 35), or the derivation of unrealistic shapes for features beneath low-velocity layers (Fig. 33).

An analysis which fails to account for diffraction effects could lead to imprecise location of the boundary between horizontal sediments and an emergent peak (Fig. 38), the misinterpretation of side echoes as diapirs (Ball, 1969), or the conclusion that the sea floor is plunging beneath an oceanic trench. Even though reflector resolution of less than 7 m is possible, the noise introduced by bubble pulse oscillations, secondary ray paths, and instrumental distortions reduces resolution to 25 m or more. Other hazards to instantaneous correlations include variable vertical exaggerations, variations in amplitudes of reflected signals, and failure to reconcile differing reflection models with different geologic regimes. Even though the drawbacks to collection and interpretation of reflection seismic data seem overwhelming, the seismic method remains the most rapid procedure for developing a reasonable and consistent quantitative geological model of the sea floor and its covering layers of sediments.

VIII. References

Albers, Vernon M. (1965). Underwater Acoustics Handbook-II: University Park, Penn., The Penn. State Univ. Press, 290 p.

Allen, F.T. (1972). Some Characteristics of Marine Sparker Seismic Data. Geophysics, V. 37, p. 462-470.

Anderson, V.D. (1953). Wide Band Sound Scattering in the Deep Scattering Layers: San Diego, CA, Scripps Institution of Oceanography, 17 p. (SIO Ref. 53-36, Unpublished).

Anguita, F. and F. Hernan (1975). A Propagating Fracture Model Versus a Hot Spot Origin for the Canary Islands. Earth and Planet Sci. Lett., V. 23, p. 337-348.

Ball. M.M. (1969). Discussion Diapers of Magdalena Delta. Bull. Am. Assn. Petrol. Geol., V. 53, p. 2195-2196.

Ballard. J. Alan and L.G. Hemler (1969). Structure of the Cape Verde Basin. EOS: Trans. Am. Geophys. Union, V. 50, p. 251.

Ballard, J.A. and R.C. Michael-Thome (1979). The Cape Verde Islands. In: R.W. Fairbridge (ed.), Encyclopedia of World Regional Geology, Part II. New York, Dowdes, Hutchinson, and Ross, Inc. (in press, 1979).

Ballard, J. Alan and F.H. Sorensen (1968). Preglacial Structure of Georges Basin and Northeast Channel, Gulf of Maine. Bull. Am. Assn. Petrol. Geol., V. 52, p. 494-500.

Ballard, J.A., P.R. Vogt, and J. Egloff (1976). Seismic Structure of the J-Anomaly in the Eastern Atlantic. EOS, Trans. Am. Geophys. Union, V. 57, p. 289.

Barrett, D.L. and C.E. Keen (1976). Mesozoic Magnetic Quiet Zone and Sea-Floor spreading in the Northwest Atlantic. J. Geophys. Res, V. 81, p. 4875-4884.

Bebiano, J.B. (1932). "A Geologia do Arquipelago do Cabo Verde. Comm. Serv. Geol. Portugal, V. 18, 276 p.

Bedenbender, J.W., R.C. Johnson, and E.B. Neitzel (1970). Electroacoustic Characteristics of Marine Seismic Streamers. Geophysics, V. 35, p. 1054-1072.

Bond, Gerald (1978). Evidence for Late Tertiary Uplift of Africa Relative to North America, South America, Australia and Europe. J. Geol., V. 86, p. 47-65.

Brooks, M. (1970). Some Trigonometric Formulae for the Interpretation of Continuous Seismic Profiles. Int. Hydrog. Rev., V. 47, p. 65-72.

Brophy, J.J. (1976). Basic Electronics for Scientists. New York. McGraw-Hill, 471 p.

Burke, K. and J.T. Wilson (1972). Is the African Plate Stationary? Nature, V. 239, p. 387-390.

Canary Islands (1975). In: New Encyclopedia Britannica, Chicago, Encyclopedia Britannica, Inc., V. II, p. 502.

Collette, B.J., J.I. Ewing, A. Lagary, and M. Truchen (1969). Sediment Distribution in the Oceans: The Atlantic Between 10° and 19°. Marine Geology, V. 7, p. 279-346.

Collette, B.J. and K.W. Rutten (1970). Differential Compaction vs. Diapirism in Abyssal Plains. Mar. Geophys. Research, V. 1, p. 104-107.

Colom G. (1955). Jurassic-Cretaceous Pelagic Sediments of the Western Mediterranean and the Atlantic Ocean. Micropaleontology, V. 1, p. 109-124.

Dewey, John (1972). Plate Tectonics. Scientific American, V. 226, No. 5, p. 26-34.

Dillon, W.P. and J.M.A. Sougy (1974). Geology of West Africa and Canary and Cape Verde Islands. In: A. E. M. Nairn and F. G. Stehli (eds), The Ocean Basin and Margin, V. 2, The North Atlantic. New York, Plenum Press, p. 315-390.

Egloff, J. (1972). Morphology of Ocean Basin Seaward of Northwest Africa: Canary Islands to Monrovia, Liberia. Bull. Am. Assn. Petrol. Geol., V. 56, p. 694-706.

Embley, R.W. and R.D. Jacobi (1977). Exotic Middle Miocene Sediment From Cape Verde Rise and Its Relation to Piercement Structures. Bull. Am. Assn. Petrol. Geol., V. 61, p. 2004-2009.

Embley, R.W., P.D. Rabinowitz, and R.D. Jacobi (1978). Hyperbolic Echo Zones in the Eastern Atlantic and the Structure of the Southern Madeira Rise. Earth and Planet Sci. Lett., V. 41, p. 419-433.

Evenden, B.S. and D.R. Stone (1971). Seismic Prospecting Instruments, V. II: Instrument Performance and Testing. Berlin, Gebruderborn-Traeger, 195 p.

Ewing, J.I and G.B. Tirey (1961). Seismic Profiler. J. Geophys. Res., V. 66, p. 2917-2927.

Ewing, M., G. Carpenter, C. Windisch, and J. Ewing (1972). Sediment Distribution in the Oceans: The Atlantic. Bull. Geol. Soc. Am., V. 84, p. 71-88.

Fairbridge, Rhodes W., Arnold Gordon, and Eric Olaussen (1966). The Atlantic Ocean. In: R. W. Fairbridge (ed.), Encyclopedia of Oceanography, New York, Reinhold Publishing Company, 1021 p.

Fass, R.W. (1969). Analysis of the Relationship Between Acoustic Reflectivity and Sediment Porosity. Geophysics, V. 34, p. 546-553.

Gastesi, Paloma (1973). Is the Betancuria Massif Fuerteventura, Canary Islands, an Uplifted Piece of Oceanic Crust. Nature, V. 246, p. 102-104.

Giles, Ben F. (1968). Pneumatic Acoustic Energy Source. Geophys. Prospecting, V. 16, p. 21-53.

Grunau, H.R., P. Lehner, M.R. Cleintaur, P. Allenback, and G. Backer (1975). New Radiometric Age and Seismic Data from Fuerteventura (Canary Islands), Maio (Cape Verde Islands) and Sao Tome (Gulf of Guinea). Progress in Geodynamics, Amsterdam, Roy. Soc. Neth. Acad. Arts and Sci., p. 89-118.

Hallam, A. (1971). Mesozoic Geology and the Opening of the Atlantic. J. Geol., V. 79, p. 129-157.

Hamilton, E.L. (1970). Reflection Coefficients and Bottom Losses at Normal Incidence Computed from Pacific Sediment Properties. Geophysics, V. 35, p. 995-1004.

Handschumacher, D.W. and J.E. Andrews (1975). Kana Keoki Fracture Zone. Geology, V. 1, p. 25-28.

Handschumacher, D.W. and L. Kroenke (1978). An Extended Time Scale for Mesozoic Geomagnetic Reversals (abs). EOS, Trans. Am. Geophy. Union, V. 59, p. 266.

Harbison, R.N., R.K. Lattimore, and P.A. Rona (1973). Structural Lineations in the Canary Basin, Eastern Central North Atlantic. Marine Geology, V. 14, p. 269-275.

Hastrup, O.F. (1970). Digital Analysis of Acoustic Reflectivity Tyrrhenian Abyssal Plain. J. Acoust. Soc. Am., V. 47, p. 181-190.

Hayes, D.E., A.C. Pimm et al. (1972). Initial Reports of the Deep Sea Drilling Project, V. 14. U.S. Government Printing Office, Washington, DC, p. 975.

Hayes, D.E. and P.D. Rabinowitz (1975). Mesozoic Magnetic Lineations and the Mesozoic Zone off Northwest Africa. Earth and Planet. Sci. Lett., V. 28, p. 105-115.

Hays, James D. and Walter C. Pitman III (1973). Lithospheric Plate Motion, Sea Level Changes and Climatic Consequence. Nature, V. 246, p. 18-21.

Heezen, B.C., M. Tharp, and M. Ewing (1959). The Floors of the Oceans, I. North Atlantic. Denver, CO., (Geol. Soc. Am. Spec. Pap. 65). 122 p.

Heezen, B.C. and A.S. Laughton (1963). Abyssal Plains. In: M.M. Hill (ed.), The Sea. New York, Interscience, V. 3, p. 312-364.

Heirtzler, J.R. (1974). The Evolution of the North Atlantic Ocean. In: A. E. M. Nairn and F. G. Stahi (eds.), The Ocean Basin and Margins, V. 2, The North Atlantic. New York, Plenum Press, p. 191-196.

Horton, C.W. (1959). Signal Processing of Underwater Acoustic Waves. U. S. Government Printing Office, Washington, D.C., 286 p.

Houtz, R.E. and J.I. Ewing (1963). Detailed Sedimentary Velocities from Seismic Refraction Profiles in the Western North Atlantic. J. Geophy. Res., V. 68, p. 5233-5258.

Houtz, R.E., J.I. Ewing, and Xavier LePichon (1968). Velocity of Deep-Sea Sediments from Sonobuoy Data. J. Geophys. Res., V. 73, p. 2578-2596.

Junger, Arne (1964). Signal-to Noise Ratio and Record Quality. Geophysics, V. 29, p. 992-995.

Jones, E.J.W., A.S. Laughton, M.N. Hill, and D.A. Davies (1966). Geophysical Study of the Western Boundary of the Madeira - Cape Verde Abyssal Plain. Deep Sea Research, V. 13, p. 889-907.

Knott, S.T. (1973). Operational Technique for Continuous Seismic Profiling and Related Studies. Wood Hole, MA, Woods Hole Oceanographic Institution, 71 p. (WHOI Ref. 70-43, unpublished).

Kramer, F.S., R.A. Peterson, and W.C. Walter (1969). Seismic Energy Sources. Paper OTC 1119, V. 2, Preprints. Houston, TX, Offshore Technology Conference. p. 387-416.

Krause, Dale C. (1962). Interpretation of Echo Sounding Profiles. Int. Hydrog. Rev., V. 39, p. 65-123.

Lancelot, Y. and R.W. Embley (1977). Piercement Structures in Deep Oceans. Bull. Am. Assn. Petrol. Geol., V. 61, p. 1991-2000.

Larner, K.L., E.J. Mateker, and C. Wu (1973). Amplitude: Its Information Content. Mexico City, Mexico, 43rd Annual International Meeting of the Society of Exploration Geophysicists. (Preprint).

Larson, R.L. and T.W.C. Hilde (1975). A Revised Time Scale of Magnetic Reversals for the Early Cretaceous and Late Jurassic. J. Geophys. Res., V. 80, p. 2586-2594.

Larson, R.L. and W.C. Pitman IV. (1972). World-Wide Correlation of Mesozoic Magnetic Anomalies, and Its Implications. Bull. Geol. Soc. Am., V. 83, p. 3645-3662.

Leong, W.K., T.K. Kan, and C.S. Clay (1971). Use of Acoustic Scattering Theory to Interpret Marine Geophysical Data. Madison, WI, Univ. of Wisconsin, 32 p. (Univ. of Wisc. Res Rpt., Series #71-1).

LePichon, X. and P.J. Fox (1971). Marginal Offsets, Fracture Zones and the Early Opening of the North Atlantic. J. Geophys. Res., V. 76, p. 6294-6308.

LePichon, X., I. Francheteau, and J. Bonin (1973). Plate Tectonics. New York, Elsevier Scientific Publishing Company, p. 300.

Lowrie, A., J. Egloff, and W. Jahn (1978). Kane Seamount in the Cape Verde Basin, Eastern Atlantic. Marine Geology, V. 26, p. M29-M35.

Lowrie, A. and E. Escowitz (1969). KANE 9. Washington, DC, U.S. Government Printing Office. 976 p.

Luehrmann, W.H., T.R. Shugart, and W.H. Parker (1970). Marine Seismic Streamer Noise Analyses and Tests. Los Angeles, 40th Annual International Meeting of the Society of Exploration Geophysicists. (Preprint).

Luyendyk, B.P. (1970). Origin and History of Abyssal Hills in the Northeast Pacific Ocean. Bull. Geol. Soc. of Amer., V. 81, p. 2237-2260.

MacClure, D.C., H.F. Nelson, and W.B. Huckabay (1958). Marine Sonoprobe System, New Tool for Geologic Mapping. Bull. Am. Assn. Petrol. Geol., V. 42, p. 701-716.

Maury, M.F. (1855). Physical Geography of the Seas. New York: Harpers, 531 p.

Menard, H.W. and T.E. Chase (1970). Fracture Zones. In: A.E. Maxwell (ed.), THE SEAS, V. 4, Part I. New York, Wiley-Interscience. p. 421-443.

Menard, H.W. (1969). Elevation and Subsidence of Ocean Crust. Earth and Planet Sci. Lett., V. 6, p. 275-284.

Mero, Thomas and John Freitag (1974). Seismic Source Signature Analysis. Washington, DC, U. S. Naval Oceanographic Office, Technical Note 222-5-74, 29 p. (unpub.).

Morgan, W.J. (1971). Convection Plumes in the Lower Mantle. Nature, V. 230, p. 42-43.

Musgrove, A.W. (1962). Application of the Expanding Reflection Spread. Geophysics, V. 27, p. 981-993.

National Defense Research Committee (1946). Principles and Applications of Underwater Sound Summary Technical Report of Division 6. Washington, D.C., U.S. Govt. Printing Office, V. 7, 307 p.

Olhovick, V.A. (1964). The Causes of Noise in Seismic Reflection and Refraction Work. Geophysics, V. 29, p. 1015-1030.

Padberg, L.R. Jr. (1958). Subsurex - A New Approach to Geophysical Exploration Using Sonic Frequencies. World Petrol., March, p. 60-63.

Part, G.K. (1950). Volcanic Rocks from the Cape Verde Islands. Bull. Brit. Mus. (Natur. Hist.), V. 1, p. 25-72.

Part, G.M. (1951). Tertiary and Pleistocene Sediments from the Cape Verde Archipelago. Geol. Mag., V. 88, p. 65-69.

Pautot, G., J.M. Auzerde, and X. LePichon (1970). Continuous Deep-Sea Salt Layer Along the North Atlantic Margins Related to Early Phase of Rifting. Nature, V. 227, p. 351-354.

Peterson, M.N.A. et al. (1970). Initial Reports of the Deep Sea Drilling Project, V. IV. Washington, D.C., U. S. Government Printing Office, 501 p.

Pitman, W.E. III (1979). The Effect of Eustatic Sea Level Changes on Stratigraphic Sequences at Atlantic Margins. In: J.S. Watkins, Lucien Montadert, and P.W. Dickerson (eds.), Geological and Geophysical Investigations of Continental Margins. Tulsa, OK, Am. Assn. Petrol. Geol. (Am. Assn. Petrol. Geol. Mem. 26), p. 453-460.

Pitman, W.C. III and M. Talwani (1972). Sea-Floor Spreading in the North Atlantic. Bull. Geol. Soc. Am., V. 83, p. 619-646.

Pratt, Richard M. (1963). Great Meteor Seamount. Deep-Sea Research, V. 10, p. 17-25.

Ricker, N. (1953). Wavelet Contraction, Wavelet Expansion, and the Control of Seismic Resolution. Geophysics, V. 18, p. 769-792.

Rona, P.A., J. Brakl, and J. R. Heirtzler (1970). Magnetic Anomalies in the Northeast Atlantic between the Canary and Cape Verde Islands. J. Geophys. Res., V. 75, p. 7412-7420.

Rona, P.A. and H.S. Fleming (1973). Mesozoic Plate Motions in the Eastern Central North Atlantic. Marine Geology, V. 15, p. 239-252.

Rona, P.A. (1969). Possible Salt Domes in the Deep Atlantic off Northwest Africa. Nature, V. 224, p. 141-143.

Rona, P.A., R.N. Harbison, and S.A. Bush (1974). Abyssal Hills of the Eastern Central North Atlantic. Marine Geology, V. 16, p. 275-292.

Rothe, P. and H.V. Schmincke (1968). Contrasting Origins of the Eastern and Western Islands of the Canarias Archipelago. Nature, V. 218, p. 1152-1154.

Rothe, Peter (1973). Sedimentation in the Deep-Sea Areas Adjacent to the Canary and Cape Verde Islands. Marine Geology, V. 14, p. 191-206.

Sangree, J.B. and J.M. Widmier (1977). Seismic Stratigraphy and Global Changes of Sea Level, Part 9: Seismic Interpretation of Clastic Depositional Facies. In: C.E. Payton (ed.), Seismic Stratigraphy Applications to Hydrocarbon Exploration, Tulsa, OK, Amer. Assn. Petrol. Geol., p. 165-184.

Sarnthein, Michael (1977). Neogene Sand Layers off Northwest Africa: Composition and Source Environment. In: Lancelot, Y., E. Seibold et al. (1977). Initial Reports of the Deep Sea Drilling Project, V. 41, Washington, U.S. Government Printing Office, p. 939-960. (Supplement to V. 41).

Schmincke, H.U. (1967). Cone Sheet Swarm, Resurgence of Tejedas Caldera, and the Early Geologic History of Gran Canaria. Bull. Volcanology, V. 31, p. 153-162.

Schmincke, H.U. (1973). Magnetic Evolution and Tectonic Regime in the Canary, Madeira, and Azores Island Groups. Bull. Geol. Soc. Am., V. 84, p. 633-648.

Schneider, E.D. and G.L. Johnson (1970). Deep Ocean Diapiric Structures. In: F.M. Delaney (ed.), The Geology of the East Atlantic Continental Margin. Great Britain Inst. Geol. Sci. Dept. 70/13, p. 153-175.

Schoenberger, M. and F.K. Levin (1974). Apparent Attenuation Due to Intrabed Multiples. Geophysics, V. 39, p. 278-291.

Schoenberger, M. and J.F. Mifsud (1974). Hydrophone Streamer Noise. Geophysics, V. 39, p. 781-793.

Schoenberger, Micheal (1970). Optimization and Implementation of Marine Seismic Arrays. Geophysics, V. 35, p. 1038-1053.

Sclater, J.G., R.N. Anderson, and M.L. Bell (1971). Elevation of Ridges and Evolution of the Central Eastern Pacific. J. Geophys Res., V. 76, p. 7888-7915.

Sclater, J.G. and R. Detrick (1973). Elevation of Midocean Ridges and the Basement Age of the JOIDES Deep Sea Drilling Sites. Bull. Geol. Soc. Am., V. 84, p. 1547-1554.

Seibold, Eugene and Karl Hinz (1974). Continental Slope Construction and Destruction, West Africa. In: C.A. Burk and C.L. Drake (eds.), The Geology of Continental Margins. New York, Springer-Verlap, p. 179-196.

Sheriff, R.E. (1976). Inferring Stratigraphy from Seismic Data. Bull. Am. Assn. Petrol. Geol., V. 60, p. 528-542.

Shipley, T.H. (1978). Sedimentation and Echo Characteristics in the Abyssal Hills of the West-Central North Atlantic. Bull. Geol. Soc. Am., V. 89, p. 397-408.

Smith, Mark K. (1956). Noise Analysis and Multiple Seismometer Theory. Geophysics, V. 21, p. 337-360.

Smith, Mark K. (1958). A Review of Methods of Filtering Seismic Data. Geophysics, V. 23, p. 44-47.

Smith, W.O. (1958). Recent Underwater Surveys Using Low Frequency Sound to Locate Shallow Bedrock. Bull. Geol. Soc. Am., V. 69, p. 69-98.

Sousa Torres, A. and J.M. Pires Soares (1946). Formacoes Sedimentares do Archipelago de Cape Verde. Portugal Junta Mis. Geog. Inv., V. 3, p. 1-197.

Sykes, L.R., and M.L. Sbar (1974). Focal Mechanism Solutions of Intraplate Earthquakes and Stresses in the Lithosphere. In: L. Kristjansson, (ed.), Geodynamics of Iceland and the North Atlantic Area. Boston, D. Reidel Publishing Co., p. 207-224.

Thompson, Jay F. (1963). A Technique for Solving the Low-Velocity Problem. Geophysics, V. 28, p. 869-876.

Tucholke, Brian E. (1979). Relationships Between Acoustic Stratigraphy and Lithostratigraphy in the Western North Atlantic Basin. Initial Reports of the Deep Sea Drilling Project, V. 43, Washington, U. S. Government Printing Office, p. 827-844.

Tulcholke, B.E., P.R. Vogt et al. (1979). Initial Reports of the Deep Sea Drilling Project, V. 43, Washington, U.S. Government Printing Office, 1115 p.

Tucker, P.M. and H.J. Yorston (1973). Pitfalls in Seismic Interpretation. Tulsa, OK, Society of Exploration Geophysicists, Monograph 2, 50 p.

Turcotte, D.L. and E.R. Oxburgh (1973). Mid-plate Tectonics. Nature, V. 244, p. 141-144.

Uchupi, Elazar, K.O. Emery, C.O. Bowin, and J.D. Phillips (1976). Continental Margin Off Western Africa: Senegal to Portugal. Bull. Am. Assn. Petrol. Geol., V. 60, p. 809-878.

Urick, R.J. (1967). Principles of Underwater Sound for Engineers. New York, McGraw-Hill, 342 p.

U.S. Naval Oceanographic Office (1965). Oceanographic Atlas of the North Atlantic, Sect. 5, Marine Geology. Washington, U.S. Naval Oceanographic Office, H. O. Pub. No. 700, 89 p.

U. S. Naval Oceanographic Office (1966). Handbook of Oceangraphic Tables, (SP-68). Washington, U.S. Government Printing Office, 427 p.

Van Hinte, J. E. (1976a). A Cretaceous Time Scale. Bull. Am. Assn. Petrol. Geol., V. 60, p. 498-516.

Van Hinte, J.E. (1976b). A Jurassic Time Scale. Bull. Am. Assn. Petrol. Geol., V. 60, p. 489-497.

Van Padang, M.N., A.F. Richards, F. Machado, T. Bravo, P.E. Baker, and R.W. Maitre (1967). Volcano of Fogo. In: Catalog of Active Volcanoes, Part XXI, Atlantic Ocean, p. 109-114.

Vogt, P.R. and A.M. Einwich (1979). Magnetic Anomalies and Sea Floor Spreading in the Western North Atlantic and a Revised Calibration to the Keathley (M) Geomagnetic Reversal Chronology. In: B. Tucholke and P.R. Vogt, (eds.), Initial Reports of the Deep Sea Drilling Project, V. 43, Washington, U.S. Government Printing Office. (Preprint).

Vogt, P.R., G.L. Johnson, T.L. Holcombe, J.G. Gilg, and O.E. Avery (1971). Episodes of Sea-Floor Spreading Recorded by the North Atlantic Basement. Tectonophysics, V. 12, p. 211-234.

Vogt, P.R. (1974a). Volcano Spacing, Fractures and Thicknesses of the Lithosphere. Earth and Planet Sci. Lett., V. 26, p. 235-252.

Vogt, P.R. (1974b). Volcano Height and Plate Thickness. Earth and Planet Sci. Lett., V. 23, p. 337-348.

Watkins, Joel S. and K.W. Hoppe (1979). Seismic Reflection Reconnaissance of the Atlantic Margin of Morocco. In: 2nd M. Ewing Symp. (Preprint).

Weigel, W. and G. Wissmann (1977). A First Crustal Section from Seismic Observations West of Mauretania. Publ. Inst. Geophys. Pol. Acad. Sci., A-4, V. 115, p. 369-380.

Widness, M.B. (1973). How Thin is a Thin Bed? Geophysics, V. 38, p. 1176-1180.

Wilkes, Charles (1845). Narrative of the United States Exploring Expedition, 1838-1842. 5 Vols., Philadelphia, Lee and Blanchard.

Wilson, J.T. (1973). Mantle Plumes and Plate Motions. Tectonophysics, V. 19, p. 149-164.

Wissman, G. (1979). The Cape Bojador Slope, an Example for Potential Pitfalls in Seismic Interpretation without the Information of Outer Margin Drilling. In: W.F.B. Ryan and V. von Rad (eds.), Initial Reports of the Deep Sea Drilling Project, V. 47, Washington, U.S. Government Printing Office. (Preprint).

UNCLASSIFIED

SECURITY CLASSIFICATION OF THIS PAGE (When Data Entered)

REPORT DOCUMENTATION PAGE	READ INSTRUCTIONS BEFORE COMPLETING FORM
1 REPORT NUMBER: NORDA Report 45	2. GOVT ACCESSION NO. AD-A122 623 / 3 RECIPIENT'S CATALOG NUMBER
4 TITLE (and Subtitle): Geology of a Stable Intraplate Region: The Cape Verde/Canary Basin	5 TYPE OF REPORT & PERIOD COVERED
	6 PERFORMING ORG. REPORT NUMBER
7 AUTHOR(s): J. Alan Ballard	8. CONTRACT OR GRANT NUMBER(s)
9 PERFORMING ORGANIZATION NAME AND ADDRESS: Naval Ocean Research & Development Activity, Ocean Programs Management Office, Code 541, NSTL Station, Mississippi 39529	10. PROGRAM ELEMENT, PROJECT, TASK AREA & WORK UNIT NUMBERS
11 CONTROLLING OFFICE NAME AND ADDRESS: Same	12. REPORT DATE: March 1982
	13. NUMBER OF PAGES: 127
14 MONITORING AGENCY NAME & ADDRESS(if different from Controlling Office)	15. SECURITY CLASS. (of this report): UNCLASSIFIED
	15a. DECLASSIFICATION DOWNGRADING SCHEDULE
16. DISTRIBUTION STATEMENT (of this Report): Distribution Unlimited	
17. DISTRIBUTION STATEMENT (of the abstract entered in Block 20, if different from Report)	
18. SUPPLEMENTARY NOTES	
19. KEY WORDS (Continue on reverse side if necessary and identify by block number): Tectonic development; Cape Verde/Canary Basin; Seismic-stratigraphy; J-Anomaly; M-sequence; Jurassic 'Quiet Zone'; Seismic energy sources; Seismic signal processing; Seismic record interpretation	

20. ABSTRACT (Continue on reverse side if necessary and identify by block number)

This report evaluates a unique bathymetric, magnetic, and seismic data set in terms of the geological history of a major ocean basin. It develops a seismic-stratigraphic classification for deep sea sediments and proposes a tectonic development history within the framework of sea floor spreading theory. The study will be useful to oceanographers, geologists, and geophysicists attempting to synthesize large quantities of data to construct a model for regional development.

DD FORM 1 JAN 73 1473 EDITION OF 1 NOV 65 IS OBSOLETE
S/N 0102-LF-014-6601

UNCLASSIFIED

SECURITY CLASSIFICATION OF THIS PAGE (When Data Entered)

☆U.S. GOVERNMENT PRINTING OFFICE 1982 573 926

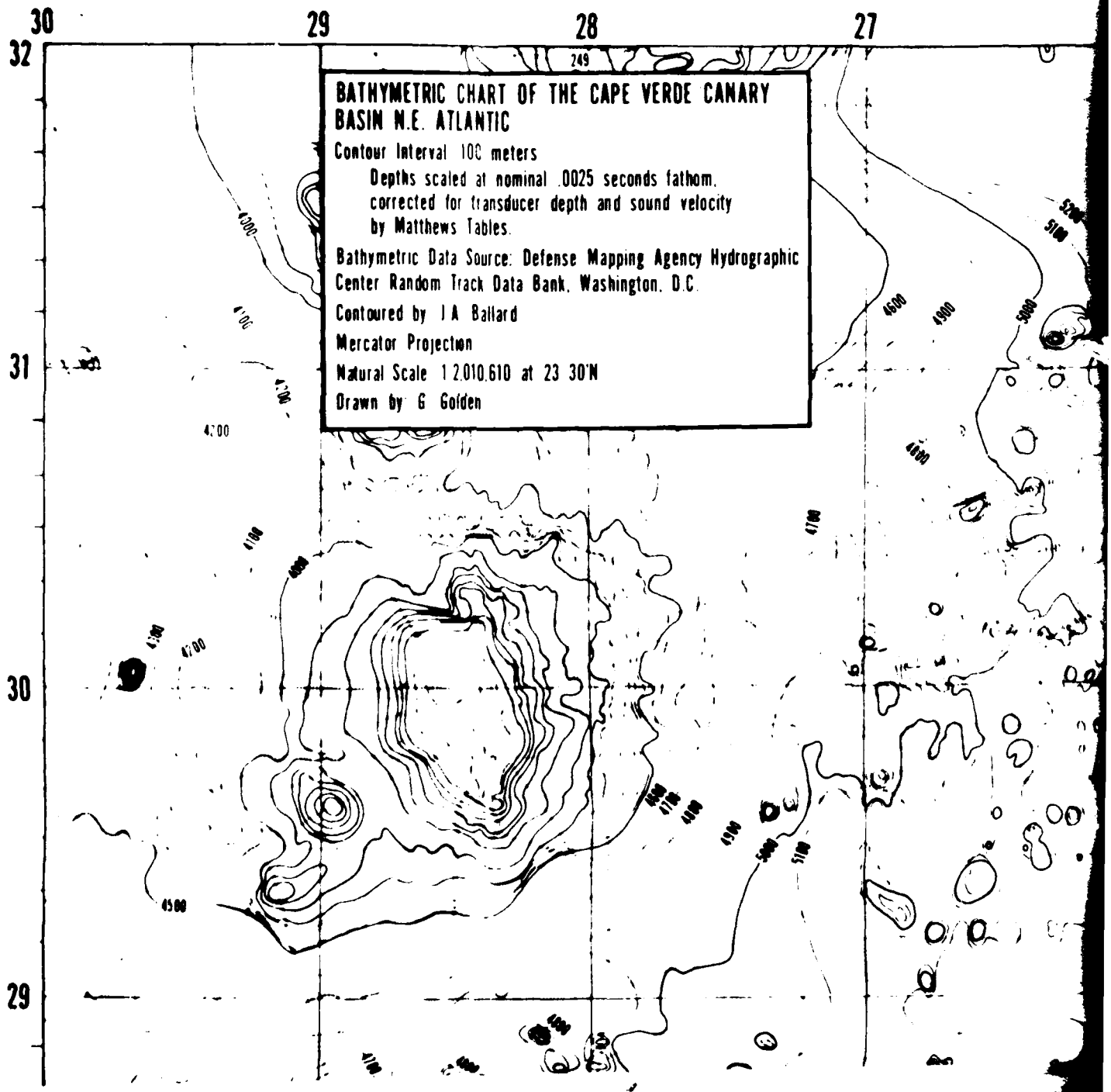
30
29
28
27
32
31
30
29
BATHYMETRIC CHART OF THE CAPE VERDE CANARY BASIN N.E. ATLANTIC
Contour Interval 100 meters
Depths scaled at nominal .0025 seconds fathom, corrected for transducer depth and sound velocity by Matthews Tables.
Bathymetric Data Source: Defense Mapping Agency Hydrographic Center Random Track Data Bank, Washington, D.C.
Contoured by J A Ballard
Mercator Projection
Natural Scale 1:2,010,610 at 23 30'N
Drawn by G Golden

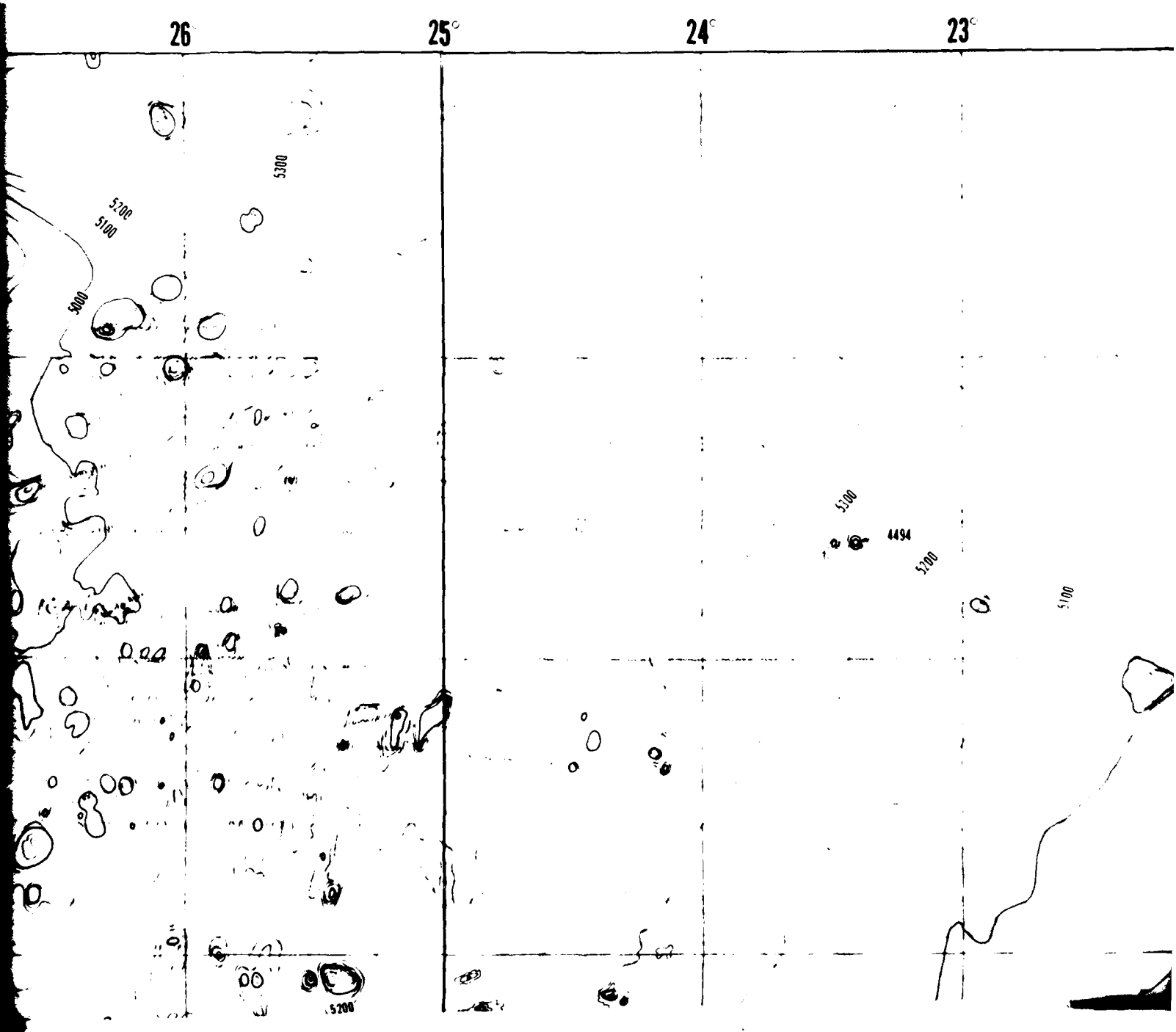
26
25°
24°
23°
5300
5200
5100
5000
5200
4494
5200
5100
5200

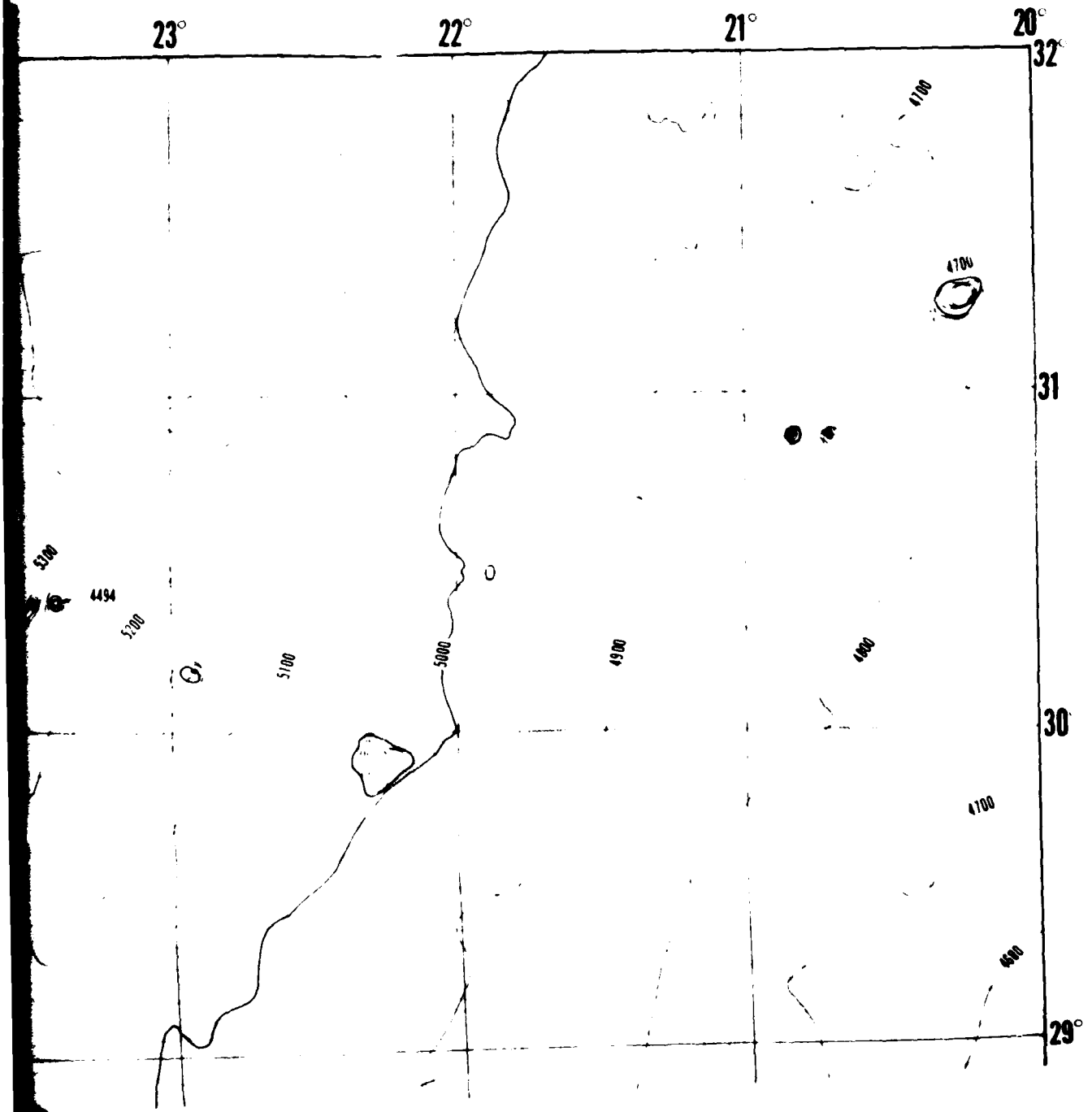
23°
22°
21°
20°
32°
31
30
29°
4100
4700
5100
4494
5200
5100
5000
4900
4800
4700
4900

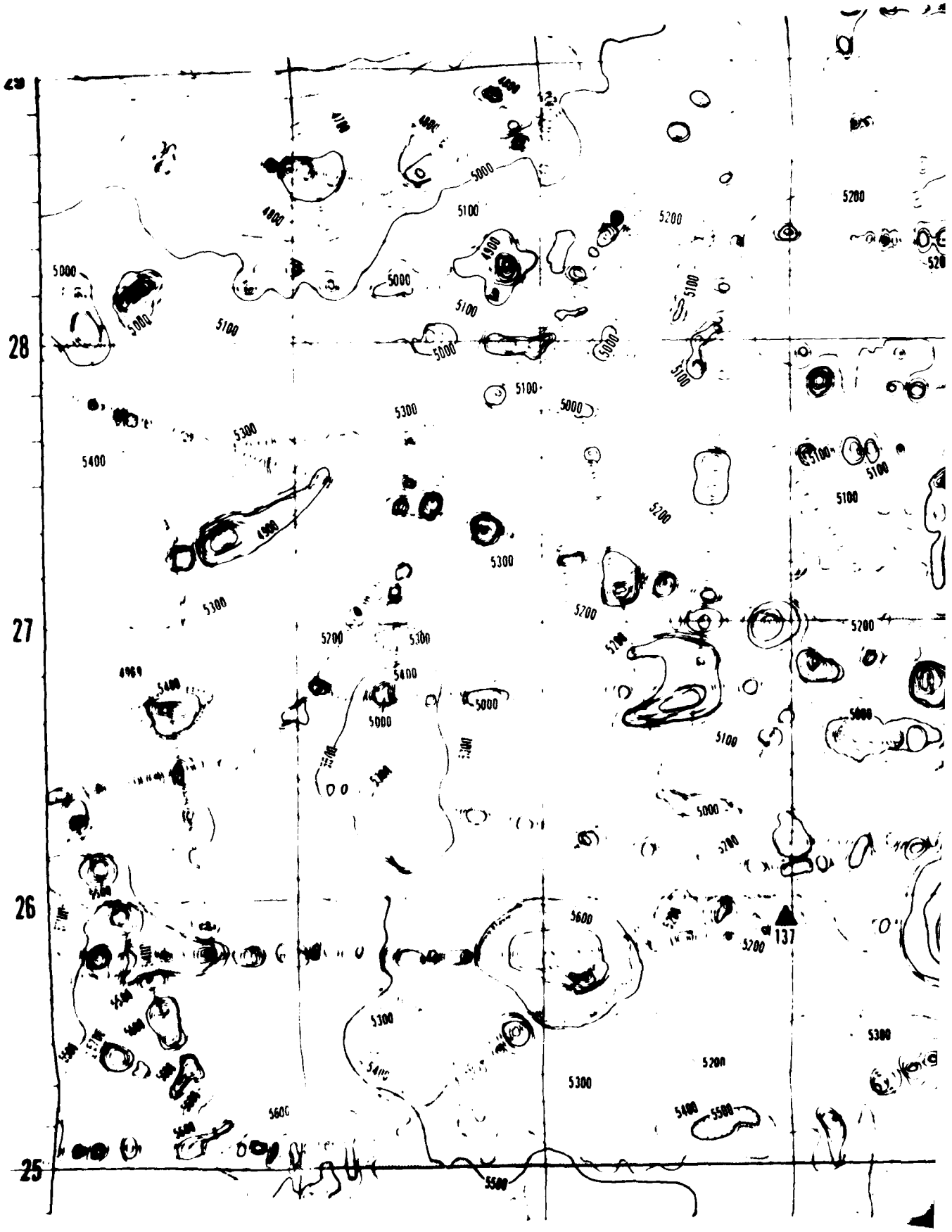
28
27
26
25
5000
5100
5200
5300
5400
5500
5600
137

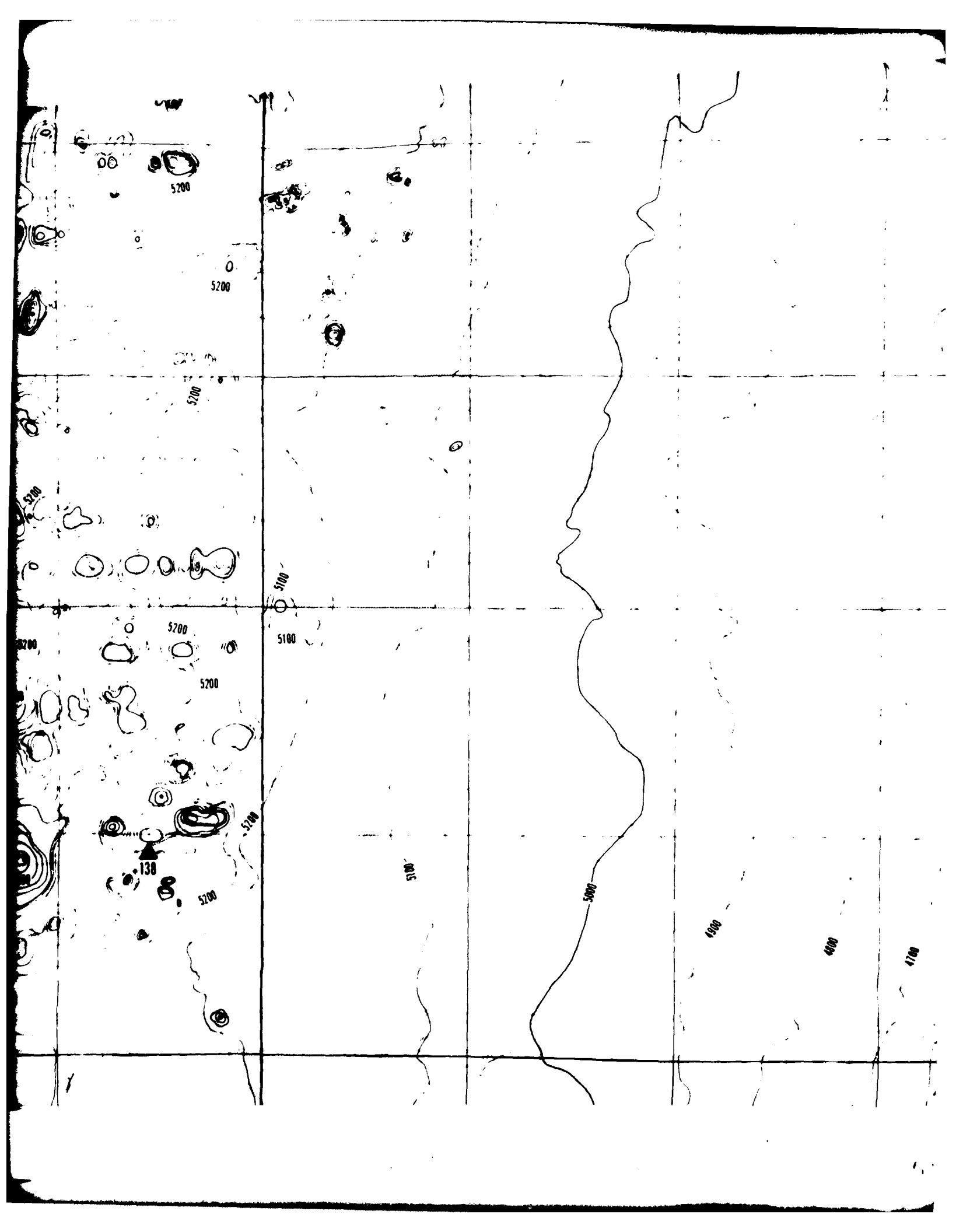
5200
5200
5200
5200
5100
5200
5200
5200
5200
5100
5100
5000
4900
4800
4700
138

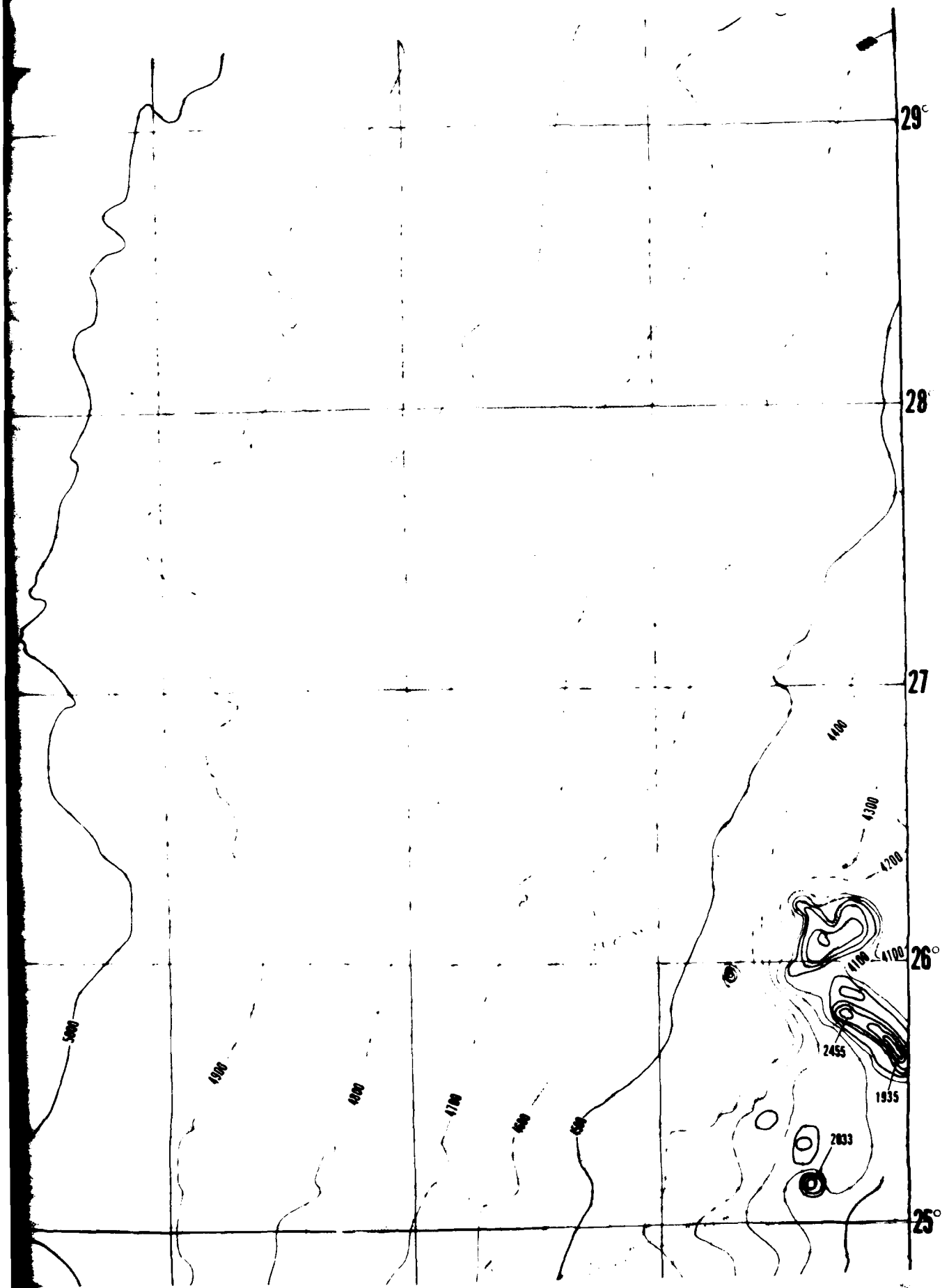
29°
28°
27
26°
25°
4400
4300
4200
4100
4100
2455
1935
2033

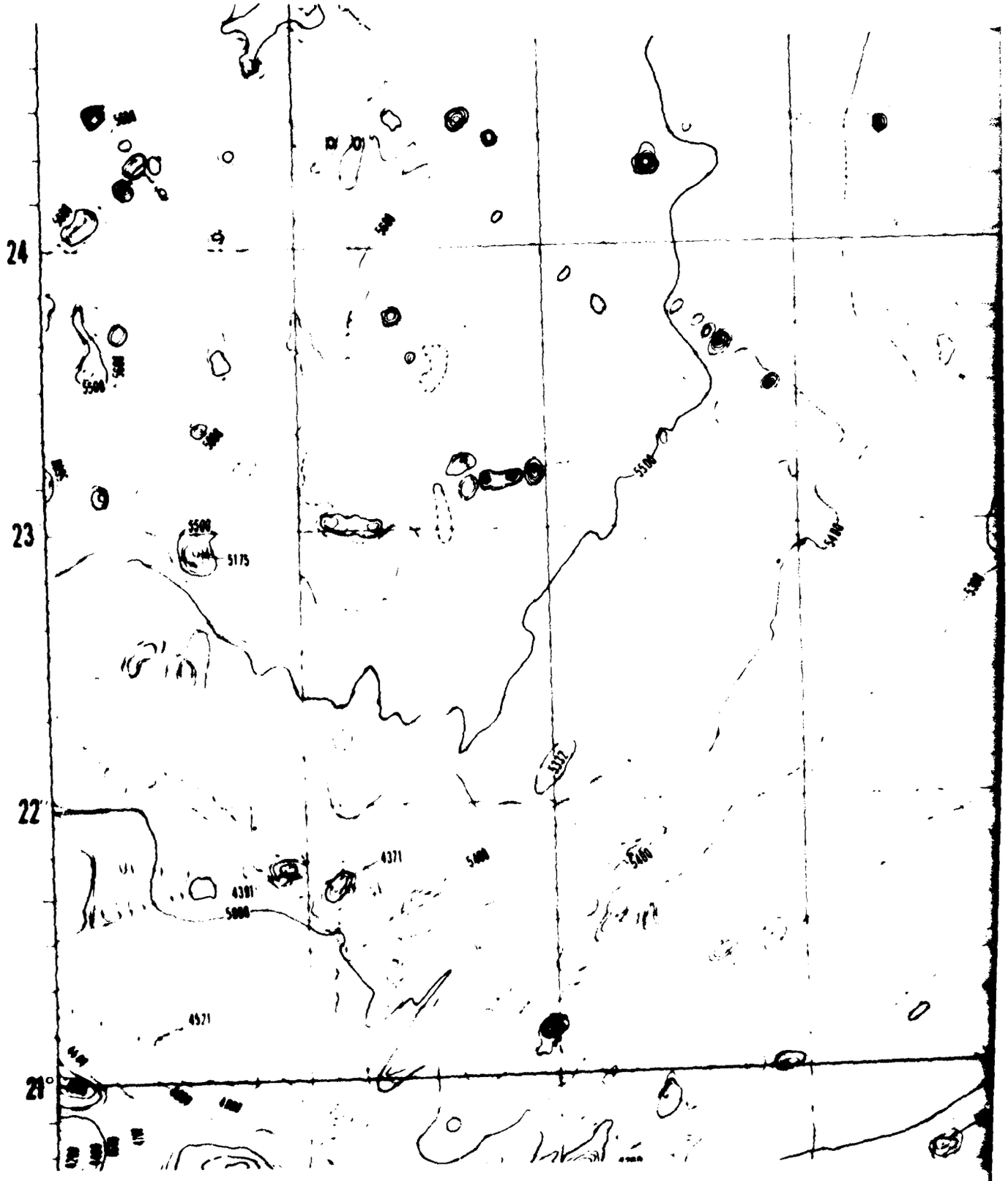
24
23
22
21°
5500
5175
5100
5400
4371
4381
5000
4571


5200
5100
5000
4900
4800
4700
4600
4500
4400
4350
4790

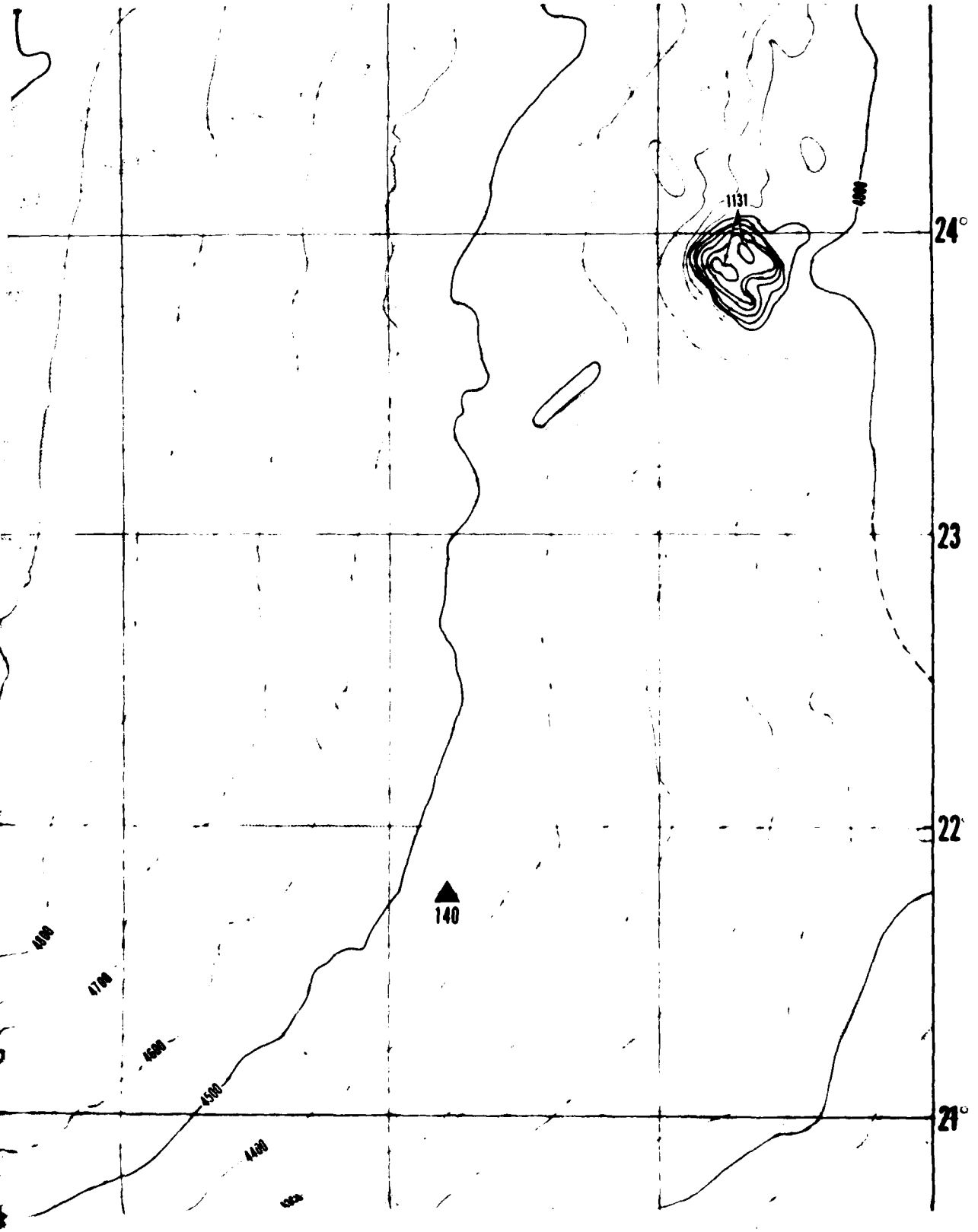
1131
4800
24°
23
22
140
4800
4700
4600
4500
4400
21°

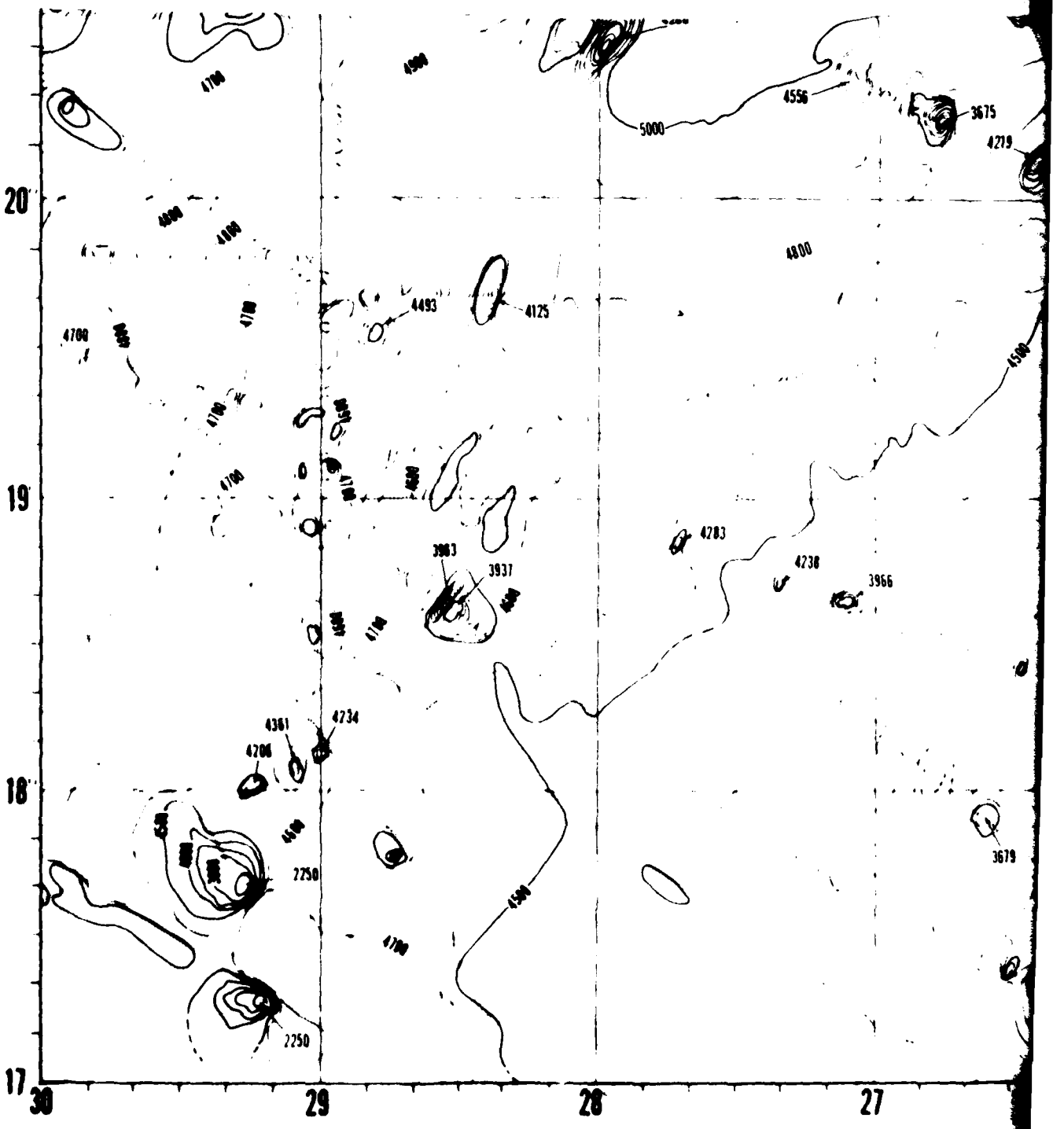
20
19
18
17
30
29
28
27
4700
4800
4900
5000
4556
3675
4279
4493
4125
4783
4238
3966
3983
3937
4361
4234
4206
2750
2250
3679
4500

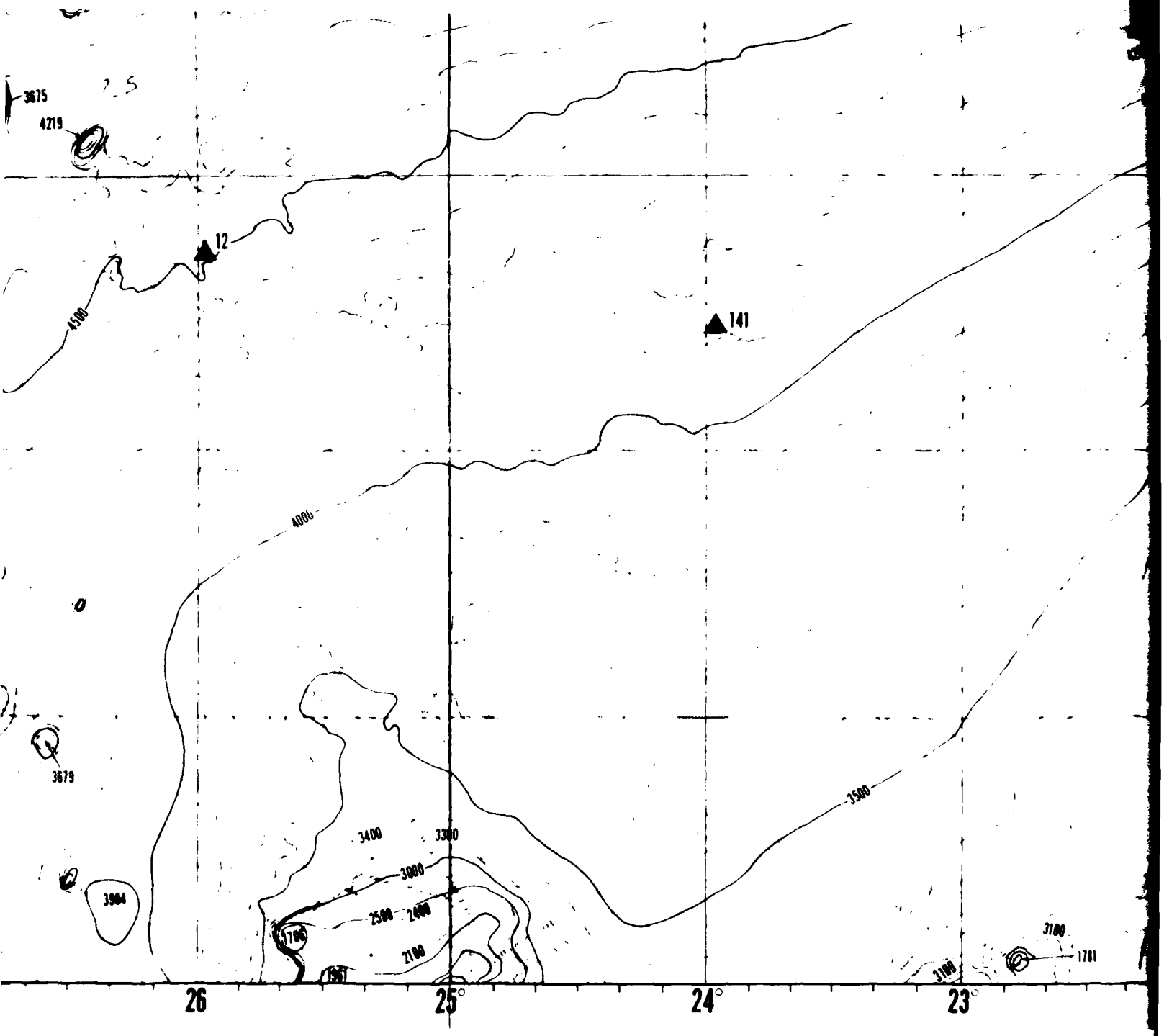
3675
4219
12
4500
141
4000
3679
3500
3400
3300
3000
3904
2500
2400
2100
1781
3100
1781
26
25°
24°
23°

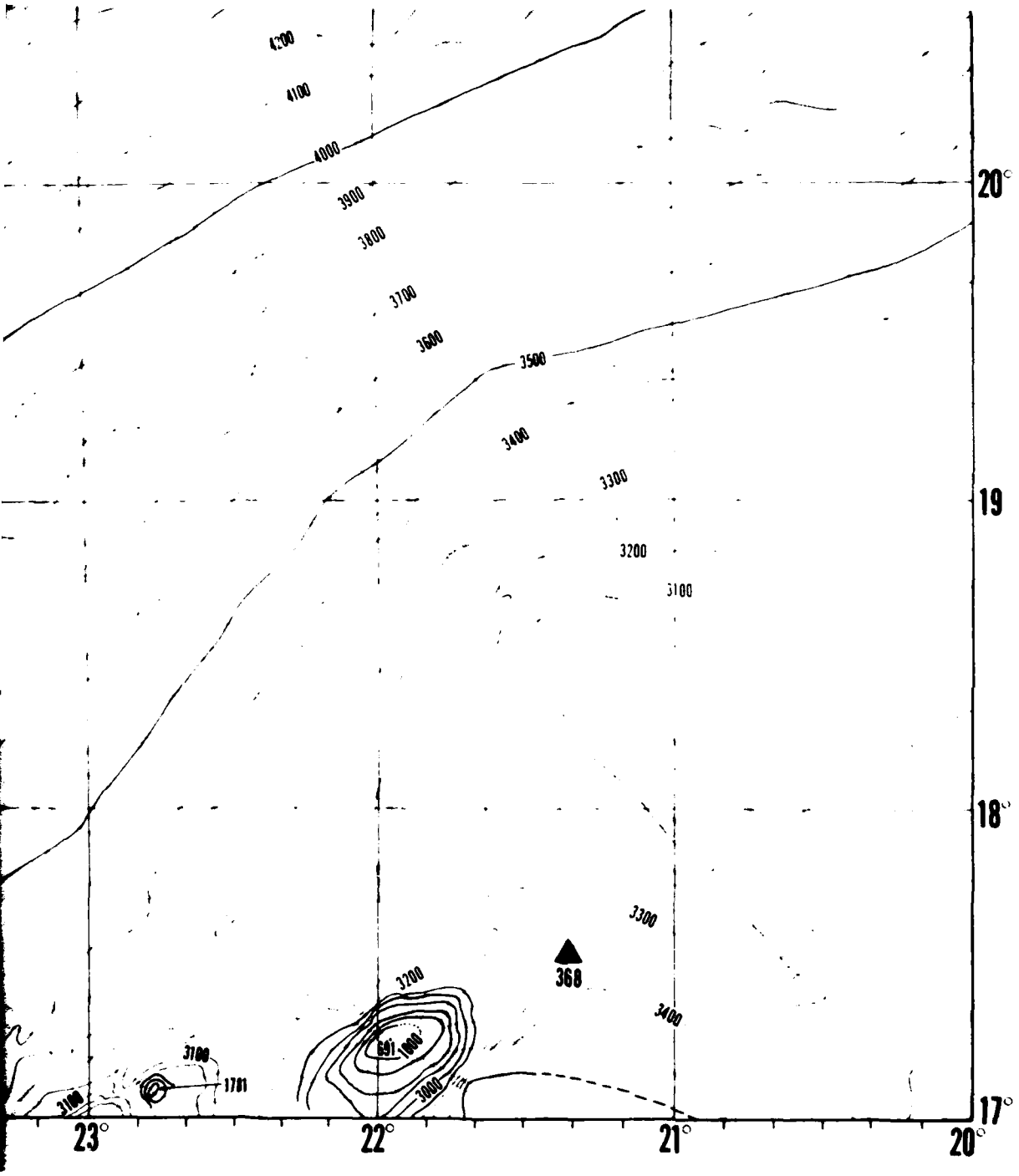
4200
4100
4000
3900
3800
3700
3600
3500
3400
3300
3200
3100
3300
3400
3200
3100
1781
691
1000
3000
368
20°
19
18°
17°
23°
22°
21°
20°

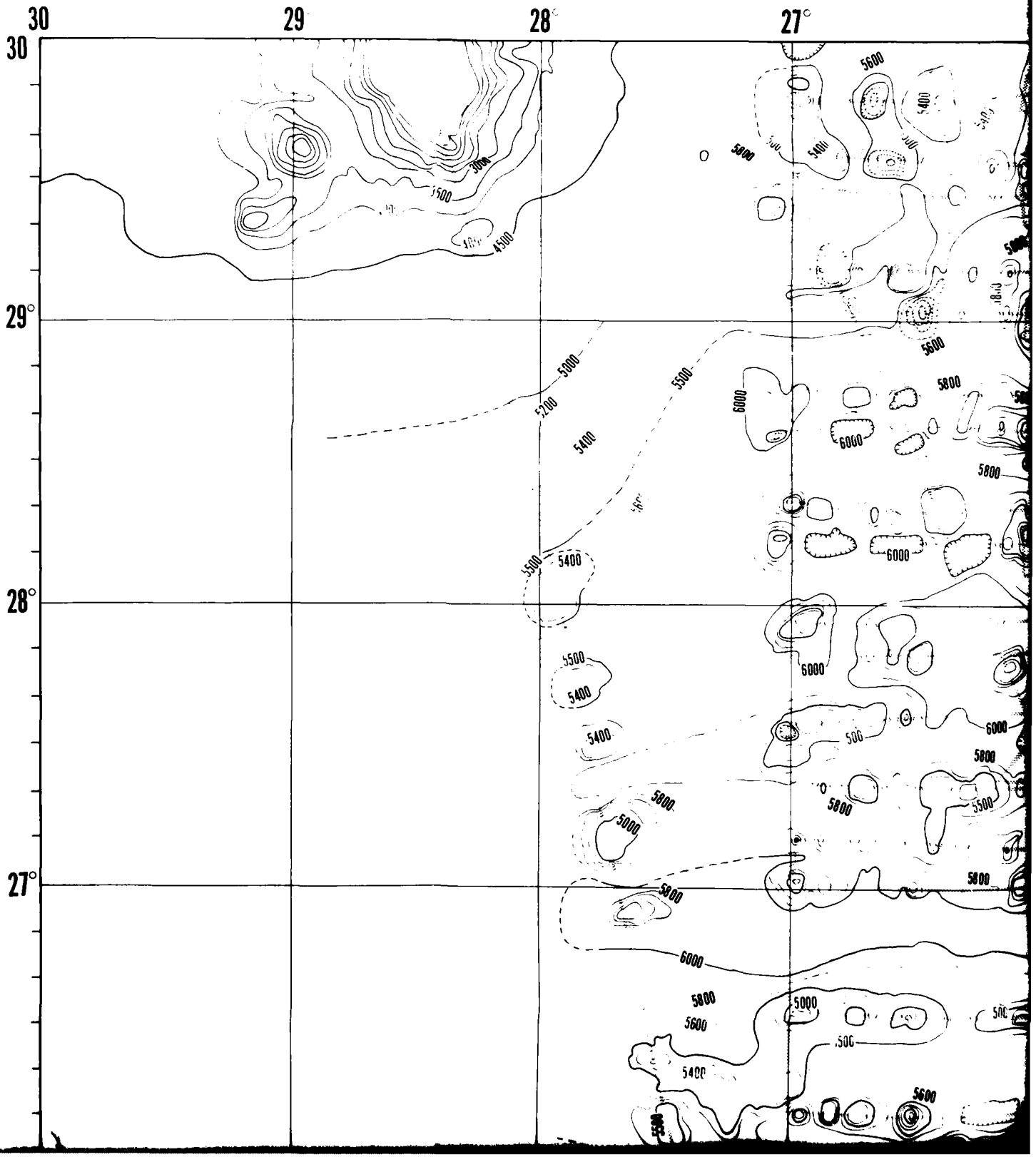
30
29
28
27°
30
29°
28°
27°
5600
5400
5000
5500
5200
6000
5800
4500


26
25
24
23

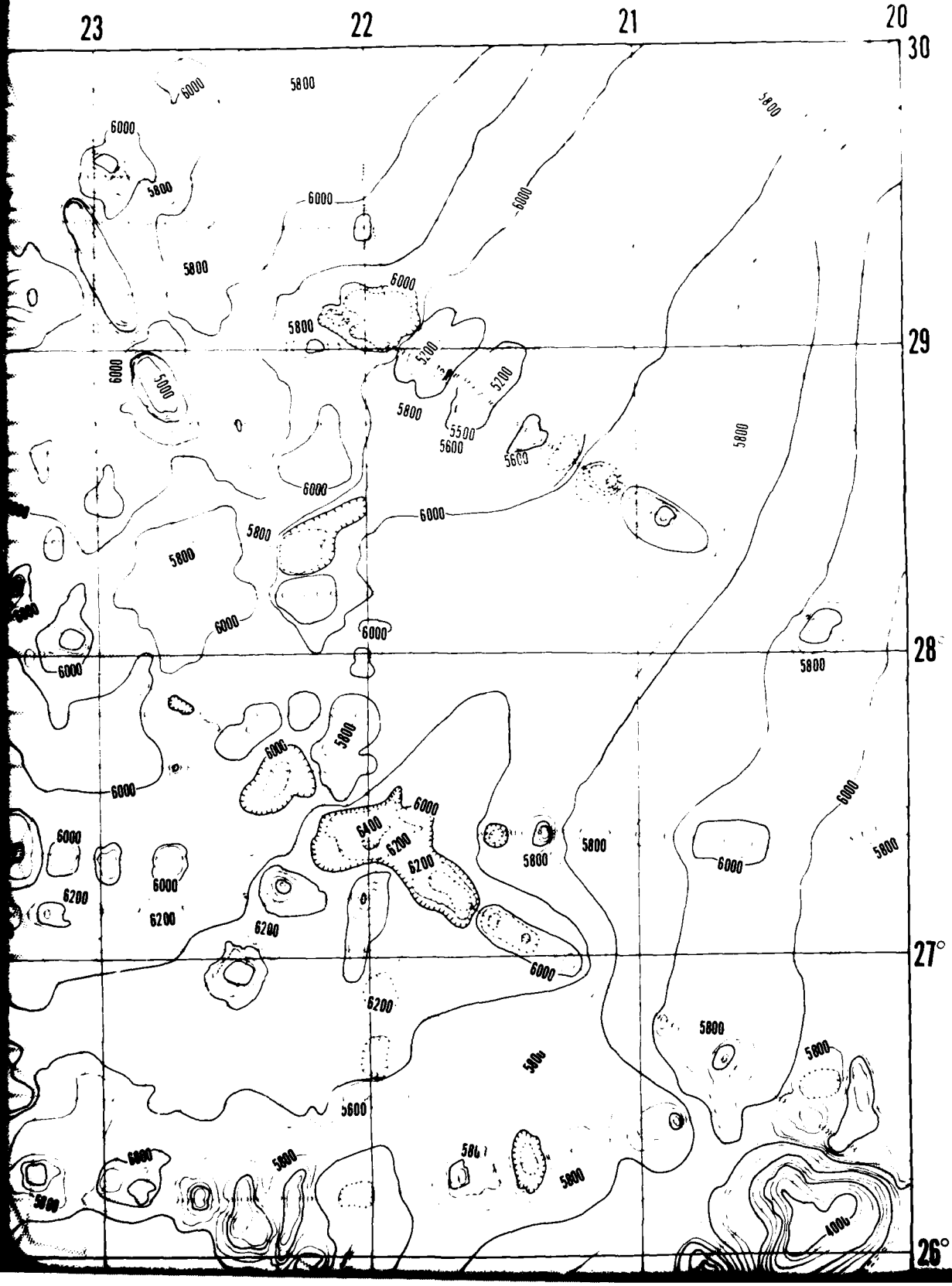
23
22
21
20
30
29
28
27°
26°
6000
5800
6200
6400
5600
5500
5200
5000
4800

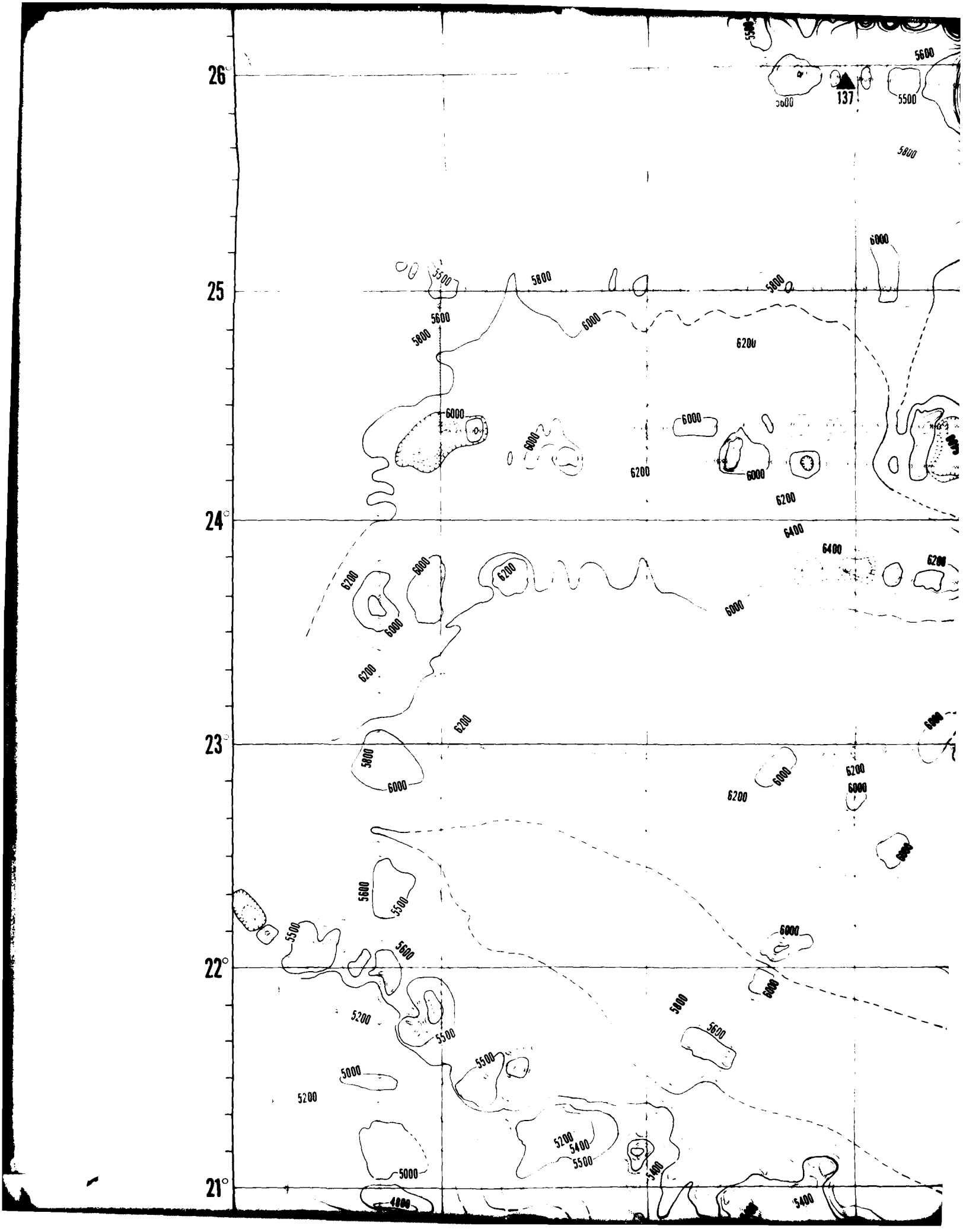
26°
25°
24°
23°
22°
21°
137
5600
5500
5800
6000
6200
6400
5400
5200
5000
4800

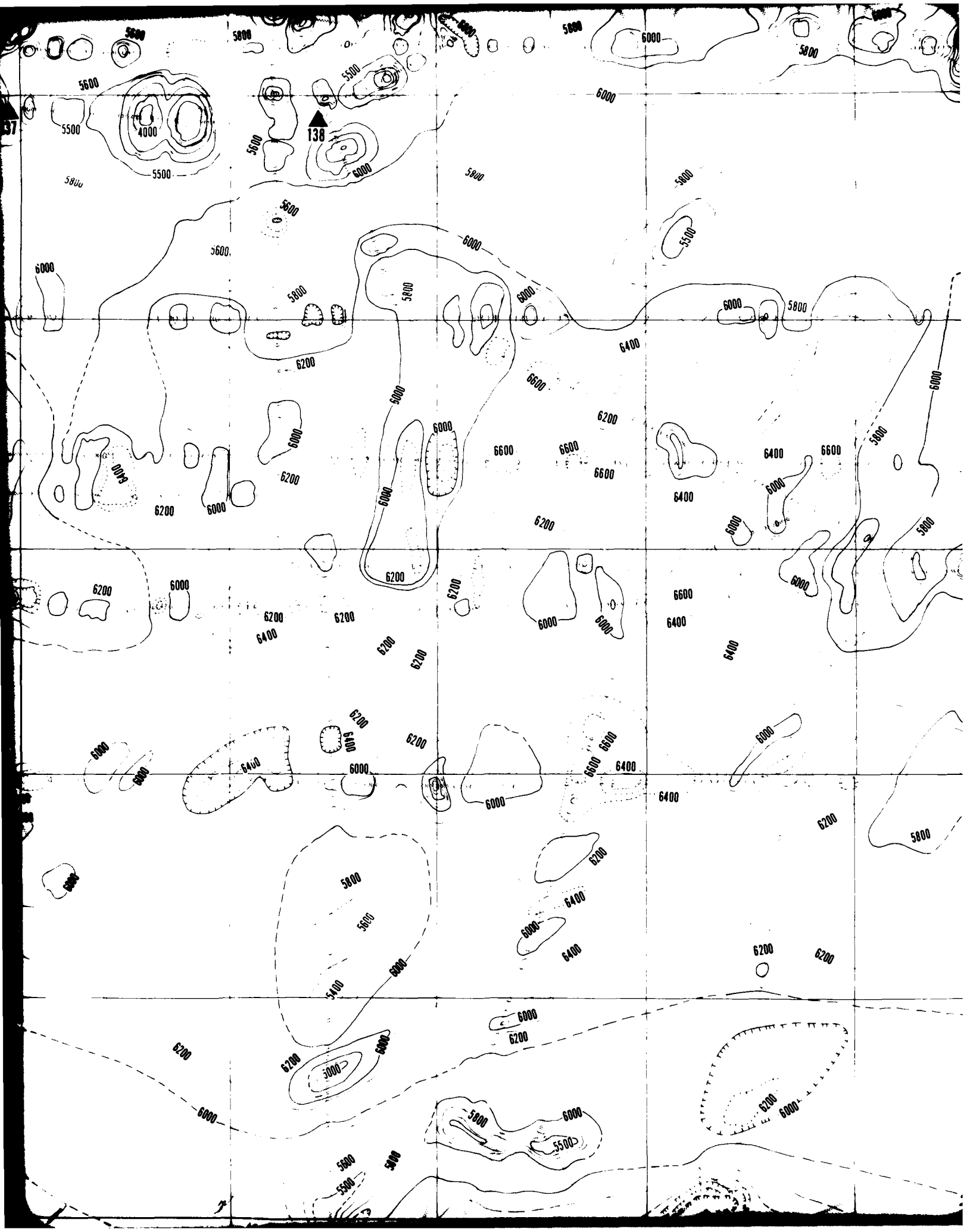
137
138
4000
5500
5600
5800
6000
6200
6400
6600

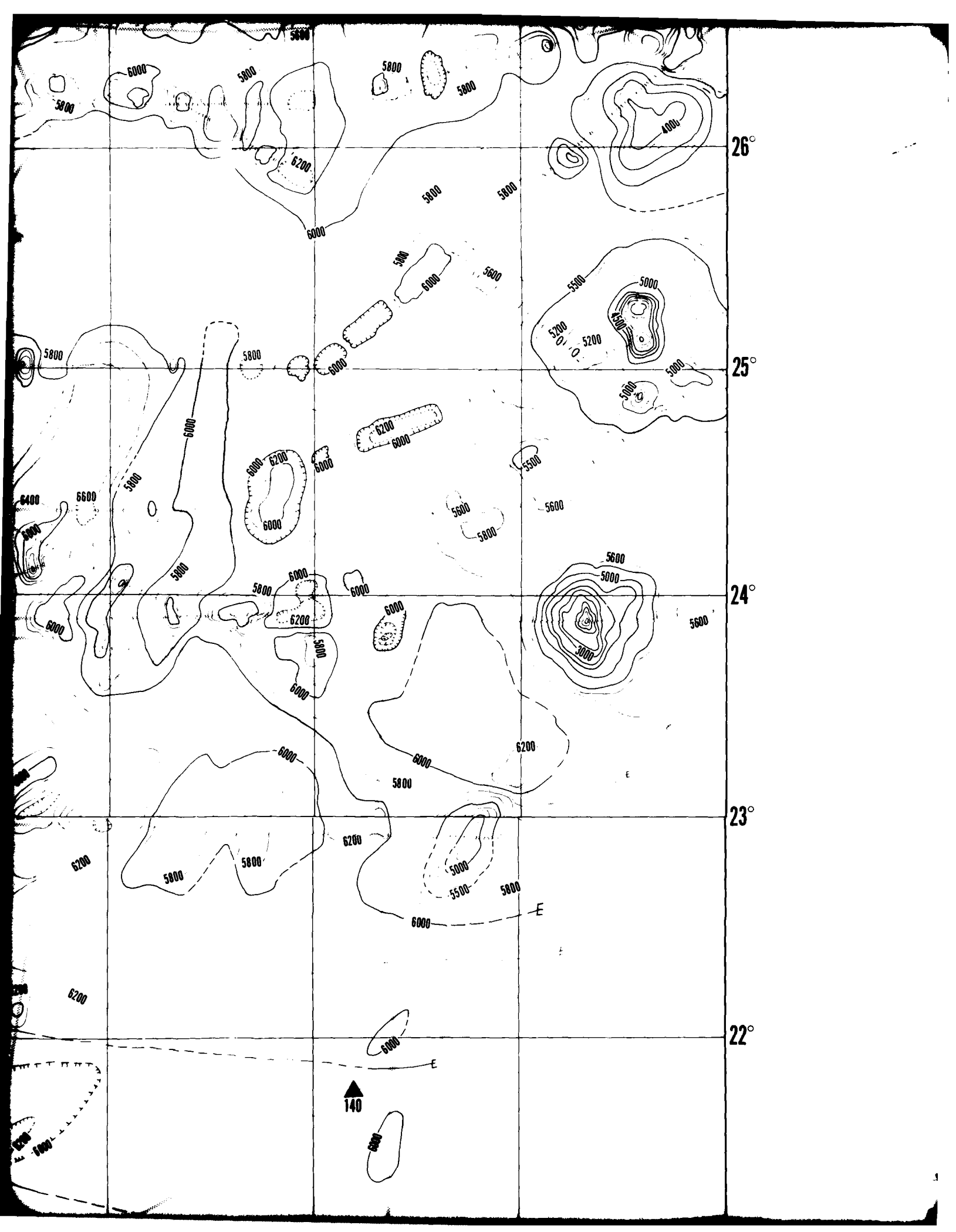
26°
25°
24°
23°
22°
140

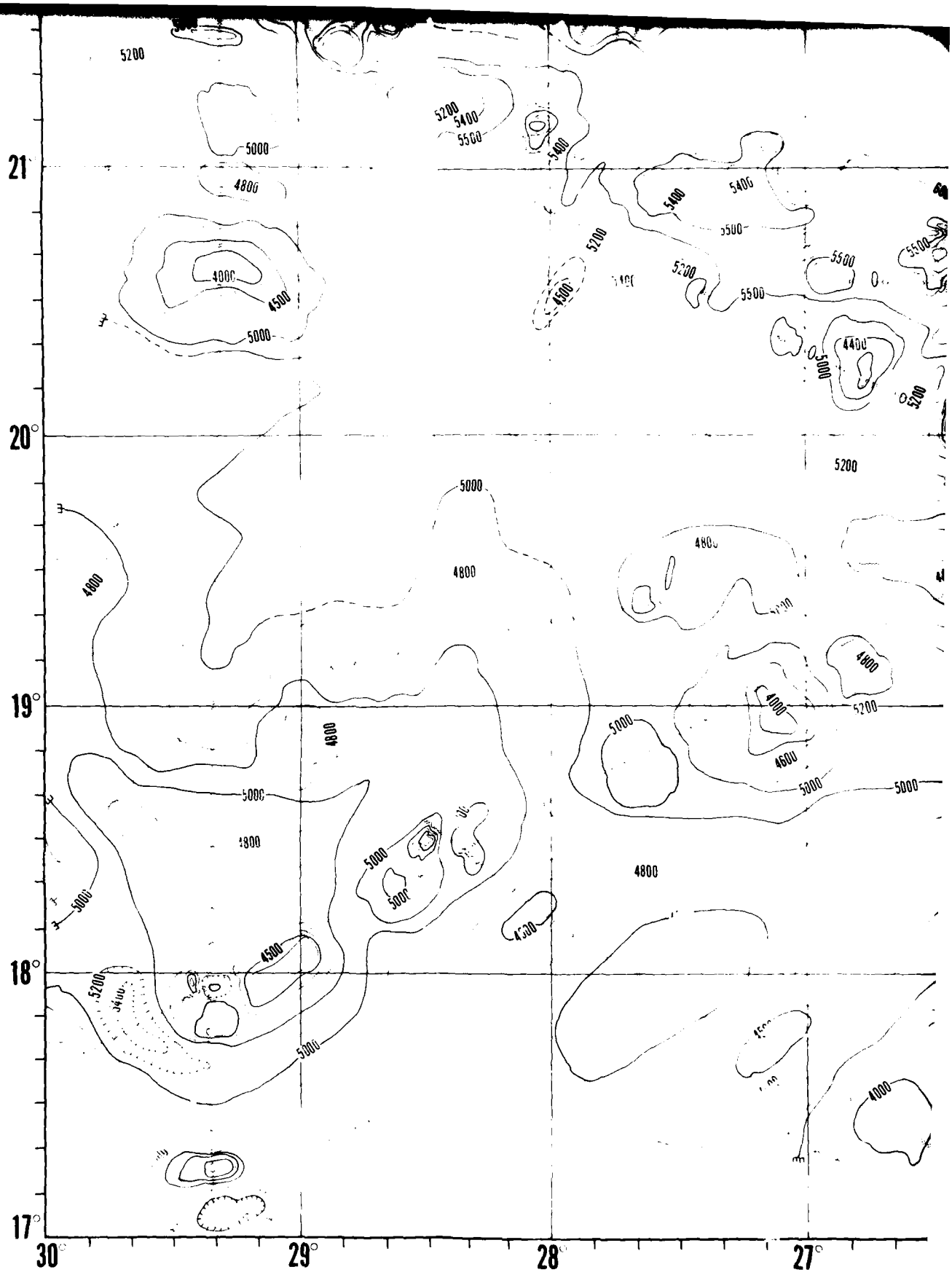
21
20°
19°
18°
17°
30°
29°
28°
27°
5200
5400
5500
5000
4800
4500
4400
4000
4600

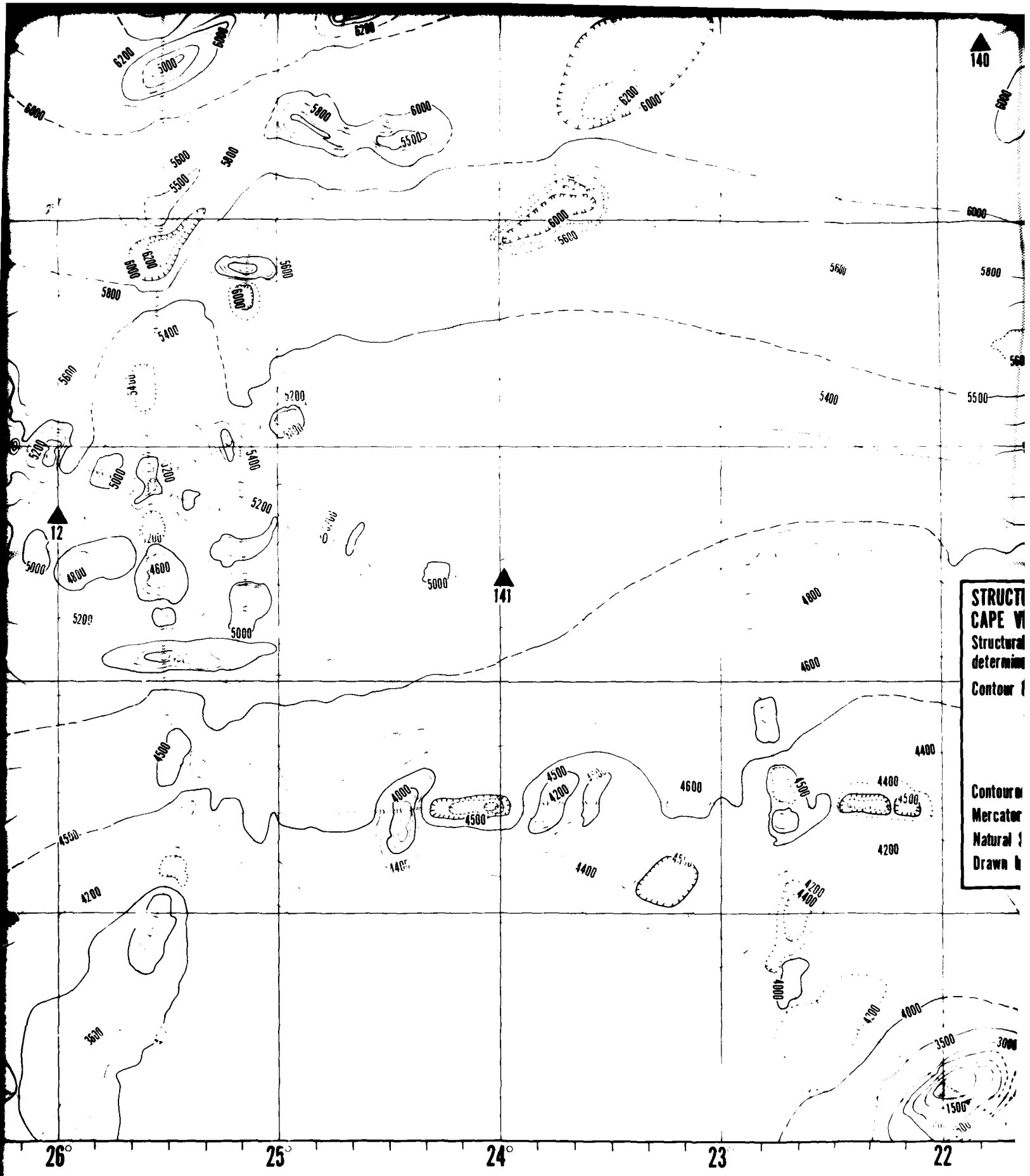
140
141
12
STRUCTU
CAPE VI
Structural
determinu
Contour
Contoure
Mercator
Natural
Drawn
26°
25°
24°
23
22

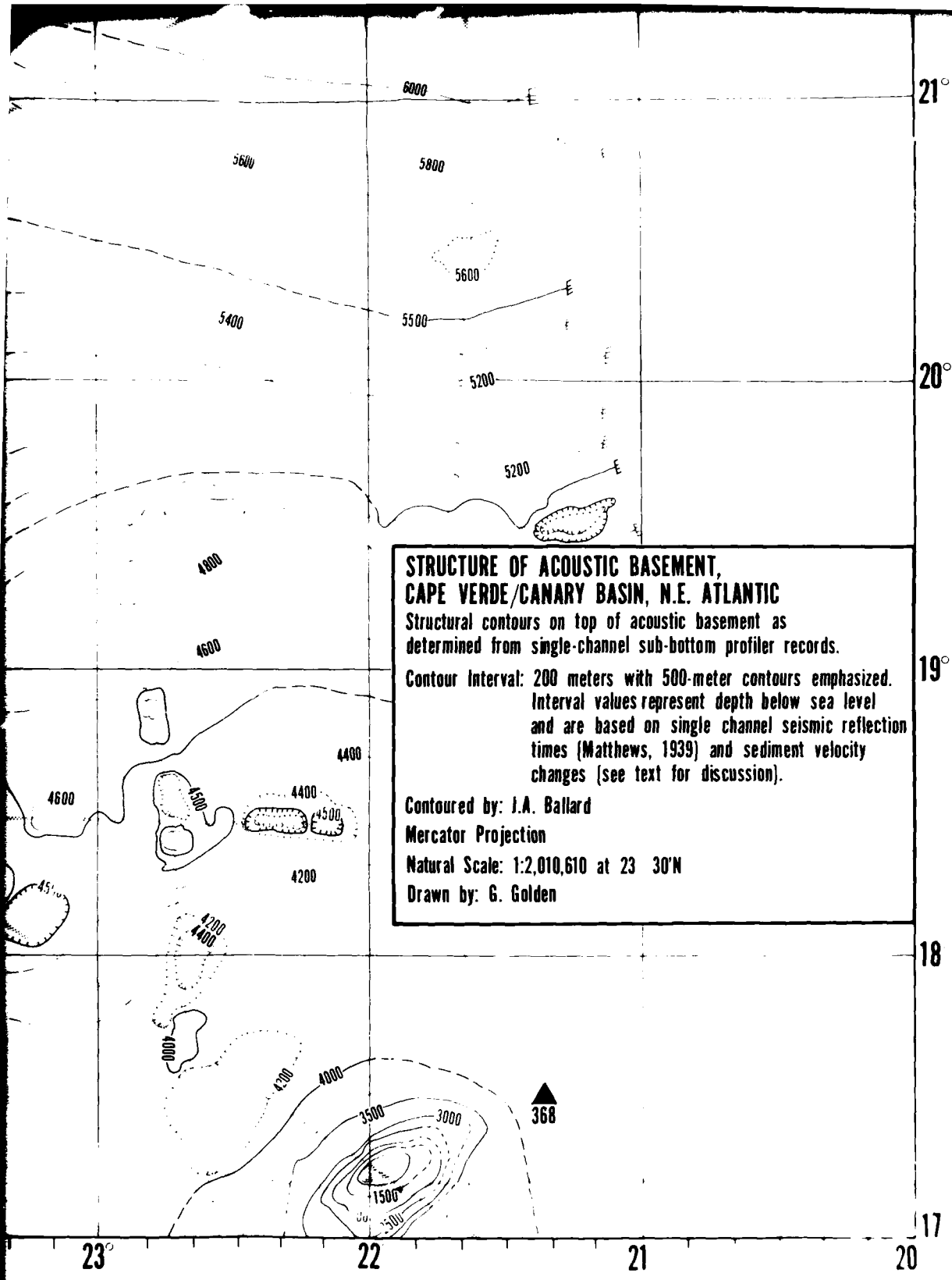

STRUCTURE OF ACOUSTIC BASEMENT, CAPE VERDE/CANARY BASIN, N.E. ATLANTIC

Structural contours on top of acoustic basement as determined from single-channel sub-bottom profiler records.

Contour Interval: 200 meters with 500-meter contours emphasized. Interval values represent depth below sea level and are based on single channel seismic reflection times (Matthews, 1939) and sediment velocity changes (see text for discussion).

Contoured by: J.A. Ballard

Mercator Projection

Natural Scale: 1:2,010,610 at 23 30'N

Drawn by: G. Golden

PLATE III

ISOPACH OF SEDIMENTS ABOVE ACOUSTIC BASEMENT
CAPE VERDE/CANARY BASIN

Sediment thickness calculated by $h=V_0(e^{at} - 1)/a$.

Velocity gradient in sediment - 1.79 sec^{-1}.

Contour interval--200 m and 500 m.

Data Base--Single channel, normal incidence seismic reflection profiles from NAVOCEANO, NORDA, and NGSDC Data Banks.

Track control underprinted.

DSDP Drill Sites indicated by numbered triangles.

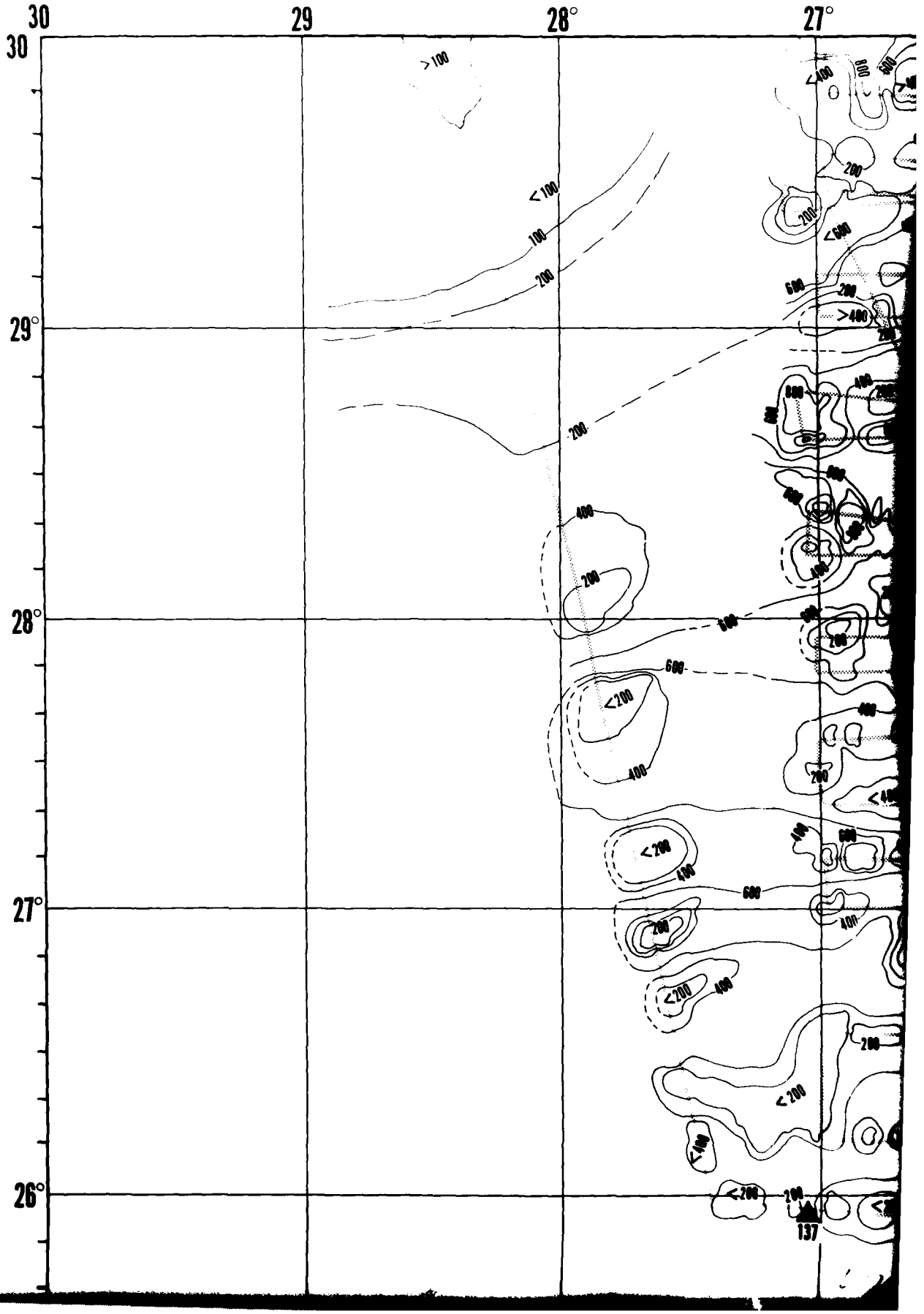
30
29
28°
27°
30
29°
28°
27°
26°
>100
<100
100
200
400
600
800
137

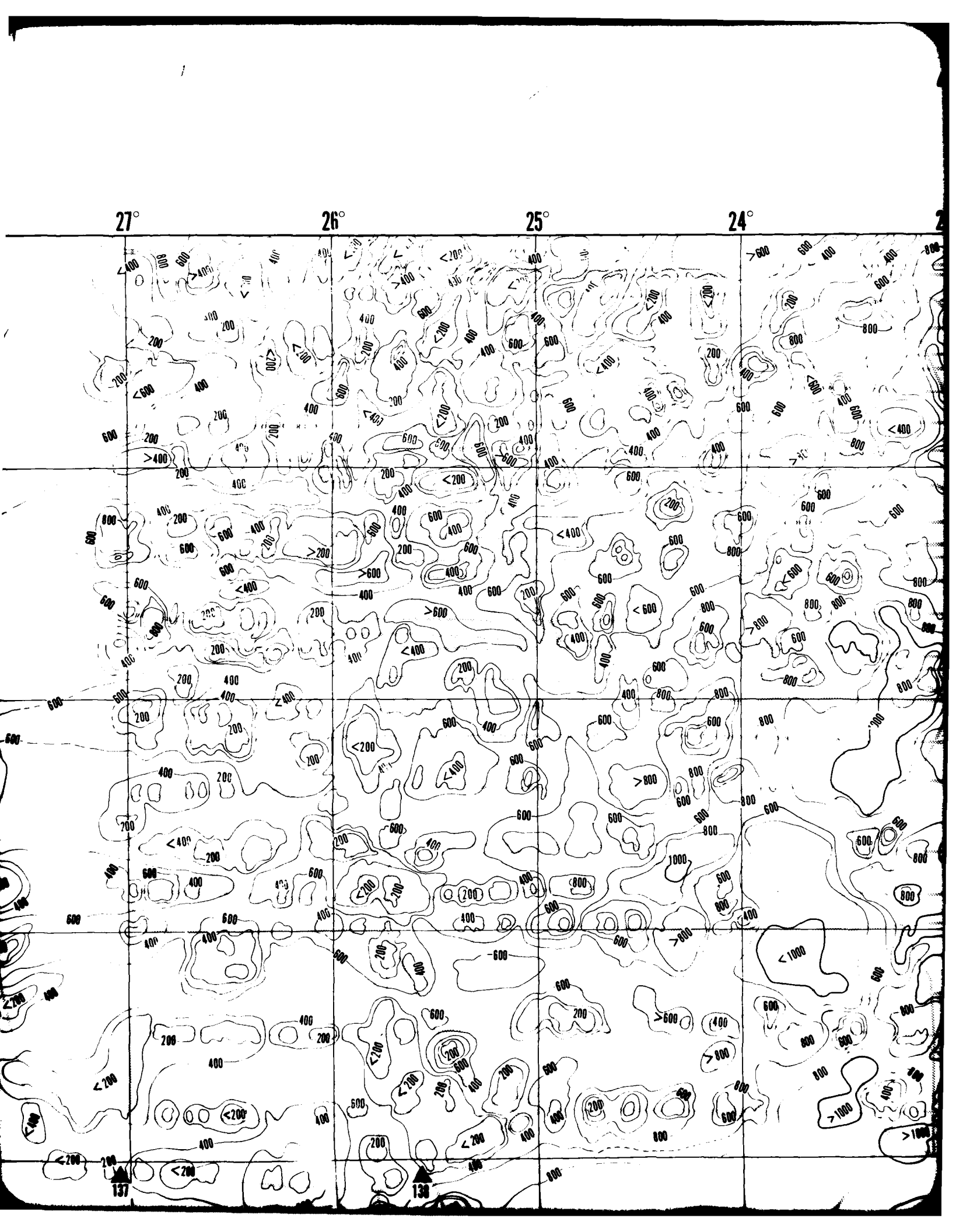
27°
26°
25°
24°
137
138

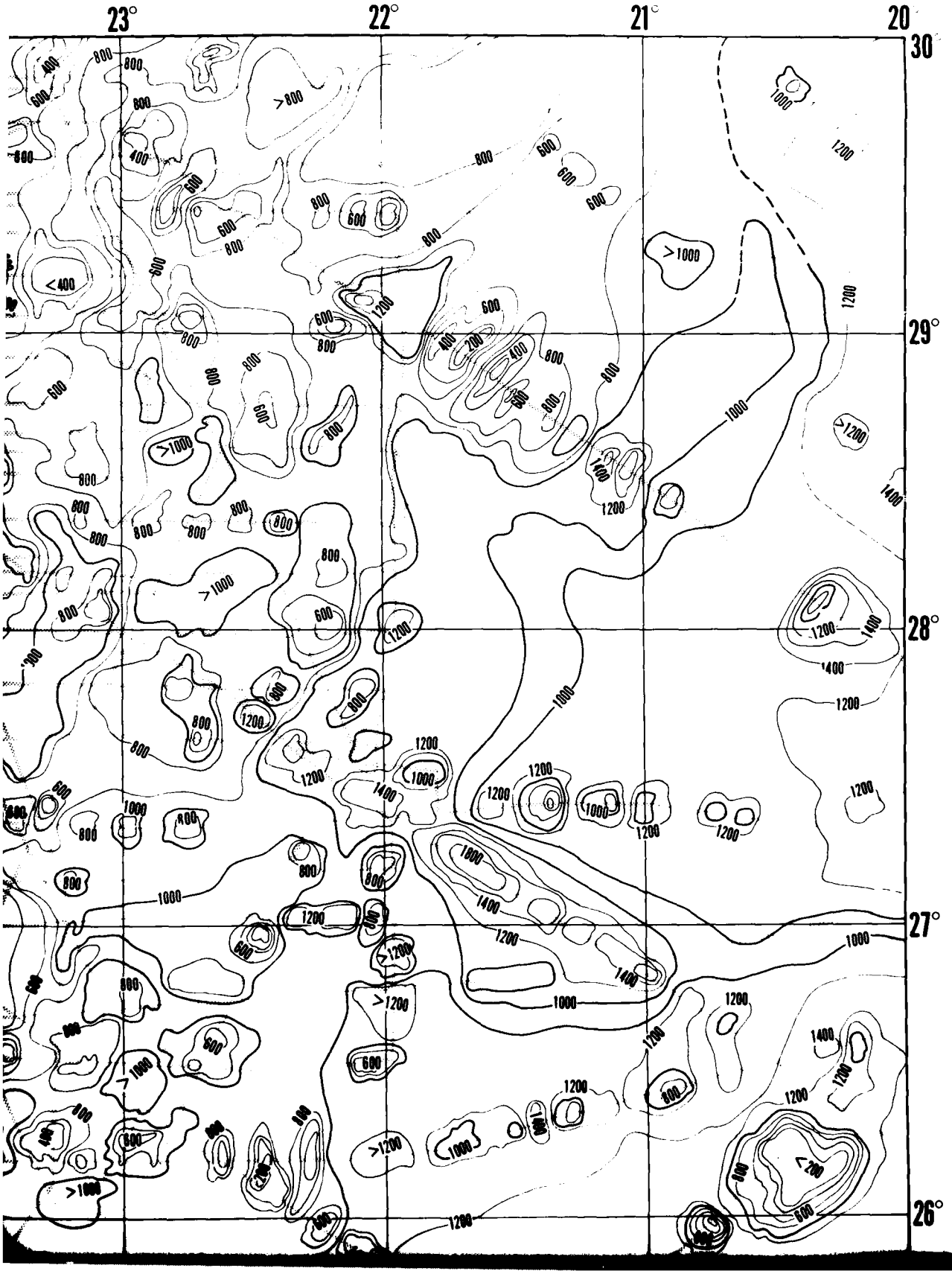
23°
22°
21°
20
30
29°
28°
27°
26°

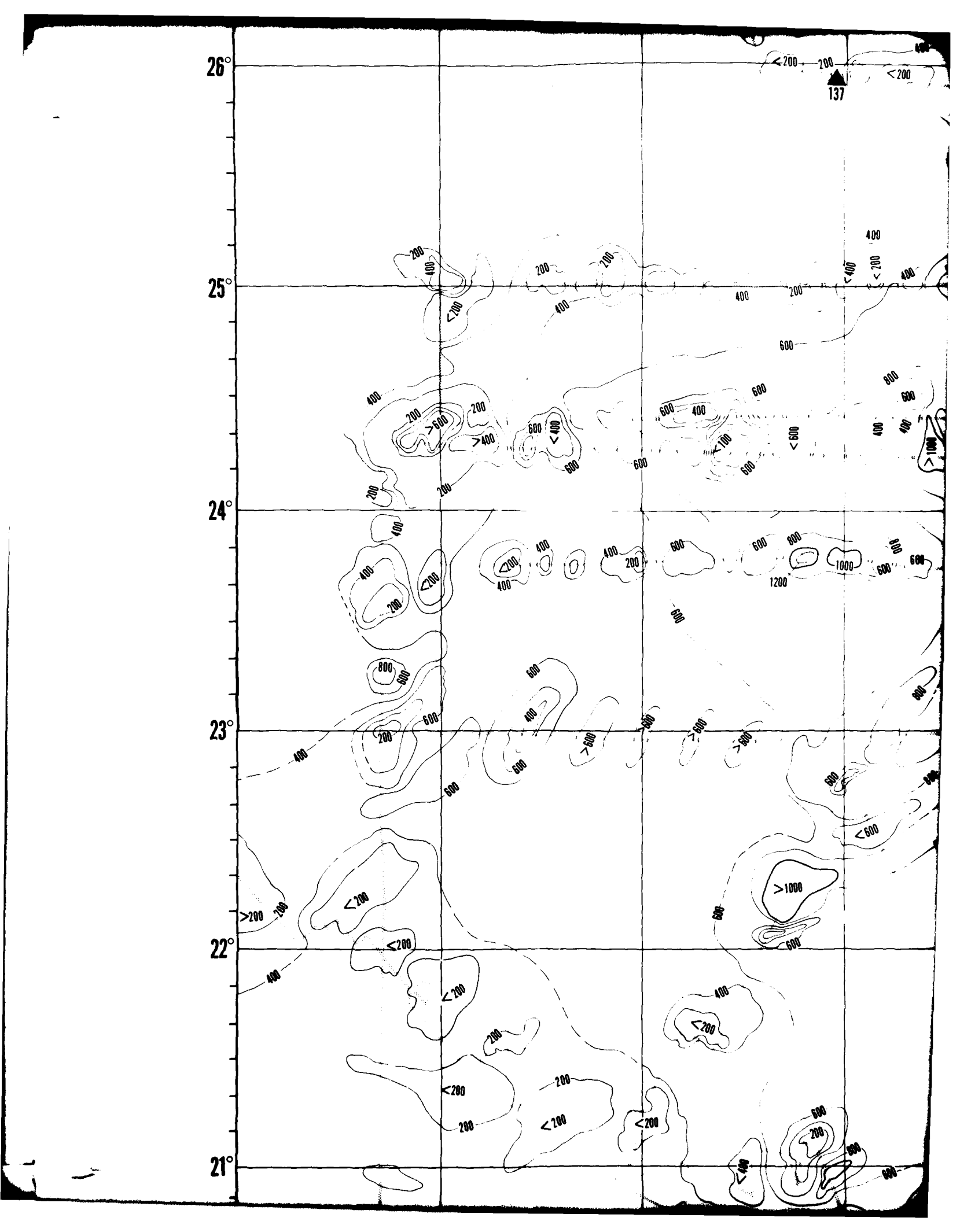
26°
25°
24°
23°
22°
21°
137
<200
200
400
600
800
1000
1200
>1000


138
140

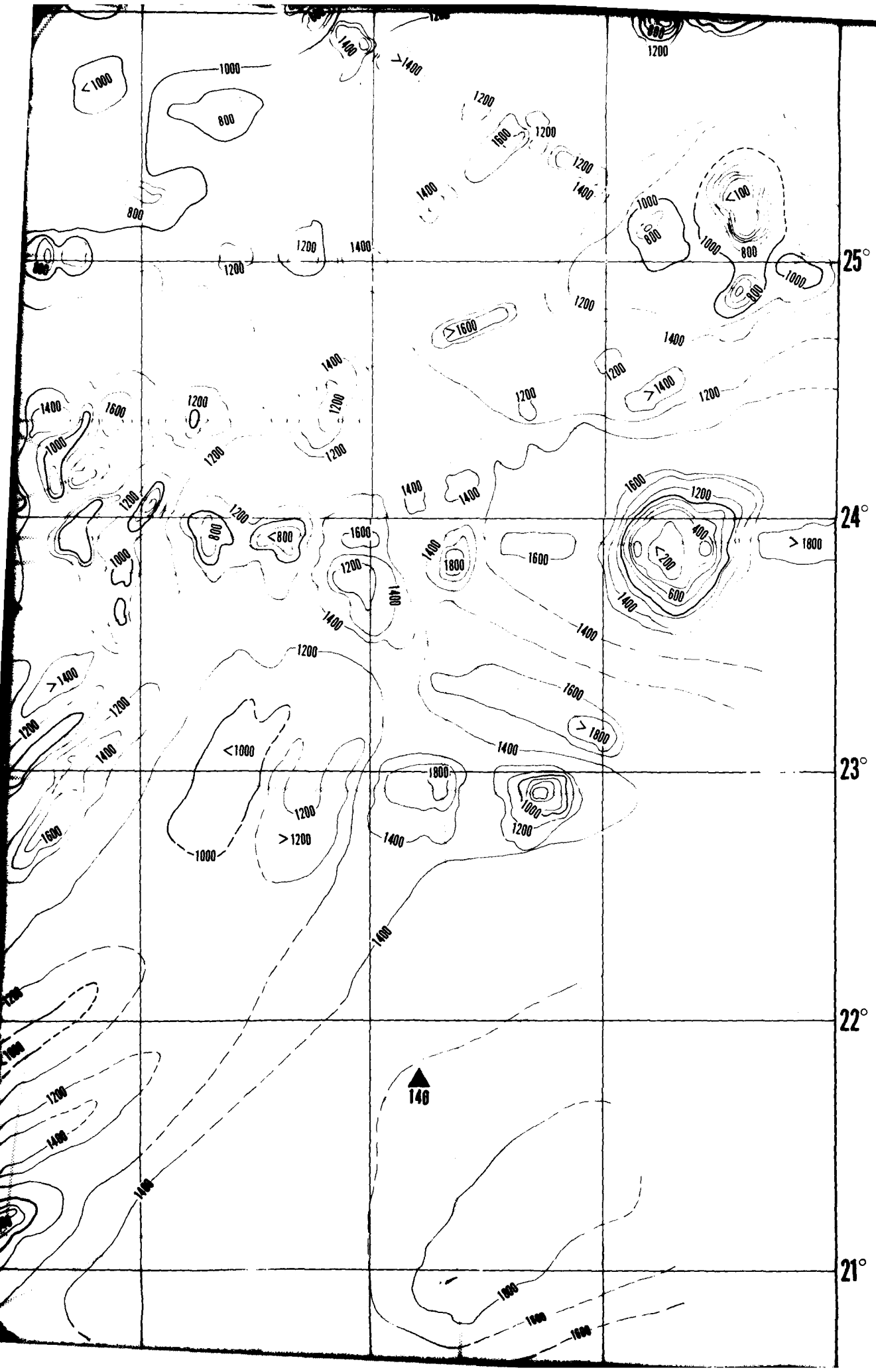
25°
24°
23°
22°
21°
146

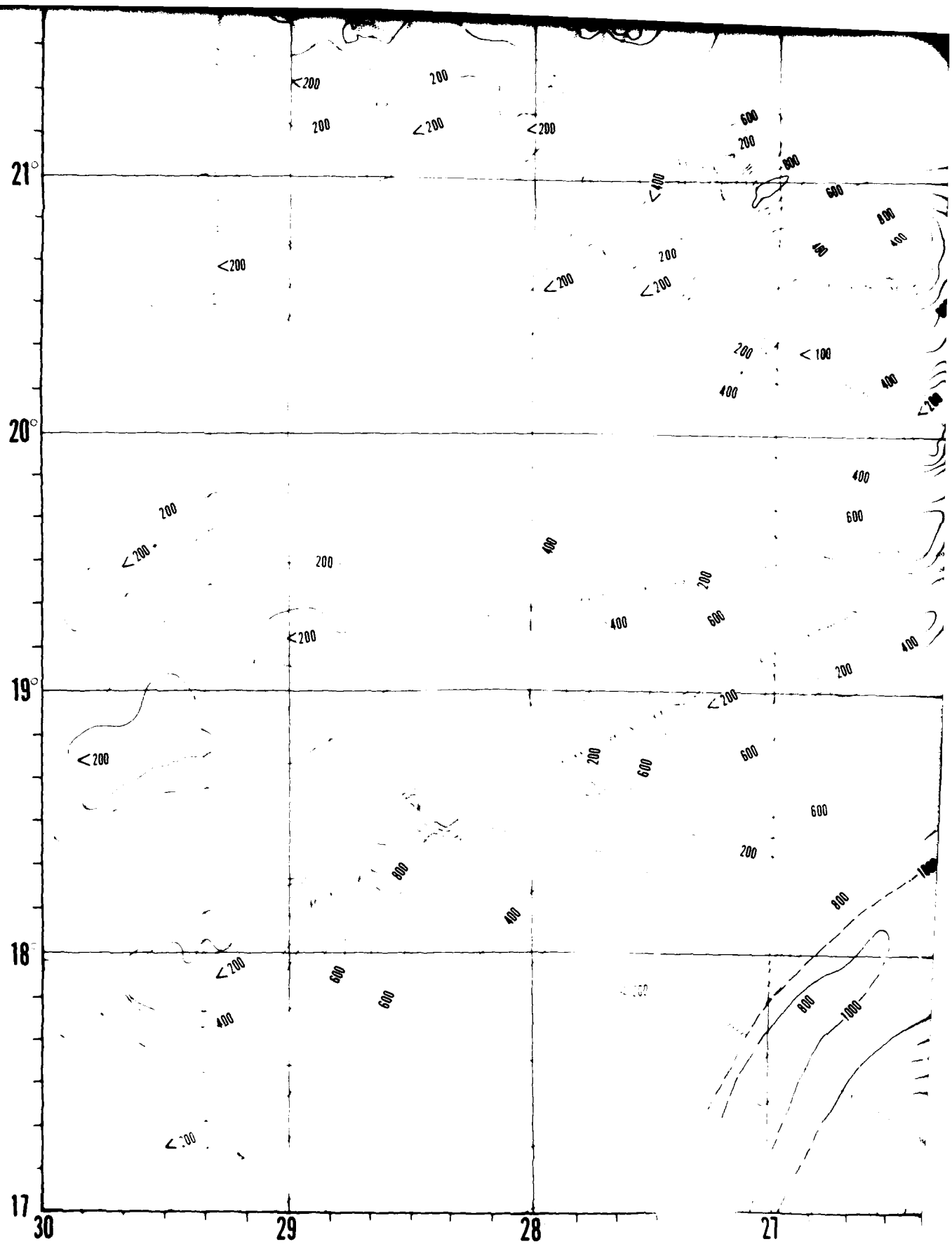
21°
20°
19°
18°
17
30
29
28
27
<200
200
400
600
800
1000
<100

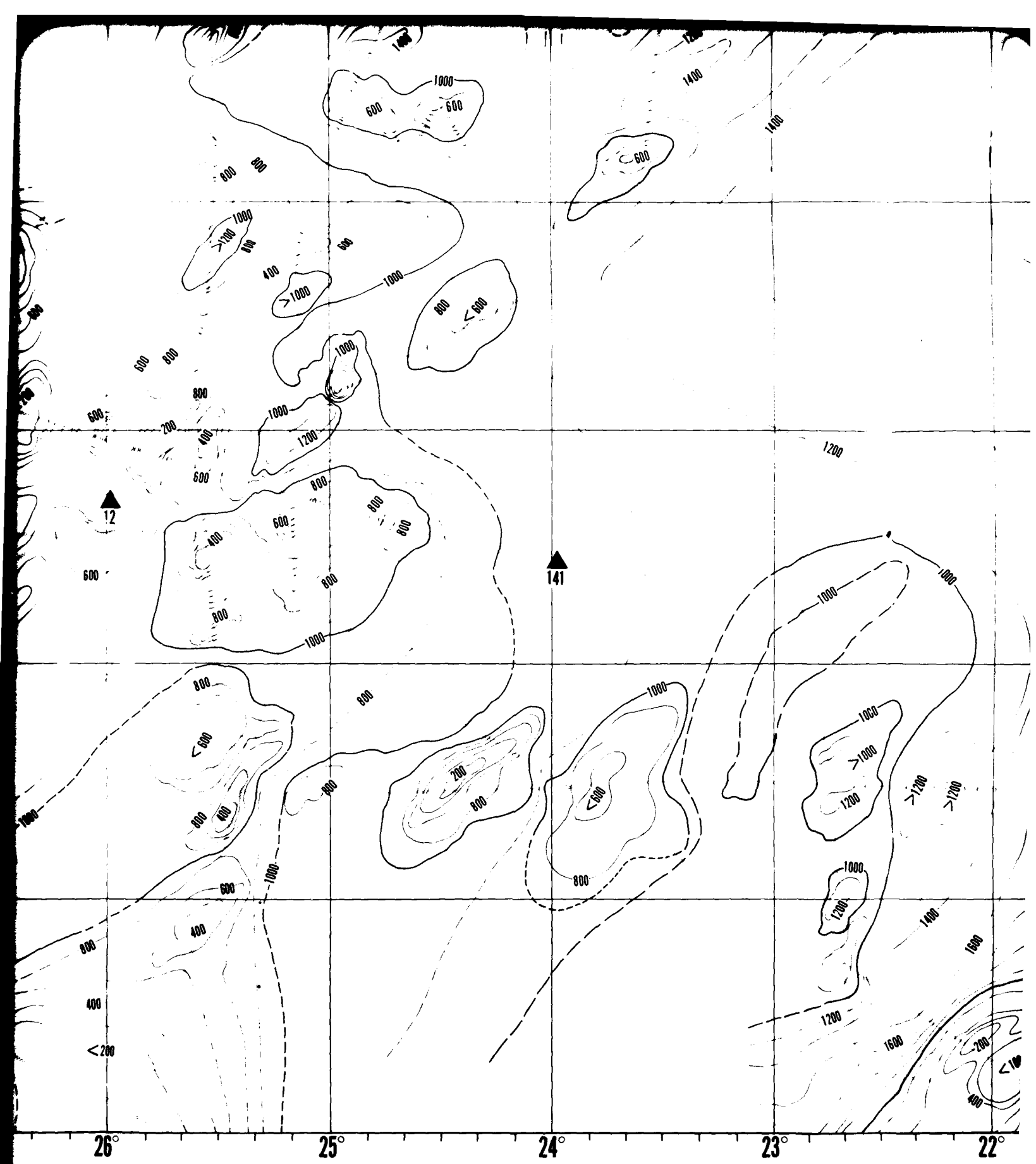
12
141
26°
25°
24°
23°
22°

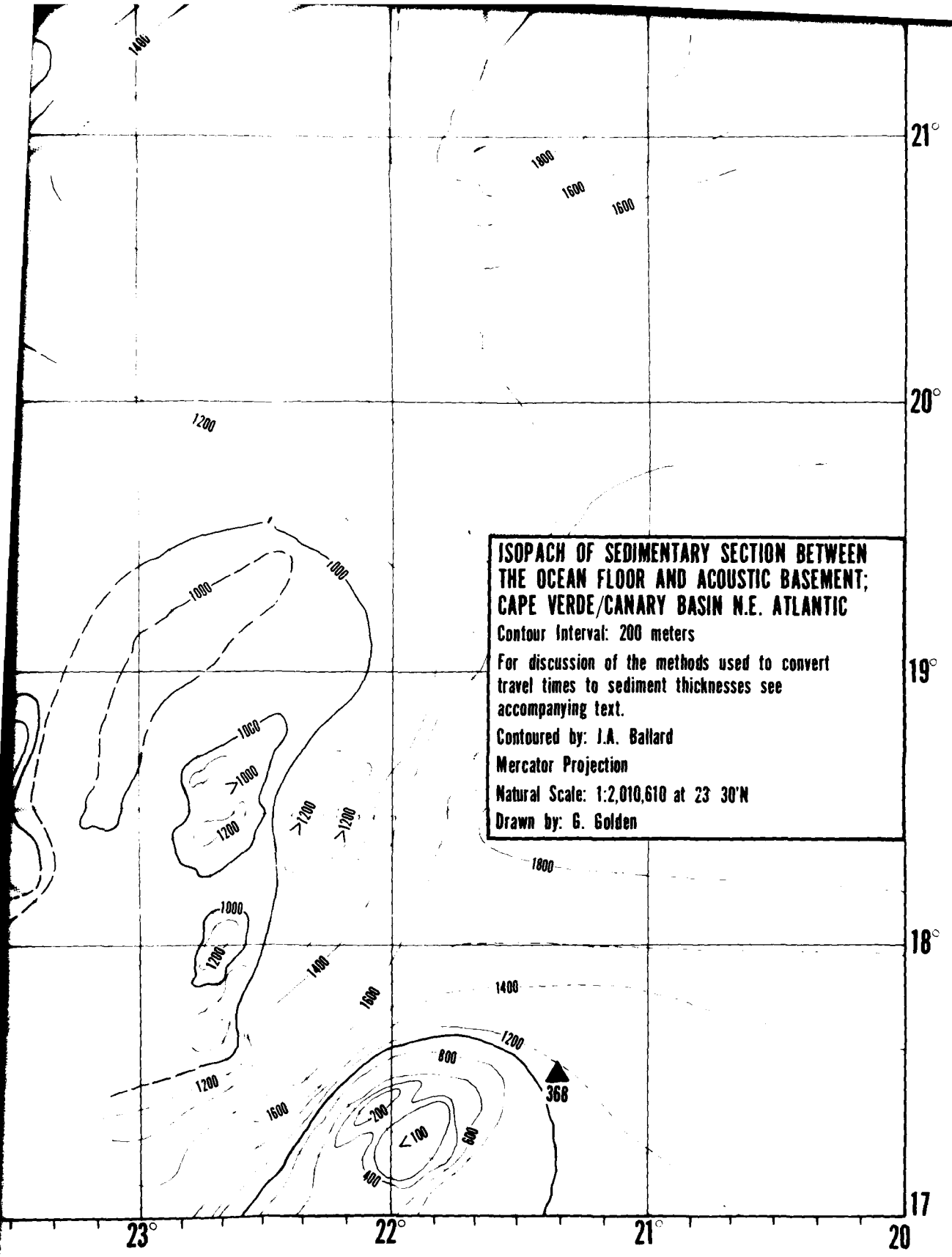

ISOPACH OF SEDIMENTARY SECTION BETWEEN THE OCEAN FLOOR AND ACOUSTIC BASEMENT; CAPE VERDE/CANARY BASIN N.E. ATLANTIC

Contour Interval: 200 meters

For discussion of the methods used to convert travel times to sediment thicknesses see accompanying text.

Contoured by: J.A. Ballard

Mercator Projection

Natural Scale: 1:2,010,610 at 23° 30'N

Drawn by: G. Golden

PLATE IV

STRUCTURAL FABRIC
CAPE VERDE/CANARY BASIN

Acoustic basement structure map used as base.

Faults identified from normal incidence, seismic reflection profile.

South of 26°N dimensions and distribution of features are controlled by data density.

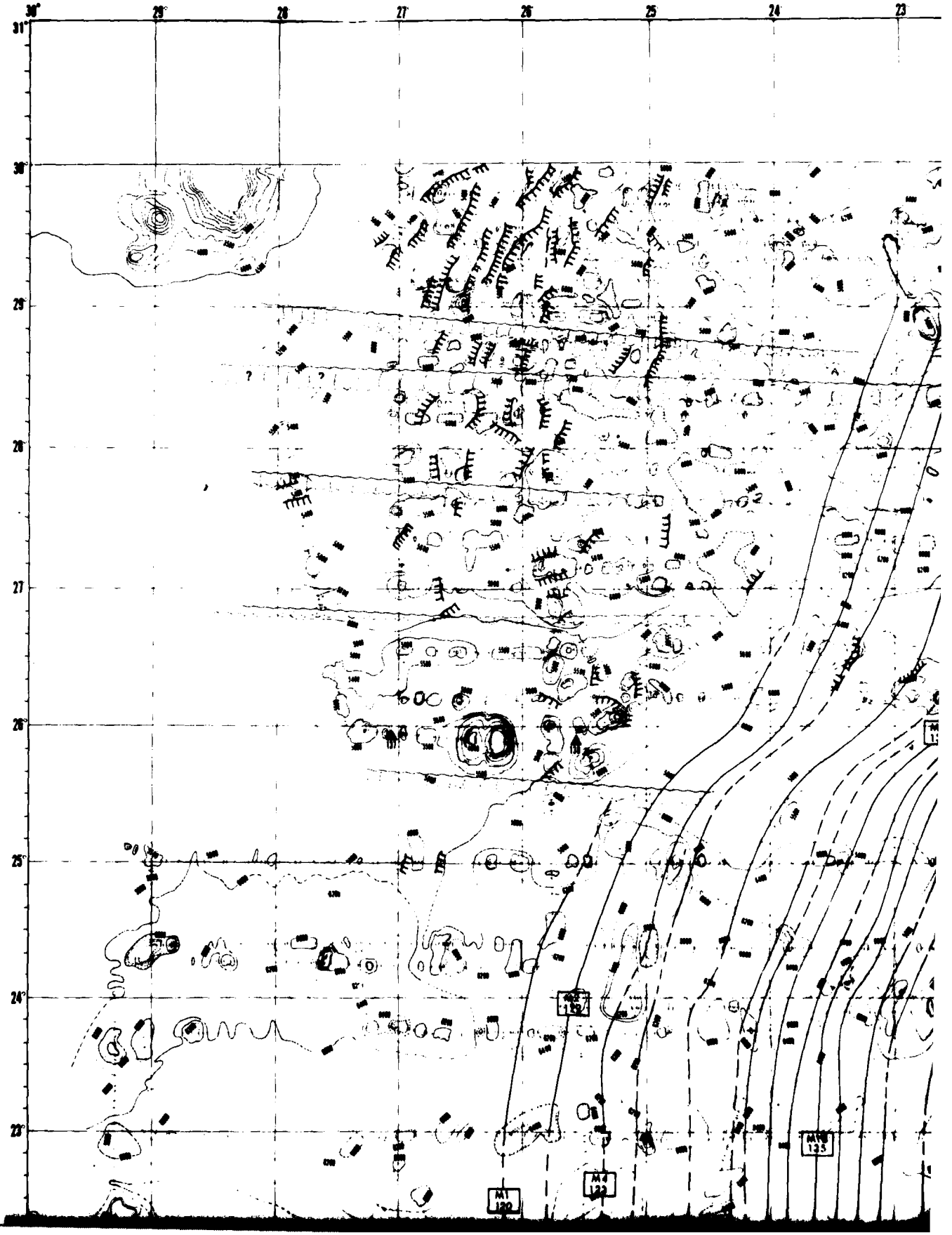
30°
29°
28°
27°
26°
25°
24°
23°
31°
30°
29°
28°
27°
26°
25°
24°
23°
M1
120
M2
122
M3
123

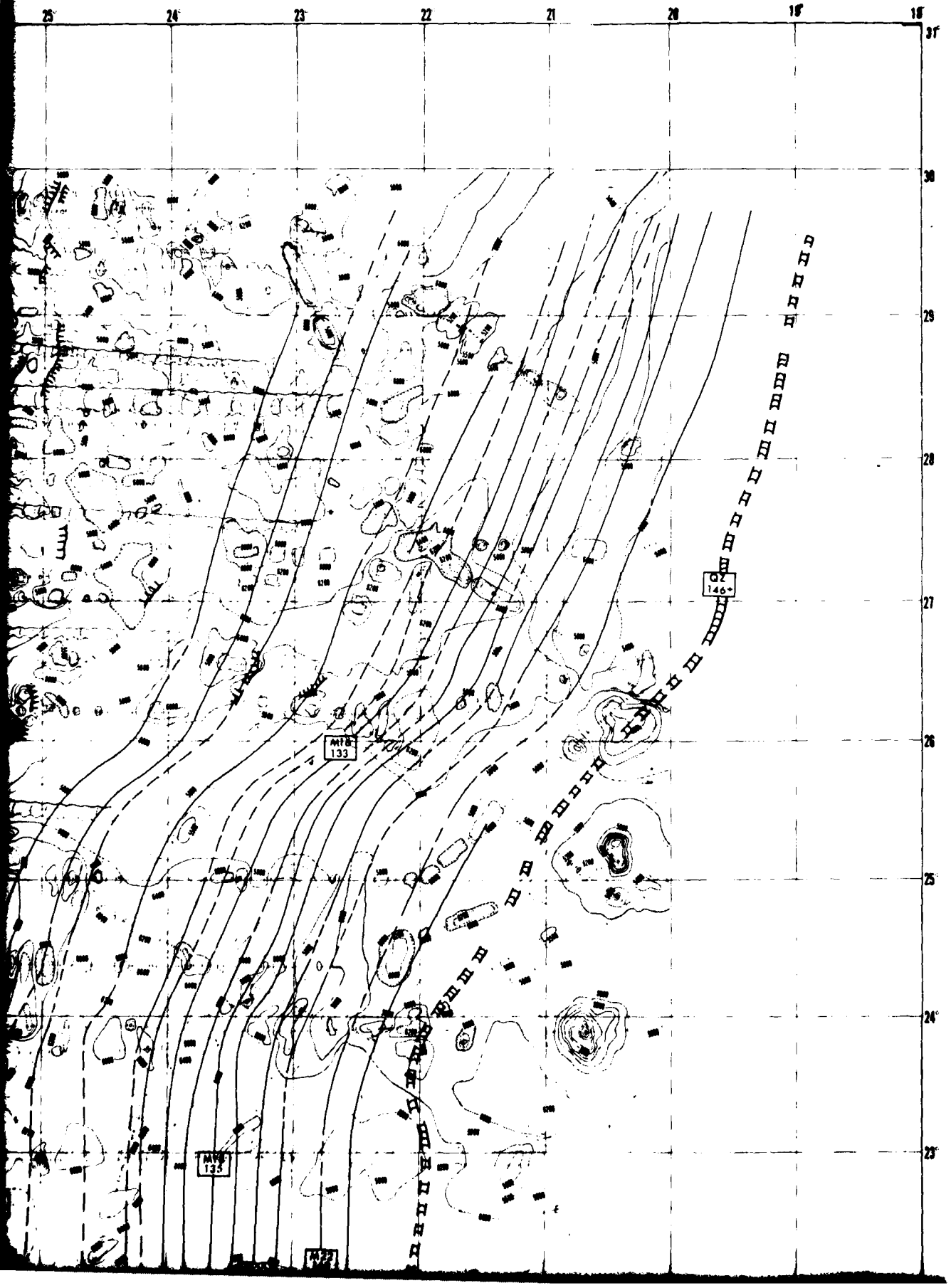
25
24
23
22
21
20
19
18
31
30
29
28
27
26
25
24
23
MTB
133
MTB
135
MTB
137
QZ
146

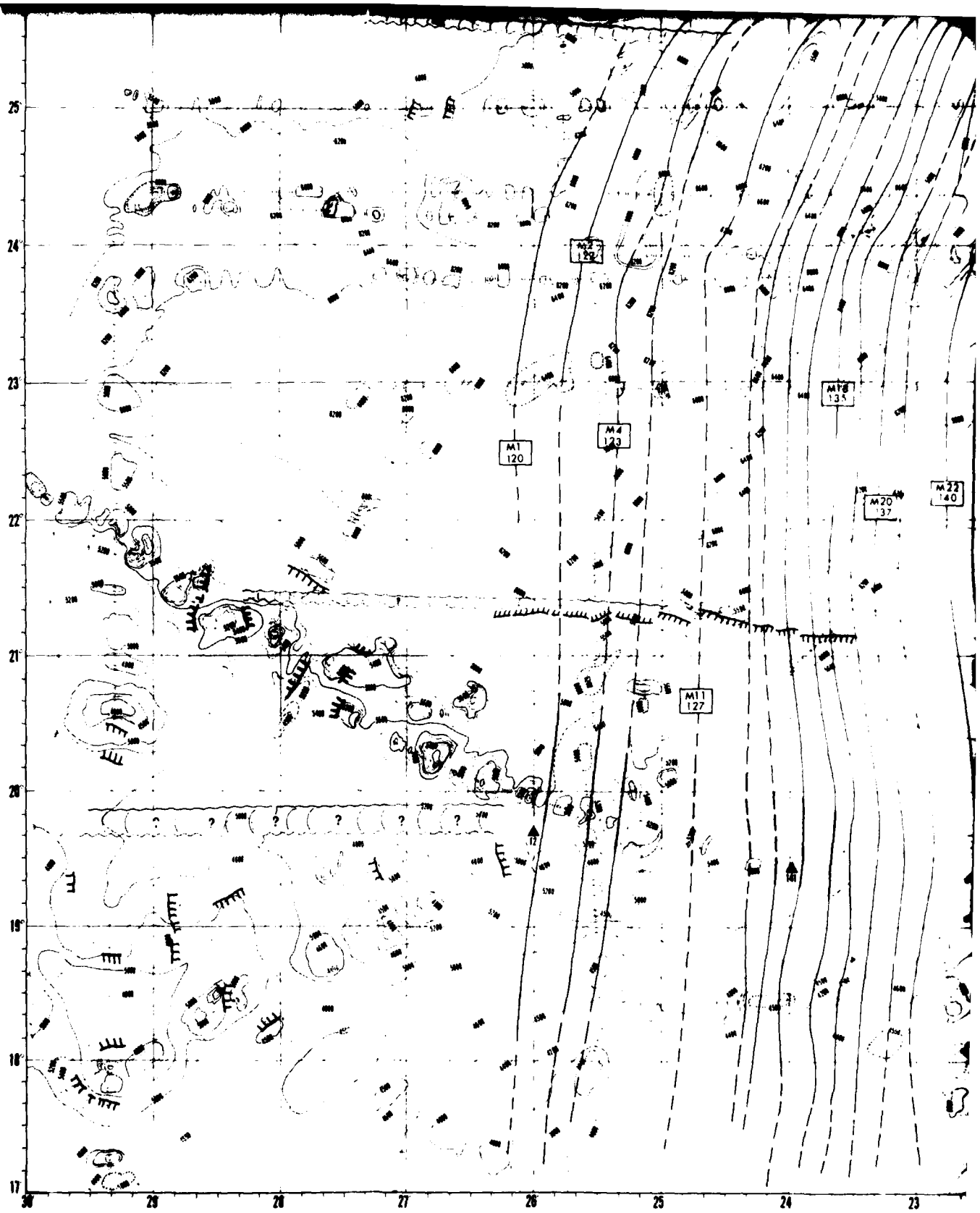
M1
120
M4
123
M11
127
M20
137
M22
140

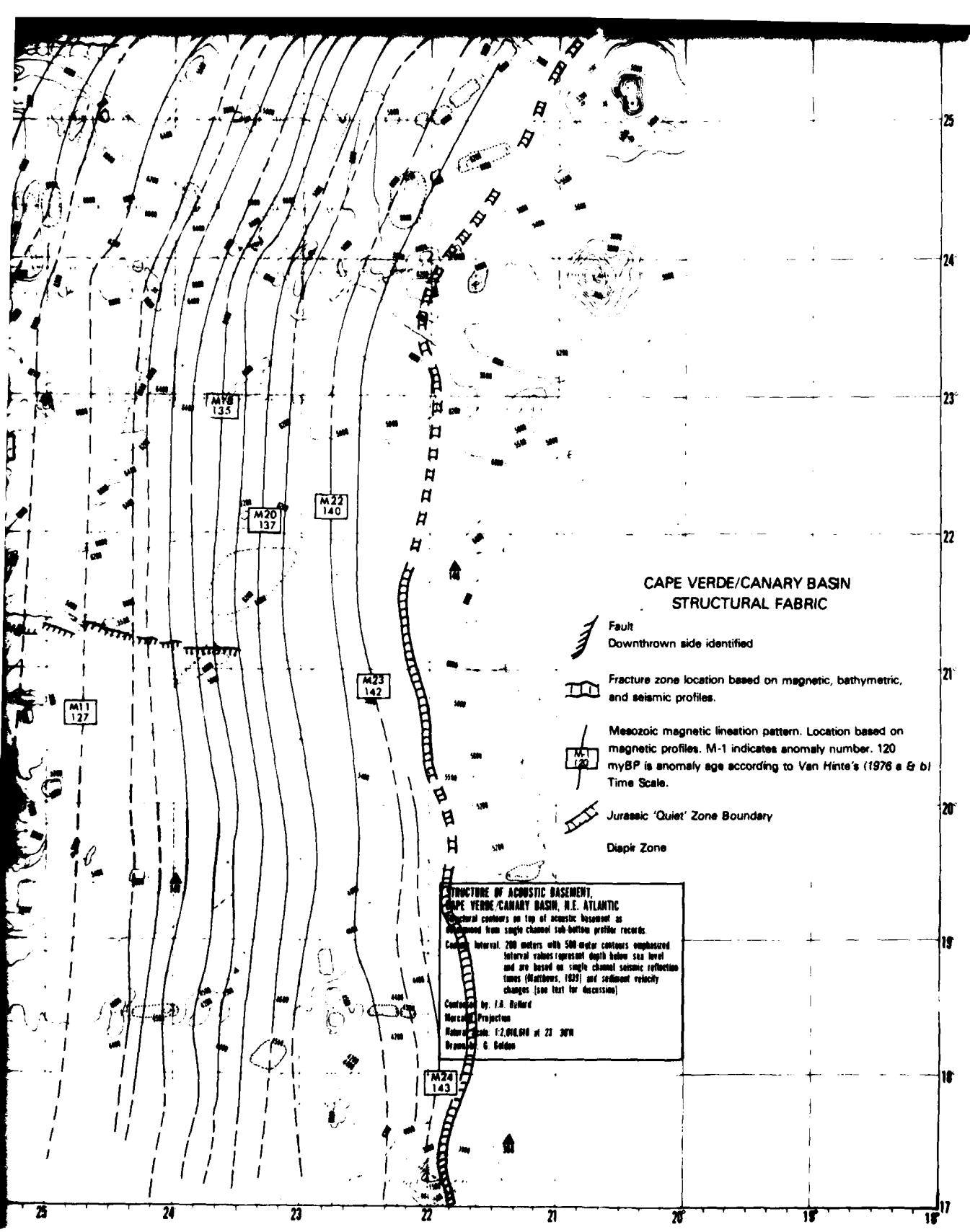

CAPE VERDE/CANARY BASIN
STRUCTURAL FABRIC

Fault
Downthrown side identified

Fracture zone location based on magnetic, bathymetric, and seismic profiles.

M-1
120

Mesozoic magnetic lineation pattern. Location based on magnetic profiles. M-1 indicates anomaly number. 120 myBP is anomaly age according to Van Hinte's (1976 a & b) Time Scale.

Jurassic 'Quiet' Zone Boundary

Diapir Zone

STRUCTURE OF ACOUSTIC BASEMENT, CAPE VERDE/CANARY BASIN, N.E. ATLANTIC

Structural contours on top of acoustic basement as determined from single channel sub-bottom profiler records.

Contour Interval: 200 meters with 500-meter contours emphasized. Interval values represent depth below sea level and are based on single channel seismic reflection times (Matthews, 1939) and sediment velocity changes [see text for discussion].

Contoured by: I.A. Bullard

Mercator Projection

Natural Scale: 1:2,000,000 at 23° 30'N

Drawn by: G. Seldon

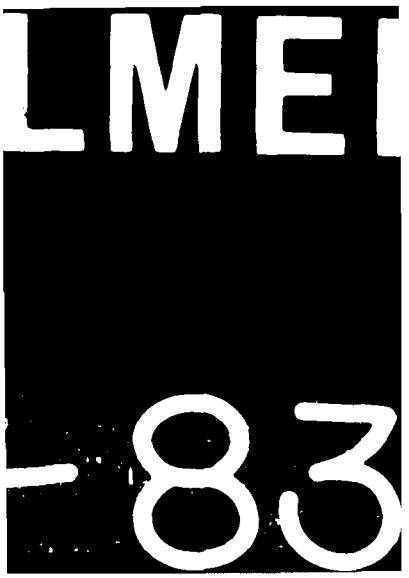
LME
83